SC

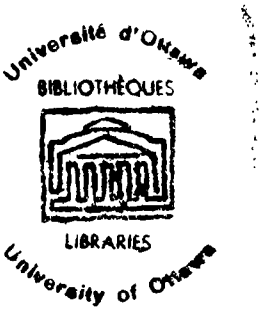

PHOTOCHEMISTRY OF ETHYLENE WITH INFRARED AND ULTRAVIOLET RADIATION

by

Louis Giroux

Thesis submitted to
the School of Graduate Studies and Research
in partial fulfillment of the requirements
for the Ph.D. degree in Chemistry

University of Ottawa
August, 1988

M.H. Back
Professor of Chemistry
Research Supervisor

Louis Giroux
Ph.D. Candidate

ACKNOWLEDGEMENTS

Many people have supported me in both a scientific and a personal way throughout the course of my graduate studies. Here, I wish to acknowledge the parts played by all of those who, on a large or small scale, have contributed to my quest at better understanding the intimate world of the interaction between light and molecules.

First of all, I am indebted to Professor M.H. Back, my research director, who has provided extraordinary scientific guidance and the required financial support through my entire graduate career. Her constant enthusiasm and unfailing availability as well as her encouragements and helpful suggestions were especially appreciated during the writing of this thesis.

I am equally very grateful to her husband, Dr. R.A. Back, who besides allowing me to use his equipment in the Photochemistry and Kinetics section at the National Research Council of Canada in Ottawa, was instrumental in showing me the importance of clear and concise scientific thought and writing. Our numerous discussions dealing with the experimental and interpretation parts of this work and his constructive comments are also gratefully acknowledged.

I would like to thank Drs. J. Sloan, S. Mitchell and G. Paraskevopoulos at the NRCC for allowing me to use their excimer lasers.

Special thanks are given to J. Parsons and P. Lawrence at the NRCC for their expert technical assistance over the duration of the experiments.

I am also thankful to all members of the support and teaching staffs in the Chemistry Department at the University of Ottawa and especially to Professor B.A. Morrow for letting me use his FTIR spectrometer and to Professor H. Teitlebaum for several interesting discussions.

A number of my former fellow graduate students including Drs. J. R. Cao, S. Ahmed, R. McFarlane and C. Tripp are to thank for their invaluable help and companionship as well as for many fruitful discussions and suggestions about the present work.

Several postdoctoral fellows and visiting scientists including Drs. A. Kumar, D. Perrin, A. Bossard, P. Roussel, S. Yamamoto and Y. Ishikawa also contributed greatly to my scientific development both at the university and at the NRCC.

Dr. A. Kumar, D. Lauzon and C. Carruthers deserve my special gratitude for help in the writing of the computer programs used in the model calculations.

Mrs. D. Tam's skillful and efficient typing and editing of the text of this manuscript as well as her patient cooperation during this quite lengthy process are gratefully appreciated. Many thanks are also due to Mrs. E. Szabo for her expert craftsmanship in the drawing of figures.

During the final stages of preparation of the thesis, I am grateful to Sylvie Marengère and to her family for their support and friendship.

Finally, from the bottom of my heart, I wish to express my deepest and most sincere appreciation for the support, the understanding, the patience and encouragements, but most of all for the love provided by my parents, Jean-Guy and Thérèse, my brothers Marc, Guy and Claude and sisters Hélène, Danielle and Martyne. I shall forever be indebted to them for being directly responsible for my achievements through their constant interest in my education. To them, with my love and admiration, I dedicate this thesis.

TABLE OF CONTENTS

LIST OF FIGURES

LIST OF TABLES

GLOSSARY OF SYMBOLS

A	absorbance of light, $\log_{10} (E_0/E_T)$
A_f, A_r	forward and reverse preexponential factors of a reaction
c	speed of light
c_s	speed of sound
C_p	heat capacity at constant pressure
C_v	heat capacity at constant volume
CW	continuous wave
E	energy
E_0	energy per pulse incident on the gas (behind front window of cell)
$(E_0)_E$	energy per pulse incident on ethylene
E_a	energy of activation
E_{abs}	energy per pulse absorbed per mole of ethylene
E_{cell}	energy per pulse transmitted by the empty cell
E_T	energy per pulse transmitted by ethylene
F	fluence
F_0	incident fluence on the gas (behind front window of cell)
FWHM	full width at half-maximum
h	Planck constant
Hz	hertz
ΔH_i	enthalpy of reaction i
ΔH_f°	standard molar enthalpy of formation
I	intensity
J	joule
k_i	rate constant of reaction i
K_c	equilibrium constant with respect to concentration

l	path length
l_1	thickness of an "effective reaction zone"
<N>	average number of photons absorbed per molecule
R	molar gas constant ($J\ K^{-1}\ mol^{-1}$)
R_f	reflectance factor
S	cross-section area of laser beam
S°	standard molar entropy
t	time
t_{eff}	effective reaction time
T	temperature
T_0	initial temperature (300 K)
T_{eff}	effective reaction temperature
T_{max}	maximum temperature
v_i	vibrational quantum number of i^{th} mode
V	electric potential (volt)
V_{eff}	effective reaction volume
V_{vessel}	volume of vessel
γ	ratio of heat capacities
ϵ	molar (decadic) absorption coefficient
ϵ_{eff}	effective molar (decadic) absorption coefficient
η	index of refraction
λ	wavelength
ν_i	frequency of i^{th} mode of vibration
$\tilde{\nu}$	wave number
ρ	normal reflectance
σ	molecular cross-section
ϕ	quantum yield

In this thesis, all units adhere to the "système international d'unités" except for the use of the following non SI units (given along with their corresponding values in SI units):

1 Torr = 101325/760 Pa. = 133.322 N m^{-2}

1 cm^{-1} = 0.01 m^{-1}

ABSTRACT

The decomposition of ethylene was investigated at pressures ranging from 500 to 3000 Torr, using the unfocussed beam of a pulsed infrared CO_2 TEA laser tuned to the 10 P(12) line at 951.19 cm^{-1} and to the 10 P(14) line at 949.48 cm^{-1}. Deviations from the Beer-Lambert law were observed in the dependence of absorption on ethylene pressure and incident fluence. Absorption of these laser frequencies, which are close to a number of rotational features in the central region of the Q-branch of the ν_7 out-of-plane wagging mode of ethylene, was enhanced by pressure-broadening in the absorption spectrum.

Knowledge of the energy absorbed permitted the calculation of temperature profiles and of effective reaction zones immediately following the laser pulse. Under the experimental conditions, (500-3000 Torr and incident fluences between 0.1 and 1 J cm^{-2}), the reaction zone is a thin disc at the front window.

The occurrence of the reversible reaction $2C_2H_4 \rightleftarrows c\text{-}C_4H_8$, for which the rate parameters are known, allowed an estimation of an "effective reaction temperature" assuming an equilibrium concentration of cyclobutane was attained. Simple computer modelling of the reaction by numerical integration for different maximum temperatures (T_{max}) reached at the end of the pulse (110 ns FWHM) showed the relation between the "effective reaction temperature" and T_{max}.

Other products of the decomposition included 1,3-butadiene, acetylene, hydrogen, ethane, 1-butene, propylene, methane, allene, n-butane and 2-butene in approximate order of diminishing importance. These were suggested to arise

from free-radical chain reactions initiated by the bimolecular reaction of ethylene, $2C_2H_4 \rightarrow C_2H_5^{\cdot} + C_2H_3^{\cdot}$, followed by a series of decomposition, addition and disproportionation reactions of ethyl and vinyl radicals and of the higher radicals thus formed.

A study was also made of the ethylene photolysis in the UV region between 193 and 308 nm using unfocussed excimer lasers operated at pulse rates from 1 to 100 Hz. Radiation at 193 nm (ArF laser) excites ethylene from its ground electronic state, N, in which the molecule is planar, into its first excited electronic singlet state, V, in which one CH_2 group has been twisted by 90° relative to the other. The energy of the absorbed quantum exceeded the energy thresholds of the following three primary dissociation reactions:

$$C_2H_4 + h\nu\,(\lambda = 193\ \text{nm}) \rightarrow C_2H_2 + H_2 \quad (1)$$

$$\rightarrow C_2H_2 + 2H^{\cdot} \quad (2)$$

$$\rightarrow C_2H_3^{\cdot} + H^{\cdot} \quad (3)$$

A measurement of the absorption coefficient at 193 nm, $\epsilon = 5.6\ M^{-1}\ cm^{-1}$, allowed the determination of quantum yields as a function of both pressure (50-3000 Torr) and time (10-250 pulses) using a laser pulse rate of 1 Hz. The products obtained in order of decreasing importance were acetylene, hydrogen, n-butane, 1-butene, ethane, 1,3-butadiene, propane, propylene, methane, allene, 2-butene and methylcyclopropane. It was concluded that primary process (1) was the main decomposition reaction occurring at 193 nm, with $\phi(1)$, decreasing with pressure from 0.36 at 50 Torr to 0.28 at 3000 Torr and decreasing slightly with number of pulses. Primary process (2) was found to decrease slightly

with pressure from 0.11 at 50 Torr to 0.09 at 3000 Torr and to increase slightly with number of pulses. Primary process (3) appeared to increase with pressure from 0.11 at 50 Torr to 0.15 at 3000 Torr and to decrease sharply with number of pulses; this was shown to be due to secondary photolysis of products. The total primary quantum yield was always less than 1. A mechanism was proposed, and it was concluded that the V state of ethylene was very short lived ($t \leq 3 \times 10^{-11}$ s).

Preliminary experiments were also made in which ethylene at 1 atmosphere pressure was irradiated at 222 nm (KrCl laser), 249 nm (KrF laser) and 308 nm (XeCl laser). While absorption at 222 nm, located near the origin of the V $\leftarrow$ N transition, probably involves the V state, absorption at 249 and 308 nm may proceed by excitation into the triplet state. Despite the very weak absorption of ethylene at these longer wavelengths, ($\epsilon \sim 10^{-3}$-10^{-4} M^{-1} cm^{-1}), products including acetylene, hydrogen, ethane, n-butane, propylene, methane and 1-butene were obtained following long irradiations (1 h) at a laser pulse rate of 100 Hz. Possible mechanisms are discussed.

PART I

Thermal decomposition of ethylene induced by pulsed infrared CO_2 laser radiation

GENERAL INTRODUCTION

Ever since the realization of the first laser by Maiman in May 1960 [1], many areas of physics and chemistry have benefited greatly from their unique properties. The special features of laser radiation such as narrow bandwidth, high intensity and short pulse duration have made possible a variety of studies probing the details of the interaction of molecules with intense radiation fields.

In 1971, two Canadians, Isenor and Richardson [2], first suggested that a molecule could be decomposed in the field of a focussed CO_2 laser, even though the energy of the photon was much lower than the dissociation energy of the molecule. They observed fluorescence from electronically excited products of dissociation from molecules such as NH_3, SiF_4 and CCl_2F_2. In 1973, the Canadian group [3] and the Soviet group of Letokhov, Ryabov and Tumanov [4] identified two distinct components in the observed luminescence: an "instantaneous" emission and a delayed emission. The former was not influenced by collisional events during the pulse and was thus the result of direct dissociation of isolated molecules following absorption of the IR radiation. Subsequently, Ambartzumian, Letokhov, Ryabov and Chekalin [5] observed for the first time the isotopically selective dissociation of a polyatomic molecule, BCl_3. This experiment pointed the way to the practical application of powerful infrared lasers for isotope separation. Since 1974, other isotope separations have been accomplished with lasers in systems providing isotopic enrichment for about a dozen elements, including uranium [6], hydrogen [7] and carbon [8]. At the same time, significant efforts have been made both by experimentalists and theoreticians to understand the process of infrared multiphoton absorption and dissociation in polyatomic molecules in strong radiation fields.

Perhaps the most successful and currently accepted model for infrared multiple photon absorption (IRMPA) and dissociation (IRMPD), was proposed by Black, Yablonovitch, Bloembergen and Mukamel in 1977 [9]. In this model, shown in Figure 1, the vibrational energy levels of a molecule are divided into three regions of excitation: a region of discrete levels, a quasi-continuum and a dissociation region. In region I, tuning a monochromatic IR laser in resonance with an allowed transition between the ground state and the first vibrational level (v=1) of a particular mode, readily promotes molecules to this level. Successive transitions to higher vibrational levels of the same mode, however, become more and more out of resonance due to anharmonicity. Various effects such as degeneracy splitting [10], rotational energy compensation [11], Coriolis coupling [12], power-broadening [13] and pressure-broadening [14], have been invoked to compensate for the vibrational anharmonicity and enable the further excitation of molecules up the ladder of a single vibrational mode. It is in this first region that selective excitation of isotopic molecules occur, and the excitation efficiency depends on laser intensity rather than fluence. As the vibrational energy of the molecule increases, the density of rotational-vibrational states grows rapidly and eventually these merge into a "quasi-continuum". The onset of this region (II) is strongly dependent on molecular size, i.e., the number of vibrational modes, and on the magnitudes of their frequencies. The probability of absorption in region II is greatly increased because of the high density of vibrational states, and laser fluence rather than the laser intensity appears to be the important parameter for excitation efficiency. If the fluence is high enough, some molecules will accumulate an amount of energy during the pulse comparable to the dissociation threshold. Above this threshold, the model defines a third

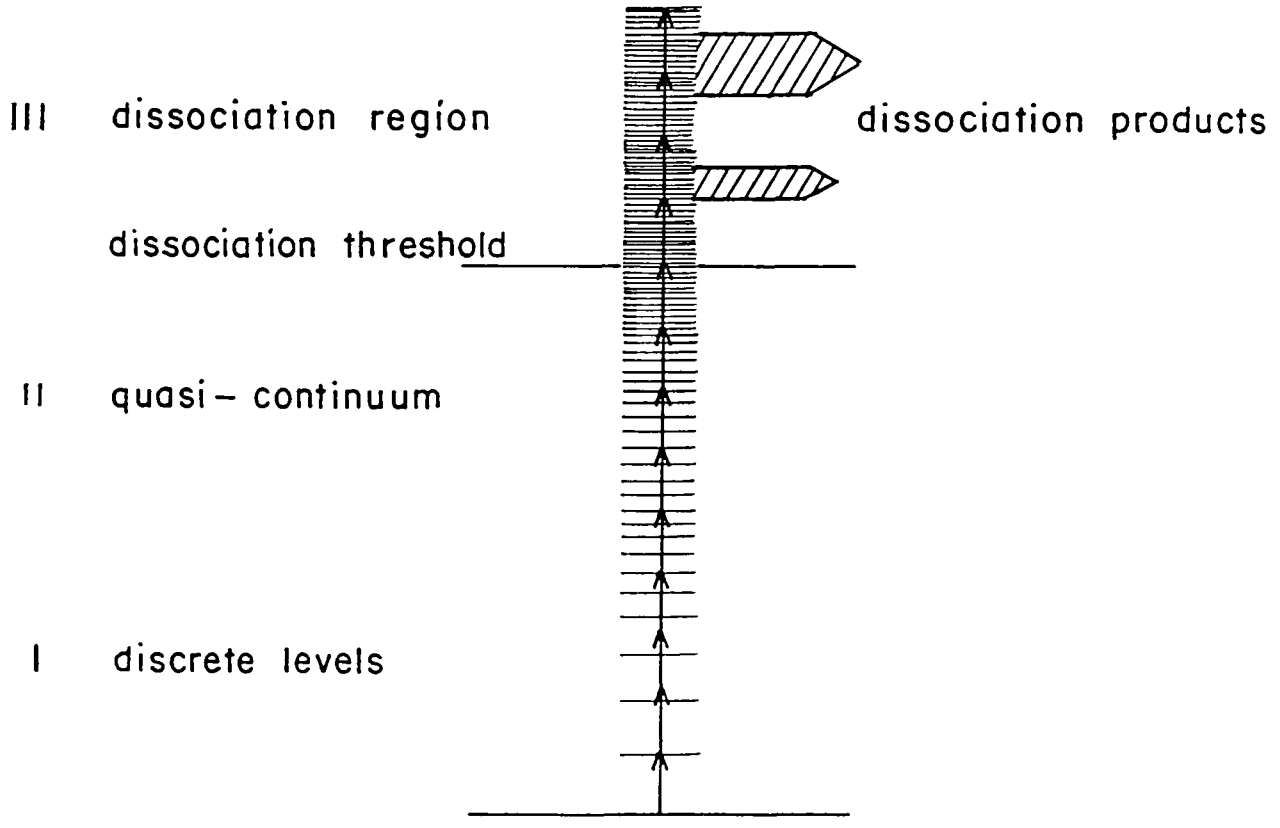

Figure 1. Schematic energy-level diagram for multiple photon absorption (IRMPA) and dissociation (IRMPD).

region, in which the states of the molecule are coupled with dissociation products through unimolecular dissociation processes. In region III, dissociation competes with excitation and the RRKM statistical theory of unimolecular decomposition relates the lifetime of the dissociating species to the energy in excess of the dissociation threshold [15]. The laser intensity determines the excess energy content of the molecule which is available for partitioning among the dissociation fragments [16].

A number of characteristics of the laser radiation and of the absorbing molecule play important roles in both the infrared multiple-photon absorption and the dissociation processes [17]. The absorption is sensitive to such inter-related variables as the total energy of the laser pulse, the pulse length, the beam profile and the focussing geometry of the system, the optical path length and the small-signal absorption cross-section, as well as to the exact matching of the sharp frequency of the laser radiation with features of the absorption spectrum of the absorbing molecule. As will be seen in the present work, the probability of absorption depends on the width of the absorption band, which is a function of the total pressure in the system. The coherence of the laser radiation can also be a factor in its interaction with absorbing molecules, as these are pumped in phase with the radiation field. The primary absorption can in fact be regarded as a dephasing process, and further dephasing occurs by rapid collisional relaxation. While such dephasing processes were occurring in the systems studied here, the nature of the measurements and conditions of the experiments, which involved no measurements in the very short time domain in which dephasing occurred, were such that no information could be obtained about these processes. In particular, at the pressures and relatively low radition intensities of the present infrared experiments, collisional

dephasing during the pulse will be such that molecules are effectively dephased from the laser field between absorption of successive photons, and hence no in-phase multiphoton pumping is occurring. In the decomposition process, properties of the molecule such as the density of vibrational states and the bond strength are important in determining the rate of decomposition.

Studies of IRMPA and IRMPD of polyatomic molecules have suggested that molecules may be classified as "small" or "large" according to their absorption behavior in the radiation field of a pulsed IR laser. The differences between these categories have in recent years been clarified by the Kansas State University group of Danen, Setser and coworkers [18-22]. They described molecular properties which accounted for these differences in molecules of different size. Large molecules have a high density of rotational-vibrational states at room temperature giving ready access to the "quasi-continuum". Small molecules, with their much smaller density of states, are subject to saturation effects, or "hole-burning" in which rapid absorption by the intense laser pulse can effectively deplete the absorbing rotational state. This phenomenon is not observed in "large" molecules. "Small" molecules showed deviations from Beer's law where the absorption cross-section increased with total pressure, but this was not observed with large molecules. On the other hand, the absorption cross-section for "large" molecules was insensitive to fluence.

Important experimental parameters in IRMP systems are fluence, intensity and pressure.

Fluence is the radiation flux integrated over the duration of a single pulse, usually expressed as J cm^{-2}. Intensity is the radiation flux itself, usually expressed as W cm^{-2}, which may be given as an average value,

averaged over the pulse duration, or as a peak value. In most IRMP studies, fluence and intensity have not been varied independently, but with recent developments of short-pulse CO_2 lasers (1-10 ns), pulses of equal fluence but much different length, and hence different intensity, can be compared, and the effects of fluence and intensity separated [23-28]. Fluence determines the total energy deposited by the pulse in the molecules, while intensity determines the rate of deposition. One or the other may be the more important parameter, depending on the system.

The effects of pressure on IRMP decompositions are complex. At a pressure of 1 Torr, the average time between collisions is about 100 ns, comparable to the half life of a typical CO_2 laser pulse. At this pressure and below, the absorption process is thus almost unaffected by collisions and independent of pressure. The study of collision-free absorption has recently been extended to higher pressures by the use of shorter pulses of 1-10 ns duration [29-32]. The decomposition process, on the other hand, may occur during the pulse, or after the pulse, or both, depending on fluence, intensity and molecular properties such as absorption cross-section, bond dissociation energy, and number of vibrational modes, and thus may be affected by collisions even at pressures below 1 Torr. Decomposition in a molecular beam is probably the only way to ensure that effects of collisions are entirely eliminated [33]. At low pressures, the effect of collisions may be considered in terms of the 3-level model (Figure 1). In region I, collisions will tend to increase the number of molecules interacting with the laser field by coupling rotational states not directly excited by the laser, to those that are, i.e. rotational "hole filling". In region II, collisions will increase the rate of energy flow from the vibrational mode excited to the other internal and

translational modes of the molecule; this is more important for "small" molecules than for "large" ones because of the much greater density of states of the latter. In region III, collisions may have a negative effect, causing a significant decrease in the dissociation rate. As the pressure is increased above 1 Torr, collisions become progressively more important in both absorption and decomposition. The overall pressure dependence can be quite complicated, as the decomposition changes from the unimolecular decomposition of isolated molecules at low pressure to something close to a bulk thermal decomposition of a gas at high pressure.

Some molecules are either non-absorbing or too weakly absorbing to be efficiently decomposed by multiple-photon absorption in the emission region, 9-11 μm, of the CO_2 laser. In such cases, an unreactive molecule which absorbs the IR radiation may be used as a sensitizer to transfer some of this energy to the reactant molecule. This technique has been termed "cold pyrolysis" since the often complicating and detrimental heterogeneous processes occurring at the walls of hot reaction cells are avoided [34]. The group of Keehn, Steel and coworkers at Brandeis University [35-38] have used such molecules as SiF_4, SF_6, C_6F_6 and NH_3 as sensitizers for many organic decompositions.

Sensitizer molecules have also been used to distinguish between a selective, non-equilibrium reaction and a thermally-equilibrated reaction. The first example of this was the study of mixtures of ethyl acetate and isopropyl bromide [39]. Only ethyl acetate absorbed the infrared radiation, but when the system was thermally equilibrated decomposition of both reactants was observed. It was shown that at low pressure and high laser fluences, ethyl acetate was selectively decomposed, showing that the system was far from thermal equilibrium.

An important question in decomposition reactions induced by IR radiation is the temperature reached by the reacting system. Attempts have been made to use a thermal monitor in a pulsed IR laser experiment in which Boltzmann conditions are established. A molecule, R, which undergoes reaction via two channels yielding products A and B provides a convenient monitor. By measuring the ratio of the products formed, the temperature corresponding to this ratio may be obtained from the known Arrhenius parameters [18].

$$R \xrightarrow{k_a = A_a \exp(-E_a/RT)} P_a \qquad (1a)$$

$$R \xrightarrow{k_b = A_b \exp(-E_b/RT)} P_b \qquad (1b)$$

$$T_{eff} = (E_a - E_b)/R[\ln(A_a/A_b) - \ln(P_a/P_b)] \qquad (2)$$

An example of such a molecule is cyclobutanone, which decomposes by the following reactions,

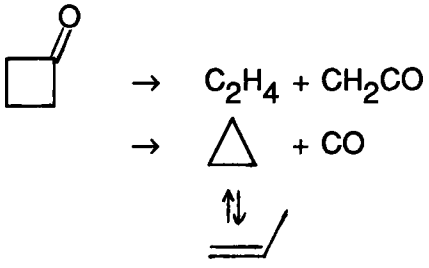

$$\rightarrow \quad C_2H_4 + CH_2CO \qquad (3a)$$

$$\rightarrow \quad \triangle \quad + CO \qquad (3b)$$

The ratio of the rates of formation of ethylene and (cyclopropane and propylene) therefore provided a measurement of the effective reaction temperature:

$$k_{3a}/k_{3b} = 1.6 \exp(25000/RT) \quad [40] \qquad (4)$$

Studies of this reaction as a function of pressure and fluence showed the

complexity of the absorption and decomposition processes, which involved redistribution of energy by collisions at various stages of the heating and cooling cycle [30, 41-46].

Other molecules which have been used as monitors are ethyl vinyl ether [47] and perfluorocyclobutane [48].

The present study was undertaken with the aim of continuing the search for an effective probe of the temperature distribution and the related reaction time in pulsed IR laser-induced absorption and decomposition processes. In thermally reacting ethylene at temperature in the neighborhood of 750 K, the formation and dissociation of cyclobutane

$$2C_2H_4 \rightleftharpoons c\text{-}C_4H_8 \qquad (5)$$

was shown to occur by a reversible process and equilibrium concentrations of cyclobutane were measured [49]. Since the rate constants for both forward and reverse reactions are known, measurement of this product in the laserinduced reaction could therefore indicate an effective reaction temperature in the system. The method was improved by using a simple computer model involving the numerical integration of the forward and reverse rate expressions of the equilibrium reaction, (5), and the approach to equilibrium was explored under different conditions. At the same time, measurement of the absorption of the CO_2 laser radiation allowed an estimate of the energy absorbed and hence of the temperature of the reacting gas under thermally-equilibrated conditions. Beside cyclobutane, other products formed were also measured and their distribution also gave information on the temperature of the reacting system [50].

At the opposite end of the spectrum from the CO_2 laser, lasers are also providing powerful new light sources for the more conventional photochemistry in the ultraviolet region. Particularly notable are the rare-gas halide excimer lasers, which are now available commercially with tens of watts average power at a number of wavelengths from 193 to 350 nm. Table 1 includes the output wavelengths available with the various combination of rare gas and halogen.

Table 1. Emission wavelengths of rare-gas halide excimer lasers.

	ArF	KrCl	KrF	XeCl	XeF
Wavelength/nm	193	222	249	308	350

The high power outputs of the rare-gas halide lasers have led to conversion of their emission into a wide range of tunable coherent radiation sources in both the VUV, the extreme UV (XUV) and the soft X-ray regions via harmonic generation and sum frequency mixing and into the UV and visible regions via the optical pumping of dyes and by the Raman shifting technique [51].

The spectroscopic states responsible for laser transitions in the rare-gas halide (RgX) molecules are most likely the $^2\Sigma_{\frac{1}{2}}$ excited state, which possesses similar properties to the ionic ground state of an alkali halide, and the $^2\Sigma_{\frac{1}{2}}$ ground state [52]. While the excited state is bound by several thousand wavenumbers, the ground state is much more weakly bound and undergoes rapid dissociation in one vibrational period. This is an important characteristic of these systems which allows the achievement of population inversion with subsequent lasing action.

The production of excited rare-gas halide molecules involves two types of processes:

$$\underset{(RgX)}{Rg + X_2} \rightarrow \underset{(Rg)}{RgX^* + X} \qquad (6)$$

the neutral channel route, and

$$Rg^+ + X^- + M \rightarrow RgX^* + M \qquad (7)$$

the ion-recombination route.

Ethylene, whose infrared photochemistry is the topic of the first part of this thesis, has also been thoroughly studied in the ultraviolet region, both spectroscopically [53] and photochemically [54]. The photochemistry has been examined largely using rare-gas resonance lamps in the vacuum ultraviolet (VUV) and with a mercury resonance lamp at 185 nm. At longer wavelengths, the absorption becomes too weak to permit studies with conventional light sources, and a number of questions about both the photochemistry and the spectroscopy remain unresolved in this region. The ArF excimer laser should certainly provide enough power to examine the photolysis at 193 nm, while the other excimer lasers may even allow studies at longer wavelengths well out on the very weak tail of the singlet V $\leftarrow$ N absorption band, and perhaps even in the extremely weak triplet absorption region around 300 nm.

It is useful to compare the infrared photolysis, which almost certainly proceeds through the vibrationally excited ground state, with the ultraviolet photolysis, in which the decomposition may occur from an electronically excited state, or, after internal conversion, may also involve the ground state. As a supplement to the infrared studies in the first part of this thesis, the photolysis of ethylene in the ultraviolet region was also investigated at several wavelengths, using excimer lasers as light sources.

GENERAL EXPERIMENTAL

1. Irradiation system

The optical system for both the absorption measurements and the irradiation experiments is shown schematically in Figure 2. The reaction vessel showing valves and connections to the gas chromatograph and to the vacuum line is shown in Figure 3.

The laser was a line-tuneable Lumonics model 203 multimode CO_2 TEA laser delivering maximum pulse energies of about 2 J and was operated at a pulse frequency of 0.5 Hz. With a mixture of $He:CO_2:N_2$ in the ratio of 95.1:4.3:0.6, the laser pulse consisted of a sharp spike containing ~ 75% of the total energy in the first 110 ns (FWHM) followed by an exponentially decaying tail containing the remaining fraction of the total pulse energy. On average, the total pulse duration was 600 ns. A typical profile averaged over 10 pulses obtained with a Rofin photon drag detector interfaced with a programmable digitizer (Tektronix type 7912 AD), is shown in Figure 4.

The emission lines used in this study were the P(12) at 951.19 cm^{-1} and the P(14) at 949.48 cm^{-1} of the 00°1-10°0 transition of CO_2. Tuning was accomplished by rotation of a gold-coated diffraction grating located at the rear end of the laser cavity. The setting was calibrated using a CO_2 laser spectrum analyzer (Optical Engineering model 16A).

A small fraction (~ 4%) [55] of the incident beam was reflected from a polished NaCl window (Harshaw Chemical Company, Solon, Oh.) to a pyroelectric detector. Such a detector consists of a Li/Ta disc, 5 cm in diameter, mounted on a heat sink. This disc has the electrical properties of

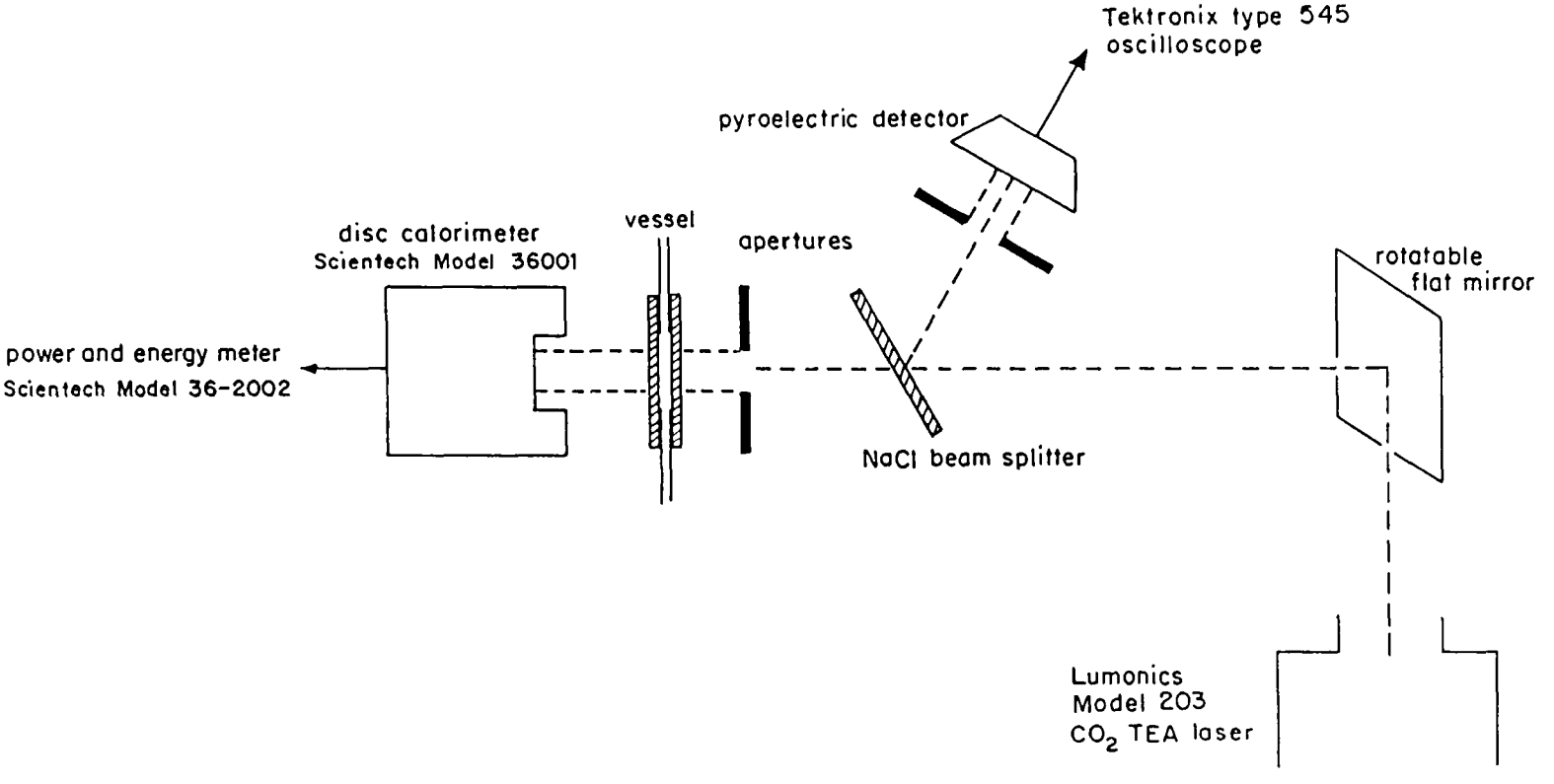

Figure 2. Schematic diagram of the optical system for both the absorption measurements and the irradiation experiments.

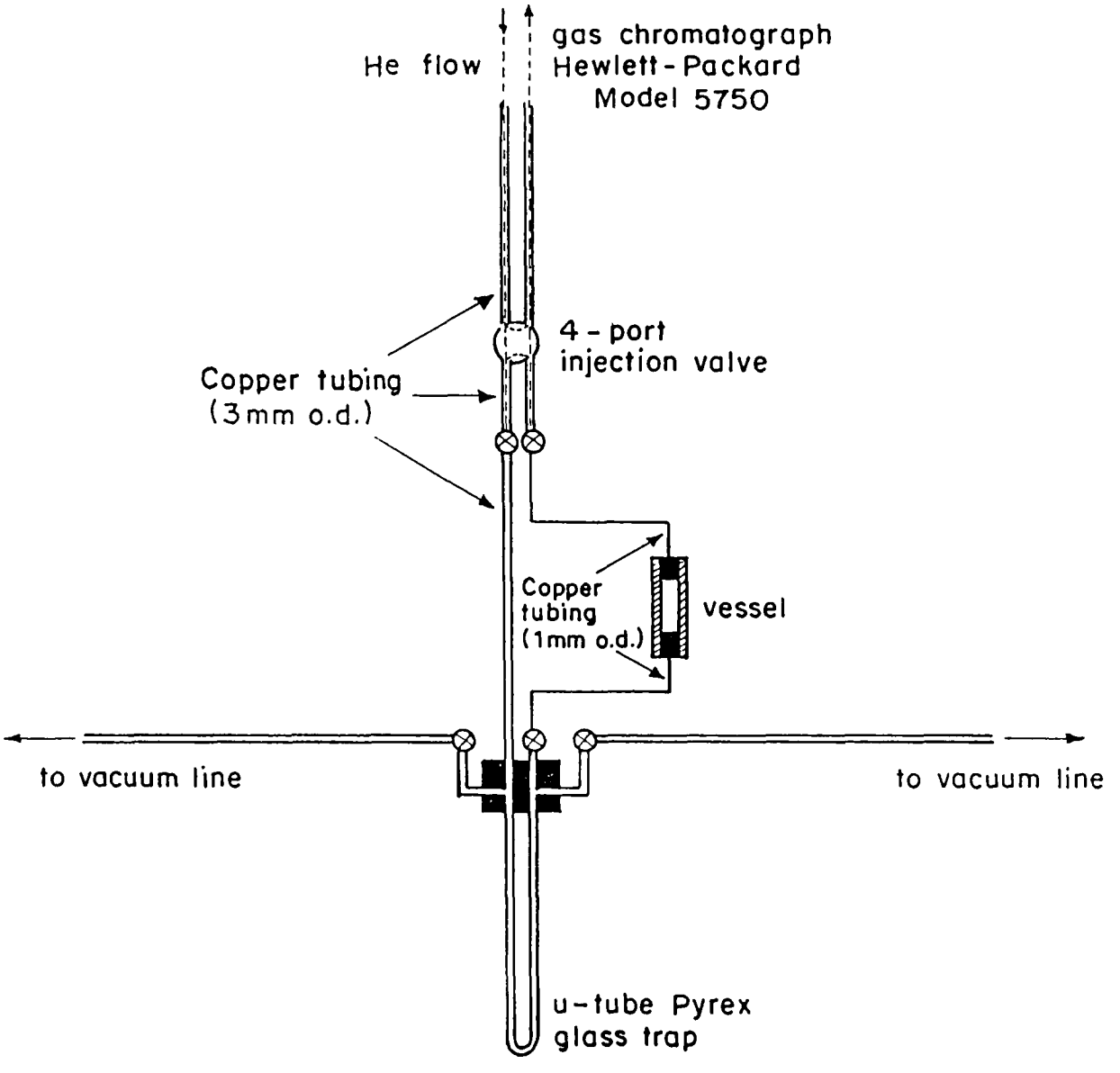

Figure 3. Reaction vessel showing valves and connections to gas chromatograph and vacuum line. ⊗ : Metal Hoke valve.

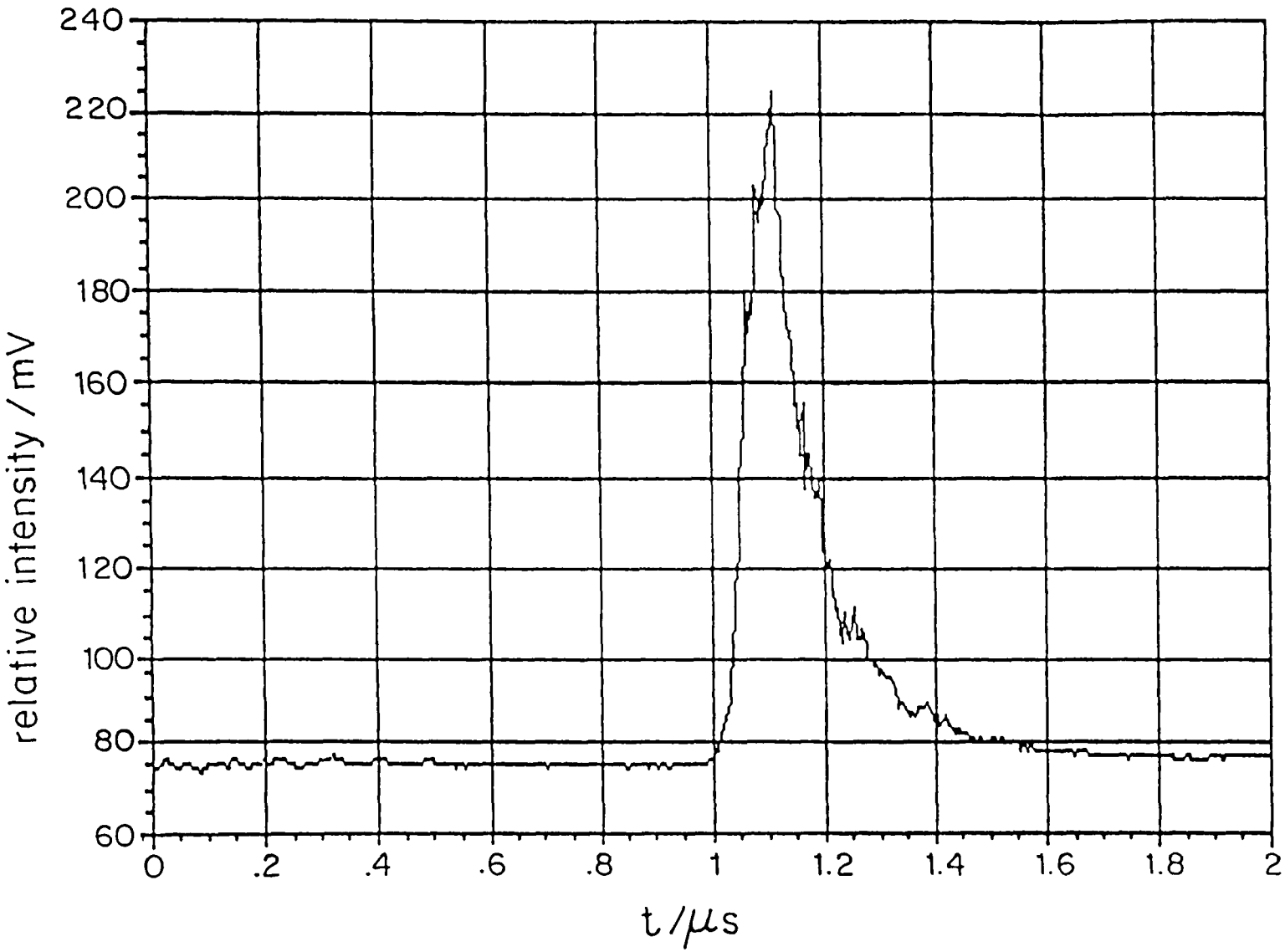

Figure 4. Time profile of CO_2 laser pulse.

an array of partially ordered dipoles, and thus there is a potential difference across it. When radiant energy is absorbed, the temperature of the disc rises, causing a decrease in the dipole ordering and thus of the observed potential difference. As heat subsequently flows from the disc into the heat sink, the original potential difference is restored.

The remaining fraction of the beam passed through an aperture, of 0.98 cm diameter and area 0.75 cm^2, to the reaction vessel. The beam reflected from the beam splitter passed through an identical aperture, carefully placed to select the same central portion of the beam, with both apertures equidistant from the beam splitter. This ensured that the energy reaching the pyroelectric detector was always the same fraction of that incident on the reaction cell.

After passing through the cell, the energy of the beam was measured with a disc calorimeter (Scientech Model 36-0001). This consists of a radiation-absorbing disc connected by a heat-conducting pipe to a heat sink. The temperature difference between disc and heat sink is measured by a thermopile. The integral of the thermopile voltage over time is proportional to the energy falling on the disc. To minimize the effect of stray sources of heat or radiation, such as thermal fluctuations produced by air currents for example, the disc calorimeter was surrounded by insulation. When it was necessary to reduce the intensity of radiation falling on the calorimeter to prevent damage, a flat Ge disc (reflecting ~ 36% at 10.5 μm [56]) was inserted as an attenuator between the cell and the disc calorimeter. The signal from the pyroelectric detector was displayed on an oscilloscope (Tektronix type 545) while the calorimeter outputs were measured with a power and energy meter (Scientech Model 36-2002). On the energy mode, the meter was capable of

measuring the total energy of a single pulse and all measurements were made in this way.

The optical system was carefully aligned by means of a 25 mW He-Ne laser (Optikon, Aerotech, Inc. Model LSR2P) placed behind the cell. The peak maximum signal from the pyroelectric detector measured by the oscilloscope was calibrated relative to the energy measured with the disc calorimeter after passing through the cell. The measurements showed the variation in the pulse-to-pulse average energy delivered by the laser to be 5-10%. Such calibrations were performed regularly throughout the course of the experiments. Results of these calibrations are described in the experimental section of the absorption measurements.

Before each experiment, the uniformity of the beam passing through the cell was checked by examining the pattern burned on exposed polaroid film, and the front optic of the laser was adjusted if necessary to give as uniform a pattern as possible.

With the unfocussed beam, the maximum fluence was approximately 1 J cm^{-2}. Attenuation of the fluence to values down to 0.1 J cm^{-2} was achieved by placing a 10 cm cell fitted with NaCl windows, filled with the appropriate pressure of ethylene, in the laser beam in front of the beam splitter. Values of fluence reported throughout this study were average values for the entire beam, calculated from the equation,

$$\text{Fluence} = \frac{\text{Total energy per pulse}}{\text{Cross-sectional area of beam}} \qquad (8)$$

With the optical arrangement described above, pulse energies incident on the cell were monitored with the pyroelectric detector during irradiation experiments with high pressures of ethylene (500-3000 Torr), in which the absorption in the 0.52 cm vessel was virtually complete.

2. Vacuum apparatus

The reaction vessel was connected to a Pyrex glass vacuum system illustrated in Figure 5. The cell and vacuum line were evacuated to less than 10^{-4} Torr before an experiment using an oil diffusion pump (Consolidated Vacuum Corporation, Rochester, N.Y., type 9F-21), backed by a rotary oil pump (Welch Duo Seal Model 1400). Low pressures were measured with an LKB Autovac gauge type 3294 B. Apiezon N grease was applied on the glass stopcocks on the vacuum manifold. Metal Hoke valves were used to connect the reaction vessel to the vacuum line and to the analysis system. Pressure in the manifold was measured using a Wallace and Tiernan Bourdon pressure gauge (Model series 1000) with a range 0-800 Torr. The error associated with pressure readings in this range was approximately ± 0.2 Torr. Pressures greater than 760 Torr in the vessel were achieved by condensing a known quantity of ethylene from the manifold into the U-trap connected to the vessel. Pressures below 1 Torr were calculated by gas expansion from calibrated volumes.

3. Reaction vessels

All irradiation experiments as well as some of the absorption measurements were performed in a cylindrical cell consisting of a central brass annulus having the following dimensions: an outer diameter of 5.1 ± 0.05 cm, an inner diameter of 1.97 ± 0.005 cm measured with a vernier caliper, and a width of 0.50 ± 0.003 cm measured with a C-shaped micrometer. Polished NaCl windows (5 cm diameter, 0.6 cm thick) were sealed on each side of the brass

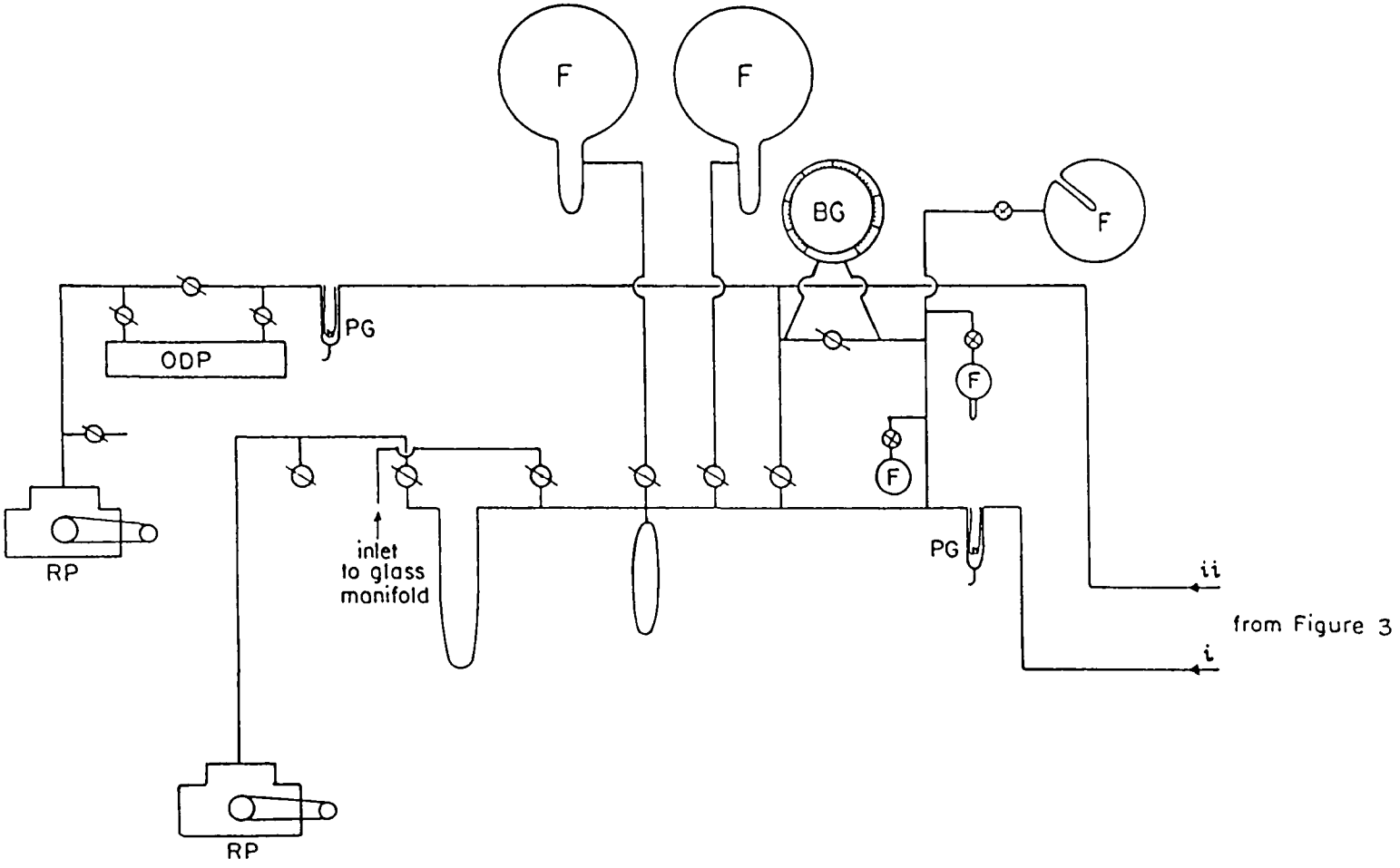

Figure 5. Schematic diagram of the vacuum apparatus.
RP: Rotary pump; ODP: Oil diffusion pump;
PG: Pirani gauge; BG: Bourdon gauge;
F: Flask; ⊘ : glass stopcock;
⊗ : Metal Hoke valve.

annulus with layers (approximately 0.01 cm thick) of Apizon W black wax. Taking the thickness of the wax into consideration, the actual cell width between the windows becomes 0.52 ± 0.003 cm. The cell volume was 1.58 ± 0.02 cm^3. This cell, referred to as cell A, is shown in Figure 6A. Two copper tubes of 0.1 cm bore led from opposite sides of the central annulus and as illustrated in Figure 3, appropriate valves permitted evacuation or filling from the vacuum line. The reaction vessel (cell A) also formed part of the sample loop for the gas chromatograph (Figure 3) so that the entire contents of the vessel could be injected and analyzed after each experiment.

Absorption measurements with high pressures of pure ethylene were performed in a cell with a pathlength of 0.051 ± 0.0003 cm, referred to as cell B and shown in Figure 6B. One polished NaCl window was sealed to the outside of a central brass annulus while the second window was inset to meet the 0.051 cm spacer at the front window. The width of the cell was determined with a Bausch and Lomb binocular microscope (Rochester, N.Y.) of magnifying power 250X, which could focus on the surfaces of the NaCl windows.

Throughout the course of the experiments, the NaCl beam splitter and windows were kept warm to prevent absorption of moisture. A jet of Freon gas was used to clean dust from the surfaces. Cell windows sometimes required polishing to remove films and carbon deposits created during irradiations. If hot spots developed at the surfaces, causing damage, the windows were promptly replaced.

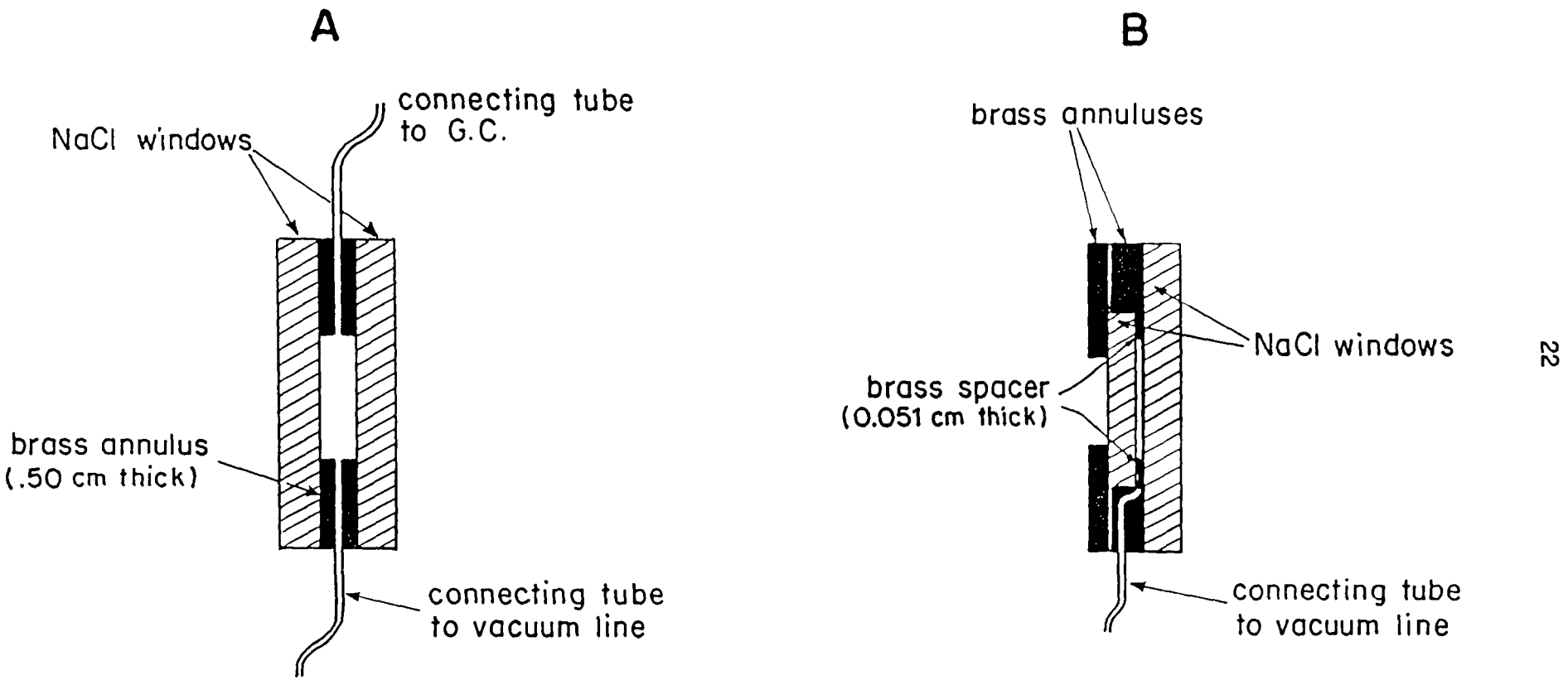

Figure 6. Schematic diagram of the IR cells.
A: Cell A; B: Cell B.

4. Materials

Research-grade ethylene with a stated minimum purity of 99.98% was obtained from Matheson Canada, Limited, Whitby, Ont. Analysis revealed trace impurities (1.3×10^{-3}%) of both ethane and acetylene. Because both of these hydrocarbons are products of the irradiation experiments, corrections were made to the yields when required. Ethane was Phillips 66 research-grade with a stated minimum purity of 99.97% obtained from the Phillips Petroleum Company, special products division, Bartlesville, Okla. Hydrocarbon gases used for calibrations were Matheson research grade or chemically pure grade with stated minimum purities of 99.9% and 99.0% respectively. An exception was cyclobutane (Columbia Organic Chemicals, Columbia, S.C.) which contained 6% of n-butane and 0.5% of both 1-butene and the 2-butene isomers. All hydrocarbons were subjected to multiple de-gassing at liquid nitrogen temperature prior to use to remove possible traces of air.

ABSORPTION MEASUREMENTS

1. Introduction

The absorption of IR radiation from high-powered pulsed CO_2 lasers has been measured for a variety of molecular gases under a wide range of conditions [17-23,26-32,57-70]. These investigations have shown that at high intensity, multiple-photon absorption can occur, and departures from the Beer-Lambert law may be observed. Three parameters commonly used as measures of absorption are: σ, the molecular cross-section; <N>, the average number of photons absorbed per molecule; and ϵ, the molar (decadic) absorption coefficient. Note that in the low intensity limit, σ and ϵ are expected to be independent of intensity, while <N> should have a linear dependence. It should also be noted that in the usual measurements with pulsed radiation including those in the present work, these parameters are of necessity average values, averaged over the time duration of the pulse, and over the spatial extent of the laser beam, both across the beam profile and along the absorption path.

Many absorption measurements have been made at pressures below 1 Torr [17-23,26-32]. In this low pressure region, the absorption process can be considered almost "collision-free" since the average time between gas kinetic collisions for polyatomic molecules is about 50-100 ns at a pressure of 1 Torr, a time comparable to the pulse width of a typical CO_2 TEA laser. The main process occurring is multiple-photon absorption by individual isolated molecules. Absorption coefficients decrease with increasing fluence as the populations of molecules in rotational levels resonant with the laser frequency are depleted (sometimes termed rotational "hole burning"). Absorption from higher

vibrational levels also tends to decrease because of anharmonic shifts and lack of rotational lines coincident with the laser frequency. At sufficiently high vibrational levels the increasing density of states begins to overcome these effects, which are more severe for smaller molecules than large ones, but at intermediate levels, a "bottleneck" in the multiphoton pumping process can occur. In the absence of collisions, intramolecular vibrational reorganization is the only relaxation mechanism available to alternate these effects but as the pressure is raised towards 1 Torr and above, a variety of collisional processes combine to increase the absorption coefficient and lessen its dependence on fluence. These include rotational and vibrational relaxations, collision-induced internal vibrational relaxation, and pressure-broadening of absorption lines.

While some absorption studies have been made at intermediate pressures (1-10 Torr) [57-70] where about 2 to 25 collisions would occur during a typical 200 ns laser pulse, fewer measurements have been made at the higher pressures used in the present investigation (25-3000 Torr). At these pressures, rotational and translational relaxation is very fast and would be complete in times much shorter than the laser pulse. Vibrational relaxation is somewhat slower. Nevertheless, at 500 Torr or higher, relaxation will be largely complete during our laser pulse. To a good approximation at these higher pressures, the energy distribution in the gas during the pulse will be close to thermal equilibrium, and the absorbed radiation can be regarded as simple heating of the gas. (See Appendix B, p. 217). Even under these conditions, however, there can be substantial deviations from the Beer-Lambert law.

Studies on absorption by NH_3 were made jointly by groups at Brandeis and Heriot-Watt Universities. Measurements of the absorption by the ν_2 mode of NH_3 with the 9 R(16) CO_2 laser line at 1076.0 cm^{-1}, were made at pressures

between 5-244 Torr and fluences from 0.04 to 1.2 J cm^{-2} [60-61]. Steel and his group [62] later made absorption measurements on several polyatomic molecules including silicon tetrafluoride, cyclobutanone and hexafluorobenzene over a range of pressures (0.4-50 Torr) and fluences (0.03-0.8 J cm^{-2}). These investigations indicated significant deviations from the Beer-Lambert law. The average number of photons absorbed per molecule in a volume element with pressure P and fluence F, was represented by the following empirical equation:

$$<N>(P,F) = [(A_1F + A_2F^2)/(1 + B_1F)](1/h\nu)(RT/P) \quad (9)$$

where ν is the laser frequency and A_1, A_2 and B_1 are empirical parameters which may be functions of pressure.

A study with a pulsed CO_2 laser has been reported by Blazejowski and Lampe [66] who measured absorption in the ν_2 and ν_4 vibrational modes of phosphine, PH_3. At a fixed laser frequency and constant incident fluence, the pressure dependence of the optical density from 10 to 150 Torr was found to deviate from the Beer-Lambert law. The data was fitted by the following empirical expression:

$$\ln [E_0/(E_0 \quad E_{abs})] = [A(P/P_0)^n + B](LP) \quad (10)$$

where E_0 and E_{abs} represent the incident energy and the energy absorbed in the gas, L = length of cell, while P is the pressure of phosphine and P_0 = 760 Torr. The quantity $A(P/P_0)^n + B$ corresponds to an absorption coefficient corrected for pressure dependence, with A and B empirical constants, and n can take values between 0 and 1. An additional term $C(P_f/P_0)^m$ was also added to this absorption coefficient to account for increased absorption in the presence of a non-absorbing foreign gas at a pressure P_f. In this term, C is an empirical constant and m, as in the case of n, can also vary between 0 and 1. In a more recent study, these same authors examined the

absorption of pulsed CO_2 laser radiation by SiH_4 [67]. Deviation from the Beer-Lambert law in this system was also described in terms of an empirical expression similar to that of equation (10).

The approach of these investigations was to search for an equation with adjustable parameters to describe the absorption behavior. No such curve fitting has been attempted in the present experiments. We have been concerned rather with an accurate estimate of energy absorbed at the pressures used in our experiments to permit calculations of temperature profiles along the reaction vessel, and to draw some conclusions about the influence of pressure and fluence on the absorption process.

Measurements have been made over a range of pressure (25 to 3000 Torr) and fluence (0.1 to 0.7 J cm^{-2}), for two CO_2 laser lines, the 10 P(12) (951.19 cm^{-1}) and the 10 P(14) (949.48 cm^{-1}), both lying near the center of the strong ν_7 absorption band in the ethylene spectrum. Some experiments were also made with ethane, a non-absorbing diluent, added to examine the effects of pressure on the absorption.

2. Experimental

Measurements of the absorption by ethylene of the 10 P(12) and 10 P(14) lines of the CO_2 laser

A. Calibration of the energy of the beam before and after passage through the vessel

The optical system was first aligned using the He-Ne laser as described in the general experimental section. The relation between the energy recorded by the pyroelectric detector (V, volt) and by the calorimeter (E, joule), was determined with cell A (l = 0.52 cm), evacuated, in the optical system. The results are shown in Figure 7. From the slope a calibration factor of 0.69 ± 0.07 volt joule^{-1} was obtained. The 10% uncertainty in the calibration factor arises from 5% uncertainties in both the peak voltage and the energy per pulse values. Thus from the measurement of the peak voltage per pulse, V, from the pyroelectric detector, the energy just behind the rear window of the cell, E, was obtained. To obtain the energy incident on the gas, E_0, a correction for the losses in energy by the rear NaCl window was made. In polished NaCl windows at a wavelength of 10.5 μm, these losses are 3.9% [55]. The corrected calibration factor relating the voltage measured on the pyroelectric detector to the energy incident on the gas, V/E_0, is therefore 0.66 ± 0.07 volt joule^{-1}. Regular calibrations of the optical system throughout the duration of this study showed that the beam splitter and cell windows consistently reflected ~ 4% of the incident radiant energy at 10.5 μm.

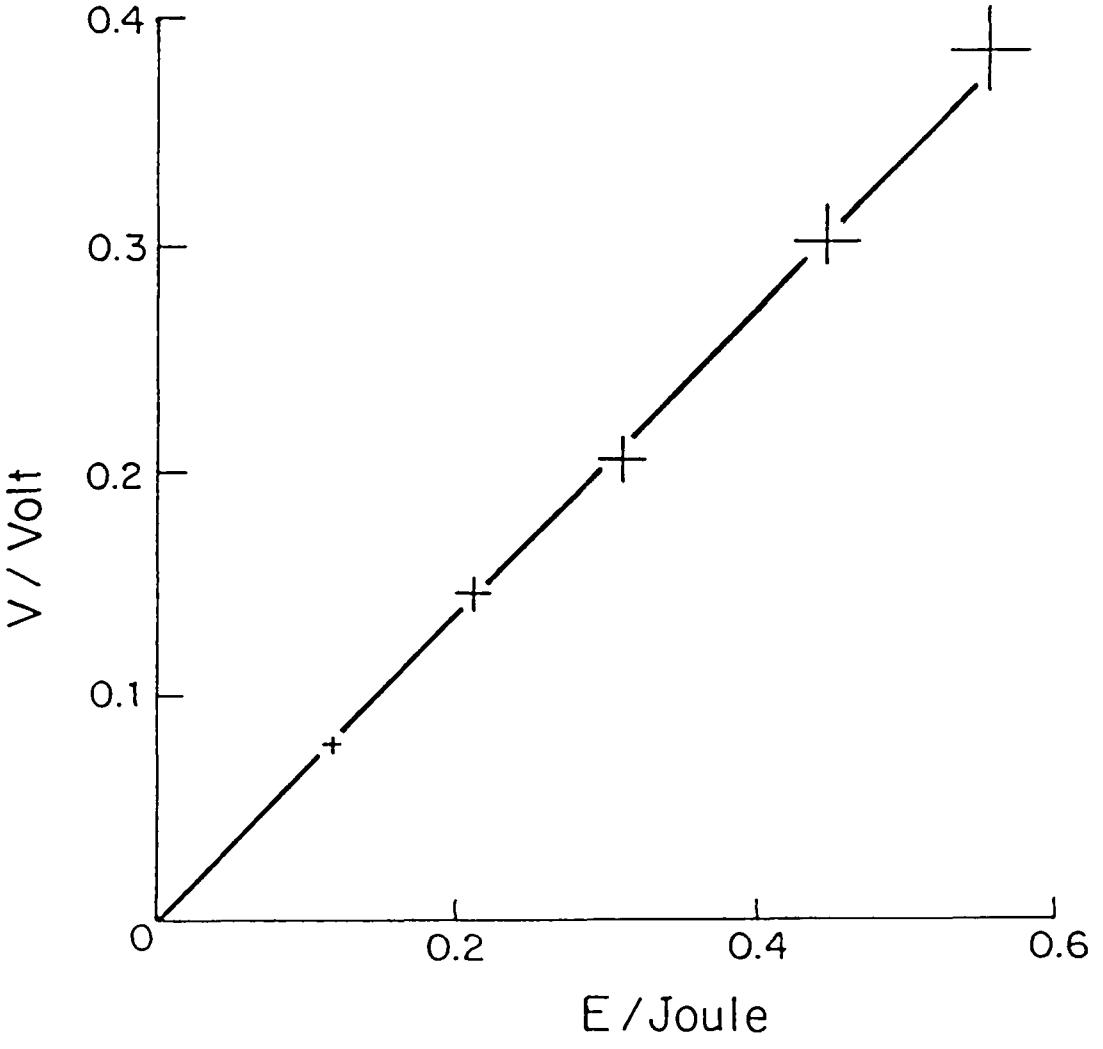

Figure 7. Calibration relating the peak voltage of the pyroelectric detector in the split beam to the energy transmitted by the empty cell.

The optical system was again calibrated for absorption using cell B (l = 0.051 cm). Because of a slightly different position of this cell, and a realignment of the optical system, a calibration factor of 0.80 ± 0.08 volt joule^{-1} was obtained, with both windows in the beam, and a calibration factor for the energy incident on the gas was therefore 0.77 ± 0.08 volt joule^{-1}.

B. Procedure for absorption measurements

Single pulse measurements were made of the peak voltages, V, and of the pulse energies, E, when the cell was evacuated to check the calibration. The cell was then filled with a known pressure of ethylene and between 6-12 single pulse measurements of V and E_T, the energy transmitted by the ethylene, were made at each pressure. Using the calibration factor obtained previously and checked before the absorption measurements, a value for $(E_0)_E$, the energy incident on ethylene was obtained from the values of V to correspond to each measurement of E_T. From these measurements, an average value for $E_T/(E_0)_E$, the fraction of light transmitted by the ethylene, was calculated for each pressure.

The absorption measurements were made in the cylindrical cells of pathlengths 0.52 cm (cell A) and 0.051 cm (cell B) described in the general experimental section. Cell B, used exclusively for the absorption measurements, was connected to the vacuum line by one brass tube of 0.1 cm bore. The internal diameters of the cells were slightly more than twice the diameter of the beam, so that wall reflections were avoided. By use of these two cells, absorption measurements with pure ethylene were performed over the

pressure range of 25 to 3000 Torr. In the 0.52 cm cell, almost total absorption by ethylene occurred at pressures above 500 Torr. Measurements in this cell were extended to higher total pressures by the addition of the non-absorbing gas ethane. Measurements were made with mixtures of ethane and ethylene in the ratios 5, 10 and 21 with total pressures up to about 3000 Torr.

To investigate the effect of pressure-broadening on the individual rotational features of ethylene in the region of the 10 P(12) and 10 P(14) lines, low intensity, high resolution spectra of pure ethylene at pressures of 1, 5 and 25 Torr, and of 5 Torr of ethylene diluted to 380 and 760 Torr with ethane were measured using a 10 cm cell fitted with NaCl windows in a BOMEM FTIR spectrometer, DA3.02 series, with a resolution of 0.05 cm^{-1}.

3. Results

Values of the absorbance, A, (defined as $\log_{10}(E_0/E_T)$ where E_0 and E_T are the incident and transmitted pulse energies) measured in cell A (0.52 cm long) are shown in Figure 8 as a function of ethylene concentration for several incident fluences for the 10 P(12) and 10 P(14) laser lines. Similar results using cell B (0.051 cm long) are shown in Figure 9. Fluences ranged between 0.18 and 0.65 J cm^{-2} for the 10 P(12) line and between 0.10 and 0.69 J cm^{-2} for the 10 P(14) line. All these plots show upward curvature indicating that the absorption does not follow the Beer-Lambert law. It is nevertheless useful to define an effective molar absorption coefficient, ϵ_{eff}, in terms of the Beer-Lambert equation,

$$\epsilon_{eff} = A/cl \qquad (11)$$

and to evaluate ϵ_{eff} for each data point in Figures 8 and 9 (note that ϵ_{eff} is determined simply from the slope of the straight line joining the point to the origin, not from dA/dc, the slope of the curve). These results are shown in Figures 10 and 11, from which it is seen that ϵ_{eff} increases with increasing pressure of ethylene, and varies inversely with fluence. Similar results have been reported by Gowenlock, John and coworkers [60] in a study of absorption by ammonia with a CO_2 laser, although they found that ϵ reached a maximum at 125 Torr of NH_3, and then declined at higher pressures. Blazejowski and Lampe [66,67] also found a pressure dependence of the absorption coefficient for phosphine between 10 and 150 Torr and for silane between 5 and 100 Torr.

To explore further the effect of pressure on ϵ, absorption measurements were made in cell A with ethane (which is transparent around 950 cm^{-1}) added to the ethylene. Figure 12 shows plots of A as a function of ethylene

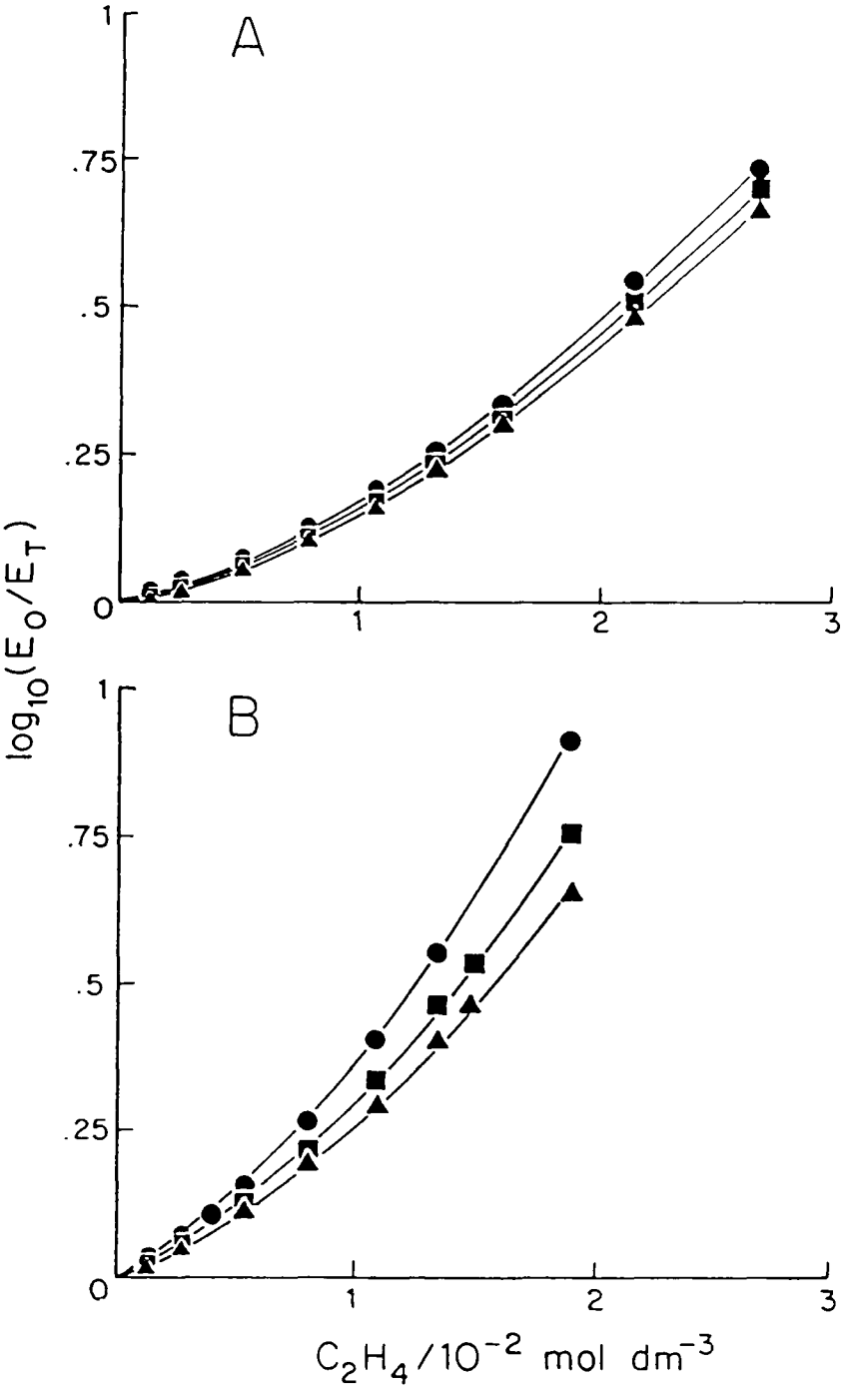

Figure 8. Absorbance of CO_2 laser radiation as a function of ethylene concentration in cell A, l=0.52 cm.

A. 10 P(12) line
F_0: ● : 0.18 J cm^{-2}, ■ : 0.30 J cm^{-2}, ▲ : 0.65 J cm^{-2}

B. 10 P(14) line
F_0: ● : 0.10 J cm^{-2}, ■ : 0.36 J cm^{-2}, ▲ : 0.69 J cm^{-2}

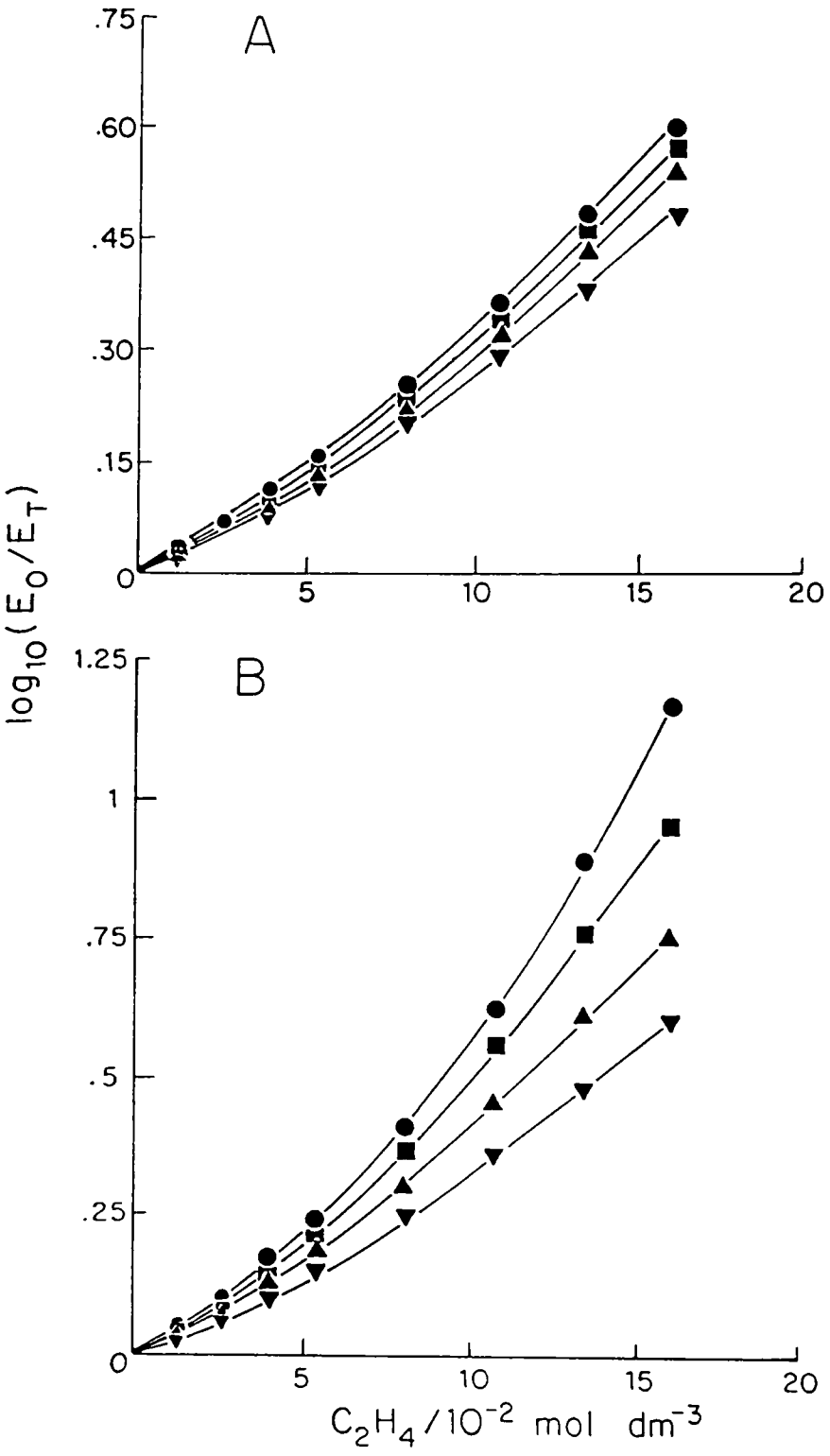

Figure 9. Absorbance of CO_2 laser radiation as a function of ethylene concentration in cell B, l=0 051 cm

A 10 P(12) line
F_0 ● : 0.20 J cm^{-2} ■ : 0 29 J cm^{-2}, ▲ 0 37 J cm^{-2},
▼ : 0.52 J cm^{-2}

B 10 P(14) line
F_0 ● : 0.18 J cm^{-2} ■ : 0 25 J cm^{-2}, ▲ 0 38 J cm^{-2},
▼ : 0.53 J cm^{-2}

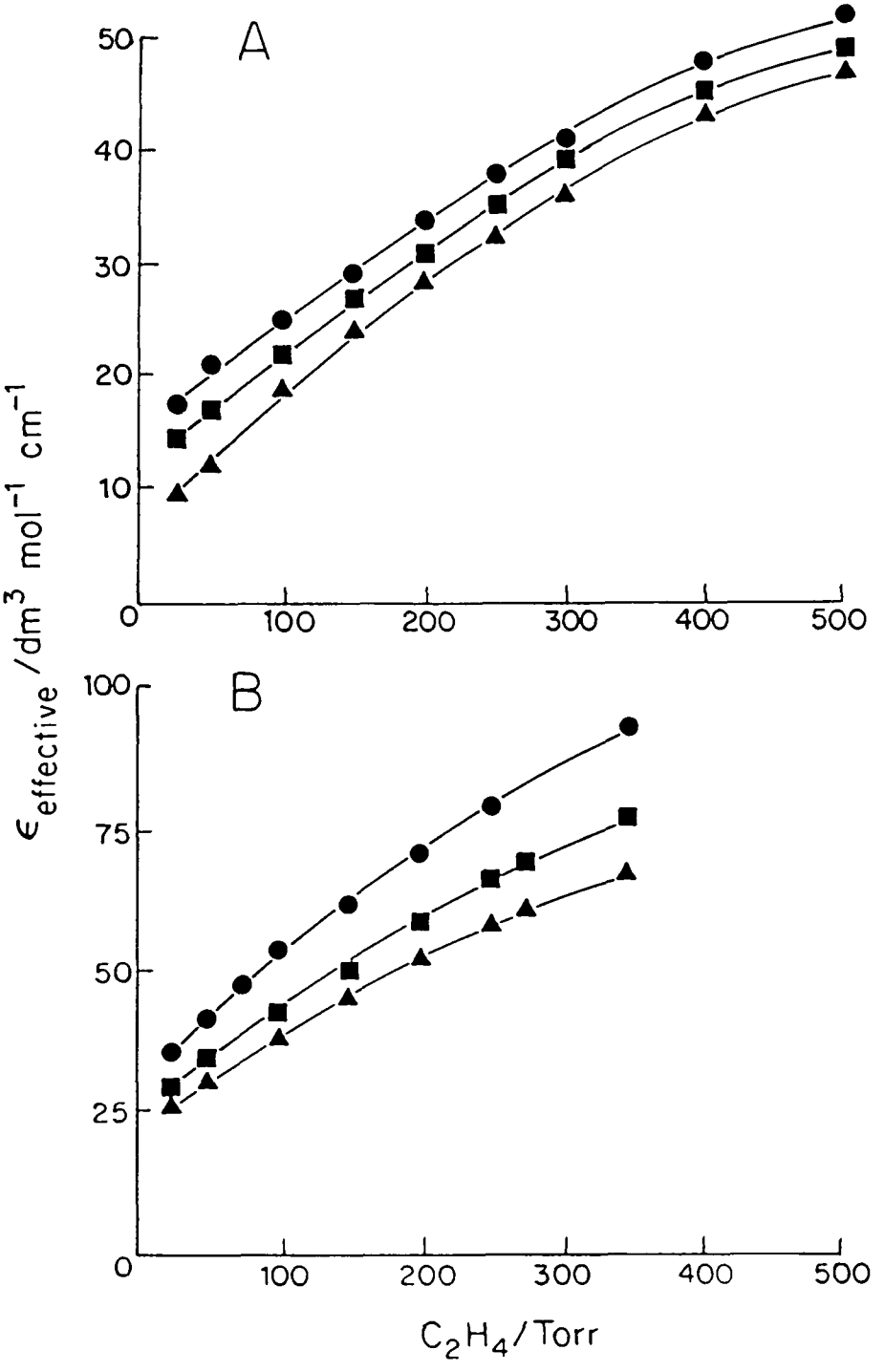

Figure 10. Effective molar absorption coefficient as a function of ethylene pressure in cell A, l = 0.52 cm.

A. 10 P(12) line
F_0: ● : 0.18 J cm^{-2}, ■ : 0.30 J cm^{-2}, ▲ : 0.65 J cm^{-2}

B. 10 P(14) line
F_0: ● : 0.10 J cm^{-2}, ■ : 0.36 J cm^{-2}, ▲ : 0.69 J cm^{-2}

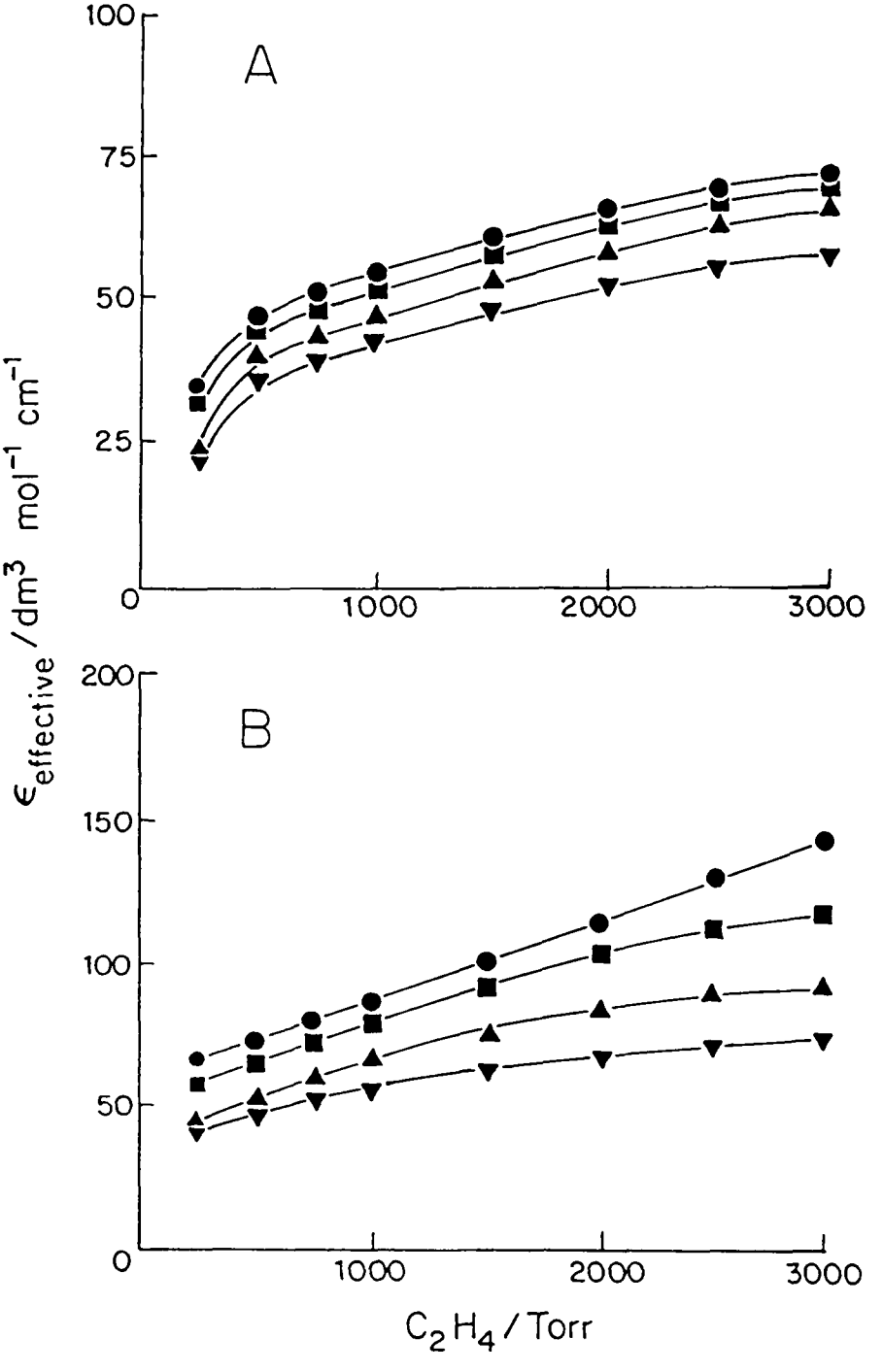

Figure 11. Effective molar absorption coefficient as a function of ethylene pressure in cell B, l = 0 051 cm

A 10 P(12) line
F_0 ● 0 20 J cm^{-2} ■ 0 29 J cm^{-2}, ▲ 0 37 J cm^{-2},
▼ 0 52 J cm^{-2}

B 10 P(14) line
F_0 ● 0 18 J cm^{-2} ■ · 0 25 J cm^{-2}, ▲ 0 38 J cm^{-2},
▼ 0 53 J cm^{-2}

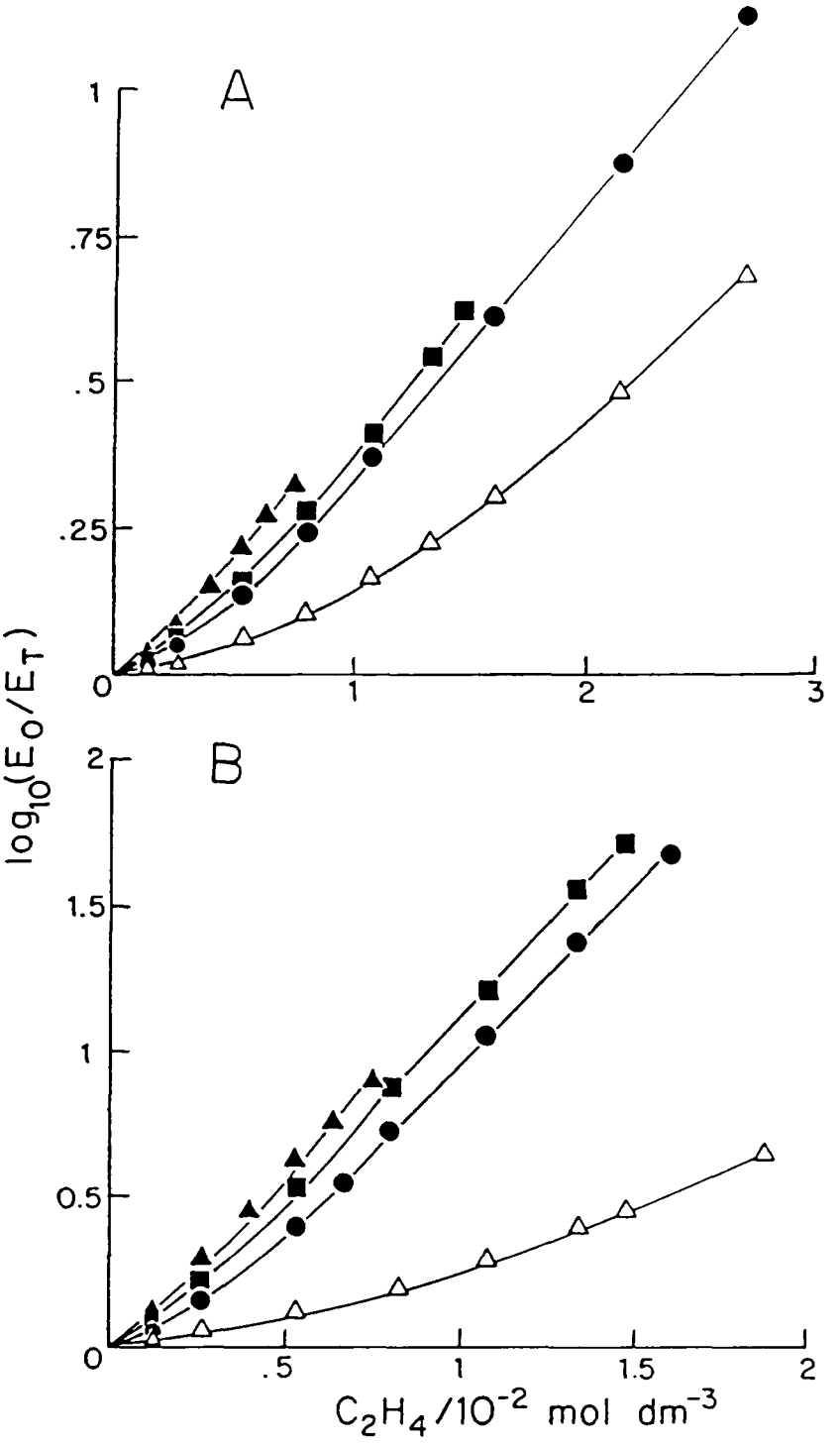

Figure 12. Absorbance of CO_2 laser radiation as a function of ethylene concentration in ethylene-ethane mixtures in cell A, l = 0.52 cm.

A. 10 P(12) line, incident fluence of 0.65 J cm^{-2}

△ : pure C_2H_4

C_2H_6/C_2H_4: ● : 5.2, ■ : 10.3, ▲ : 20.8.

B. 10 P(14) line, incident fluence of 0.69 J cm^{-2}

△ : pure C_2H_4

C_2H_6/C_2H_4: ● : 5.2, ■ : 10.3, ▲ : 20.8.

concentration for several ratios of C_2H_6/C_2H_4 ranging from 5 to 21. Values of ϵ_{eff} obtained from these data as before are shown as a function of pressure of ethylene in Figure 13. Comparison with Figure 10 shows that ethane has a significant effect on the value of ϵ_{eff}. Figure 14 shows ϵ_{eff} as a function of total pressure (C_2H_4 + C_2H_6), which confirms the pressure dependence of ϵ_{eff}. Values of ϵ_{eff} measured in pure ethylene and in mixtures of ethylene and ethane are compared in Figure 15. The data accompanying Figures 8-15 are given in Appendix A, as Tables A-1-A-8 inclusively. Although the overlap in the range of pressure is limited, the values of ϵ_{eff} obtained in the mixtures are significantly higher than those obtained in pure ethylene at the same pressure and fluence; this will be discussed later.

As noted earlier, since rotational and vibrational relaxation is largely complete at 100 Torr it seems unlikely that these effects could explain the observed pressure dependence of ϵ_{eff}. A more probable cause would appear to be pressure-broadening of the rotational lines of the ethylene absorption spectrum (known to be sharp at low pressure), leading to improved overlap with the CO_2 laser lines. To examine this possibility, absorption spectra were taken at moderately high-resolution (0.05 cm^{-1}) using a 10 cm long cell in the FTIR spectrometer. Figures 16A-E show spectra obtained at pressures of ethylene of 1, 5 and 25 Torr, and with 5 Torr of ethylene made up to 380 and 760 Torr by the addition of non-absorbing ethane. The positions of the 10 P(12) and 10 P(14) CO_2 laser lines are also indicated.

Even at the lowest pressure (1 Torr), individual rotational lines are not fully resolved. An average value of 2.121 x 10^{-4} cm^{-1} $Torr^{-1}$ has been reported [71] for the self-broadened line width of C_2H_4 at 300 K, well below the 0.05 cm^{-1} resolution of the instrument. At 5 and 25 Torr some effects of

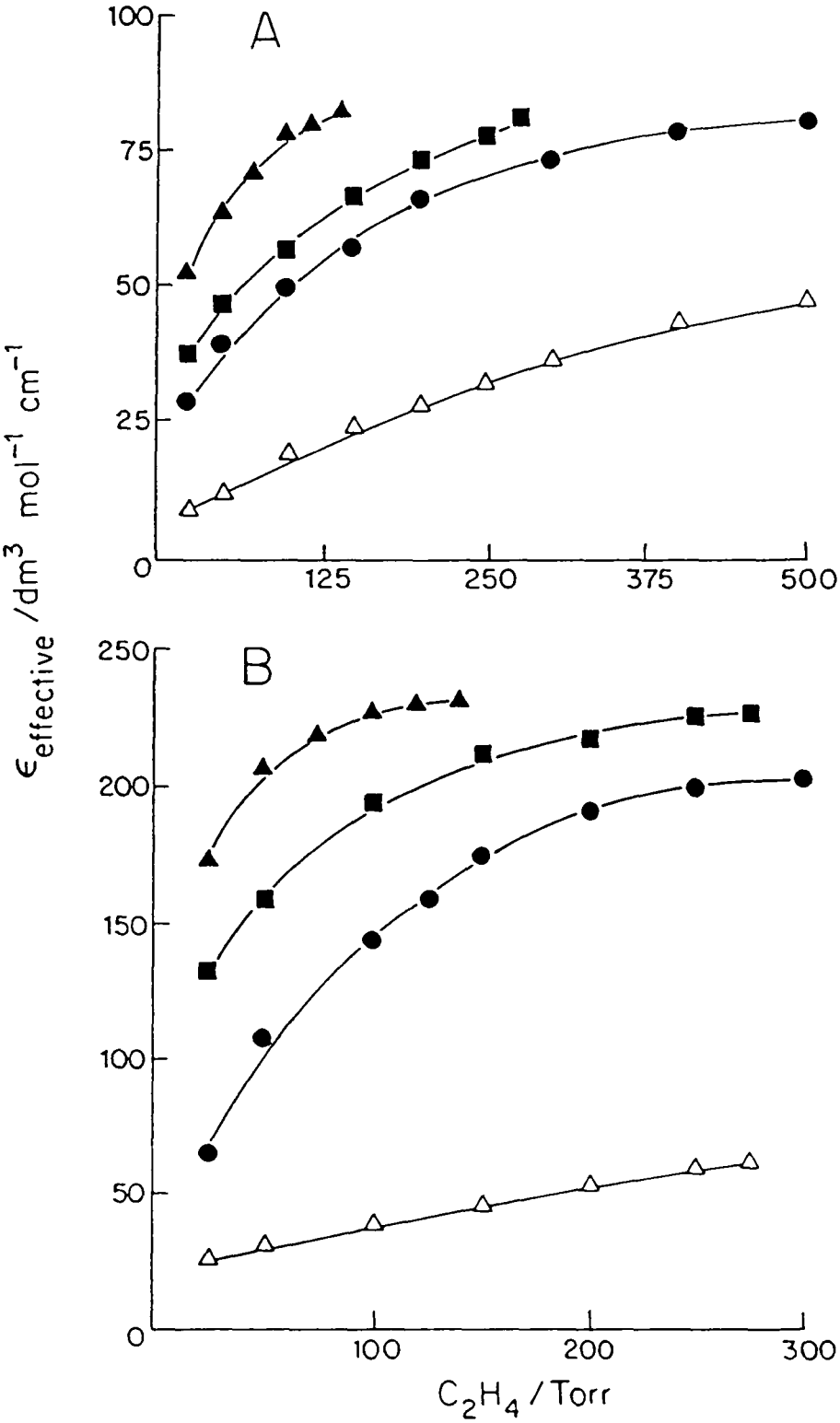

Figure 13. Effective molar absorption coefficient as a function of ethylene pressure in ethylene-ethane mixtures in cell A, l = 0.52 cm.

A. 10 P(12) line, incident fluence of 0.65 J cm^{-2}

△ : pure C_2H_4

C_2H_6/C_2H_4: ● : 5.2, ■ : 10.3, ▲ : 20.8.

B. 10 P(14) line, incident fluence of 0.69 J cm^{-2}

△ : pure C_2H_4

C_2H_6/C_2H_4: ● : 5.2, ■ : 10.3, ▲ : 20.8.

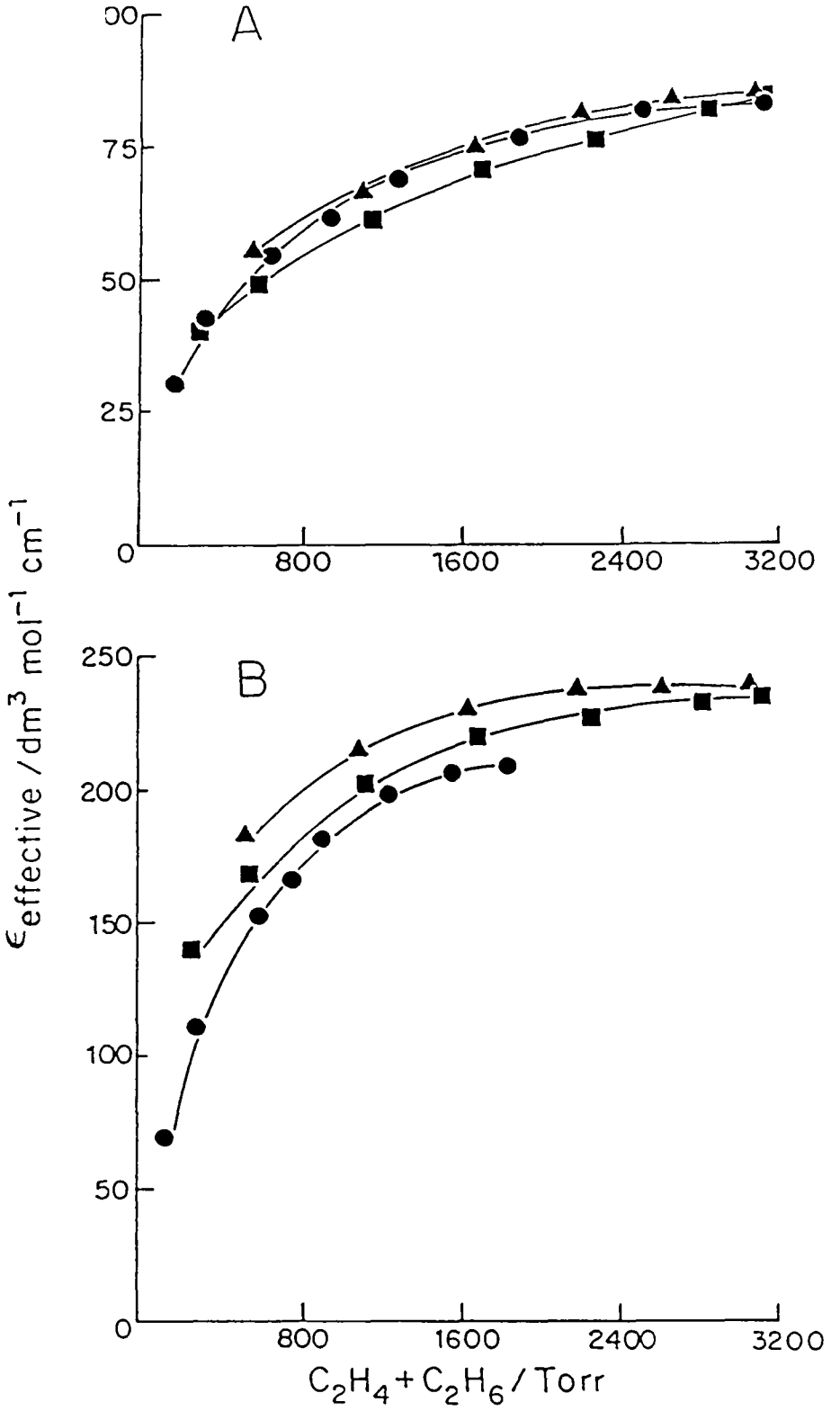

Figure 14. Effective molar absorption coefficient as a function of total pressure of ethylene and ethane in cell A, l = 0.52 cm.

A. 10 P(12) line, incident fluence of 0.65 J cm^{-2}

C_2H_6/C_2H_4: ● : 5.2, ■ : 10.3, ▲ : 20.8.

B. 10 P(14) line, incident fluence of 0.69 J cm^{-2}

C_2H_6/C_2H_4: ● : 5.2, ■ : 10.3, ▲ : 20.8.

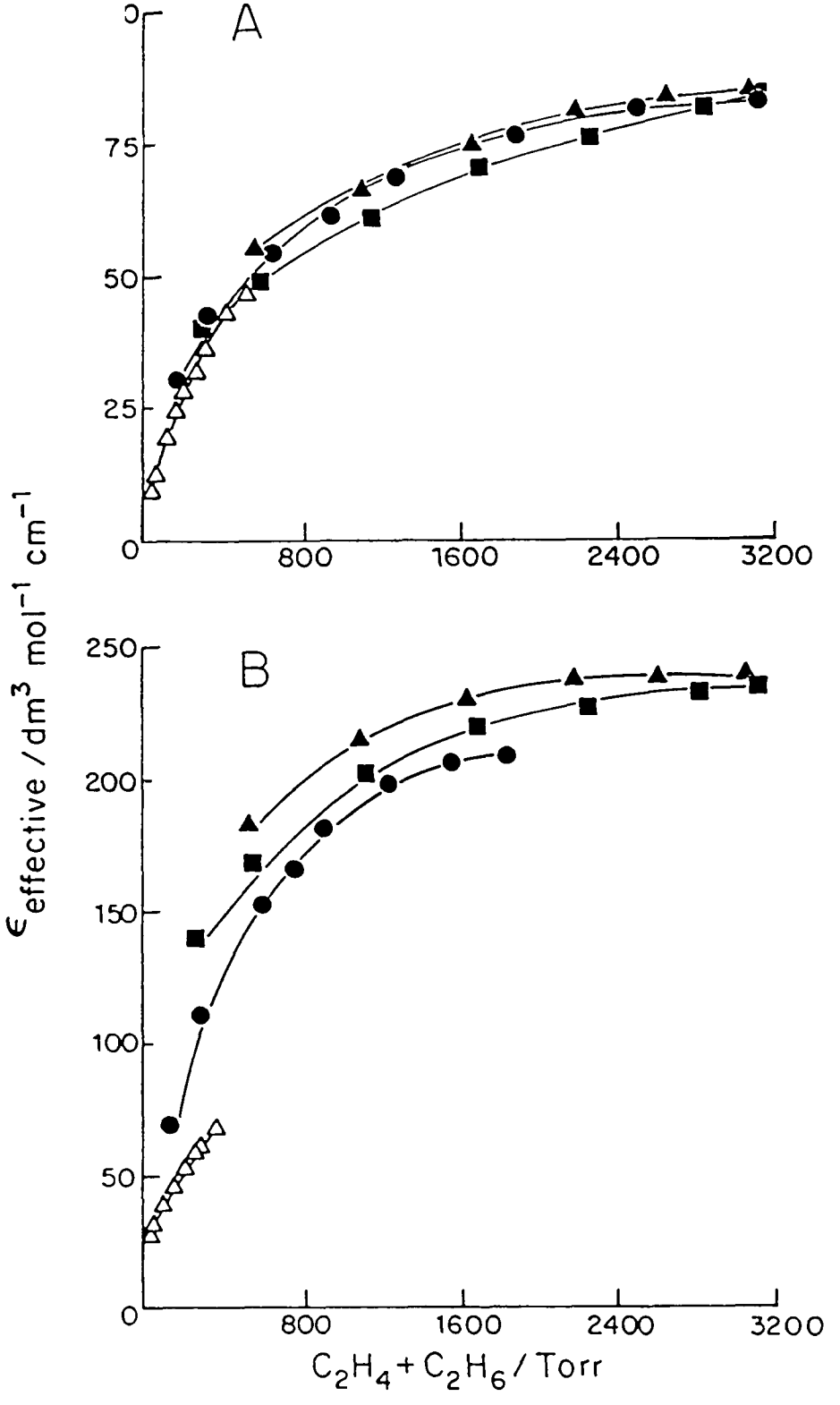

Figure 15. Effective molar absorption coefficient as a function of total pressure of ethylene and ethane in cell A, l = 0 52 cm

A 10 P(12) line, incident fluence of 0 65 J cm^{-2}

△ pure C_2H_4

C_2H_6/C_2H_4 ● 5 2, ■ 10 3, ▲ 20 8

B 10 P(14) line, incident fluence of 0 69 J cm^{-2}

△ pure C_2H_4

C_2H_6/C_2H_4 ● 5 2, ■ 10 3, ▲ 20 8

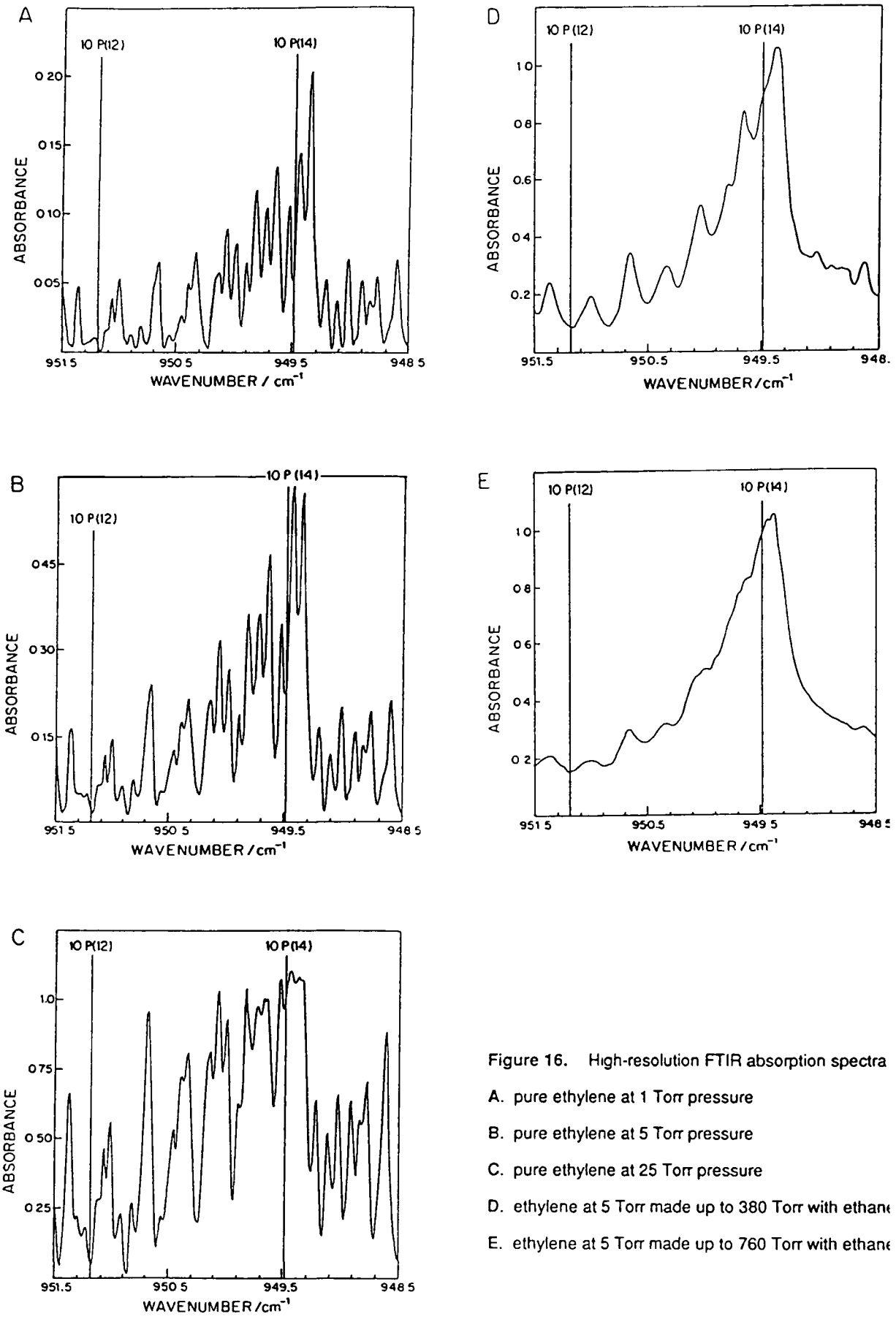

Figure 16. High-resolution FTIR absorption spectra

A. pure ethylene at 1 Torr pressure

B. pure ethylene at 5 Torr pressure

C. pure ethylene at 25 Torr pressure

D. ethylene at 5 Torr made up to 380 Torr with ethane

E. ethylene at 5 Torr made up to 760 Torr with ethane

broadening can be seen while at 380 and 760 Torr, pressure-broadening largely obscures the sharp bands observed at lower pressure. It is seen that at the lowest pressure of ethylene (1 Torr), in the spectrum in Figure 16A, the 10 P(14) line lies well down on the steep side of a sharp absorption feature, and any broadening of this feature would lead to a greater overlap with the emission line and enhanced absorption.

To explore and illustrate this effect in more detail, we have plotted in Figures 17A-B the positions and relative intensities of rotational lines in the ν_7 absorption band of ethylene close to the 10 P(12) and 10 P(14) lines of the CO_2 laser, taken from the very high-resolution data of Herlemont, Lambeau and coworkers [72-74]. Pressure-broadened Lorentzian profiles are shown for the ethylene absorption lines, calculated from the pressure dependent linewidth of 2.121×10^{-4} cm^{-1} $Torr^{-1}$ reported for ethylene by Tejwani and Yeung [71]. Also shown is a rather arbitrary profile for the CO_2 laser lines, based on reported gain profiles and making some allowance for narrowing by the grating in the laser cavity. The width at the base of 3.33×10^{-2} cm^{-1}, corresponds to 1 GHz.

While there is much uncertainty in the data used in Figures 17A-B, they serve to show in a qualitative way how the overlap between the absorption lines and the laser emission lines may be expected to increase with increasing pressure, (refer to caption of Figure 17).

From the FTIR spectrum of pure ethylene at 25 Torr (Figure 16C) values of ϵ were estimated for both the 10 P(12) and 10 P(14) lines, using the standard baseline correction procedure supplied with the spectrometer software. In Table 2, these are compared with values of ϵ_{eff} measured with the CO_2 laser at the same pressure of ethylene. For the 10 P(12) line it is

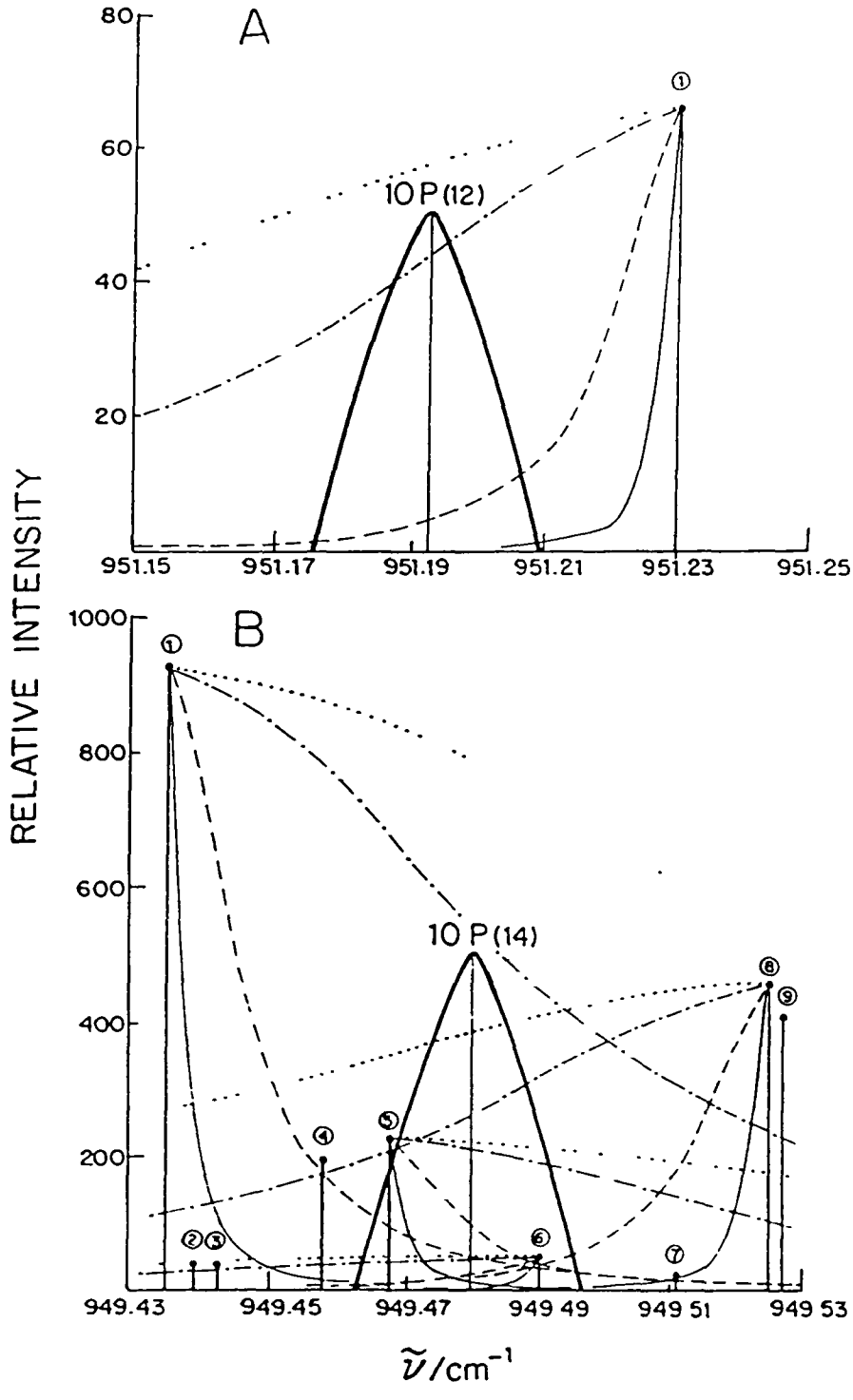

Figure 17. Effect of pressure-broadening leading to improved overlap between absorption lines of ethylene [73] and emission lines from the CO_2 laser [74].

A 10 P(12) line, $\tilde{\nu}_l$ = 951.1923 cm^{-1}

B 10 P(14) line, $\tilde{\nu}_l$ = 949 4793 cm^{-1}

C_2H_4 pressure

—· 25 Torr
—·— 100 Torr
- - : 500 Torr
····. 1000 Torr

For clarity, absorption line profiles have been normalized to the same maximum intensities at all pressures For true comparison of different pressures, intensities must be scaled downwards by factors proportional to the line widths, i.e., by factors of 1, 4, 20 and 40 at pressures of 25, 100, 500 and 1000 Torr respectively Also to avoid confusion, profiles have been drawn for only 4 of the 9 absorption lines close to e 10 P(14) line.

interesting that values of ϵ measured at low intensity in a spectrometer and measured at high intensity with a pulsed CO_2 laser are similar. On the other hand, for the 10 P(14) line the values are significantly different. It will be argued later that this difference can be attributed to temperature effects. Grunwald, Dever and Keehn [35] have discussed the relation of ϵ_{eff} to the molar absorption coefficient measured spectrophotometrically, and have noted that they are not necessarily related, and depend on the overlap of the laser line and the absorption band as well as other properties of the absorbing molecule.

Table 2. Molar absorption coefficients measured in a low-intensity FTIR spectrometer and in a high-intensity CO_2 laser at 25 Torr.

laser line	frequency/cm^{-1}	ϵ/$dm^3mol^{-1}cm^{-1}$ FTIR	CO_2 laser
10 P(12)	951.19	12	14
10 P(14)	949.48	72	31

4. Discussion

To summarize, the absorption measurements in pure ethylene with the CO_2 laser showed significant deviations from the Beer-Lambert law. The increase in ϵ_{eff} with increasing pressure can be accounted for by pressure-broadening of the rotational lines in the absorption spectrum leading to increased overlap with the laser emission lines. This conclusion is supported by experiments with ethylene-ethane mixtures and by low-intensity measurements in the infrared spectrometer.

While the pressure dependence of ϵ_{eff} was the dominant factor in the laser absorption measurements, several observations indicate additional deviations from a simple absorption law:

(1) At constant pressure, ϵ_{eff} in pure ethylene showed an inverse dependence on fluence, and was larger in the long cell (Figure 10) than in the short one (Figure 11).

(2) These effects were more pronounced with the more strongly absorbed 10 P(14) line than with the 10 P(12) line.

(3) At the same total pressure and otherwise similar conditions, values of ϵ_{eff} were substantially higher in ethylene-ethane mixtures than in pure ethylene (Figure 15).

All these observations could be explained if ϵ_{eff} were to decrease with increasing temperature. As noted earlier, the ethylene is heated by the laser pulse, and the extent of this heating will depend in an obvious way on the fluence, the difference in absorption of the 10 P(12) and 10 P(14) lines, and the addition of ethane diluent. The dependence on the length of the

absorption cell is not quite so obvious; it arises from the greater attenuation of the laser fluence in traversing the longer cell, so that for a given incident fluence and ethylene pressure, the average temperature rise in the longer cell will be less. To illustrate this effect, approximate temperature gradients were calculated for each cell, based on the absorption measurements at an ethylene pressure of 1000 Torr, for both the 10 P(12) and 10 P(14) lines at an incident fluence of 0.3 J cm^{-2}. The absorption coefficient was taken to be equal to ϵ_{eff} measured in the short cell, and as a first approximation, assumed to be constant throughout both cells. The temperature rise was calculated from values of C_v, the heat capacity of ethylene at constant volume. Details of the calculations are given in Appendix B, and the calculated profiles are shown in Figure 18. It is clear that the average temperature of the gas following the pulse is much lower in the long vessel, and is lower with the 10 P(12) line than with the 10 P(14) line. The most probable cause of a decrease in ϵ_{eff} with increasing temperature would appear to be the simple thermal population of excited vibrational states of ethylene and the consequent depopulation of the vibrational ground state. Since temperatures in the neighborhood of 1000 K may be attained during the pulse this effect could be considerable. The equilibrium thermal populations of the $v = 1$ level of each of the vibrational modes in ethylene were calculated from their Boltzmann factors at several temperatures and are given in Table 3.

The effect of the thermal population of these vibrational levels on the absorption will be two-fold. The first and most direct effect comes from the population of $v_7 = 1$. For a transition in a two-level system, if the population of the upper level is not negligible compared with that in the lower, the concentration term in Beer's law must be replaced by a term (c_0 c_1) where

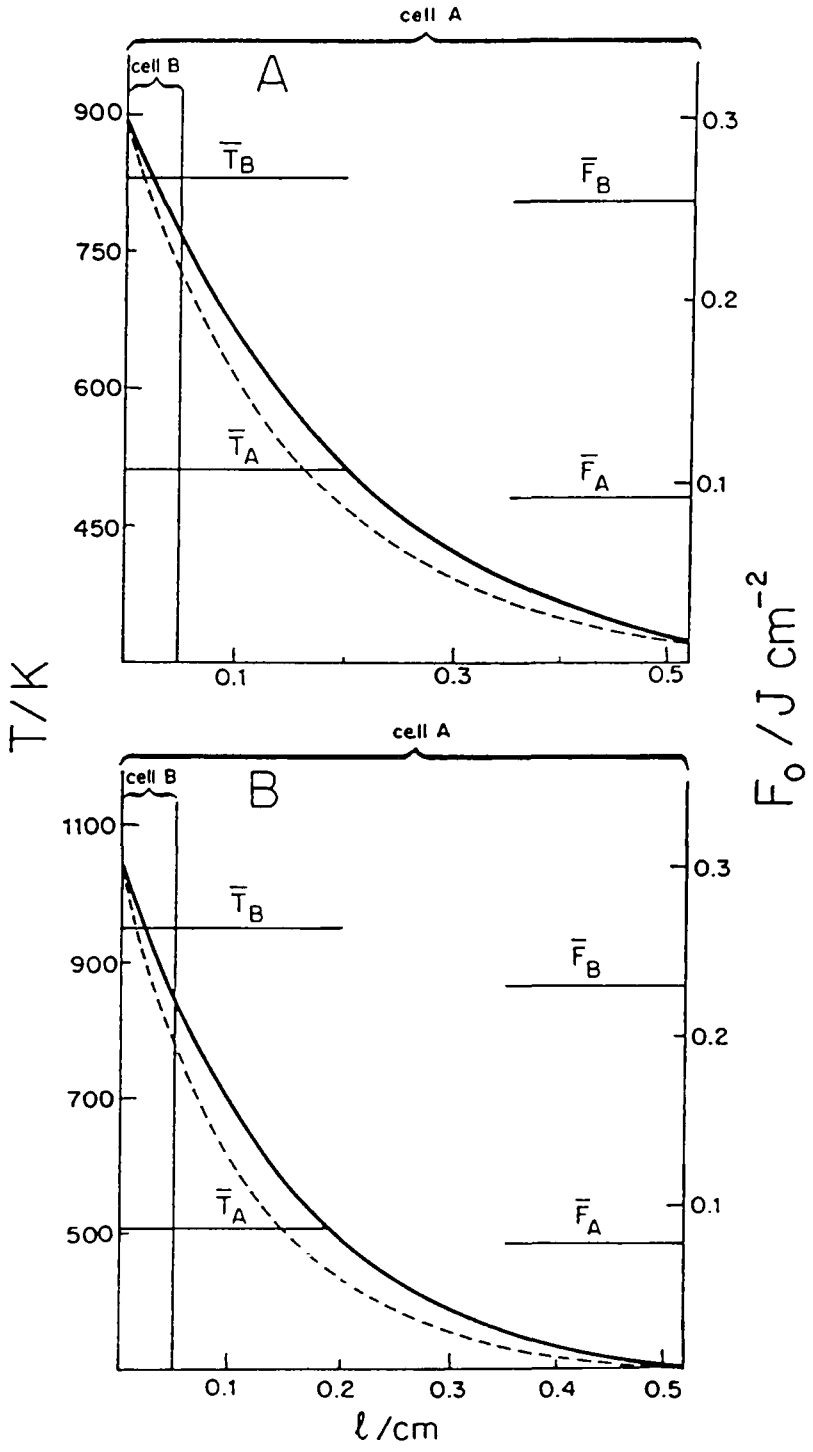

Figure 18. Temperature and fluence profiles as a function of distance at an ethylene pressure of 1000 Torr with an incident fluence of 0.3 J cm^{-2}

A. 10 P(12) line

—: Temperature
---: Fluence

B. 10 P(14) line

—: Temperature
---: Fluence

Average temperatures and fluences in the two cells are indicated by horizontal lines.

Table 3. Thermal equilibrium population of vibrationally excited states of ethylene*.

vibrational state	energy/cm^{-1} above ground state	300 K		650 K		1000 K	
		Boltzmann factor	fraction of molecules in state	Boltzmann factor	fraction of molecules in state	Boltzmann factor	fraction of molecules in state
$v = 0$	0	1.0	0.950	1.0	0.588	1.0	0.380
$v_{10} = 1$	825.9	0.019	0.018	0.161	0.095	0.305	0.116
$v_8 = 1$	940.1	0.011	0.010	0.125	0.073	0.258	0.098
$v_7 = 1$	948.8	0.010	0.007	0.122	0.072	0.255	0.097
$v_4 = 1$	1026.4	0.007	0.003	0.103	0.060	0.228	0.086
$v_6 = 1$	1222.0	0.003	0.002	0.067	0.039	0.172	0.065
$v_3 = 1$	1345.5	0.002	0.001	0.051	0.030	0.144	0.055
$v_{12} = 1$	1443.5	0.001	0.0	0.041	0.024	0.125	0.047
$v_2 = 1$	1625.4	0.0	0.0	0.027	0.016	0.096	0.036
$v_{11} = 1$	2988.6	0.0	0.0	0.001	0.001	0.014	0.005
$v_1 = 1$	3021.2	0.0	0.0	0.001	0.001	0.013	0.005
$v_5 = 1$	3083.4	0.0	0.0	0.001	0.001	0.012	0.005
$v_9 = 1$	3105.0	0.0	0.0	0.001	0.001	0.011	0.004

* To first approximation, only equilibrium populations of $v_i = 1$ were considered while equilibrium populations of vibrational states with $v_i > 1$ were ignored. The population of $v_i = 2$ for the ν_6, ν_3, ν_{12} and ν_2 modes and of $v_i = 3$ for the ν_{10}, ν_8, ν_7 and ν_4 modes have greater populations than $v_i = 1$ for the stretching modes ν_{11}, ν_1, ν_5, and ν_9.

c_0 and c_1 are the concentrations in the lower and upper levels respectively. This takes into account the stimulated emission from level 1 to level 0 which will detract from the net absorption of radiation. The effect of this "down-pumping", as it is sometimes called, will be to reduce the value of ϵ_{eff} in the present measurements by a fraction c_1/c_0, which for $v_7 = 1$ at 1000 K (Table 3) will be 0.255.

The second effect on the absorption comes from the depletion of the vibrational ground state, and is less easy to assess. Thermal excitation of any of the vibrational modes listed in Table 3 leaves the ethylene molecule still capable of absorbing in the ν_7 mode, but with a small shift in the frequency of the ν_7 band center caused by small changes in geometry. The change is largest for excitation of ν_7 itself, in which case the shift corresponds simply to the anharmonicity of the ν_7 vibration. For excitation of the other modes, the shift is generally not known accurately, being probably less than 1 cm^{-1}, but could still be sufficient to shift the absorption out of the fairly close resonance with the laser lines which we have seen is responsible for their strong absorption. If as an extreme limiting assumption it is assumed that these shifts reduce the absorption of the 10 P(12) and 10 P(14) laser lines to zero, then the depopulation of the ground vibrational state should directly reflect the reduction in ϵ_{eff}. From Table 3, the fraction of molecules remaining in the vibrational ground state at 1000 K is given, from the definition of the Boltzmann factor, and ignoring higher vibrational levels, by

$$\begin{aligned} f_{(\text{ground state})} &= 1/[1 + \sum_{i=1}^{12} f(v_i = 1)] \\ &= 1/[1 + 1.63] \\ &= 0.38 \end{aligned} \qquad (12)$$

Quantitative treatment of the change in ϵ_{eff} due to these thermal effects would be very difficult because of the gradients in fluence (and hence in temperature) in both time and in space, both along and across the laser beam. It should be noted that the average temperature rise during the pulse would be about half that calculated at the end of the pulse, shown in Figure 18. It seems unlikely that vibrational excitation would lead to complete loss of ν_7 absorption of the laser lines, as we have assumed as a limiting case, and at higher pressures, as the absorption lines broaden, small anharmonic shifts will become much less effective in reducing the overlap. The "down-pumping" from $v_7 = 1$ on the other hand, should be unaffected by pressure-broadening. All things considered, it seems at least possible that stimulated emission from $v_7 = 1$, combined with the effects of depopulation of the vibrational ground state, could account for most of the apparent temperature dependence of ϵ_{eff}.

Alternative explanations are not attractive. Non-equilibrium depopulation of absorbing levels (vibrational or rotational "hole burning") would not appear to be of much importance at the pressures employed. Simple radial expansion of the heated gas, with consequent decrease in the number of molecules in the absorption path and related thermal lensing effects, are too slow to affect the absorption measurements, as will be shown later.

Finally, the relatively low levels of excitation of ethylene reached in the present work should be noted. Table 4 shows some typical values of <N>, the average number of photons absorbed per molecule in a single pulse. Included are values determined with each laser line at an incident fluence of 0.3 J cm^{-2} averaged over the entire lengths of the cell (I), and the higher values at the front window (II). An appreciable fraction of the absorption will be from the vibrational ground state, and, given the rapidity of inter and intramolecular

Table 4. Number of photons absorbed per molecule, <N>, in cells A an B at an incident fluence of 0.3 J cm^{-2}

10 P(12) line

	cell A, l = 0.52 cm C_2H_4/Torr					cell B, l = 0.051 cm C_2H_4/Torr				
<N>*	25	50	100	200	300	250	500	1000	2000	3000
I	0.8	1.0	1.2	1.5	1.6	1.8	2.4	2.6	2.5	2.3
II	0.8	1.0	1.3	1.9	2.3	1.9	2.6	3.1	3.7	4.2

10 P(14) line

	cell A, l = 0.52 cm C_2H_4/Torr					cell B, l = 0.051 cm C_2H_4/Torr				
<N>*	25	50	100	200	300	250	500	1000	2000	3000
I	1.0	1.7	2.2	2.6	2.4	2.4	3.0	3.4	3.3	2.7
II	1.0	1.8	2.5	3.7	4.5	2.5	3.3	4.2	5.6	6.3

* I: <N> averaged over total length.
II: <N> at the front window.

energy transfer at the high pressures of the experiments, most of the absorption will be from vibrational states with $v_7 = 0$, with the postulated temperature effects indicating less efficient absorption as other vibrational modes become populated. The characteristics of the absorption of the CO_2 laser radiation under these conditions are very different from those in the low-pressure multiphoton unimolecular decomposition of ethylene in which individual molecules are pumped to much higher levels, and requiring much higher fluence.

MODEL

Electrocyclic and cycloaddition reactions are types of pericyclic reactions which occur through cyclic transition states. A number of cycloaddition reactions of alkenes and polyenes are known in which two molecules react to form a cyclic product. A well known example is the cycloaddition of two ethylene molecules to form a molecule of cyclobutane:

$$2C_2H_4 \rightarrow c\text{-}C_4H_8 \qquad (5)$$

By orbital symmetry rules [75], the concerted thermal [2+2] cycloaddition reaction is forbidden and probably occurs through a biradical mechanism [76]. An ionic intermediate (zwitterion) has also been suggested [77].

The reaction was studied by Quick, Knecht and Back [49] who measured the rate of formation of cyclobutane amongst other products formed in the thermal reaction of ethylene over the temperature range 723-786 K and at pressures between 300 and 1300 Torr. They suggested that the reaction to form cyclobutane occurred through the intermediate formation of a biradical, but the lifetime of the radical was so short that under the conditions of the measurements, the reaction was effectively a one-step process. The initial rate of formation of cyclobutane was second order with respect to ethylene and the rate constant for its formation was expressed as follows:

$$\log_{10} k_f\,(dm^3\,mol^{-1}\,s^{-1}) = 7.84 \quad (183000/2.3RT) \qquad (13)$$

From measurements of the equilibrium concentration of cyclobutane, they obtained the equilibrium constant for reaction (5), as follows:

$$\log_{10} K_5\,(dm^3\,mol^{-1}) = (-147/2.3R) + (80300/2.3RT) \qquad (14)$$

The equilibrium constant obtained using the measured value for k_f and the rate constant for the unimolecular dissociation of cyclobutane to ethylene [78] was in good agreement with this expression.

It seemed possible that measurement of an equilibrium concentration of cyclobutane might be used to estimate a reaction temperature in the decomposition of ethylene induced by a pulsed CO_2 laser, using the equilibrium expression for reaction (5):

$$[c\text{-}C_4H_8]_{equil.} = K_5[C_2H_4]^2 \qquad (15)$$

and the known dependence of K_5 on temperature. While this idea is a simple one, its application to the present system, with its large spatial and temporal variations in temperature seems at first sight impractical. The reagent gas is heated rapidly by the laser pulse, reaching some temperature T_{max} then cools rather more slowly back to room temperature by some combination of adiabatic expansion and thermal conduction. The laser fluence, and thence the value of T_{max} achieved, falls off rapidly with distance from the front window, as discussed earlier, and there may also be some radial fluence gradients in the laser beam. The concept of a single "effective reaction temperature" in such a system is clearly an approximation and it is only made practical at all by a sharp dependence of reaction rates on temperature inherent in the Arrhenius equation. Table 5 shows relative rates for a reaction with E = 190 kJ mol^{-1} at temperatures between 1200 and 1500 K, parameters typical of the present system.

Table 5. Relative rates for a reaction with E = 190 kJ mol^{-1}.

T/K	relative rate
1500	1.00
1450	0.59
1400	0.34
1350	0.18
1300	0.10
1250	0.05
1200	0.02

From these relative rates, it is seen that most of the reaction during a heating-cooling cycle caused by a laser pulse will tend to occur at temperatures fairly close to the maximum. It follows also, from the attenuation of the laser fluence, and thence the temperature, across the reaction cell, that most of the reaction will tend to occur in a thin disc of gas close to the front window. Thus, to a first approximation, the system can be treated in terms of an effective reaction temperature, somewhat below T_{max} at the front window, and an effective reaction volume. For practical purposes, there are further complications because a sequence of pulses, rather than a single pulse, is required to provide enough product for analysis, and between pulses, reagent and product gases in the reaction volume will mix by diffusion and convection with the rest of the reaction vessel.

In order to explore the approach of the cyclobutane concentration towards a steady-state or equilibrium value in such a system, simple computer modelling calculations were performed, using numerical integration of the differential equation for the rate of formation of cyclobutane:

$$d[c\text{-}C_4H_8]/dt = k_f[C_2H_4]^2 \quad k_r[c\text{-}C_4H_8] \qquad (16)$$

The reverse rate constant, k_r, is that of the unimolecular dissociation of cyclobutane to ethylene measured by Carr and Walters [78],

$$\log_{10} k_r\,(s^{-1}) = (15.62 \pm 0.01) \quad (262000 \pm 1700)/2.3RT \qquad (17)$$

while the forward rate constant, k_f, was calculated from this using the thermodynamic data for ethylene and cyclobutane compiled by Benson [79], giving the following value*,

$$\log_{10} k_f(dm^3\,mol^{-1}\,s^{-1}) = (9.2 \pm 0.8) \quad (196000 \pm 15000)/2.3RT \qquad (18)$$

These data and the errors associated with them are given in Appendix C.

---

* In most of the calculations, a slightly lower value for k_f was used, but no significant changes in the results or conclusions arise because of this difference.

For simplicity, the model assumes that a sample of ethylene gas is heated and cooled uniformly, so that temperatures and concentrations are homogeneous at all times. A linear rate of heating was assumed, raising the temperature from 300 K to T_{max} in a time of 110 ns, the average measured value of the laser pulse width at half its maximum intensity. Cooling was also assumed to be linear with time but slower, and calculations were made for several rates of cooling. Finally, it was necessary to make an assumption about the volume of the gas during the heating-cooling cycle induced by the laser pulse. Two limiting cases were considered, constant volume and constant pressure, and a third more complex case in which the gas remained at constant volume during the 110 ns heating period, then cooled by adiabatic expansion, and finally cooled more slowly at constant pressure. In the first case thermal expansion is assumed to be negligibly slow compared to the heating and cooling rates, while in the second case it is much faster so that the expansion and contraction follows closely the changes in temperature. The third case perhaps comes closest to the real behavior expected in the system. These are referred to as follows:

Case I: constant volume

Case II: constant pressure

Case III: constant volume, adiabatic expansion, constant pressure.

Calculations were made for a range of pressures of ethylene, values of T_{max}, and cooling rates, for each of the three assumptions about the gas volume. A more detailed description of the calculations and the computer program used are found in Appendix D.

Calculations for a single pulse were made first, in which the cyclobutane was followed as a function of time from its initial zero concentration through

both the heating period from 300 K up to the T_{max}, and the cooling from T_{max} back to 300 K. Results of these calculations for ethylene pressures of 1000 and 3000 Torr and maximum temperatures of 1000, 1500 and 2000 K are shown in Figures 19-21 for each of the three assumptions about reaction volume previously discussed. Each figure shows only the central part of a single pulse calculation covering the temperatures at which most of the chemical change is occurring. The logarithm of the cyclobutane concentration is plotted against time; the time scale in the heating period is the same in all cases, but in the cooling period, while several cooling rates were assumed, the time scale shown for Cases I and II corresponds only to equal rates of cooling and heating. For Case III, in which the cooling period was divided in two parts, the times shown are actual times during the calculation. A corresponding common linear temperature scale is included at the top of each figure, symmetric about T_{max}, which applies to all rates of cooling. Equilibrium cyclobutane concentrations corresponding to these temperatures have also been plotted.

In these figures, all cyclobutane concentrations have been corrected to correspond to the original volume at 300 K. In this way, the data reflect changes in the amount of cyclobutane present, eliminating the changes in concentration due to transient changes in volume. This permits meaningful comparison between the calculations based on different assumptions about thermal expansion, and also permits direct comparison with experiment, in which final concentrations in the cell volume at 300 K were measured. In the calculations themselves, of course, true concentrations must be employed throughout. The equilibrium values of cyclobutane concentration plotted in Figures 19-21 have been corrected in the same way. It may be noted that

Figure 19. Single pulse calculations of cyclobutane concentrations for T_{max} = 1000 K.

A: Case I (constant volume), 1000 Torr C_2H_4
B: Case I (constant volume), 3000 Torr C_2H_4
C: Case II (constant pressure), 1000 Torr C_2H_4
D: Case II (constant pressure), 3000 Torr C_2H_4
E: Case III (constant volume, adiabatic expansion, constant pressure), 1000 Torr C_2H_4
F: Case III (constant volume, adiabatic expansion, constant pressure), 3000 Torr C_2H_4.

For Cases I and II,

△ : cooling rate = heating rate
◭ : cooling rate = 1/10 heating rate
◭ : cooling rate = 1/100 heating rate
▲ : cooling rate = 1/1000 heating rate.
Times in the cooling period for the latter three cooling rates must be multiplied by 10, 100 and 1000 respectively.

For Case III, the cooling period is divided in two parts:

(i) cooling by adiabatic expansion occurs at a rate 10 times slower than the heating rate followed by
(ii) cooling under constant pressure at a rate 100 times slower than the heating rate.

In all cases, equilibrium concentrations are also shown as a function of temperature and are indicated by ○.

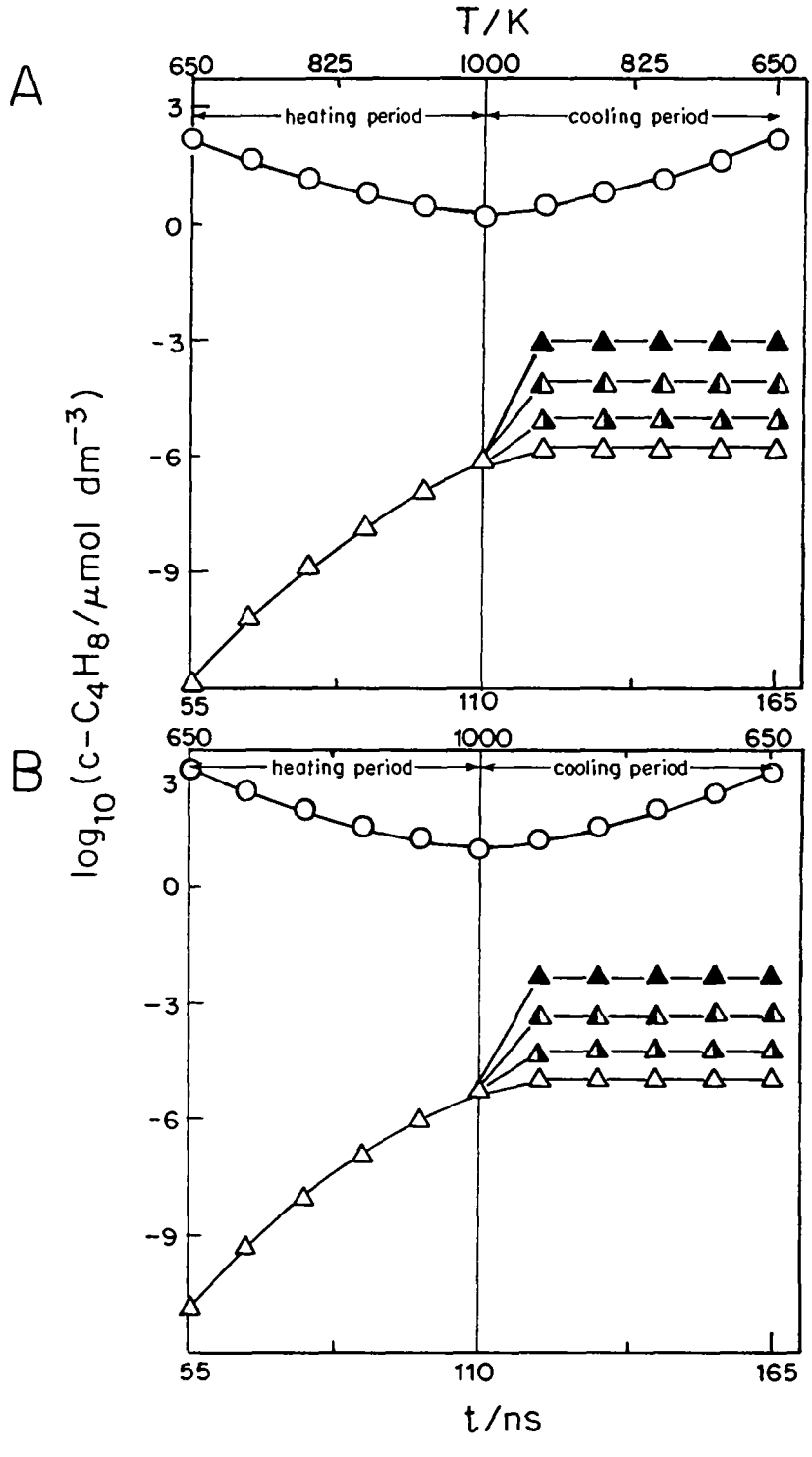
T/K
650
825
1000
825
650
A
heating period
cooling period
3
0
-3
-6
-9
55
110
165
B
650
1000
650
heating period
cooling period
3
0
-3
-6
-9
55
110
165
t/ns
log10(c-C4H8/μmol dm-3)

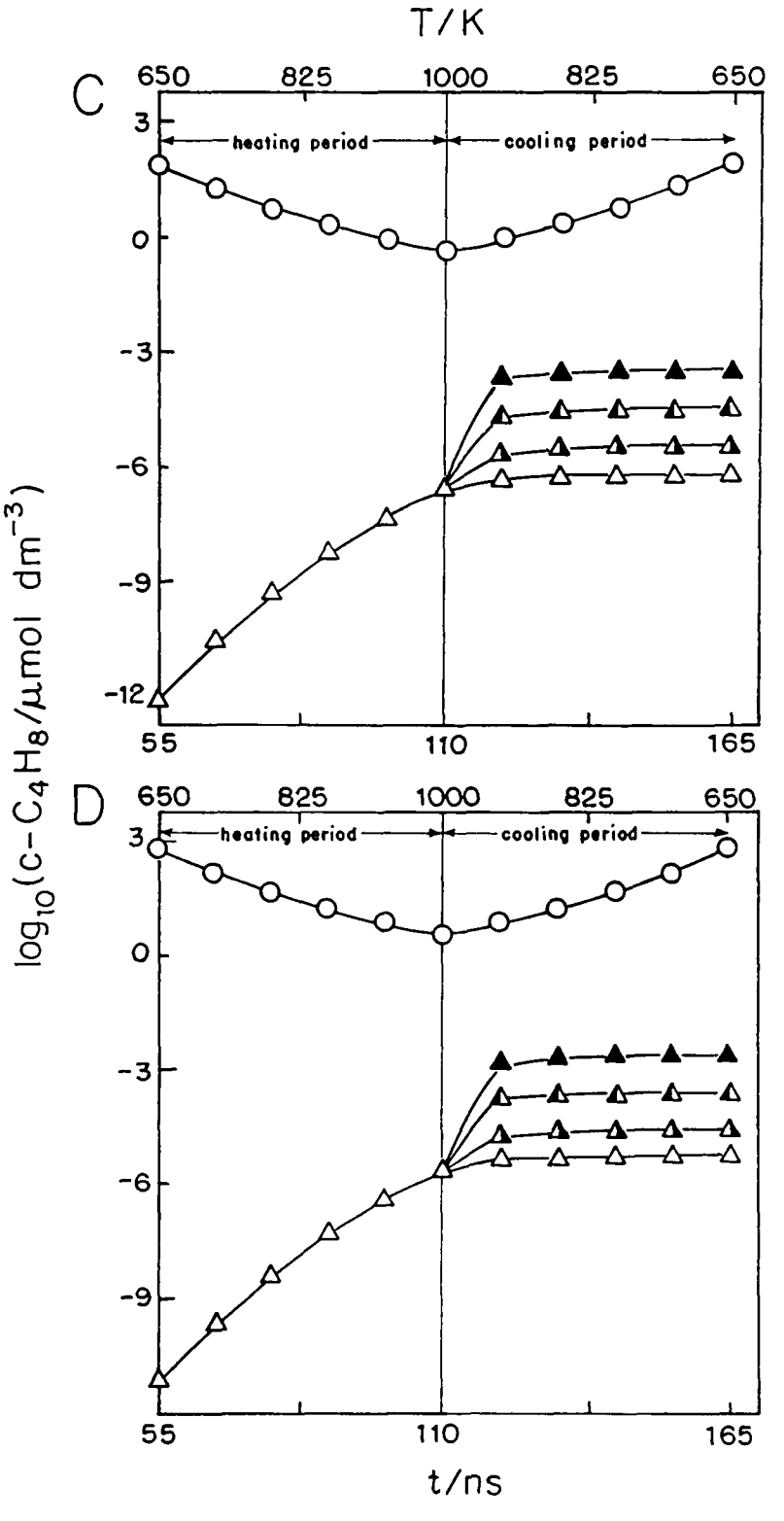
T/K
650
825
1000
825
650
C
heating period
cooling period
3
0
-3
-6
-9
-12
55
110
165
D
heating period
cooling period
3
0
-3
-6
-9
55
110
165
t/ns
log10(c-C4H8/μmol dm-3)

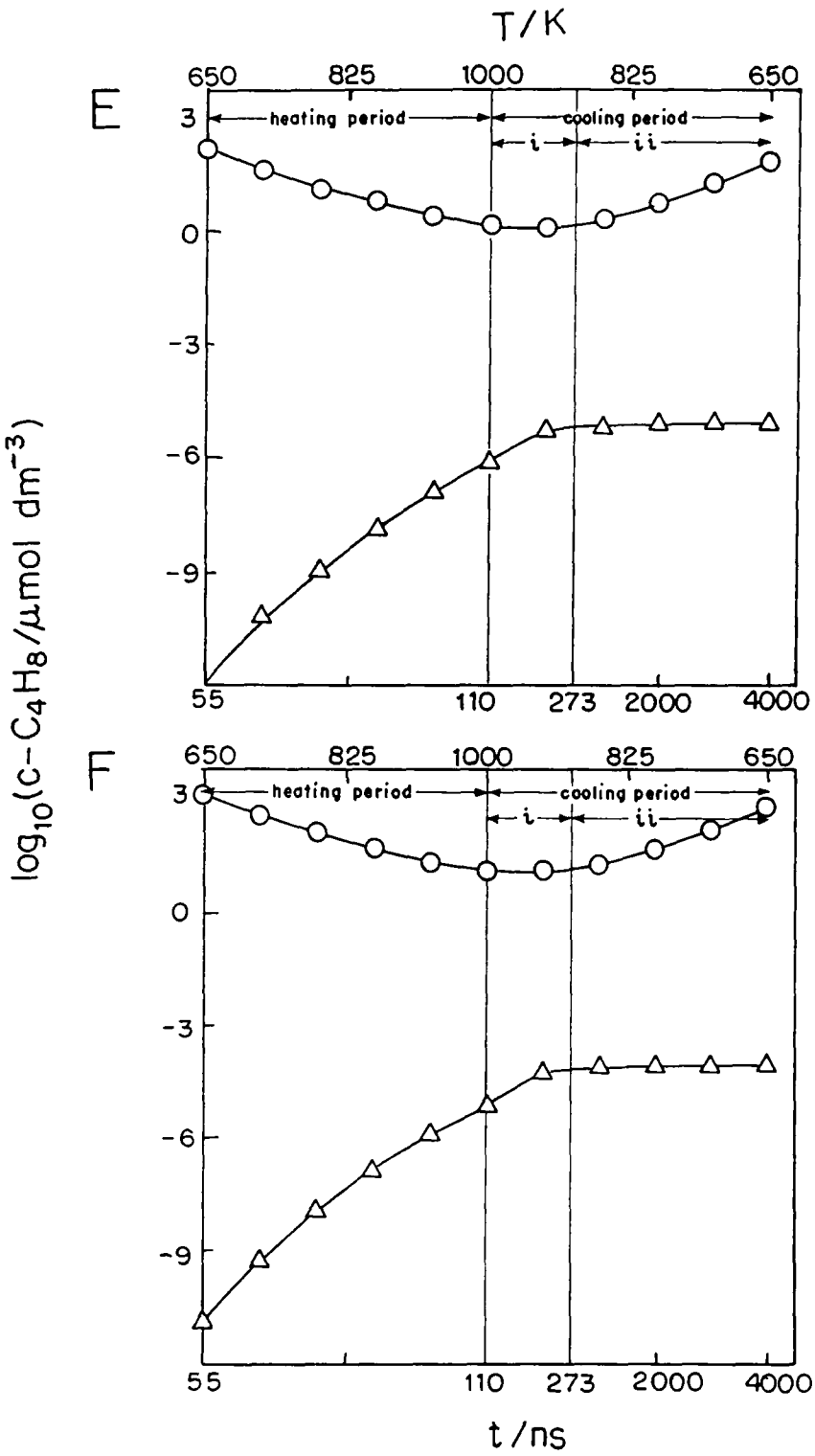
T/K
650
825
1000
825
650
E
heating period
cooling period
i
ii
3
0
-3
-6
-9
55
110
273
2000
4000
F
heating period
cooling period
i
ii
3
0
-3
-6
-9
55
110
273
2000
4000
t/ns
log10(c-C4H8/μmol dm-3)

Figure 20. Single pulse calculations of cyclobutane concentrations for T_{max} = 1500 K.

A: Case I (constant volume), 1000 Torr C_2H_4
B: Case I (constant volume), 3000 Torr C_2H_4
C: Case II (constant pressure), 1000 Torr C_2H_4
D: Case II (constant pressure), 3000 Torr C_2H_4
E: Case III (constant volume, adiabatic expansion, constant pressure), 1000 Torr C_2H_4
F: Case III (constant volume, adiabatic expansion, constant pressure), 3000 Torr C_2H_4.

For Cases I and II,

△ : cooling rate = heating rate
▲ : cooling rate = 1/10 heating rate
◭ : cooling rate = 1/100 heating rate
▲ : cooling rate = 1/1000 heating rate.
Times in the cooling period for the latter three cooling rates must be multiplied by 10, 100 and 1000 respectively.

For Case III, the cooling period is divided in two parts:

(i) cooling by adiabatic expansion occurs at a rate 10 times slower than the heating rate followed by
(ii) cooling under constant pressure at a rate 100 times slower than the heating rate.

In all cases, equilibrium concentrations are also shown as a function of temperature and are indicated by○.

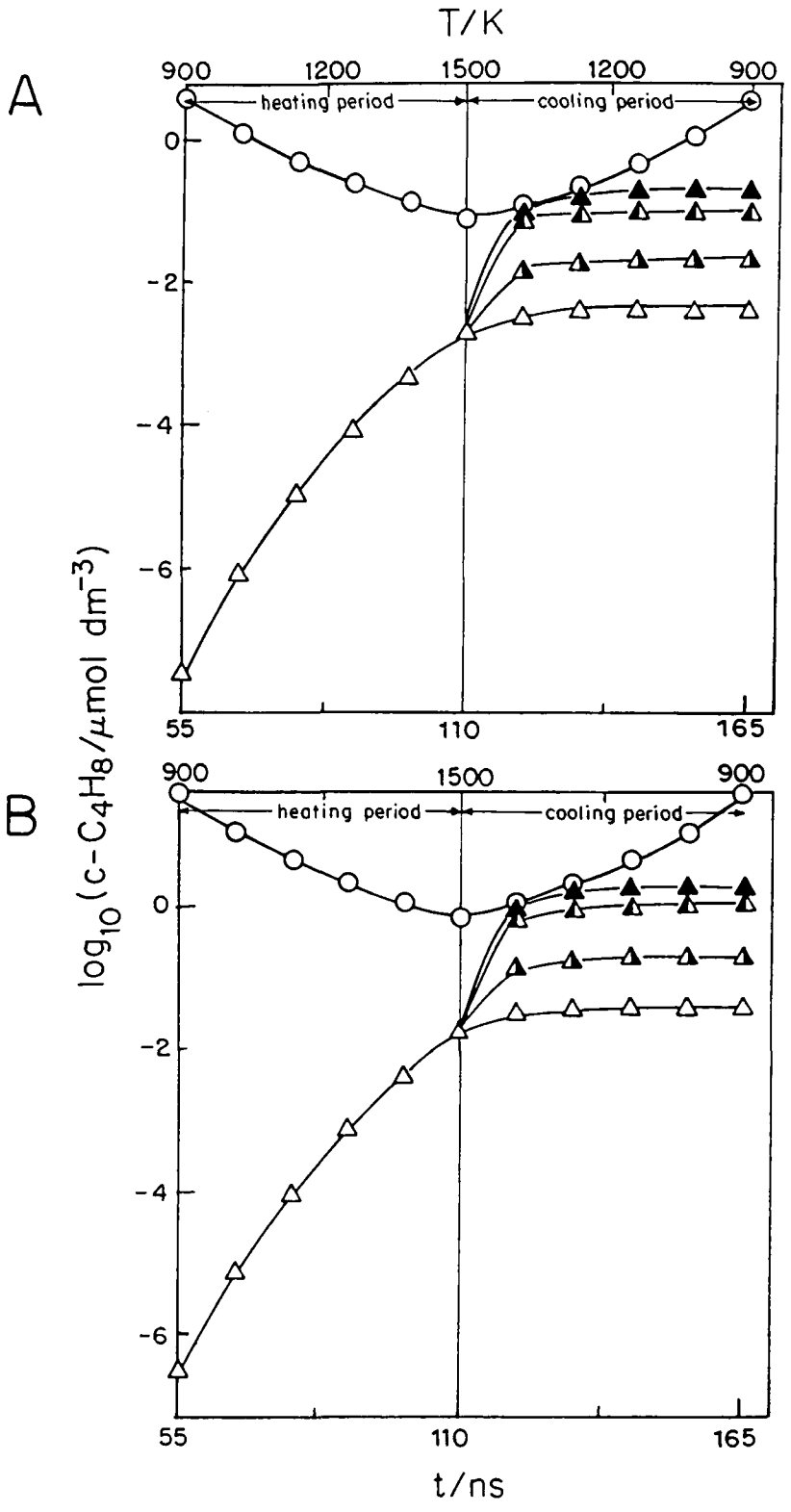
T/K
A
900
1200
1500
1200
900
heating period
cooling period
0
-2
-4
-6
55
110
165
B
900
1500
900
heating period
cooling period
0
-2
-4
-6
55
110
165
$\log_{10}(c\text{-}C_4H_8/\mu mol\ dm^{-3})$
t/ns

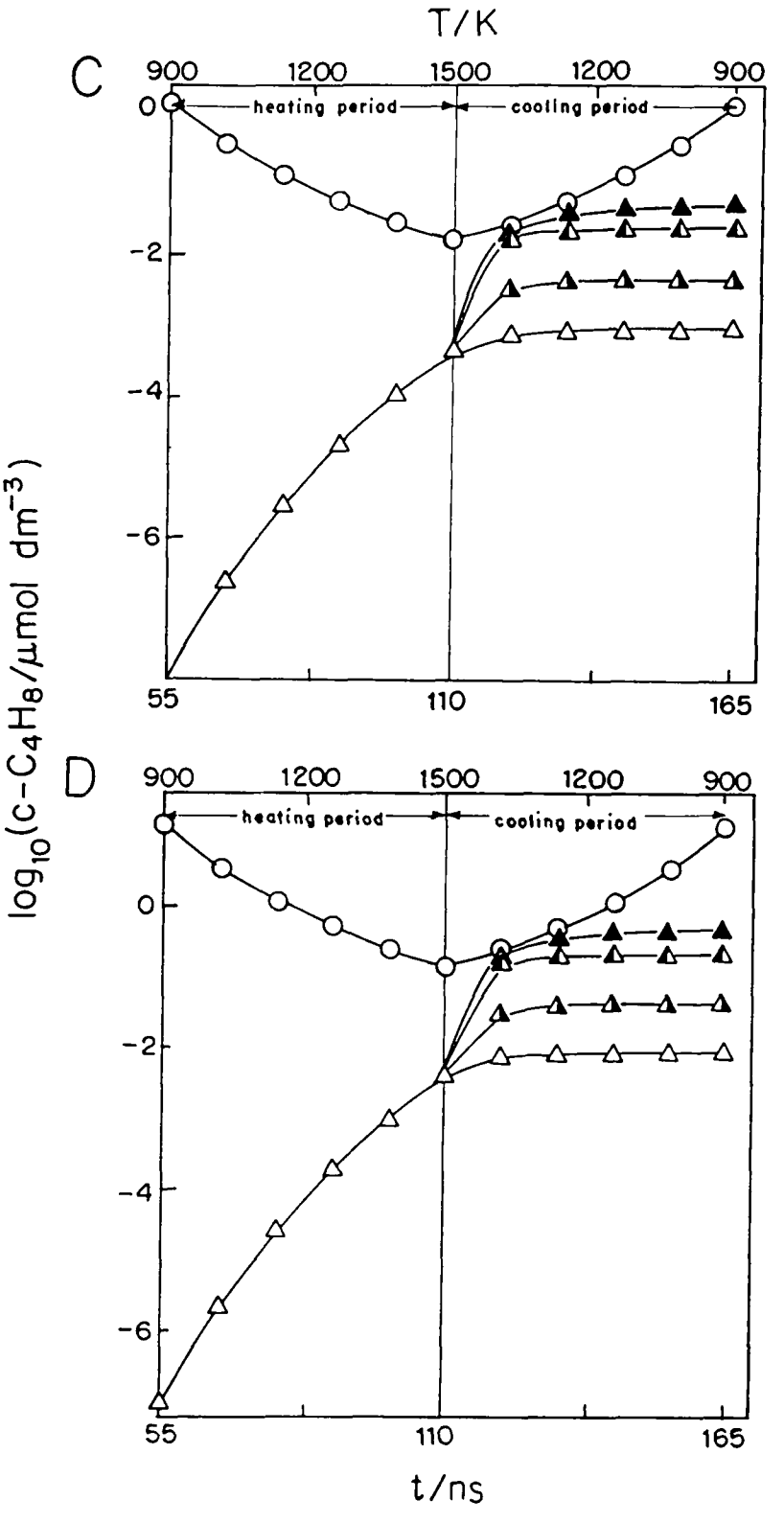
T/K
C
900
1200
1500
1200
900
heating period
cooling period
0
-2
-4
-6
55
110
165
D
900
1200
1500
1200
900
heating period
cooling period
0
-2
-4
-6
55
110
165
t/ns
log10(c-C4H8/μmol dm-3)

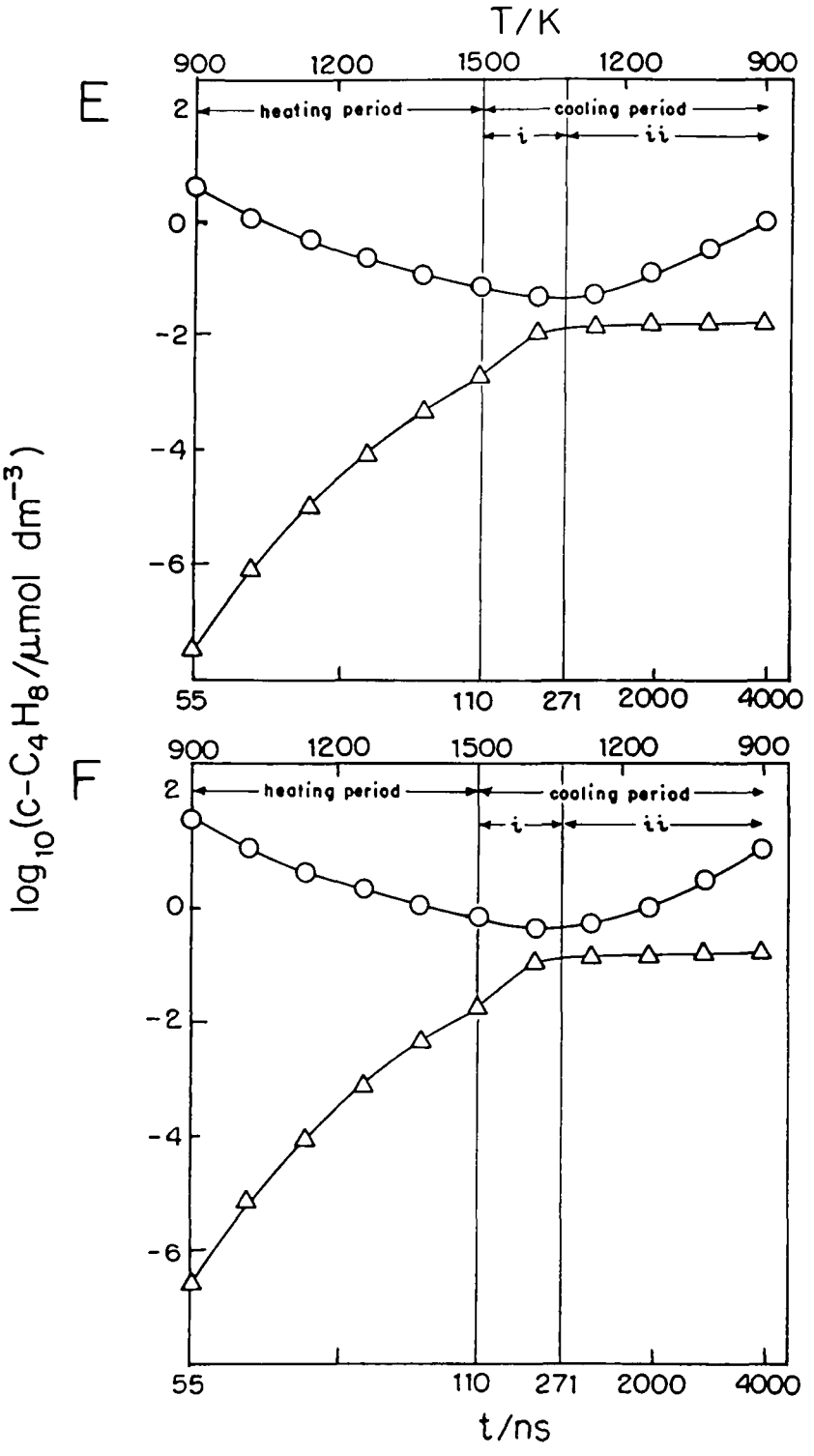
T/K
900
1200
1500
1200
900
E
heating period
cooling period
i
ii
2
0
-2
-4
-6
55
110
271
2000
4000
F
$\log_{10}(c\text{-}C_4H_8/\mu mol\ dm^{-3})$
t/ns

Figure 21. Single pulse calculations of cyclobutane concentrations for T_{max} = 2000 K.

A: Case I (constant volume), 1000 Torr C_2H_4
B: Case I (constant volume), 3000 Torr C_2H_4
C: Case II (constant pressure), 1000 Torr C_2H_4
D: Case II (constant pressure), 3000 Torr C_2H_4
E: Case III (constant volume, adiabatic expansion, constant pressure), 1000 Torr C_2H_4
F: Case III (constant volume, adiabatic expansion, constant pressure), 3000 Torr C_2H_4.

For Cases I and II,

△ : cooling rate = heating rate
◭ : cooling rate = 1/10 heating rate
◭ : cooling rate = 1/100 heating rate
▲ : cooling rate = 1/1000 heating rate.
Times in the cooling period for the latter three cooling rates must be multiplied by 10, 100 and 1000 respectively.

For Case III, the cooling period is divided in two parts:

(i) cooling by adiabatic expansion occurs at a rate 10 times slower than the heating rate followed by
(ii) cooling under constant pressure at a rate 100 times slower than the heating rate.

In all cases, equilibrium concentrations are also shown as a function of temperature and are indicated by○.

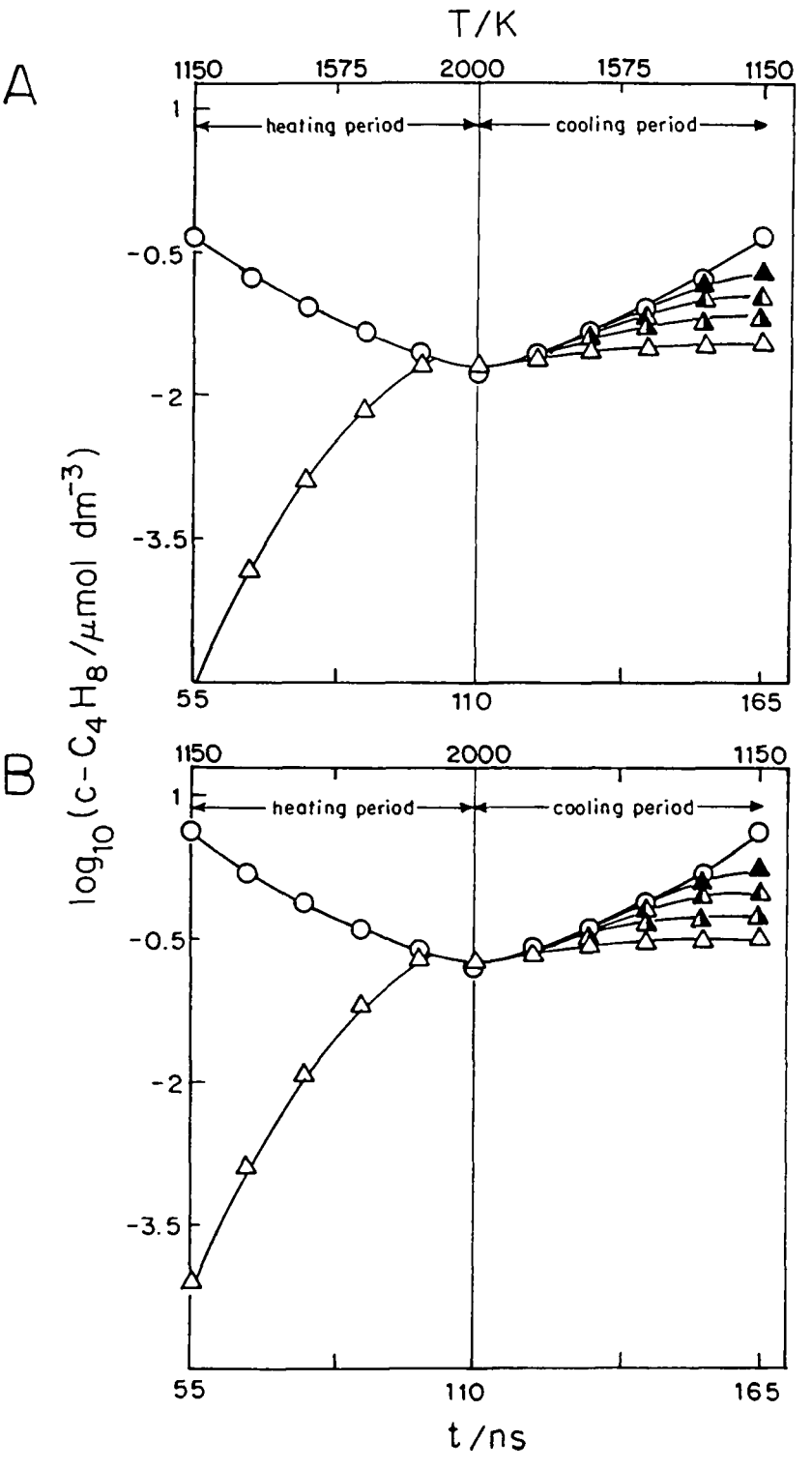
T/K
A
1150
1575
2000
1575
1150
1
heating period
cooling period
-0.5
-2
-3.5
55
110
165
B
1150
2000
1150
1
heating period
cooling period
-0.5
-2
-3.5
55
110
165
t/ns
log10(c-C4H8/μmol dm-3)

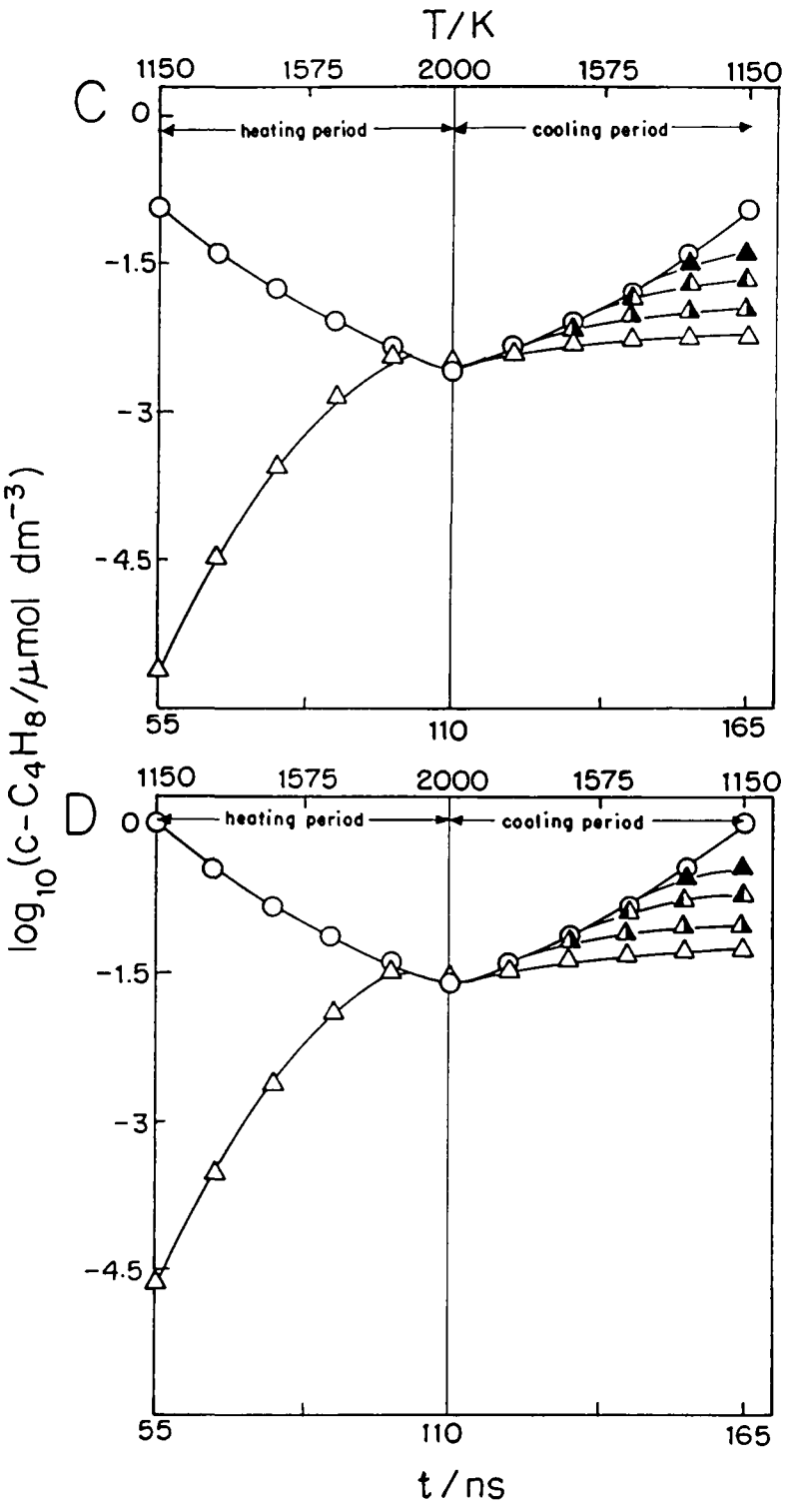
T/K
1150
1575
2000
1575
1150
C
D
heating period
cooling period
0
-1.5
-3
-4.5
55
110
165
$\log_{10}(c\text{-}C_4H_8/\mu mol\ dm^{-3})$
t / ns

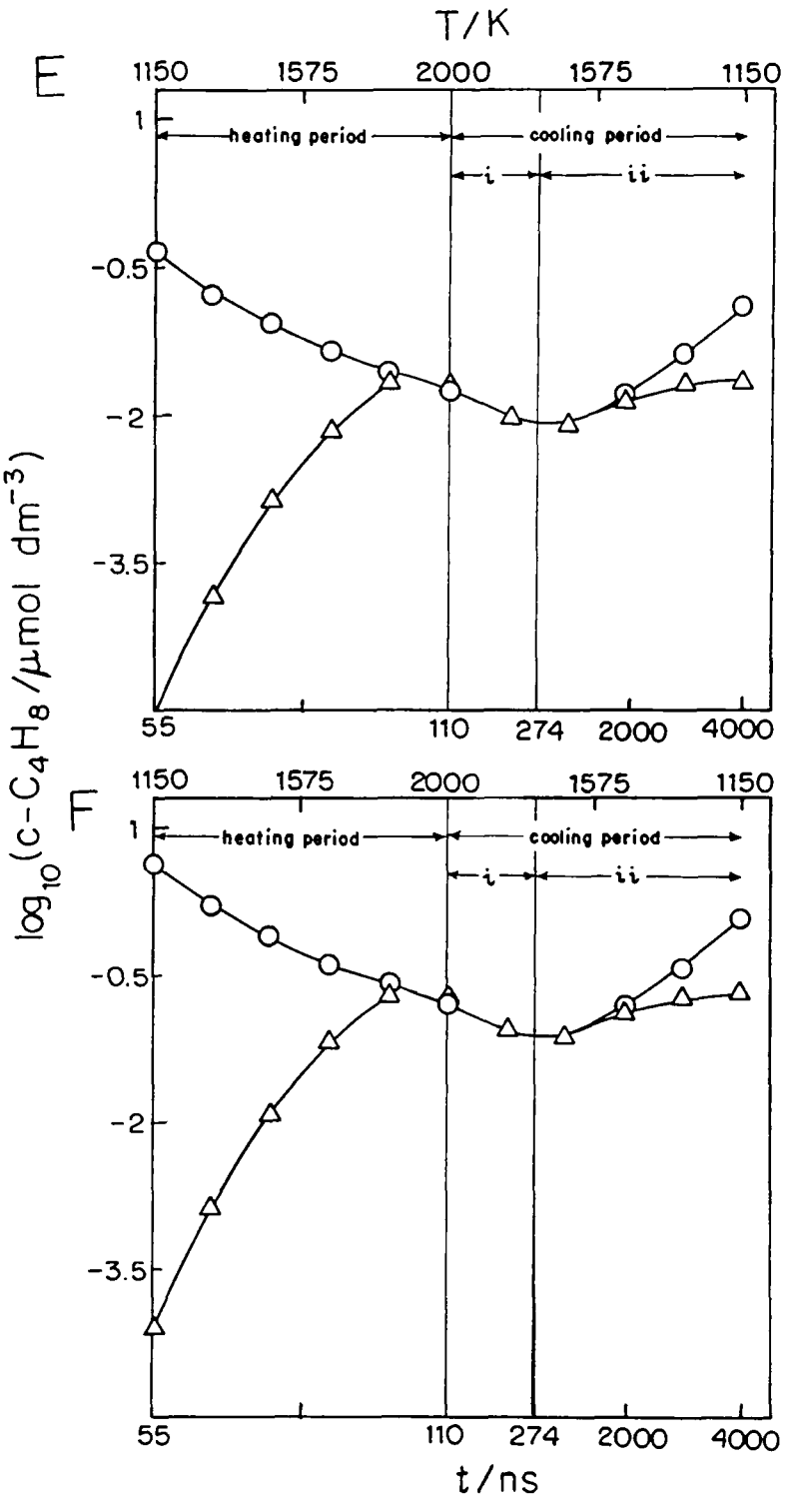
T/K
E
1150
1575
2000
1575
1150
heating period
cooling period
i
ii
1
-0.5
-2
-3.5
55
110
274
2000
4000
F
log10(c-C4H8/μmol dm-3)
t/ns

these values are somewhat different for the three assumptions about thermal expansion, reflecting associated changes in concentrations of ethylene due to changes in the gas volume with time in the heating-cooling cycle.

Several conclusions may be drawn from Figures 19-21.

(1) The calculations are very little affected by the different assumptions made about thermal expansion of the gas.

(2) Slower cooling rates allow the cyclobutane concentration to approach closer to equilibrium, as the heated gas spends a longer time at higher temperatures where the equilibration reactions are faster.

(3) The extent of approach of the cyclobutane concentration towards equilibrium is independent of the ethylene pressure. Thus, although the rate of formation of cyclobutane is faster at higher ethylene pressure, the equilibrium concentration is also higher, and the pressure has little influence on the time required to reach equilibrium.

(4) The approach of the cyclobutane concentration towards its equilibrium value depends strongly on the value of T_{max}. The three values chosen for the calculations, 1000, 1500 and 2000 K, correspond to three distinct situations. With T_{max} = 1000 K, the final cyclobutane concentration after a single pulse falls far short of the equilibrium value at T_{max}. For T_{max} = 1500 K, the final cyclobutane concentration comes close to the equilibrium value at T_{max}, while for T_{max} = 2000 K, the cyclobutane concentration reached equilibrium during the laser pulse and remained in equilibrium for part of the cooling period, levelling out finally at a value above that for equilibrium at T_{max}.

Noting that the equilibrium concentration of cyclobutane falls as the temperature rises, it can be seen that if the final values of cyclobutane

concentration after a single pulse were used to estimate T_{max}, assuming these to be equilibrium values, the calculations indicate that for T_{max} = 1000 K, the temperature would be overestimated and for T_{max} = 2000 K it would be underestimated while for T_{max} = 1500 K it would be roughly correct. The estimation of the temperature also depends on the cooling rate. The results in Figures 19-21 show that the final values for the concentration of cyclobutane increase as the cooling rate is progressively decreased.

In practice, a number of pulses must be used to provide enough product for analysis, and calculations were therefore undertaken to determine how this would affect the final concentrations of cyclobutane attained. Such a multipulse calculation consisted simply of a series of single pulse calculations, made in the same way as before, except that the cyclobutane concentration at the beginning of each pulse was taken to be the value at the end of the previous pulse. Again homogeneous temperatures and concentrations were assumed, with no mixing with unirradiated ethylene between pulses. Each multipulse calculation is continued until there is no further net change in the cyclobutane concentration. Because the last stages of the approach to this final value are very slow, the final value was in fact obtained by a graphical method of approximation. Several single-pulse calculations were made with initial concentrations slightly above and below the expected final value, which was then obtained by interpolation from a plot of Δ[cyclobutane] against initial concentration. An example is shown in Figure 22.

Results of typical multipulse calculations are shown in Figure 23 for an initial ethylene pressure of 1000 Torr and T_{max} = 1250 K. This shows the

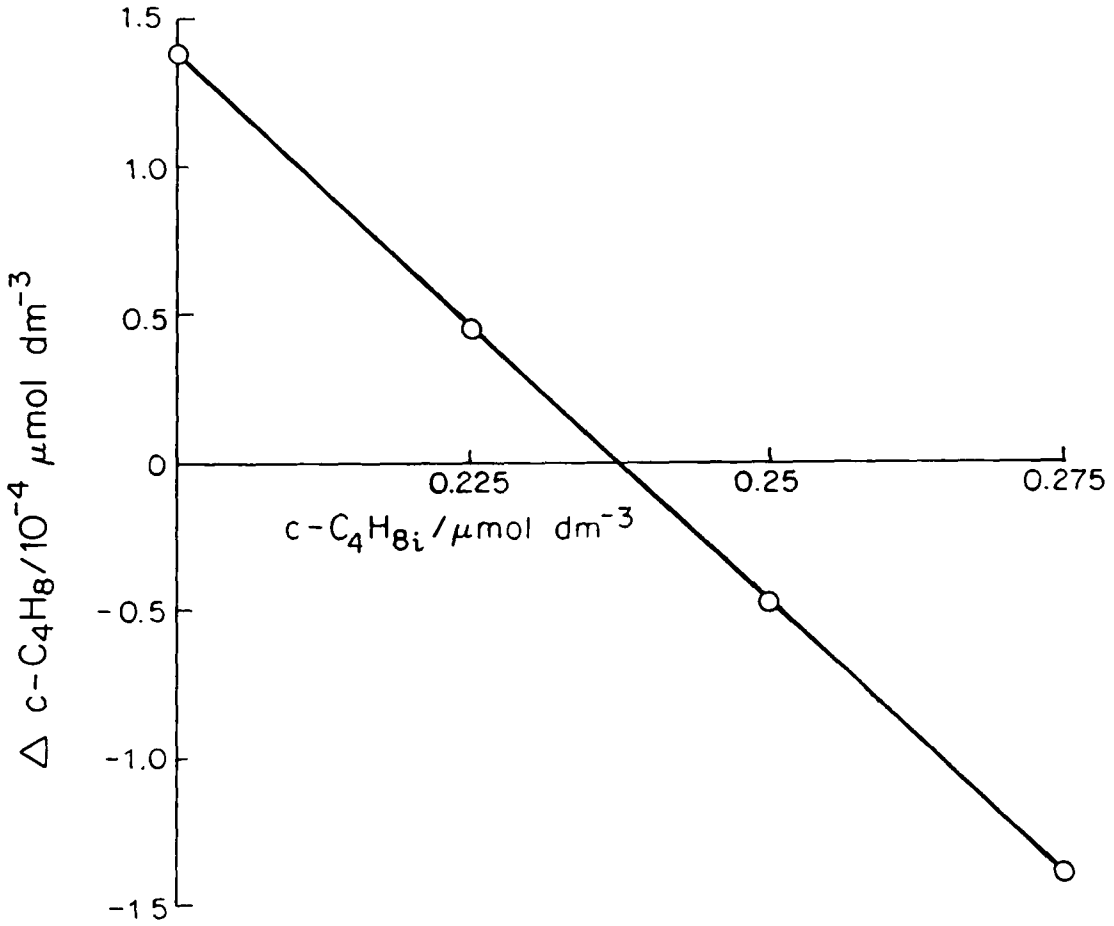

Figure 22. Graphical method of approximation yielding the constant final cyclobutane concentration.

Example of Case III,
heating under constant volume, cooling first by adiabatic expansion at a cooling rate equal to 1/10 the heating rate and further cooling under constant pressure at a cooling rate equal to 1/100 the heating rate,
$P_{C_2H_4}$ = 1000 Torr, T_{max} = 1250 K.

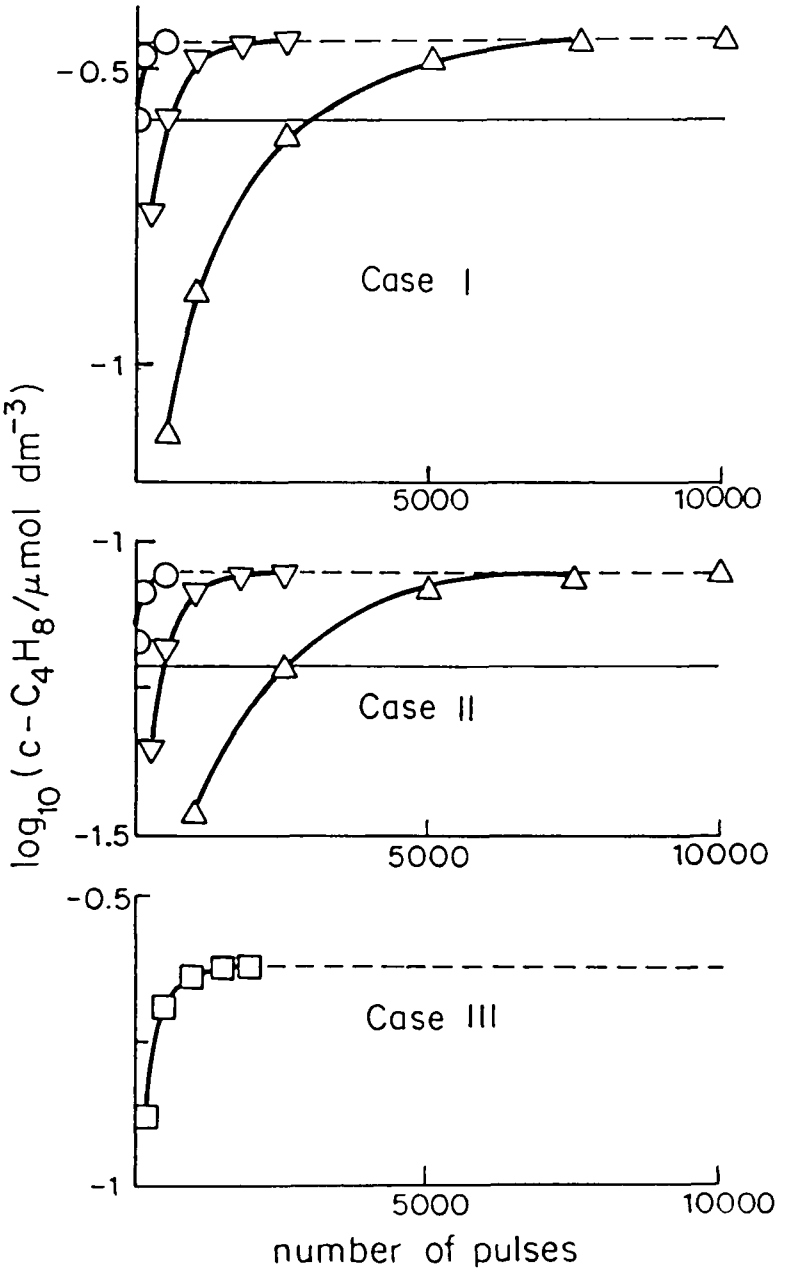

Figure 23. Multipulse calculations at $P_{C_2H_4}$ = 1000 Torr, T_{max} = 1250 K.

Calculated values for cyclobutane.

For Cases I and II,

cooling rate / heating rate △	▽	○	constant final value	equilibrium value
1	1/10	1/100	- - -	———

For Case III,

□ : cooling rate of adiabatic expansion = 1/10 heating rate and cooling rate under constant pressure = 1/100 heating rate

----: constant final value.

approaches to the constant final values of the cyclobutane concentration for the three assumptions about thermal expansion considered earlier, and for several rates of cooling. Also shown are values of the cyclobutane concentration corresponding to equilibrium at T_{max} (1250 K). As before, all concentrations shown are corrected to the original volume of the system at 300 K. It is interesting that the rate of cooling had no effect on the final value reached, but did have a major effect on the number of pulses required to reach this value. Multipulse calculations at higher maximum temperatures showed that a constant final value was reached much more quickly, while for T_{max} = 1000 K or 750 K, a very large number of pulses was required. In contrast to Cases I and II, no single set of equilibrium values for cyclobutane can be given for Case III because the values during the heating period are different from those at the same temperatures in the cooling period. It is interesting to note that the constant final value in Case III is intermediate between those for Cases I and II, but somewhat closer to Case I. Thus, expansion following heating at constant volume will not significantly affect an estimate of the final temperature.

Typical changes in the concentration of cyclobutane during the final stages in the approach to the constant final value for an ethylene pressure of 1000 Torr and a maximum temperature of 1500 K are shown in Figures 24A-B for limiting cases I and III respectively. These figures show the concentration of cyclobutane as a function of time (on the main axis) or temperature (at the top of each figure) during a single pulse, where the initial concentration of cyclobutane was close to the constant final value. Also shown in the upper half of these figures are equilibrium concentrations on a logarithmic scale, while in the lower half of these figures, changes in the

Figure 24. Single pulse calculation at an initial cyclobutane concentration close to the constant final value, $P_{C_2H_4}$ = 1000 Torr, T_{max} = 1500 K.

O : equilibrium values
Δ : calculated values
----: constant final value

A. Case I

Heating and cooling under constant volume, with cooling rate = 1/100 heating rate.

B. Case III

Heating under constant volume while cooling consists of two parts: (i) cooling by adiabatic expansion at a rate 10 times slower than the heating rate and (ii) cooling under constant pressure at a rate 100 times slower than the heating rate.

For A and B, the lower curve is an expanded linear plot of the cyclobutane concentration shown in the upper curve on a logarithmic plot. Note the change in time scale for the cooling periods.

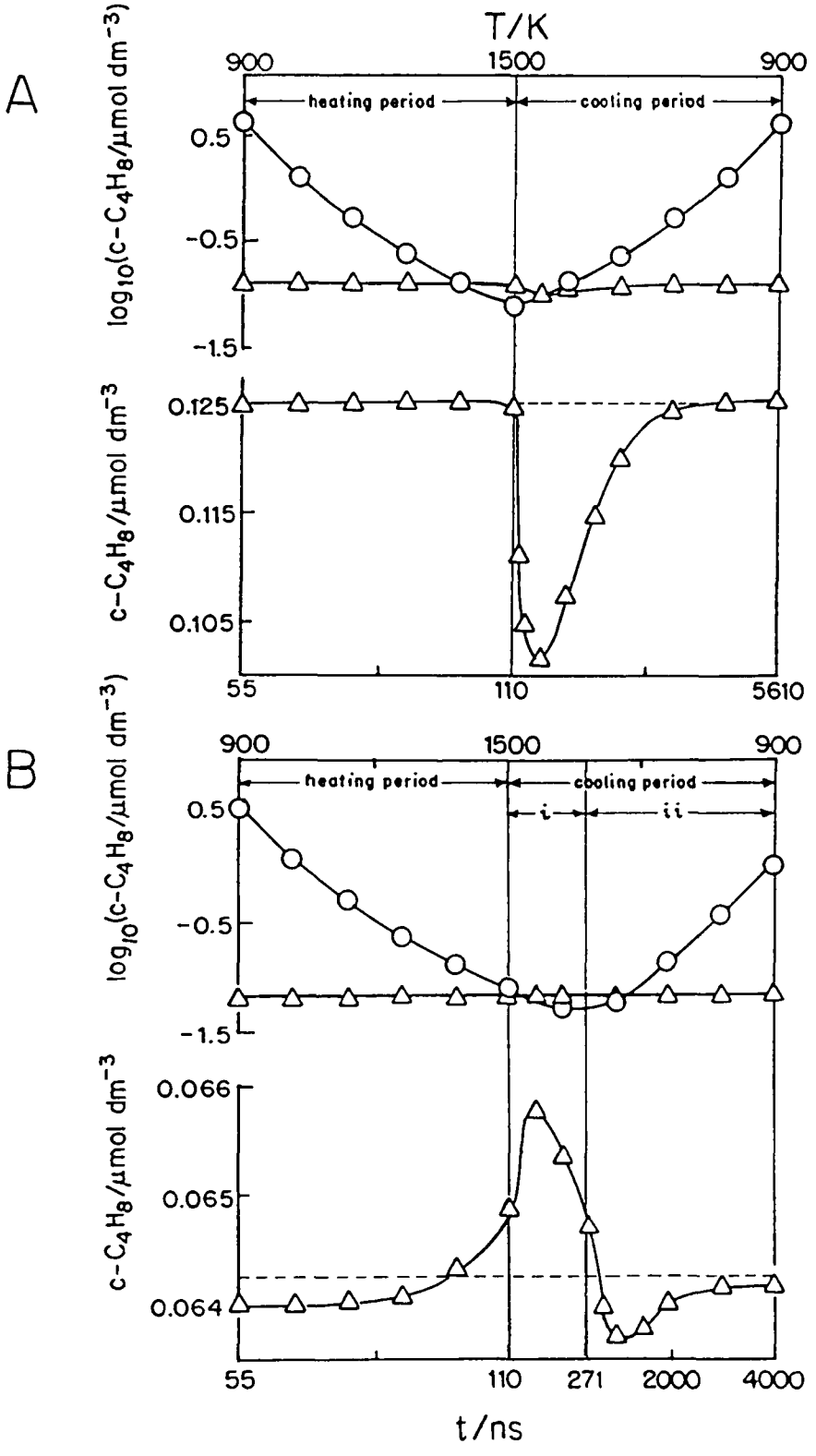
A
T/K
900
1500
900
heating period
cooling period
0.5
-0.5
-1.5
log10(c-C4H8/μmol dm-3)
0.125
0.115
0.105
c-C4H8/μmol dm-3
55
110
5610
B
900
1500
900
heating period
cooling period
i
ii
0.5
-0.5
-1.5
log10(c-C4H8/μmol dm-3)
0.066
0.065
0.064
c-C4H8/μmol dm-3
55
110
271
2000
4000
t/ns

concentration of cyclobutane are shown on an expanded linear scale. This demonstrates that the constant final value following a series of pulses corresponds neither to an equilibrium nor to a normal steady-state. During the heating-cooling cycle, there are both increases and decreases in the cyclobutane concentration, corresponding to times when the concentration is below and above its equilibrium value, and the constant final value is reached when the net change, over the entire cycle, is zero. It is important to understand the nature of this constant final value, as it will be seen that this is what will be measured in a multipulse experiment.

Table 6 shows constant final values obtained from multipulse calculations under the limiting cases of constant volume and constant pressure of gas, at ethylene pressures in the range 500-3000 Torr and at maximum temperatures of 1000, 1250 and 1500 K. These calculations were performed assuming a cooling rate of the gas one hundred times slower than the heating rate. Also shown are "effective reaction temperatures" obtained by assuming that the constant final values are in fact equilibrium values. These temperatures were obtained from plots of the equilibrium cyclobutane concentration as a function of temperature. An example is shown in Figure 25 for assumptions of constant volume and of constant pressure, the latter data corrected to the original volume at 300 K. The equilibrium cyclobutane concentrations for constant volume lie above those for constant pressure because of the increase in volume with increasing temperature in the latter case, with a consequent decrease in ethylene concentration. For the case of constant volume heating followed by adiabatic expansion, no simple relation exists between equilibrium concentration of cyclobutane and temperature because of the complex asymmetric dependence of volume on temperature.

Table 6. Calculated constant final cyclobutane concentrations.

Case I (constant volume)

T_{max} = 1000 K

C_2H_4/Torr	c-C_4H_8/μmol dm^{-3}	T_{eff}/K
500	4.92×10^{-1}	970
1000	1.96	970
2000	7.89	970
3000	$1.77 \times 10^{+1}$	970

T_{max} = 1250 K

C_2H_4/Torr	c-C_4H_8/μmol dm^{-3}	T_{eff}/K
500	8.65×10^{-2}	1200
1000	3.46×10^{-1}	1200
2000	1.40	1200
3000	3.12	1200

T_{max} = 1500 K

C_2H_4/Torr	c-C_4H_8/μmol dm^{-3}	T_{eff}/K
500	3.13×10^{-2}	1390
1000	1.25×10^{-1}	1390
2000	5.01×10^{-1}	1390
3000	1.13	1390

Case II (constant pressure)

T_{max} = 1000 K

C_2H_4/Torr	c-C_4H_8/μmol dm^{-3}	T_{eff}/K
500	1.53×10^{-1}	970
1000	6.16×10^{-1}	970
2000	2.46	970
3000	5.54	970

T_{max} = 1250 K

C_2H_4/Torr	c-C_4H_8/μmol dm^{-3}	T_{eff}/K
500	2.19×10^{-2}	1200
1000	8.73×10^{-2}	1200
2000	3.49×10^{-1}	1200
3000	7.86×10^{-1}	1200

T_{max} = 1500 K

C_2H_4/Torr	c-C_4H_8/μmol dm^{-3}	T_{eff}/K
500	6.82×10^{-3}	1390
1000	2.72×10^{-2}	1390
2000	1.09×10^{-1}	1390
3000	2.45×10^{-1}	1390

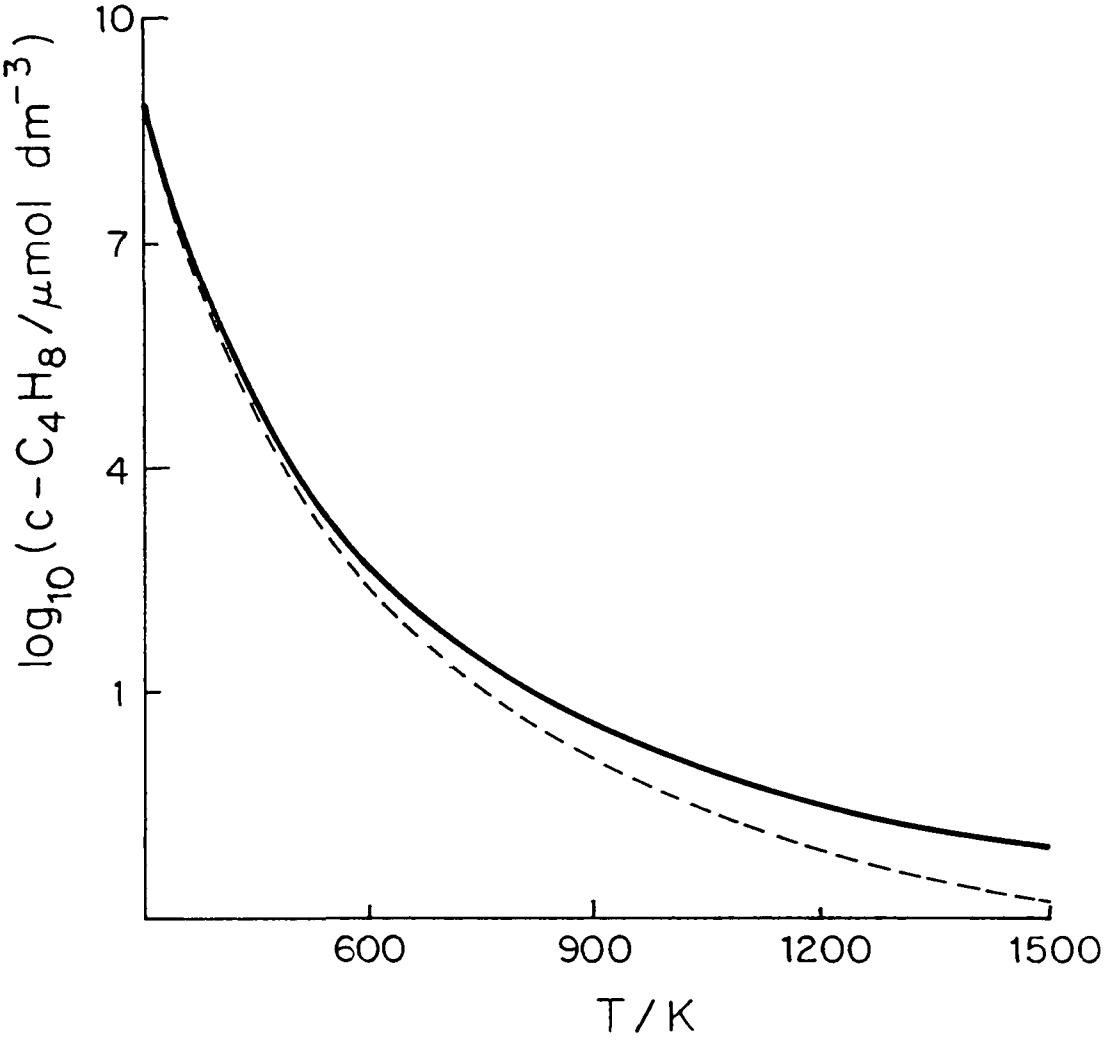

Figure 25. Equilibrium cyclobutane concentration as a function of temperature for an initial ethylene pressure of 1000 Torr at 300 K.

—: Case I (constant volume)
---: Case II (constant pressure)

Values in Case II have been corrected to gas volume at 300 K (see text).

For the two limiting assumptions about the thermal expansion of the heated gas (constant volume and constant pressure), Table 6 shows that at a specific T_{max}, identical "effective reaction temperatures" were obtained even upon changing the ethylene pressure. This result lends further support to the previous observation made concerning the unimportance of ethylene pressure in establishing the constant final cyclobutane concentrations used in the calculations of the "effective reaction temperatures". Furthermore, very similar "effective reaction temperatures" were obtained in the range of 1000 to 1500 K for the two limiting assumptions considered.

The "effective reaction temperatures" in Table 6 were all found to be somewhat lower than T_{max} since the calculated constant final cyclobutane values exceeded the true equilibrium values. The "effective reaction temperature" may be regarded as a sort of weighted average temperature at which the bulk of the reaction occurs during a heating-cooling cycle.

A. Discussion of the cooling mechanisms in ethylene heated with a pulsed CO_2 laser

The cooling of a pulsed laser-heated gas is a very complex process and some aspects of this phenomenon have been discussed in the literature [18,36,37,48,80-87]. At very low pressures, cooling most likely occurs by simple thermal diffusion; but at high pressures, such as used in the present study, other cooling mechanisms become important. Among these are cooling by adiabatic expansion and by thermal conduction. The more rapid of these two mechanisms is cooling by adiabatic expansion.

Three questions are important in a consideration of the relation of the rate of cooling to the rate of the chemical reaction:

(1) Does expansion of the gas occur during the laser pulse?

(2) What is the relation between the time taken for cooling by expansion and the duration of the laser pulse?

(3) To what extent does the cooling by expansion reduce the rate of the reaction?

Only very approximate answers to these questions will be attempted here, but the discussion may nevertheless serve to clarify the characteristics of the system.

To answer the first question, the duration of the laser pulse must be compared to the time required for the gas to expand through a distance comparable to the reaction zone.

The pulse from the CO_2 laser used in this investigation consisted of an initial spike of 110 ns (FWHM), containing about 75% of the energy, followed by a short exponential tail of about 500 ns duration and containing approximately 25% of the energy (Figure 4).

The absorption measurements obtained in the short cell (cell B, $l = 0.051$ cm) revealed that at pressures of ethylene in the range 500-3000 Torr, the laser pulse energy was entirely absorbed in a "thin disc" of gas near the front window of the reaction vessel (Figure 18). This "thin disc" defines an "effective reaction zone" whose thickness will depend on the pressure, the absorption coefficient and the activation energy of the reaction concerned. For such a thin disc, to a first approximation, expansion of the heated gas can be considered to occur in a single dimension along the laser beam axis. The thickness of the "effective reaction zone" is assumed to be given by the distance l_1 from the front window, where the rate of reaction of

the radical-chain decomposition of ethylene and of the formation of cyclobutane, which both require an activation energy of about 190 kJ mol^{-1}, have decreased by two orders of magnitude relative to that at the front window. Taking, for example, the temperature at the window to be 1330 K (at 1000 Torr C_2H_4, for an incident fluence of 0.65 J cm^{-2}, at which ϵ_{eff} = 51 M^{-1} cm^{-1}), the temperature at l_1 will be 1050 K. From the temperature profile calculated, assuming no energy loss during the pulse and no expansion of the gas during the pulse, the distance l_1 = 0.075 cm was obtained. If it is now assumed that the gas expands at the speed of sound, which for an average temperature of 1190K is given by $c_s = [(\bar{\gamma}_{1190K} \times RT)/M]^{\frac{1}{2}}$, equal to 6.2 x 10^4 cm s^{-1}, then the time for expansion over a distance corresponding to the reaction zone is, t = 0.075 cm/6.2 x 10^4 cm s^{-1} = 1.2 x 10^{-6} s, about 11 times longer than the laser pulse. It may be concluded that the initial absorption and thermalization of the absorbed energy is fast compared to expansion of the gas, and that little expansion occurs during the pulse.

The second question requires an estimate of the time taken for cooling of the gas by adiabatic expansion. The magnitude of the cooling by this process was shown in Case III of the model calculations. For an initial temperature of 1000 K, the temperature decrease in ethylene will be about 65 K. In the case of a reaction requiring an activation energy of 190 kJ mol^{-1}, which is approximately that of the radical-chain decomposition of ethylene and of the formation of cyclobutane, this type of cooling would result in a decrease in the reaction rate by about a factor of 5 relative to its maximum rate at the front window of the cell. Further cooling of the gas down to a temperature of about 835 K where the reaction rate has decreased by a factor of

100 relative to that at the entrance window, and hence below which effectively no decomposition of ethylene would occur, would take place by thermal conduction to, and mixing with, the surrounding cold gas [84]. Adiabatic expansion will proceed until the pressure gradient between the hot and cold regions has been removed. Even though the drop in temperature caused by the expansion is relatively small, the gas in the "effective reaction zone" will expand to a volume approximately proportional to the increase in pressure caused by the initial heating at constant volume. Starting at 300 K, heating to a maximum temperature of 1330 K gives an increase in pressure by a factor of 4.43 and hence a similar increase in volume after expansion. Considering only axial expansion, this corresponds to a distance of $3.43l_1$. The time required for cooling by expansion from l_1 to $4.43l_1$ is $t = 3.43l_1/6.2 \times 10^4$ cm $s^{-1} = 4.1 \times 10^{-6}$ s. For ethylene pressures higher than 1000 Torr, with the same incident fluence (0.65 J cm^{-2}), since ϵ_{eff} will be larger, and the energy absorbed also larger, the temperature at the window will be higher. In this situation, the time required for expansion will be shorter. On the other hand, for a higher temperature but at a constant ethylene pressure, the reaction volume will be greater and the time for expansion will be longer.

Cooling by expansion therefore requires times appreciably longer than the duration of the laser pulse. Furthermore, as indicated earlier for a reaction requiring an activation energy of 190 kJ mol^{-1}, since cooling by expansion reduces the rate only by factors of about 5 and 2.5 for initial temperatures of 1000 and 1500 K respectively, reaction will persist after the pressure gradient has been removed. The characteristics of the system are therefore most closely described by Case III of the model, where no expansion occurred during

the pulse and cooling took place first by expansion followed by thermal conduction. (See also Appendix B, p. 217).

The estimates made in this section are of course greatly over-simplified, but are in agreement with the conclusions of a study using the thermal lens effect. This effect occurs when a radial temperature gradient is established in a gas, which by expansion produces a density gradient. In a recent application of this effect to estimate transient temperatures in IRMP reaction of cyclobutanone at pressures from 1 to 10 Torr, Guckert and Carr [86] found that density changes in this gas were delayed by several microseconds following the initiating CO_2 laser pulse. The density gradients were measured by following the intensity of a He-Ne probe laser beam, coaxially aligned with the CO_2 laser.

B. Importance of shock waves in the present system

The rapid heating of the gas during the laser pulse can produce a large pressure gradient and the subsequent expansion will cause a weak shock wave to propagate through the remainder of the gas in the reaction cell. For example, for a maximum temperature of 1500 K the maximum pressure generated, if expansion during the pulse is neglected, will be 5 times the initial pressure. Benson [88] has calculated properties of shock waves traveling in N_2 at STP. For a ratio of pressures of 5 across the shock front, a temperature increase of about 200 K would result from the passage of the shock wave. In ethylene, the rise in temperature will be smaller than for nitrogen, probably somewhat less than 100 K, because of its greater heat capacity. In the present experiments, such an increase in temperature will be unimportant in

the dissociation of ethylene outside the initially heated zone.

Shock wave generation in gases by pulsed lasers has been discussed extensively in the literature [18,36,37,80-87], and it has generally been concluded that chemical effects are usually negligible. Reheating of the laser-heated gas by reflected shock waves is the most probable cause of complications, but several factors will tend to minimize this possibility in the present system:

(1) The initial pressure gradient generated by the laser pulse is not a sharp discontinuity as in a true shock front, but is an exponential gradient dictated by Lambert's law (see Figure 18, in the absorption measurements section).

(2) The shock front will spread radially into the gas outside the laser beam which with the present reaction vessel allows an increase in cross-section of a factor of 4; the shock front will weaken, rather than sharpen up to a planar front as it does in propagating through a shock tube where it is constrained by the tube walls.

(3) There is no continuous driving force behind the shock as there is in a shock tube with a massive volume of driver gas. The entire driving force and energy in the present system comes from the adiabatic expansion of a minute volume of hot gas, which will be complete in 1 or 2 μs.

From all these considerations, it seems unlikely that shock waves play a significant part in the chemistry in the present studies.

EXPERIMENTAL MEASUREMENTS OF CYCLOBUTANE

As mentioned earlier, cyclobutane was indeed a product of the decomposition of ethylene by a pulsed CO_2 laser, and under some conditions it was found to reach a constant value after a sequence of pulses. Plots of the experimental yields of cyclobutane obtained at C_2H_4 pressures of 500-3000 Torr irradiated with the 10 P(14) laser line at an average incident fluence of 0.45 ± 0.02 J cm^{-2} are shown in Figure 26. A second set of experimental yields of cyclobutane obtained at C_2H_4 pressures of 1000-3000 Torr also irradiated with the 10 P(14) laser line, but this time with an average incident fluence of 0.67 ± 0.07 J cm^{-2}, are shown in Figure 27. The constant final values of cyclobutane concentration for various pressures and incident fluences are summarized in Table 7. From the two sets of experiments at fluences of 0.45 ± 0.02 J cm^{-2} (500-3000 Torr) and 0.67 ± 0.07 J cm^{-2} (1000-3000 Torr), the constant final concentration of cyclobutane was proportional to $[C_2H_4]^{1.8}$.

Some experiments were also made with the 10 P(12) line, but the cyclobutane failed to reach a constant value even after as many as 3000 pulses. The lower temperature reached by the ethylene at this laser line, because of the smaller absorption coefficient, is consistent with a slower approach to a steady value.

Also in Table 7 are "effective reaction temperatures" derived from the constant final concentrations of cyclobutane assuming these to be equilibrium values, and reading the temperatures from plots such as those in Figure 25, as before. The "effective reaction temperatures" estimated under the assumption of constant volume are approximately 200 K above those found under the assumption of constant pressure, reflecting the lower calculated equilibrium

Figure 26. Experimental yields of cyclobutane as a function of number of pulses. 10 P(14) line, $F_0 = 0.45 \pm 0.02$ J cm^{-2}.

A: 500 Torr
B: 1000 Torr
C: 2000 Torr
D: 3000 Torr

---: estimated constant final value.

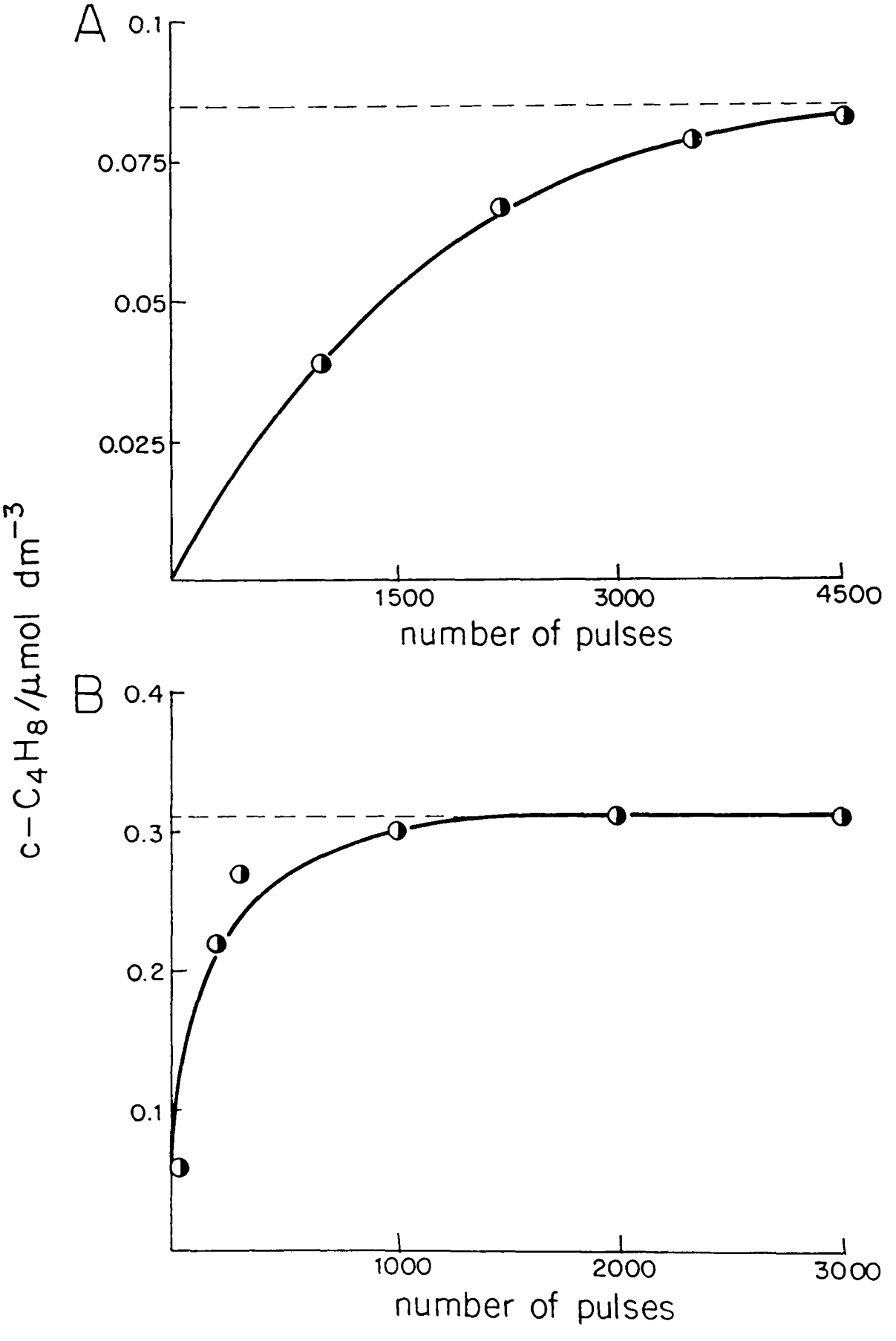
A
0.1
0.075
0.05
0.025
1500
3000
4500
number of pulses
B
0.4
0.3
0.2
0.1
1000
2000
3000
number of pulses
c-C4H8/μmol dm-3

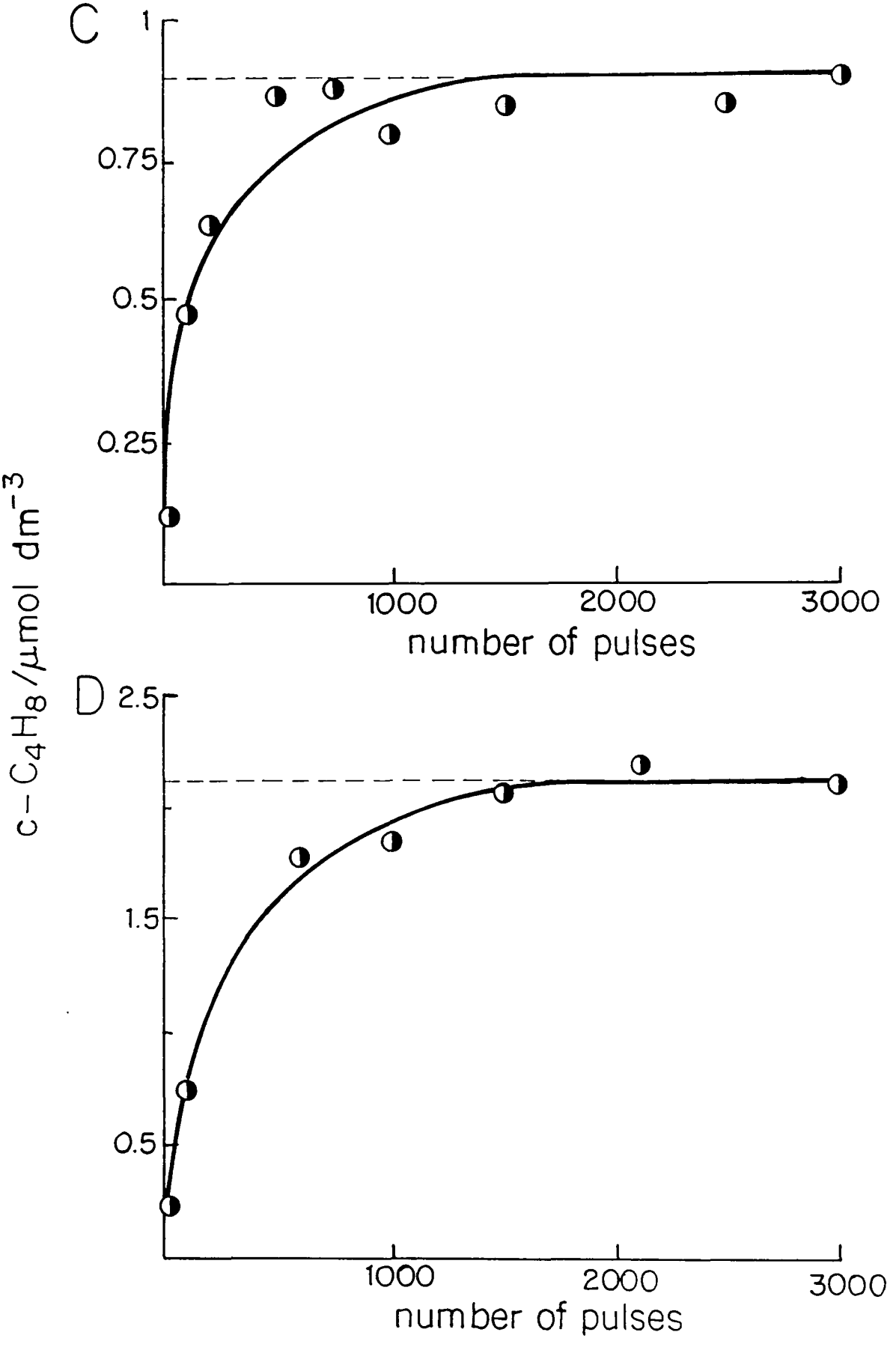
C
1
0.75
0.5
0.25
1000
2000
3000
number of pulses
D
2.5
1.5
0.5
1000
2000
3000
number of pulses
c – C4H8 /μmol dm-3

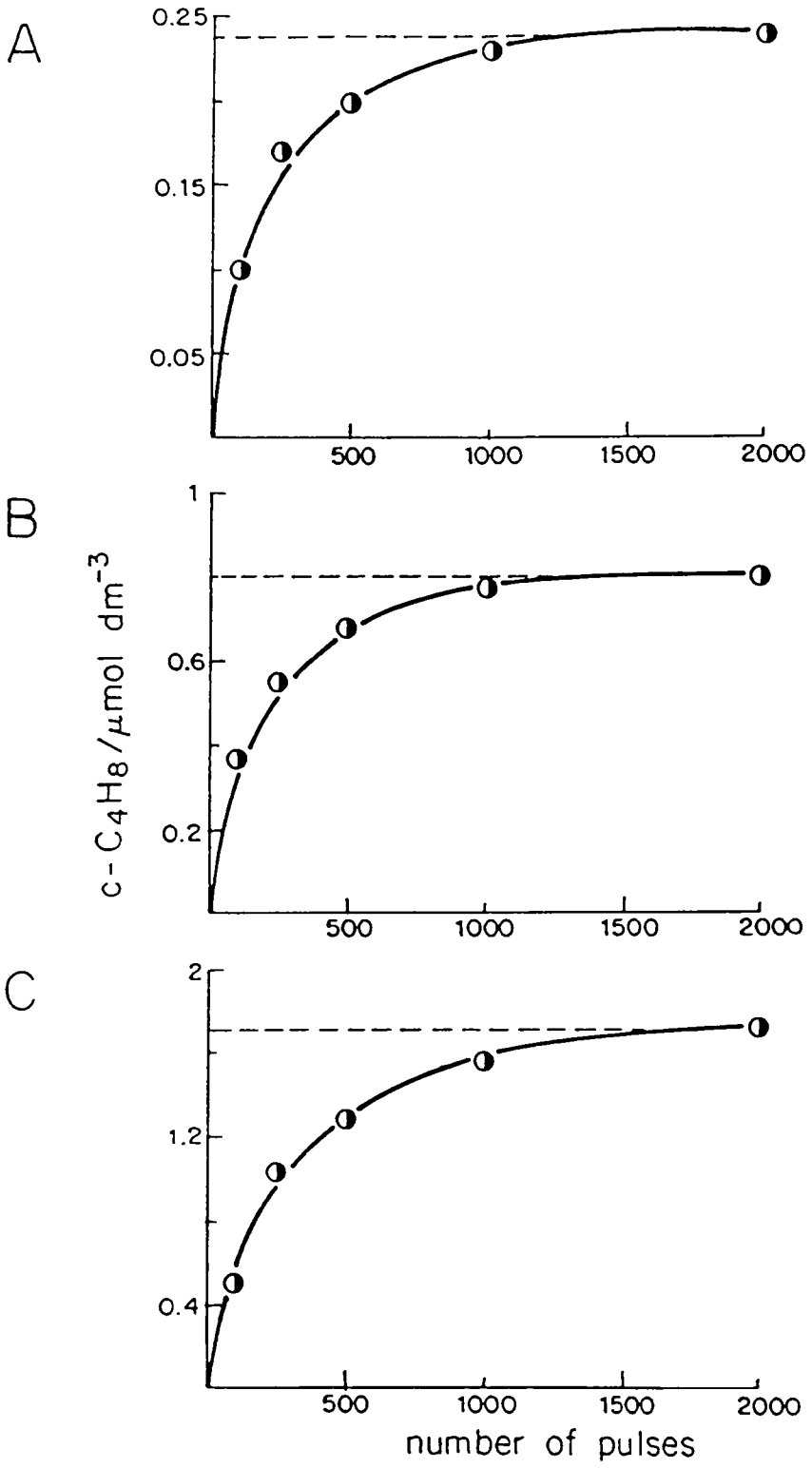

Figure 27. Experimental yields of cyclobutane as a function of number of pulses. 10 P(14) line, $F_0 = 0.67 \pm 0.07$ J cm^{-2}.

A: 1000 Torr
B: 2000 Torr
C: 3000 Torr

---: estimated constant final value.

Table 7. Experimental constant final cyclobutane concentrations.

500 Torr

$c\text{-}C_4H_8$/μmol dm^{-3}	F_0/J cm^{-2}	T_{eff}/K		T_{window}/K		T_{eff}/T_{window}	
		constant volume	constant pressure	constant volume	constant pressure	constant volume	constant pressure
0.085	0.43	1200	1030	1000	930	1.20	1.11

1000 Torr

$c\text{-}C_4H_8$/μmol dm^{-3}	F_0/J cm^{-2}	T_{eff}/K		T_{window}/K		T_{eff}/T_{window}	
		constant volume	constant pressure	constant volume	constant pressure	constant volume	constant pressure
0.31	0.45	1220	1040	1180	1110	1.03	0.93
0.24	0.69	1260	1070	1320	1240	0.95	0.86
0.19	0.97	1310	1090	1380	1300	0.95	0.84

2000 Torr

$c\text{-}C_4H_8$/μmol dm^{-3}	F_0/J cm^{-2}	T_{eff}/K		T_{window}/K		T_{eff}/T_{window}	
		constant volume	constant pressure	constant volume	constant pressure	constant volume	constant pressure
0.90	0.47	1280	1070	1350	1270	0.95	0.84
0.80	0.57	1300	1090	1370	1300	0.95	0.84

3000 Torr

$c\text{-}C_4H_8$/μmol dm^{-3}	F_0/J cm^{-2}	T_{eff}/K		T_{window}/K		T_{eff}/T_{window}	
		constant volume	constant pressure	constant volume	constant pressure	constant volume	constant pressure
2.10	0.43	1270	1070	1400	1310	0.91	0.82
1.90	0.58	1290	1090	1500	1420	0.86	0.76
1.85	0.63	1290	1090	1530	1440	0.84	0.76
1.71	0.75	1310	1090	1610	1520	0.81	0.72

concentrations in the latter case as seen in Figure 25 and discussed previously. The effect of increasing incident fluence on the constant final cyclobutane concentrations is also shown in Table 7. The decreasing trend in the constant final cyclobutane concentrations with increasing fluence is consistent with an increase in temperature of the gas.

The cyclobutane concentrations shown in Figures 26 and 27 and Table 7 were measured by analyzing the entire contents of the reaction cell. The fact that these reach a constant value implies that the entire vessel must become equilibrated with the much smaller reaction zone. This would occur by diffusion and probably convection following each pulse, and would increase the number of pulses needed to reach a constant value. The constant final cyclobutane concentration, however, should not be affected and should be determined by the reactions occurring in the reaction zone, as in the multipulse calculations.

For comparison with T_{eff}, maximum temperatures at the front window, T_{window}, immediately after the pulse, were calculated from heat capacity data and the measured absorption coefficients, under both limiting assumptions about thermal expansion of the gas during the pulse and assuming no energy loss during the pulse. These values are shown in Table 7 together with values of the ratio T_{eff}/T_{window}.

A. Comparison of T_{eff} with T_{window}, and comparison with model

Figure 28 shows values of T_{eff}/T_{window} obtained from the experiments and the model as a function of T_{window}. Values of the ratio for the assumption of constant volume are closer to 1, and closer to the model

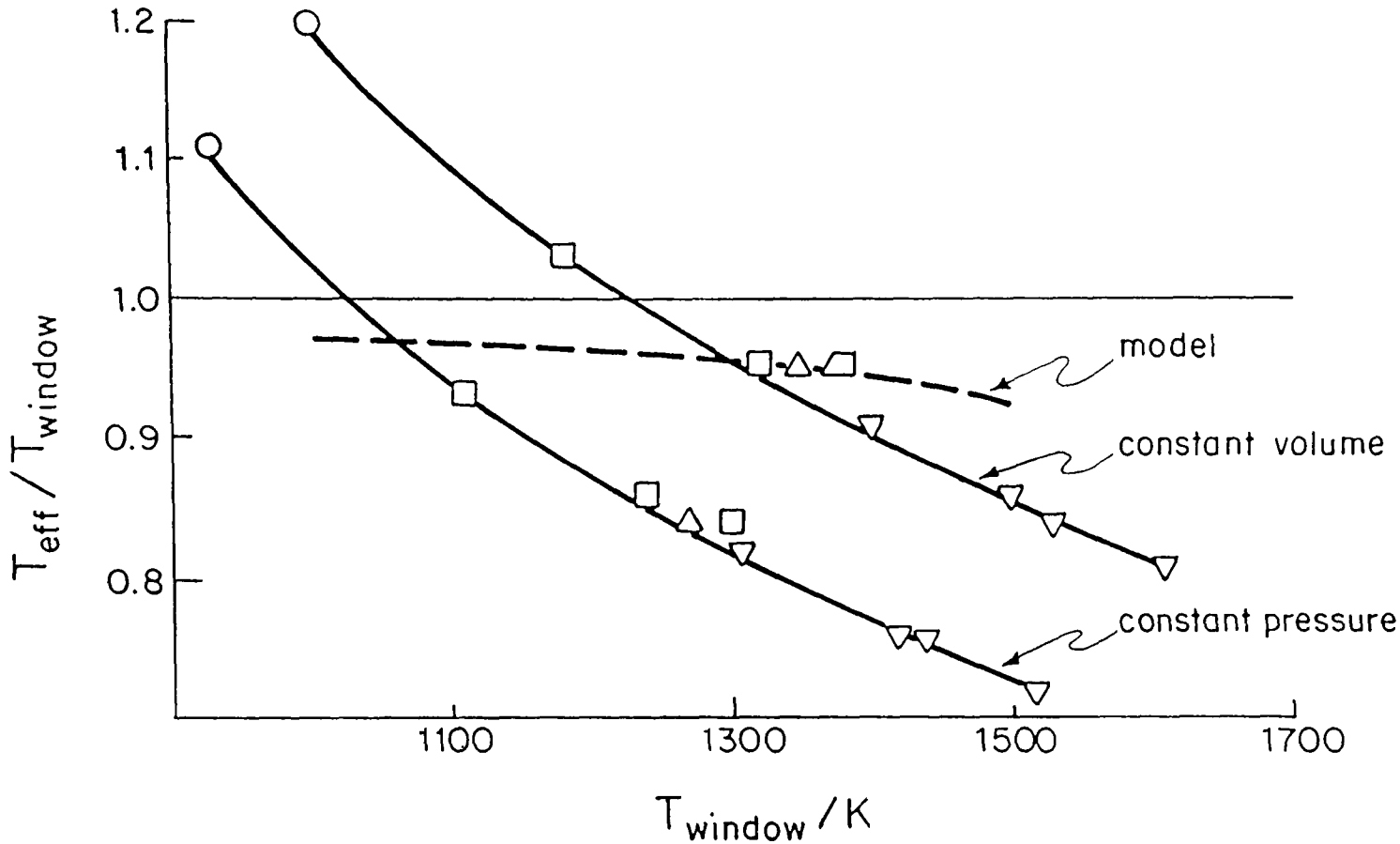

Figure 28. Values of the ratio T_{eff}/T_{window} obtained from the experiments.

For the assumptions of constant volume and pressure,

○ : 500 Torr
□ : 1000 Torr
△ : 2000 Torr
▽ : 3000 Torr

---: Predictions from the model between 1000 and 1500 K assuming $T_{max} = T_{window}$.

values, than are those for the assumption of constant pressure. Since the model predicts no difference between constant volume and constant pressure, the better fit of the former may be construed as evidence that the system is in fact closer to constant volume than constant pressure conditions. This is supported by estimates of the time required for expansion of the heated gas compared to the pulse duration.

The ratio T_{eff}/T_{window} decreases with increasing T_{window}. What at first sight in Table 7 appears to be a pressure dependence is seen in fact (see Figure 28) to be a temperature dependence, since for a given fluence, T_{window} increases with pressure because of an increase in ϵ_{eff} with pressure. Overlapping data at 3 pressures with T_{window} between 1300 and 1400 K show that there is little if any pressure dependence per se of the ratio.

The model calculation gives values of T_{eff}/T_{max} always less than unity, and decreasing with increasing T_{max}. The decrease in the experimental T_{eff}/T_{window} ratio with T_{window} is in the same direction as that from the model but perhaps 8 times larger in magnitude. Values of the ratio T_{eff}/T_{window} at T_{window} below 1225 K are greater than unity, which never occurs with the model.

Differences between the model and the experiment which might account for these differences between the ratios of T_{eff} to T_{window} and T_{max} must be considered. The chief obvious difference is that the model assumes *homogeneous uniform heating of the gas sample, while in the experiment*, there are large axial temperature gradients, and perhaps temperature variations across the laser beam. In the model, temperature varies with time, and T_{eff} falls below T_{max} because the equilibration reactions, (5) and (-5), occur to a substantial extent at temperature below T_{max}, both in the heating and cooling

portions of the cycle, mostly in the latter (see Figure 24A-B). Hence the effective temperature of the reaction is less than T_{max}. In the experimental measurements, because of the temperature gradients in space and time, there will be much more gas at temperatures below T_{window} than in the model, and T_{eff}, the effective temperature of the equilibration reactions, will be reduced further below T_{window}, as observed. These effects, both in the model and in the experiment, become more important with rising T_{max} (or T_{window}), as the equilibration reactions persist to temperatures further and further below the maximum, thus accounting for the temperature dependence evident in Figure 28.

The increase in the experimental T_{eff}/T_{window} ratio above unity at the lowest temperatures is more difficult to explain. One explanation is that constant final values of cyclobutane were not reached in the experiments; the value reported is lower than it should be and T_{eff} therefore correspondingly higher. The relatively small amounts measured at these low pressures could also lead to a sizeable error in the measurement. A second possibility is that there were substantial variations in T across the laser beam. The measured incident fluence was always an average value for the whole beam, and if parts of it were at substantially higher fluence than others, the higher temperatures resulting from the regions of higher fluence would have a large effect on the equilibrium attained. This effect would be largest at the lowest temperatures, as observed. While the fluence across the beam section was probably moderately flat, as expected for a multimode laser with an aperture selecting a central portion of the beam, and the burn pattern appeared fairly uniform, there could perhaps have been enough variation in fluence to raise the value of T_{eff} above T_{window}, based on the average fluence. A contributing factor

may have been non-uniform fluence on a sub-millimeter scale arising from complex mode patterns that can arise in a multimode laser and which would not show up in a burn pattern. Measurements at the lowest pressure (500 Torr) may also have been affected by incomplete vibrational-translational relaxation; T_{window} would then be underestimated and the points in Figure 28 shifted up and to the left, as observed. See Appendix B, p. 217.

Summary and conclusions:

(a) The model and the experiment are in qualitative agreement, both in values of T_{eff} vs. T_{max} and in the variation of the ratio with temperature.

(b) The better fit of T_{eff} based on constant volume suggests that the experiment is closer to constant volume than constant pressure conditions; this is supported by estimated times for expansion.

(c) There are significant qualitative differences between the model and experiment, which might be explained by temperature gradients in the latter which were not taken into account in the model. (These could be built into a more sophisticated model, but this is beyond the scope of the present work.)

(d) Values of T_{eff} calculated from cyclobutane concentrations for constant volume probably do correspond to a weighted average temperature at which the equilibration reactions were occurring. Cyclobutane therefore acts as an approximate thermometer.

B. Evaluation of the ethylene-cyclobutane system

The experimental finding that cyclobutane indeed reached a steady concentration in the present system enabled the estimation of "effective reaction temperatures". The usefulness of this system as a thermometer is, however, restricted by the following pressure and temperature limitations. It is useful only at a high pressure of ethylene, which favors cyclobutane formation, and where measurable concentrations are attained. If the temperature is too low, the rate of the forward reaction may be too slow to reach equilibrium in reasonable time. On the other hand, if the temperature is too high, the reaction may reach equilibrium in a single pulse, but the equilibration reactions may be so fast that the "equilibrium" concentration effectively follows the temperature of the system as it cools. The final cyclobutane concentration therefore "freezes in" at some temperature well below the maximum value.

Despite numerous accounts of pulsed infrared CO_2 laser experiments carried out under Boltzmann conditions, few systems have been studied which have served as "chemical thermometers", allowing estimates of "effective reaction temperatures" (T_{eff}) and "effective reaction times" (t_{eff}). Most of these systems emphasize the measurement of the rate of the reaction rather than the attainment of an equilibrium. The scope and limitations of these systems have been summarized recently by Moylan and Brauman [89].

The first category of "thermometers" were used primarily to distinguish between "thermal" and "non-thermal" conditions and were therefore qualitative indicators of temperature. The system ethyl acetate-isopropyl bromide described earlier was of this sort [39]. Another example was

perfluorocyclobutane, a molecule whose rate of unimolecular decomposition had been well studied [90]. The temperature calculated from the energy absorbed was compared to the rate of decomposition of c-C_4F_8, to allow conclusions regarding the extent of thermal equilibrium in the system [48].

In the second category were molecules which undergo reaction via two channels. In this case, a measure of the product ratio of the two products formed in the respective channels, and utilization of the known Arrhenius parameters, lead to the temperature required to generate that particular ratio. Examples of molecules in this category are ethyl vinyl ether and cyclobutanone. The limitation of these systems lies primarily in the difference in activation energies between the two channels. Decomposition into both channels will occur only over a limited range of energies. In fact, if the pulse energy is low, then only the channel having the lower activation energy may be observed. For example, with ethyl vinyl ether both channels were observed only with a focussed beam [47] which leads to inhomogeneity in the focal region and enhances the possibility of secondary photochemistry of primary products. Estimation of the temperature is therefore much more difficult compared with estimations using an unfocussed beam. The major problem of the cyclobutanone "thermometer" has been the disagreements about the interpretation of the effects of pressure on the system [89].

FREE-RADICAL CHAIN REACTION PRODUCTS

1. Introduction

Ever since the early work of Marchand in 1842 [91], the thermal decomposition of ethylene, the simplest of the alkene family, has been studied extensively over a wide range of conditions including static and flow systems, shock tubes and laser-induced decomposition. In static systems in the temperature range of 750-925 K and with pressures of 10-600 Torr [92-99], the main products were methane, ethane, propylene, 1-butene and 1,3-butadiene. The minor products included propane, n-butane, trans- and cis-2-butene and cyclobutane (discussed earlier), as well as unsaturated C_5 and C_6 hydrocarbons. Of the main products, all except ethane showed an induction period and the disappearance of ethylene was a second order process with an activation energy of about 170 kJ mol^{-1} [94]. The mechanism of reaction involved a radical chain polymerization initiated by the bimolecular reaction of ethylene [94-99]:

$$C_2H_4 + C_2H_4 \rightarrow C_2H_5^{\cdot} + C_2H_3^{\cdot} \qquad (19)$$

Parallel and interacting sets of addition and abstraction reactions involving the ethyl and vinyl radicals contributed to the chain propagation reactions. It was also shown that dissociation of 1-butene was an important secondary initiation process leading to further reactions [93].

From the decomposition in flow systems between 1000 and 1200 K [100], the main products were the same as those found in static systems, while in the temperature range 1200-1400 K [101] methane and acetylene were obtained in appreciable yields. The reaction was found to be second order [100,101].

The decomposition of low pressures of ethylene (15-20 Torr) (0.47% C_2H_4 + 99.53% Ar) in a shock tube in the temperature range 1380-1780 K yielded mainly hydrogen and acetylene with small amounts of 1,3-butadiene at the lower temperatures, and of methane at the higher temperatures [102]. An appreciable amount of propylene, accounting for about 15 percent of the decomposed ethylene, was formed at the lowest temperatures. The rate of formation of acetylene was first order with respect to ethylene pressure while 1,3-butadiene formation was second order. Authors of these shock tube studies [102-104] have suggested that at temperatures in the range 1300-2300 K, acetylene is formed directly by a molecular reaction,

$$C_2H_4 \rightarrow C_2H_2 + H_2 \qquad (20)$$

and 1,3-butadiene is formed through a short-lived intermediate,

$$C_2H_4 + C_2H_4 \rightarrow (C_4H_8) \rightarrow C_4H_6 + H_2 \qquad (21)$$

Benson and Haugen [105] suggested that a radical chain reaction initiated by the bimolecular reaction, (19), should predominate in the lower temperature range, while elimination of molecular hydrogen, (20), should only be favored at the higher temperature range.

Just, Roth and Damm [106] using the technique of atomic resonance absorption spectrophotometry to analyze for hydrogen atoms showed that at high temperatures (1700-2200 K), C_2H_4 decomposes simultaneously via the molecular and radical pathways:

$$C_2H_4 + M \rightarrow C_2H_2 + H_2 + M \qquad (22)$$

$$C_2H_4 + M \rightarrow C_2H_3^{\cdot} + H^{\cdot} + M \qquad (23)$$

followed by reactions of $C_2H_3^{\cdot}$ and $H^{\cdot}$ radicals:

$$C_2H_3^{\cdot} + M \rightarrow C_2H_2 + H^{\cdot} + M \qquad (24)$$

$$H^{\cdot} + C_2H_4 \rightarrow H_2 + C_2H_3^{\cdot} \qquad (25)$$

$$H^{\cdot} + C_2H_3^{\cdot} \rightarrow H_2 + C_2H_2 \qquad (26)$$

Reaction (22) was reported to have a lower activation energy (E_a = 332 kJ mol^{-1}) than reaction (23), (E_a = 411 kJ mol^{-1}). More recent results obtained by Tanzawa and Gardiner [107] at 2000-2500 K using the laser schlieren technique, supported the conclusions of Just and coworkers [106].

Interactions between the infrared field of a CO_2 laser and ethylene gas have been investigated using continuous [34,108-114] and pulsed lasers [115-126]. Most of the studies using pulsed CO_2 lasers have been made with focussed beams.

Using a focussed beam of 10.6 μm radiation from a 150 W continuous wave CO_2 laser, Bordé, Henry and Henry [108] reported the observation of a yellowish-red emission and formation of tars and carbon-rich products upon irradiating ethylene at pressures between 20 and 760 Torr. Cohen, Bordé and Henry [109] irradiated ethylene at 760 Torr with a 100 W (CW) CO_2 laser and identified as products hydrogen, acetylene, methane, 1,3-butadiene and benzene as well as tars. Similarly Quel and de Hemptinne [110] obtained appreciable amounts of methane, acetylene and 1,3-butadiene, along with smaller yields of heavier products upon irradiating ethylene in the pressure range 100-400 Torr with a focussed (CW) CO_2 laser of 37 W. With a focussed 8W continuous CO_2 laser, Bell, Edwards, Nott and Angus [111] obtained hydrogen, acetylene, 1,3-butadiene, ethane and methane as the main products in the irradiation of ethylene at 760 Torr. Except for the presence of acetylene, their product distribution was similar to that obtained by Halstead and Quinn [93] in a conventional static pyrolysis investigation. Using a focussed 660 W cm^{-2} (CW) CO_2 laser, Tardieu de Maleissye, Lempereur and Marsal [113] obtained the same products as those obtained at temperatures above 1500 K, namely hydrogen, methane, acetylene and 1,3-butadiene.

De Hemptinne and De Keuster [114] studied the effects of vibrational excitation of ethylene by intersecting at right angles a laminar stream of ethylene (1-2 Torr) with a focal region (I ~ 10 kW cm^{-2}) of a 60 W (CW) CO_2 laser focussed with a cylindrical lens. Rapid expansion after the excitation freezes the vibrational motion. The beam of ethylene molecules was sampled through a pinhole at variable distance beyond the excitation zone and analyzed mass spectrometrically. They monitored the ions of mass 26 and 27 with and without excitation of the ethylene. The results were expressed in terms of the enhancement of the signal of the fragments as follows:

$$\Delta_M = (I_M^*/I_{28}^*) \quad (I_M^\circ/I_{28}^\circ) \tag{27}$$

where I^* represents the intensity of a mass signal obtained when the sample is excited and I° is the mass signal without irradiation, and the decay of this enhancement was measured as a function of time after the irradiation. From the effect of O_2 on the decay they concluded that some of the molecules were excited into the triplet state. The conversion to triplet ethylene was estimated to be about 5%. Since the energy required is 340 kJ mol^{-1} [127], activation must have come from a multiple photon excitation process.

Directing a focussed CO_2 laser beam delivering pulses of 1-3 Joules and tuned to the 10 P(20) line at 944.2 cm^{-1} into a reaction vessel containing pressures of ethylene greater than 5 Torr, Bastiaens, De Keuster and de Hemptinne [115] reported a light-emitting and conducting plasma in the focal region of the beam. The sole products of the decomposition were hydrogen and acetylene. Irradiation with an unfocussed beam did not initiate a plasma and no reaction was observed. At very low ethylene pressures (0.1-0.3 Torr), irradiation with a focussed beam tuned to the 10 P(26) line at 938.7 cm^{-1} led to the formation of molecular hydrogen which increased linearly with the

number of pulses. Because V-V relaxation time is long compared to the pulse duration in this pressure range, a multiple photon absorption process occurred.

A number of investigations have been concerned with probing the primary products formed in the IRMPD of ethylene [116-120]. In these studies, the collisionless dissociation of ethylene took place in the focal region of the lens where the beam intensity was approximately 1 GW cm^{-2} and the laser induced fluorescence spectra of some primary products were recorded. A primary dissociation product was identified as the C_2 radical in the low-lying electronic $a^3\pi_u$ state. A mechanism proposed [118] for the formation of these radicals involved the consecutive detachment of two H_2 molecules as follows:

$$C_2H_4 + nh\nu \rightarrow H_2C{=}\ddot{C} + H_2 \quad (28a)$$

$$\rightarrow H\dot{C}\text{-}\dot{C}H + H_2 \quad (28b)$$

$$H_2C{=}\ddot{C} + n'h\nu \rightarrow C_2 + H_2 \quad (29a)$$

$$H\dot{C}\text{-}\dot{C}H + n''h\nu \rightarrow C_2 + H_2 \quad (29b)$$

In a similar study, Avatkhov, Bagratashvili and coworkers [121] found acetylene and ethane as products. Since their work also demonstrated the relatively high threshold (0.7 GW cm^{-2}) for the IR laser-induced dissociation of ethylene, they suggested that this molecule could not be dissociated in unfocussed beams. Using a focussed beam, Peterson, Manning and Braun [122] irradiated a 1% mixture of ethylene in helium with total pressures of 50-200 Torr. Hydrogen and acetylene were the only reaction products. Because products such as CH_4, C_2H_6, C_3H_6, or n-C_4H_{10} were not detected, dissociation of ethylene leading to vinyl radicals and hydrogen atoms was probably not important. Nagai and Katayama [123] also obtained molecular elimination of H_2 to yield acetylene and hydrogen upon irradiating ethylene with a focussed beam in the pressure range of 10-50 Torr. Other workers including the groups of Albrecht,

Hohmann and coworkers [124,125] and of Nemes and Székely [126] have recently reported on the dissociation of ethylene (0.1-30 Torr range) in the focussed region of a CO_2 laser. At a beam intensity at focus of about 0.2 GW cm^{-2}, the first group monitored the production of C_2 radicals via fluorescence measurements at 516 nm, whereas at a lower intensity at focus in the range 10-30 MW cm^{-2} the second group identified acetylene and methane as products.

As summarized above, the decomposition of ethylene by pulsed CO_2 lasers at low pressures has been effected almost exclusively under focussed-beam conditions of high fluence. These rather extreme requirements for exciting this molecule up to its dissociation limit is attributed to factors such as:

(1) The lack of exact coincidence between the laser emission lines and the individual vibration-rotation features in the ethylene spectrum;

(2) A high activation energy for decomposition (E_a ~ 350 kJ mol^{-1}) [105]; and

(3) The relatively inefficient pumping of a small molecule lacking low-frequency vibrations. Investigations of the ethylene dissociation under high IR laser fields have been limited to pressures below approximately 5 Torr, since at higher pressures electrical breakdown leading to the formation of a plasma sets in, preventing further study.

Few studies have been reported using an unfocussed beam [34,110]. Robinson, Moses and Boyd [112] have reported the formation of propylene as the major product upon irradiating ethylene at 25 W of power with an unfocussed (CW) CO_2 laser, while with 40 W they obtained methane, propylene and 1,3-butadiene. Shaub and Bauer [34] described the "laser powered homogeneous pyrolysis" (LPHP) of ethylene by irradiation of a gaseous mixture

made up of 10 Torr SF_6 as sensitizer, and 70 Torr C_2H_4 with a 9.5 W (CW) CO_2 laser tuned to the P(28) line of the 00°1-10°0 emission band. The pyrolysis products were acetylene, ethane, methane and other unidentified hydrocarbons. With this technique, heterogeneous processes occurring at the surfaces of the reaction vessels are eliminated.

As shown from the present work, decomposition of ethylene in the pressure range 500-3000 Torr occurs readily in an unfocussed beam, which yields a much more modest fluence and avoids breakdown. At these high pressures, the decomposition is a bulk thermal process as opposed to the IRMP excitation of isolated molecules observed at low pressures. The reaction proceeds by a free-radical chain mechanism, initiated by the bimolecular reaction of ethylene and leading to the same products as those observed in other thermal decomposition systems.

2. Experimental

The procedure for an irradiation experiment consisted of the following steps: (1) With the required pressure of ethylene in the reaction vessel, irradiations were begun with close monitoring of the incident peak pulse voltage signals with the pyroelectric detector. (2) Regular checks of these were made during the course of irradiations. (3) Following the experiment, the entire contents of the vessel were injected into a Hewlett-Packard F & M model 5750 B research gas chromatograph equipped with a flame ionization detector.

A. Columns used for analysis

The main problem in the analysis of the products was caused by the large quantity of ethylene present, particularly for the measurement of the small yields of cyclobutane among the many C_3 and C_4 hydrocarbon products. The main columns used were a 6 m x 6 mm o.d. column of propylene carbonate (15-20%) on activated F-1 alumina (60-80 mesh) at 273 K, and a tandem column consisting of 8.2 m x 6 mm o.d. of tricresylphosphate (5%) on Chromosorb P-AW (80-100 mesh) (inlet) and a 1.8 m x 3 mm o.d. section of VZ-10 (60-80 mesh) (outlet) at 298 K. The order of elution of the various products from these columns was found by comparing their retention times with those of authentic samples.

Although hydrogen was probably formed in this investigation, it was not quantitatively measured. Ethane, a product of the pyrolysis reaction of ethylene, was in most cases not sufficiently resolved from the large quantities of ethylene to allow measurement. In a few experiments however, ethane was

measured using a tandem column consisting of 3.7 m x 3 mm o.d. of VZ-7 (60-80 mesh) (inlet) and a 4.2 m x 6 mm o.d. section of phenylisocyate on Porasil C (80-100 mesh) (outlet) at 298 K. No attempt was made to measure hydrocarbon products having a carbon number greater than four.

B. Calibrations and corrections

For calibrations, standard mixtures of ethylene with the hydrocarbons required were prepared. Measured pressures of these mixtures were introduced into the reaction vessel, including the small sections of tubing of 0.1 cm bore (about 2 x 5 cm) connected directly to the cell, and the dead volume of both metal Hoke valves. In an irradiation experiment, however, the products are formed only in the vessel and the reaction time is too short to allow appreciable diffusion out of the vessel and into the connecting tubing. Consequently, for the same pressure, a larger amount of compound was analyzed in the calibration procedure. A suitable correction was applied to account for this difference. Calibrations for all measured products were obtained from the slopes of graphs of peak height or peak area as a function of concentration of gas in the vessel. The peaks were recorded on a Texas Instrument (Servo Riter II) recorder. Calibration factors along with retention times are given in Table 8. The products measured included methane, acetylene, ethane (in a few experiments), allene, propylene, propane, cyclobutane, n-butane, 1-butene, 2-butene (trans and cis) and 1,3-butadiene.

Table 8. Calibration factors and retention times of the products*.

product	calibration factor**	retention time/s
CH_4	$8.0 \pm 0.3 \times 10^1$	$4.0 \pm 0.1 \times 10^2$
C_3H_8	$2.2 \pm 0.1 \times 10^3$	$5.2 \pm 0.2 \times 10^2$
C_2H_2	$1.0 \pm 0.05 \times 10^3$	$5.8 \pm 0.3 \times 10^2$
C_3H_6	$2.0 \pm 0.1 \times 10^3$	$6.2 \pm 0.3 \times 10^2$
C_3H_4	$1.8 \pm 0.05 \times 10^3$	$7.7 \pm 0.4 \times 10^2$
n-C_4H_{10}	$2.8 \pm 0.1 \times 10^3$	$8.2 \pm 0.4 \times 10^2$
c-C_4H_8	$2.5 \pm 0.05 \times 10^3$	$1.0 \pm 0.05 \times 10^3$
1-C_4H_8	$2.7 \pm 0.08 \times 10^3$	$1.2 \pm 0.06 \times 10^3$
trans-2-C_4H_8	$2.8 \pm 0.1 \times 10^3$	$1.3 \pm 0.07 \times 10^3$
cis-2-C_4H_8	$2.8 \pm 0.1 \times 10^3$	$1.4 \pm 0.07 \times 10^3$
1,3-C_4H_6	$2.6 \pm 0.07 \times 10^3$	$1.8 \pm 0.09 \times 10^3$

* column: 8.2 m x 6 mm o.d. tricresylphosphate (5%) on Chromosorb P-AW (80-100 mesh) (inlet) and 1.8 m x 3 mm o.d. VZ-10 (60-80 mesh) (outlet) at 298 K.

** For the product methane, the calibration factor is expressed using peak height, arbitrary unit x dm^3 μmol^{-1}, while for the other products, calibration factors are expressed using peak area, mm^2 x dm^3 μmol^{-1}.

3. Results and Discussion

In contrast to the limited products obtained in the irradiation of ethylene at pressures below ~ 5 Torr with focussed CO_2 pulsed laser beams which gave almost entirely the intramolecular decomposition into acetylene and molecular hydrogen [115-126], the present investigation has shown that irradiation of ethylene at high pressures (500-3000 Torr) using the unfocussed beam of a pulsed CO_2 TEA laser gives a wide range of decomposition products. The major products measured were 1,3-butadiene, acetylene, ethane, propylene, 1-butene and methane in decreasing order of importance, while minor products were n-butane, allene, trans- and cis-2-butene, propane and cyclobutane. Only a few measurements of ethane were made using the column described in the experimental section. Its yields were comparable to those of acetylene. With the same column, a few measurements of propane, also not well separated in the regular analysis, showed it to be similar in importance to the 2-butene isomers. Traces of methylcyclopropane (c-$CH_3C_3H_5$), representing about 5% of the cyclobutane, could also be detected in a long irradiation (2000 pulses) of 3000 Torr. Hydrogen, in spite of its possible formation in the present study via the molecular decomposition reaction (20), was not measured. In addition, no attempt was made to measure hydrocarbon products having a carbon number greater than four, although some of these were probably formed under the conditions of the present experiments.

Table 9 shows a typical distribution of the products measured in order of decreasing importance for a 1000 pulse irradiation of 1000 Torr C_2H_4. In this particular experiment, the fraction of the ethylene consumed, based on the carbon content of the products was 0.32%.

Table 9. Product distribution

product	% of total
$1,3\text{-}C_4H_6$	57.6
C_2H_2	17.2
C_3H_6	12.0
$1\text{-}C_4H_8$	6.4
CH_4	4.9
$n\text{-}C_4H_{10}$	0.6
C_3H_4	0.6
$trans\text{-}2\text{-}C_4H_8$	0.3
$cis\text{-}2\text{-}C_4H_8$	0.2
$c\text{-}C_4H_8$	0.2

10 P(14) line, $\tilde{\nu}$ = 949.48 cm^{-1}
Fluence = 0.69 J cm^{-2}

A. Mechanism of reaction

The products obtained in these experiments were similar to those observed in other thermal decomposition systems [92-99] and therefore almost certainly arise from free-radical chain reactions. Two possible initiation processes may be considered: (1) the bimolecular disproportionation reaction of ethylene:

$$2C_2H_4 \rightarrow C_2H_5^{\cdot} + C_2H_3^{\cdot} \qquad (19)$$

and (2) the unimolecular decomposition of ethylene to the vinyl radical and hydrogen atom:

$$C_2H_4 \rightarrow C_2H_3^{\cdot} + H^{\cdot} \qquad (30)$$

Measurement of the rate constant for reaction (19) was reported by Ayranci and Back [99] from studies of the rate of decomposition of ethylene at temperatures in the region of 750 K. Their value was expressed as follows:

$$k_{19}\ (dm^3\ mol^{-1}\ s^{-1}) = 3 \times 10^{11} \exp(-269000/RT) \qquad (31)$$

Although other measurements relating to the endothermicity of reaction (19) suggest that the activation energy should be slightly higher [128], we used this value for the purposes of the comparison described here.

Measurements of the rate constant for reaction (30) have been reported by Just, Roth and Damm [106] and also by Tanzawa and Gardiner [107] from shock-tube studies of the decomposition of ethylene. Both of these measurements, however, were made in a region of pressure where the reaction is pressure-dependent and would therefore not be applicable to the present system. A value for k_{30} was therefore estimated using the bond dissociation energy for the C-H bond in ethylene measured from reaction (19) and a preexponential factor in accord with values estimated by Benson for simple fission reactions [79]. The reverse reaction (-30) was assumed to have no activation energy. The following estimate was obtained:

$$k_{30}\ (s^{-1}) = 1 \times 10^{14} \exp(-431000/RT) \qquad (32)$$

The ratio of the rates of formation of radicals from the bimolecular and from the unimolecular initiation reactions as a function of ethylene pressure (1000-3000 Torr) and average temperatures (1000-1500 K) are given in Table 10. Since it was shown from calculations of temperatures in the irradiation vessel that maximum temperatures achieved did not exceed ~ 1500 K, it can be concluded that reaction (19) is the only important chain initiating step in the present experiments.

Table 10. Values of the ratio of radical chain initiation rates, R_{19}/R_{30}

T/K	C_2H_4/Torr 1000	2000	3000
1000	1.4×10^4	2.8×10^4	4.2×10^4
1250	2.3×10^2	4.6×10^2	6.9×10^2
1500	1.4×10^1	2.8×10^1	4.2×10^1

$2R_{19} = 2k_{19}[C_2H_4]^2$; $2R_{30} = 2k_{30}[C_2H_4]$

A mechanism similar to the one proposed by Back and Martin [96] in their investigation of the ethylene pyrolysis at 773 K accounts for most of the products observed in the present work. The mechanism which includes a series of decomposition, abstraction and addition reactions involving the ethyl and vinyl radicals produced in reaction (19) shows boxes surrounding the final products measured:

$$C_2H_5^{\cdot} \rightleftarrows C_2H_4 + H^{\cdot} \quad (33)$$

$$C_2H_5^{\cdot} + C_2H_4 \rightarrow \boxed{C_2H_6} + C_2H_3^{\cdot} \quad (34)$$

$$C_2H_5^{\cdot} + C_2H_4 \rightleftarrows 1\text{-}C_4H_9^{\cdot} \quad (35)$$

$$1\text{-}C_4H_9^{\cdot} \rightarrow \boxed{1\text{-}C_4H_8} + H^{\cdot} \quad (36)$$

$$1\text{-}C_4H_9^{\cdot} + C_2H_4 \rightarrow \boxed{n\text{-}C_4H_{10}} + C_2H_3^{\cdot} \quad (37)$$

$$1\text{-}C_4H_9^{\cdot} + C_2H_4 \rightarrow 1\text{-}C_6H_{13}^{\cdot} \quad (38)$$

$$1\text{-}C_6H_{13}^{\cdot} \rightarrow \boxed{1\text{-}C_4H_8} + C_2H_5^{\cdot} \quad (39)$$

$$1\text{-}C_6H_{13}^{\cdot} \rightleftarrows 2\text{-}C_6H_{13}^{\cdot} \quad (40)$$

$$2\text{-}C_6H_{13}^{\cdot} \rightarrow \boxed{C_3H_6} + n\text{-}C_3H_7^{\cdot} \quad (41)$$

$$1\text{-}C_6H_{13}^{\cdot} \rightleftarrows 3\text{-}C_6H_{13}^{\cdot} \quad (42)$$

$$3\text{-}C_6H_{13}^{\cdot} \rightarrow 1\text{-}C_5H_{10} + CH_3^{\cdot} \quad (43)$$

$$CH_3^{\cdot} + C_2H_4 \rightarrow \boxed{CH_4} + C_2H_3^{\cdot} \quad (44)$$

$$C_2H_3^{\cdot} \rightarrow \boxed{C_2H_2} + H^{\cdot} \quad (45)$$

$$C_2H_3^{\cdot} + C_2H_4 \rightleftarrows n\text{-}C_4H_7^{\cdot} \quad (46)$$

$$n\text{-}C_4H_7^{\cdot} \rightarrow \boxed{1,3\text{-}C_4H_6} + H^{\cdot} \quad (47)$$

$$n\text{-}C_4H_7^{\cdot} + C_2H_4 \rightarrow \boxed{1\text{-}C_4H_8} + C_2H_3^{\cdot} \quad (48)$$

$$n\text{-}C_4H_7^{\cdot} + C_2H_4 \rightarrow 1\text{-}C_6H_{11}^{\cdot} \quad (49)$$

$$1\text{-}C_6H_{11}^{\cdot} \rightarrow 3\text{-}C_6H_{11} \quad (50)$$

$$3\text{-}C_6H_{11}^{\cdot} \rightarrow \boxed{1,3\text{-}C_4H_6} + C_2H_5^{\cdot} \quad (51)$$

It may be seen that two parallel chain reactions are occurring, propagated by ethyl and vinyl radicals. The former are regenerated by decomposition reactions such as (39) and (51) as well as (36), (45) and (47), followed by addition of $H^{\cdot}$ to ethylene, reaction (-33). Vinyl radicals are regenerated by the abstraction reactions such as (34), (37), (44) and (48). The radical chain reactions would be terminated by the following combination and disproportionation reactions:

$$2C_2H_5^{\cdot} \rightarrow \boxed{n\text{-}C_4H_{10}} \quad (52)$$

$$\rightarrow \boxed{C_2H_6} + C_2H_4 \quad (53)$$

$$H^{\cdot} + C_2H_5^{\cdot} \rightarrow \boxed{C_2H_6} \quad (54)$$

$$\rightarrow H_2 + C_2H_4 \quad (55)$$

$$2C_2H_3^{\cdot} \rightarrow \boxed{1,3\text{-}C_4H_6} \quad (56)$$

$$\rightarrow C_2H_4 + \boxed{C_2H_2} \quad (57)$$

$$C_2H_5^{\cdot} + C_2H_3^{\cdot} \rightarrow \boxed{1\text{-}C_4H_8} \quad (58)$$

$$\rightarrow \boxed{C_2H_6} + \boxed{C_2H_2} \quad (59)$$

$$\rightarrow 2C_2H_4 \quad (60)$$

$$H^{\cdot} + C_2H_3^{\cdot} \rightarrow C_2H_4 \quad (61)$$

$$\rightarrow H_2 + \boxed{C_2H_2} \quad (62)$$

The variety of hydrocarbon products found in the present experiments suggest a decomposition intermediate between shock tube and conventional pyrolysis conditions, and also perhaps occurring over an appreciable range of

temperature. Acetylene and methane are characteristic of temperatures in excess of about 1250 K, while propylene, 1-butene and ethane are characteristic of lower temperatures (~ 750 K). Furthermore, 1,3-butadiene is also an important reaction product which has been obtained both in static pyrolysis studies in the range 750-925 K [92-99] and in a shock-tube investigation conducted at temperatures between 1170 and 1425 K [102]. The products therefore suggest an average effective temperature in the range 1000-1500 K, similar to those found in our earlier treatment of cyclobutane formation.

B. Temperature profile in the vessel and effective reaction volume

An overall activation energy of about 140 to 170 kJ mol^{-1} can be expected for the free-radical chain reaction [94]. This is lower than those for the cyclobutane equilibration reactions, 190 kJ mol^{-1} for E_f, and 262 kJ mol^{-1} for E_r, (refer to Model, page 56), but as in the latter, still large enough to ensure that most of the reaction would take place close to the front window and at temperatures within 200-300 degrees of the maximum temperature at the front window. This is illustrated in Figure 29 and in Table 11 where the temperature and relative rate of reaction are shown as a function of distance from the front window.

For the purpose of the calculations of relative rates which follow in the rest of this section, the reaction volume was chosen to correspond to the distance from the front window at which the rate of the reaction had fallen to 0.01 of its value at the front window. For example, at 1000 Torr with a temperature of 1360 K at the front window (Table 11), the relative rate of reaction becomes 0.01 at a distance 0.088 cm from the front window. The

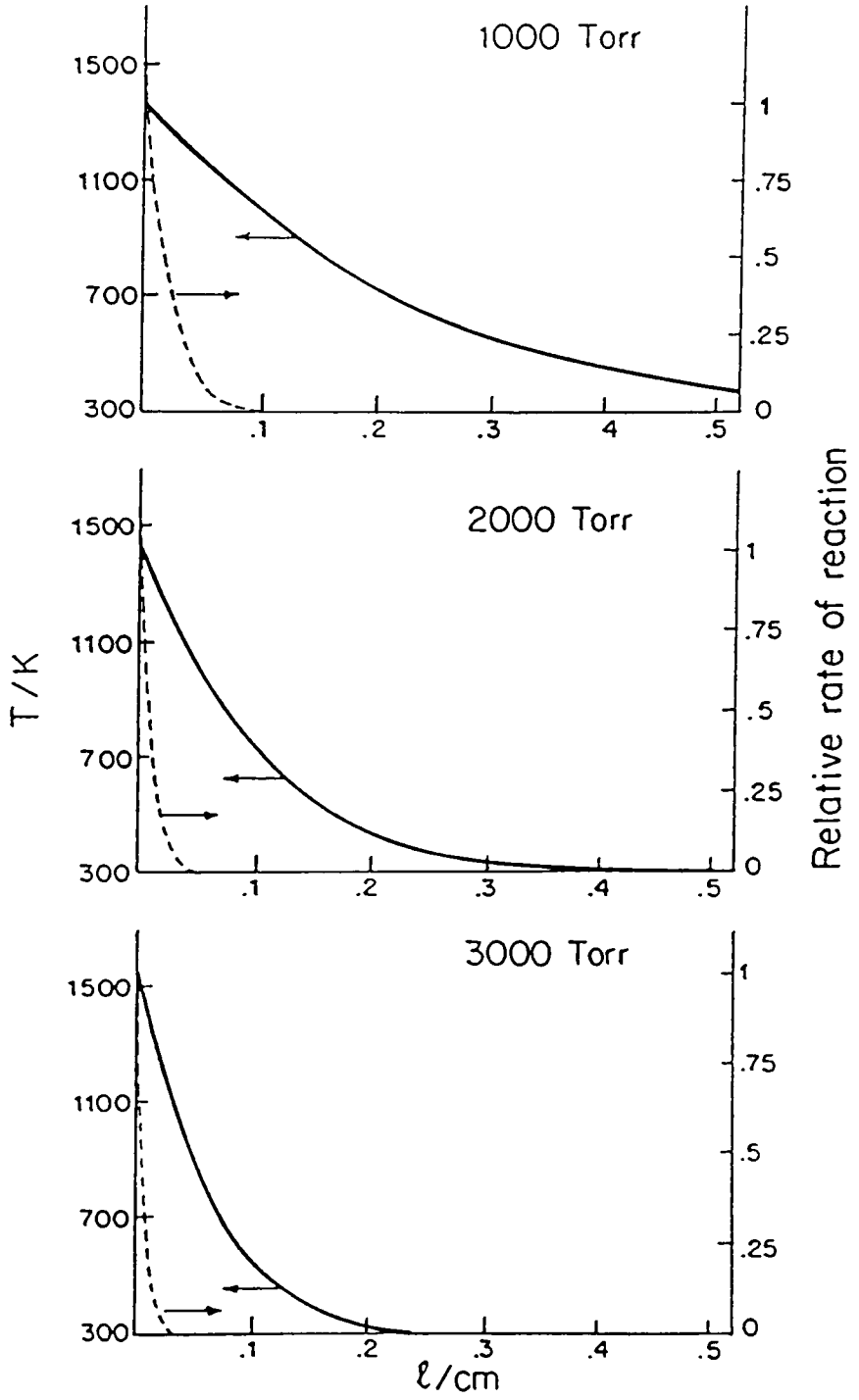

Figure 29. Temperature and relative rate of reaction profiles as a function of distance from the front window in cell A
10 P(14) line, F_0 = 0.67 J cm^{-2}

—: temperature profile
---: relative rate of reaction profile

The relative rate of reaction profiles shown were calculated for a reaction with E_a = 155 kJ mol^{-1}

Table 11. Temperature and relative rate of reaction profiles as a function of distance from the front window in cell A. 10 P(14) line, $F_0 = 0.67$ J cm^{-2}.

1000 Torr

T/K	relative rate*	l/cm
1360	1.0	0.0
1295	0.5	0.016
1235	0.25	0.032
1165	0.1	0.046
1020	0.01	0.088

2000 Torr

T/K	relative rate*	l/cm
1420	1.0	0.0
1350	0.5	0.008
1285	0.25	0.015
1210	0.1	0.024
1050	0.01	0.044

3000 Torr

T/K	relative rate*	l/cm
1550	1.0	0.0
1465	0.5	0.005
1390	0.25	0.010
1300	0.1	0.016
1120	0.01	0.028

* reaction with $E_a = 155$ kJ mol^{-1}

effective volume of reaction is therefore 0.066 cm^3 under these conditions. The measured yields of products are expressed as a concentration based on the total volume of the cell. The actual rate of formation of product in the reaction zone should be based on the concentration in the effective reaction volume, and is therefore given by the following expression:

$$R_{(actual)} = R_{(measured)} \times (V_{vessel}/V_{eff}) \quad (63)$$

where V_{eff} refers to the effective reaction volume estimated for the particular conditions.

C. Molecular decomposition of ethylene

At average effective temperatures between 1000 and 1500 K, reactions (45) and (47) are expected to be major routes for formation of acetylene and 1,3-butadiene. Nevertheless, the possibility of a direct molecular decomposition of ethylene to acetylene should be considered,

$$C_2H_4 \rightarrow C_2H_2 + H_2 \quad (20)$$

From shock-tube studies of the decomposition of ethylene between 1700 and 2200 K where the concentration of H-atoms was monitored by atomic resonance absorption spectroscopy, Just and coworkers [106] reported the following value for k_{20}:

$$k_{20} \ (dm^3\ mol^{-1}\ s^{-1}) = 3 \times 10^{14} \exp(-332000/RT) \quad (64a)$$

Tanzawa and Gardiner [107] reported the following value for k_{20}, also from shock-tube experiments between 2000 and 2500 K using the laser schlieren technique:

$$k_{20} \ (dm^3\ mol^{-1}\ s^{-1}) = 3 \times 10^{14} \exp(-340000/RT) \quad (64b)$$

Again, however, the measurements were made in the pressure-dependent region and thus not applicable to our system. The estimate made by Benson and

Haugen [105] from an interpretation of the shock-tube pyrolysis of ethylene by Skinner and Sokoloski [102] is probably more suitable for our system:

$$k_{20}\ (s^{-1}) = 3 \times 10^{13} \exp(-356000/RT) \qquad (64c)$$

Taking a pressure of ethylene of 1000 Torr where the temperature at the front window was 1360 K, the relative rate of reaction (20) has fallen to 0.01 at a temperature of 1190 K, corresponding to a distance of 0.04 cm from the front window. The effective reaction volume is therefore 0.03 cm^3 The actual rate of formation of acetylene is obtained from the measured rate (3.2×10^{-9} mol dm^{-3} $pulse^{-1}$) as follows:

$$R_{C_2H_2} = 3.2 \times 10^{-9} \text{ mol dm}^{-3} \text{ pulse}^{-1} \times (1.58/0.03)$$
$$= 1.7 \times 10^{-7} \text{ mol dm}^{-3} \text{ pulse}^{-1}$$

At an average temperature of 1275 K, the rate of formation of acetylene via the molecular pathway, (20), calculated from (64c) was 9.8×10^{-4} mol dm^{-3} s^{-1}. Thus, in order for this rate to equal the measured rate of formation, an effective reaction time of $t_{eff} = 1.7 \times 10^{-4}$ s would be required. This is much longer than the time for reaction estimated in the Model section, page 74. Similar calculations at 2000 and 3000 Torr yielded essentially similar results and it may be concluded that reaction (20) did not contribute appreciably to the measured rate of formation of acetylene in the present investigation.

D. Products of the reaction

Most of the irradiations were made using the strongly absorbed 10 P(14) line at 949.48 cm^{-1}, but some experiments were also done with the 10 P(12) line at 951.19 cm^{-1}. The products were similar, but yields were much lower and could not be measured with great accuracy and hence are not reported

here. The smaller yields of products are explained by the weaker absorption and the consequent lower temperatures at the front of the vessel.

i. Effect of irradiation time

Figures 30-32 show the dependence of the products on number of pulses for 1000-3000 Torr ethylene with the laser tuned to the 10 P(14) line. These data are summarized in Tables 12-14. The average incident fluence in this set was $F_0 = 0.67 \pm 0.07$ J cm^{-2}. Every radical chain product shows an induction period, with the rates of formation increasing sharply with irradiation time. Clearly, secondary initiation caused by reactions of the products must be occurring. In a study of the pyrolysis of ethylene at 798-924 K with reactant pressures between 10 and 270 Torr, Halstead and Quinn [93] suggested that the observed self-acceleration in the rates of formation of the products could be accounted for largely by the decomposition of 1-butene:

$$1\text{-}C_4H_8 \rightarrow C_3H_5^{\cdot} + CH_3^{\cdot} \quad (65)$$

for which k_{65} $(s^{-1}) = 1 \times 10^{16} \exp(-312000/RT)$ [129] (66)

The rate of formation of radicals by reaction (65) is therefore

$$2R_{65} = 2k_{65}[1\text{-}C_4H_8]. \quad (67)$$

Of the major products formed in the present experiments, CH_4, C_2H_6, C_2H_2, C_3H_6, $1\text{-}C_4H_8$ and $1,3\text{-}C_4H_6$, $1\text{-}C_4H_8$ is also the least stable towards thermal decomposition. Table 15 gives the rate of dissociation of 1-butene for its various experimental concentrations at 100 and 500 pulses measured in irradiations at ethylene pressures of 1000-3000 Torr, assuming an effective temperature of 1000 K. A comparison between the rate of initiation by reaction (19), R_{19}, with the rate of dissociation of 1-butene (65), R_{65}, shows that at 1000 K, the rate of dissociation of 1-butene becomes comparable to

Figure 30. Yields of products as a function of number of pulses at an ethylene pressure of 1000 Torr.

10 P(14) line, $\tilde{\nu} = 949.48\ cm^{-1}$,
incident fluence = $0.69\ J\ cm^{-2}$.

A. main products

○ : 1,3-butadiene
□ : acetylene
△ : propylene
▽ : 1-butene
◇ : methane

B. minor products

■ : n-butane
● : allene
▲ : trans-2-butene
▼ : cis-2-butene

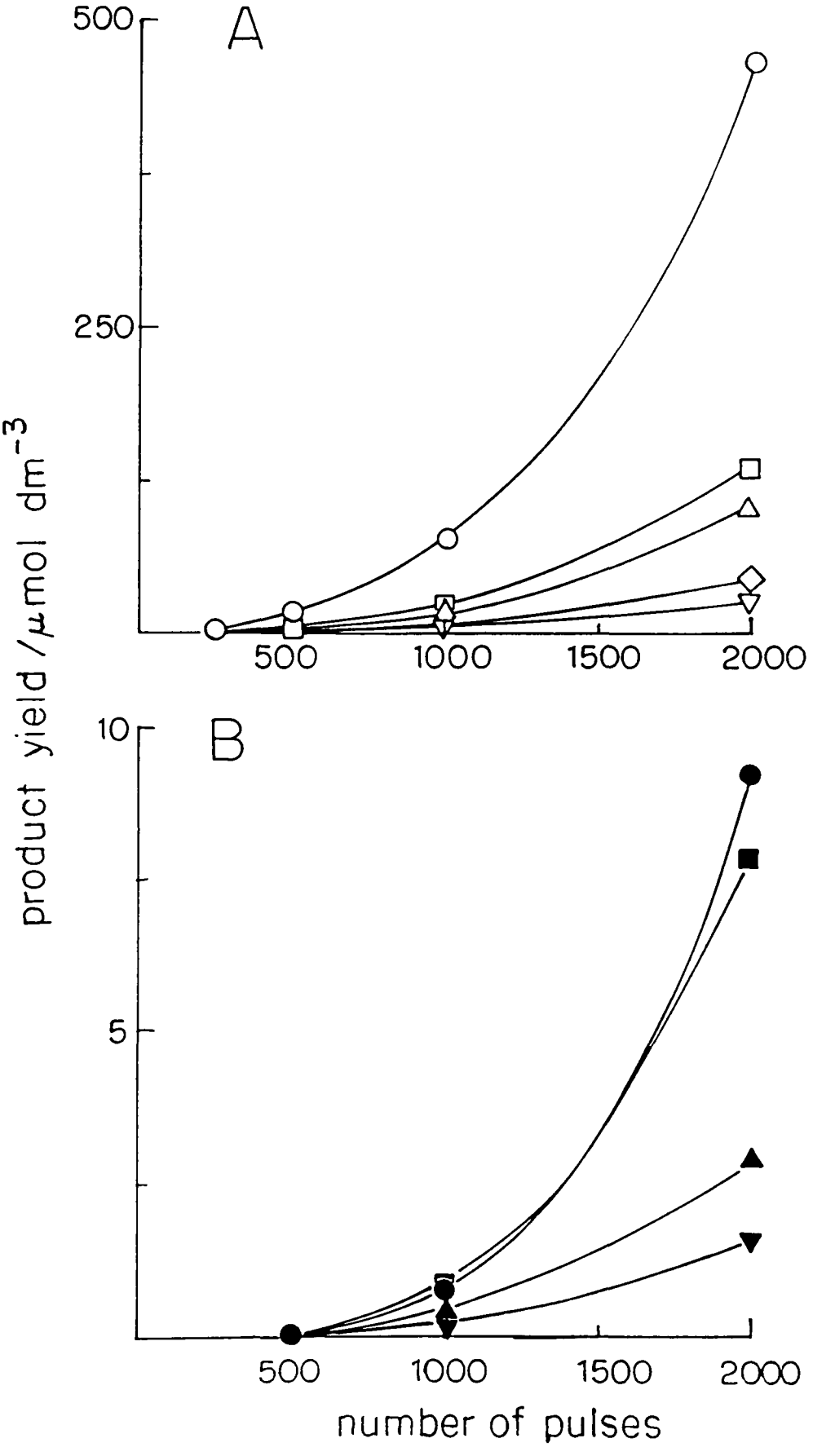
A
500
250
B
10
5
500
1000
1500
2000
product yield /μmol dm^{-3}
number of pulses

Table 12. Yields of products as a function of number of pulses at an ethylene pressure of 1000 Torr. 10 P(14) line, $\tilde{\nu} = 949.48\ cm^{-1}$, $F_0 = 0.69\ J\ cm^{-2}$.

number of pulses	product yield/μmol dm^{-3}								
	CH_4	C_2H_2	C_3H_4	C_3H_6	1,3-C_4H_6	1-C_4H_8	trans-2-C_4H_8	cis-2-C_4H_8	n-C_4H_{10}
100	—	—	—	—	0.33	0.05	—	—	—
250	0.17	0.80	—	0.50	4.5	0.62	—	—	—
500	0.97	4.0	0.05	2.6	18	2.3	0.16	0.09	0.05
1000	6.5	23	0.77	16	77	8.6	0.40	0.22	0.84
2000	44	136	9.2	103	466	26	2.9	1.6	7.8

Figure 31. Yields of products as a function of number of pulses at an ethylene pressure of 2000 Torr.

10 P(14) line, $\tilde{\nu} = 949.48\ cm^{-1}$,
incident fluence = $0.57\ J\ cm^{-2}$.

A. main products

- ○ : 1,3-butadiene
- □ : acetylene
- △ : propylene
- ▽ : 1-butene
- ◇ : methane

B. minor products

- ■ : n-butane
- ● : allene
- ▲ : trans-2-butene
- ▼ : cis-2-butene

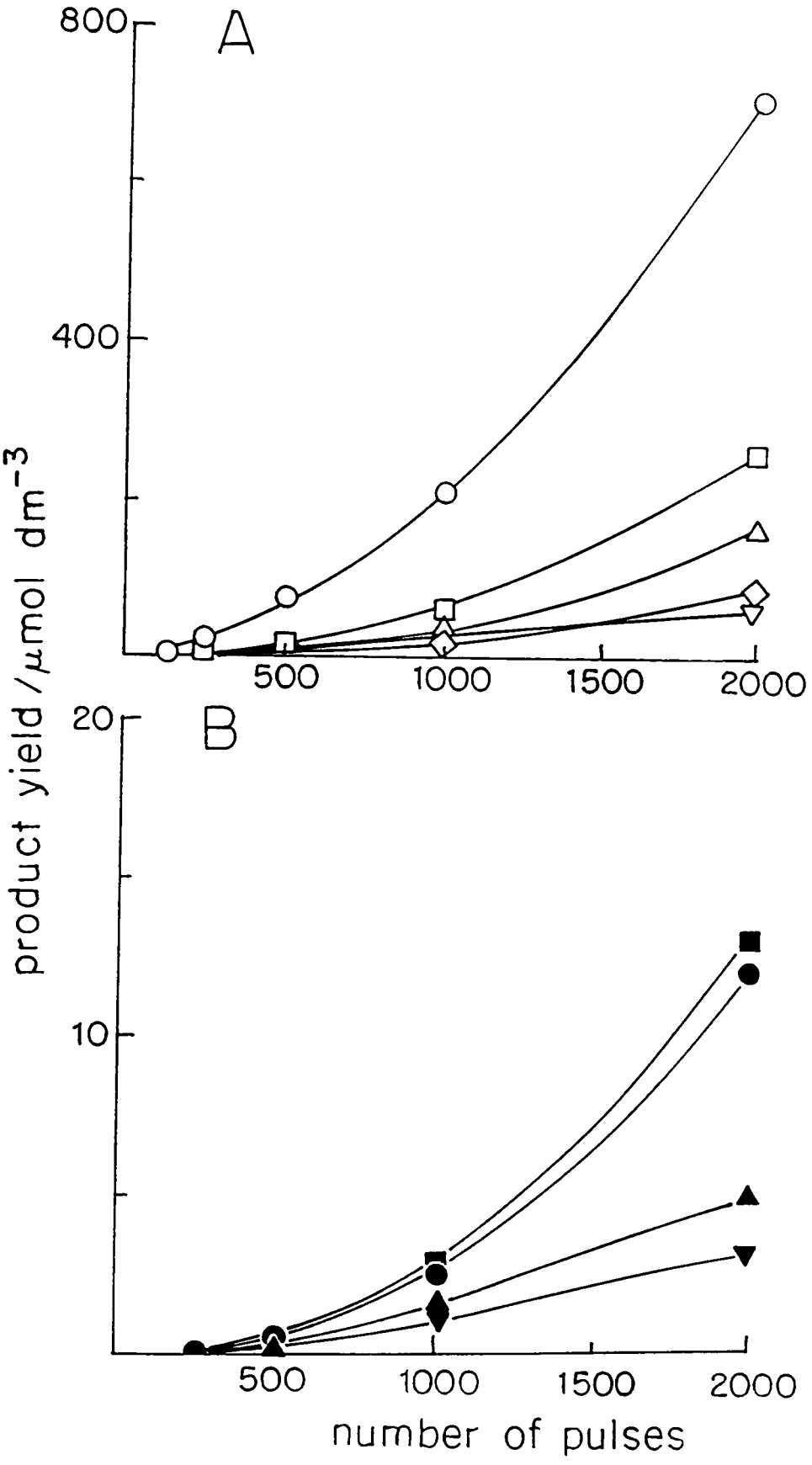
800
A
400
500
1000
1500
2000
20
B
10
500
1000
1500
2000
product yield /μmol dm^{-3}
number of pulses

Table 13. Yields of products as a function of number of pulses at an ethylene pressure of 2000 Torr. 10 P(14) line, $\tilde{\nu} = 949.48\ cm^{-1}$, $F_0 = 0.57\ J\ cm^{-2}$.

number of pulses	product yield/μmol dm^{-3}								
	CH_4	C_2H_2	C_3H_4	C_3H_6	1,3-C_4H_6	1-C_4H_8	trans-2-C_4H_8	cis-2-C_4H_8	n-C_4H_{10}
100	—	—	—	—	6.2	0.85	—	—	—
250	1.2	5.7	0.03	2.6	26	3.4	0.07	0.04	0.05
500	4.8	19	0.59	10	76	10	0.26	0.16	0.66
1000	18	62	2.6	35	211	27	1.6	1.0	2.9
2000	87	258	12	164	709	59	4.9	3.1	13

Figure 32. Yields of products as a function of number of pulses at an ethylene pressure of 3000 Torr.

10 P(14) line, $\tilde{\nu} = 949.48\ cm^{-1}$.
incident fluence = $0.75\ J\ cm^{-2}$.

A. main products

○ : 1,3-butadiene
□ : acetylene
△ : propylene
▽ : 1-butene
◇ : methane

B. minor products

■ : n-butane
● : allene
▲ : trans-2-butene
▼ : cis-2-butene

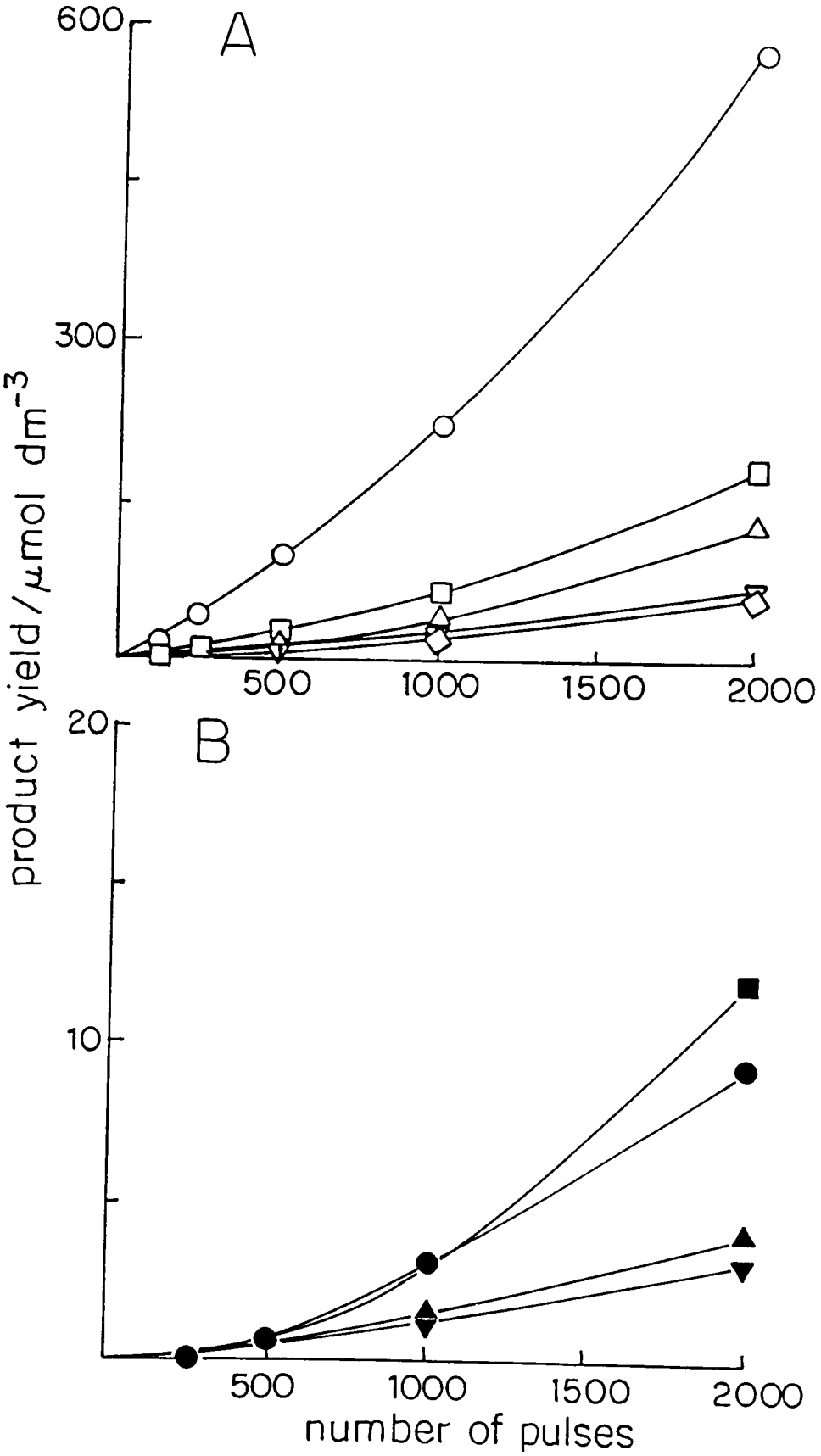
600
300
A
product yield / μmol dm⁻³
500
1000
1500
2000
20
10
B
500
1000
1500
2000
number of pulses

Table 14. Yields of products as a function of number of pulses at an ethylene pressure of 3000 Torr. 10 P(14) line, $\tilde{\nu} = 949.48\ cm^{-1}$, $F_0 = 0.75\ J\ cm^{-2}$.

number of pulses	product yield/μmol dm^{-3}								
	CH_4	C_2H_2	C_3H_4	C_3H_6	1,3-C_4H_6	1-C_4H_8	trans-2-C_4H_8	cis-2-C_4H_8	n-C_4H_{10}
100	0.55	3.2	0.04	0.75	18	3.0	0.05	0.04	0.04
250	2.0	10	0.13	3.0	43	7.0	0.09	0.08	0.14
500	7.7	29	0.70	13	100	16	0.67	0.59	0.70
1000	19	65	3.1	38	222	29	1.5	1.2	2.9
2000	60	180	9.3	130	576	69	4.0	3.2	12

the rate of initiation at a concentration of 1-butene of ~ 1.4 x 10^{-6} mol dm^{-3}, which is attained after 375 pulses at 1000 Torr. Similarly at 3000 Torr, R_{65} equals R_{19} at a 1-butene concentration of ~ 1.3 x 10^{-5} mol dm^{-3}, attained after approximately 400 pulses.

Table 15. Comparison of R_{19} and R_{65} AT 1000 K

C_2H_4/Torr	R_{19}	R_{65} 100 pulses	R_{65} 500 pulses
1000	6.8×10^{-7}	2.5×10^{-8}	1.2×10^{-6}
2000	2.7×10^{-6}	4.3×10^{-7}	5.1×10^{-6}
3000	6.2×10^{-6}	1.5×10^{-6}	8.0×10^{-6}

Therefore, dissociation of 1-butene should be an important source of additional radical formation. In this calculation, the concentrations of 1-butene refer to concentrations in the entire vessel, which assumes therefore complete mixing, between pulses, of gas from the reaction zone with the surrounding unirradiated gas. Because of the 2 s interval between pulses fairly efficient mixing would probably be expected to occur by diffusion and by convection. If, however, mixing between pulses was not complete, and some of the 1-butene formed remained in the reaction zone between pulses, this product would then decompose faster than calculated in Table 15 and hence become an even more important source of radicals.

The rate of the secondary dissociation increased by more than five orders of magnitude between 1000 and 1500 K. Secondary dissociation will therefore be increasingly important at higher temperatures.

Tables 16-18 show product ratios with respect to 1,3-butadiene as a function of number of pulses in the irradiation of ethylene at pressures between 1000 and 3000 Torr. Since formation of n-butane by reaction (37) is probably negligible on account of the short lifetime of 1-butyl radicals under the present conditions, n-butane is formed only by the termination reaction (52) involving two ethyl radicals. The ratio $n\text{-}C_4H_{10}/1,3\text{-}C_4H_6$ therefore gives some indication of the chain length of the radical reaction; the small value suggests a moderately long kinetic chain length. All ratios except $1\text{-}C_4H_8/1,3\text{-}C_4H_6$ increase moderately with number of pulses. The decrease in the ratio $1\text{-}C_4H_8/1,3\text{-}C_4H_6$ is probably due to consumption of 1-butene by secondary dissociation as discussed earlier. The increases observed in the other ratios suggest that 1,3-butadiene may be consumed in secondary reactions. The two most probable mechanisms for this consumption are (i) addition of radicals to 1,3-butadiene and (ii) addition of 1,3-butadiene to ethylene, the Diels-Alder reaction. Examination of these rates, however, shows that neither of these reactions should be fast enough to consume 1,3-butadiene in the present experiments. The ratio of the rate of addition of a methyl radical to ethylene and to 1,3-butadiene:

$$CH_3\cdot + C_2H_4 \rightarrow n\text{-}C_3H_7\cdot \qquad (68)$$

$$CH_3\cdot + 1,3\text{-}C_4H_6 \rightarrow 3\text{-}C_5H_9\cdot \qquad (69)$$

was estimated at 1000 K as ~ 1.0 from data obtained in the range 353-453 K [130]. With the low concentrations of $1,3\text{-}C_4H_6$ formed in the present experiments, reaction (69) would therefore not contribute to consumption of 1,3-butadiene.

Table 16. Product ratios with respect to 1,3-butadiene as a function of number of pulses at an ethylene pressure of 1000 Torr.

10 P(14) line, $\tilde{\nu}$ = 949.48 cm^{-1}, F_0 = 0.69 J cm^{-2}

number of pulses	ratio CH_4/1,3-C_4H_6	C_2H_2/1,3-C_4H_6	C_3H_6/1,3-C_4H_6	1-C_4H_8/1,3-C_4H_6	n-C_4H_{10}/1,3-C_4H_6
250	0.038	0.18	0.11	0.14	——
500	0.054	0.22	0.14	0.13	0.003
1000	0.084	0.30	0.21	0.11	0.011
2000	0.094	0.29	0.22	0.056	0.017

Table 17. Product ratios with respect to 1,3-butadiene as a function of number of pulses at an ethylene pressure of 2000 Torr.

10 P(14) line, $\tilde{\nu}$= 949.48 cm^{-1}, F_0 = 0.57 J cm^{-2}.

	ratio				
number of pulses	CH_4/1,3-C_4H_6	C_2H_2/1,3-C_4H_6	C_3H_6/1,3-C_4H_6	1-C_4H_8/1,3-C_4H_6	n-C_4H_{10}/1,3-C_4H_6
250	0.046	0.22	0.10	0.13	0.002
500	0.063	0.25	0.13	0.13	0.009
1000	0.085	0.29	0.16	0.13	0.014
2000	0.12	0.36	0.23	0.083	0.018

Table 18. Product ratios with respect to 1,3-butadiene as a function of number of pulses at an ethylene pressure of 3000 Torr.

10 P(14) line, $\tilde{\nu} = 949.48\ cm^{-1}$, $F_0 = 0.75\ J\ cm^{-2}$.

number of pulses	ratio $CH_4/1,3\text{-}C_4H_6$	$C_2H_2/1,3\text{-}C_4H_6$	$C_3H_6/1,3\text{-}C_4H_6$	$1\text{-}C_4H_8/1,3\text{-}C_4H_6$	$n\text{-}C_4H_{10}/1,3\text{-}C_4H_6$
100	0.030	0.18	0.042	0.17	0.002
250	0.046	0.23	0.070	0.16	0.003
500	0.077	0.29	0.13	0.16	0.007
1000	0.085	0.29	0.17	0.13	0.013
2000	0.10	0.31	0.22	0.12	0.021

The rate constant for the Diels-Alder reaction of 1,3-butadiene with ethylene forming cyclohexene [131,132]:

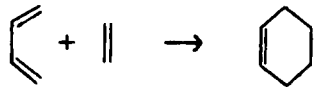

(70)

is given by the following expression,

$$k_{70}\ (dm^3\ mol^{-1}\ s^{-1}) = 3 \times 10^7 \exp(-115000/RT)\ [131] \qquad (71)$$

A comparison between the rate of removal of 1,3-butadiene by reaction (70);

$$-d[1,3\text{-}C_4H_6]/dt = k_{70}[C_2H_4][1,3\text{-}C_4H_6] \qquad (72)$$

with its experimental rate of formation was made considering two limiting assumptions about mixing of the heated gas in the present system:

(1) complete mixing in the entire vessel and

(2) no mixing between the gas in the reaction zone and the surrounding gas.

This comparison, which was made at 1000 K for a 2000 pulse irradiation of 1000 Torr ethylene, showed the rate of removal of 1,3-butadiene in both cases was negligible compared to its rate of formation.

For an average temperature of 1000 K, the effective volume was estimated as 0.14 cm^3. Assuming a reaction time of 10 μs, the rate of formation of 1,3-butadiene in the effective reaction volume is,

$$R_{f(Veff)} = (4.7 \times 10^{-4}\ mol\ dm^{-3}/2000 \times 10 \times 10^{-6}\ s) \times (1.58/0.14)$$
$$= 2.6 \times 10^{-1}\ mol\ dm^{-3}\ s^{-1}$$

If complete mixing of the 1,3-butadiene occurs between pulses only a fraction of the concentration in the entire vessel is present in the reaction zone. The rate of removal, from equation (72), is

$$R_{r(mixing)} = k_{70}[C_2H_4][1,3\text{-}C_4H_6]_{(Veff)}$$
$$= 2.0 \times 10^{-5}\ mol\ dm^{-3}\ s^{-1}$$

If no mixing occurs, the total amount of 1,3-butadiene will be in the reaction volume and the rate of removal will be greater by the fraction V_{vessel}/V_{eff} or,

$$R_{r(no\ mixing)} = 2.2 \times 10^{-4}\ mol\ dm^{-3}\ s^{-1}$$

The rate of loss of 1,3-butadiene by reaction (70) therefore appears negligible compared to its rate of formation. The rate of loss by reaction (70) becomes closer to its rate of formation at higher temperature, and at longer reaction times. Nevertheless, removal of 1,3-butadiene by reaction (70) is probably not important in the present system.

Furthermore, the rate of dissociation of 1,3-butadiene into a pair of vinyl radicals,

$$1,3\text{-}C_4H_6 \rightarrow 2C_2H_3\cdot \qquad (73)$$

which was the dominant initiation in its pyrolysis above 1000 K [102,129,133] and for which

$$k_{73}\ (s^{-1}) = 4 \times 10^{16} \exp(-391000/RT) \qquad (74)$$

estimated between temperatures of 1600 and 1900 K [133], was also negligible compared to the experimental rate of formation. At 1000 K, under the same conditions used for the previous calculation, $R_{r(73)}/R_f \sim 2 \times 10^{-7}$ and 3×10^{-6} respectively under the limiting assumptions of complete and no mixing of the gas in the vessel. Therefore, if $1,3\text{-}C_4H_6$ is not consumed in secondary reactions, the increase in the ratios of $CH_4/1,3\text{-}C_4H_6$ and $C_3H_6/1,3\text{-}C_4H_6$ suggest that 1-butene may enter into the propagation reactions as well as contributing to increased initiation. Abstraction of $H\cdot$ from 1-butene will be much faster than from ethylene and the rate of formation of products formed by abstraction, particularly methane, may be more strongly enhanced than

those formed through dissociation, such as 1,3-butadiene. Thus the ratios of products could change with conversion as 1-butene builds up in the system.

The 2-butenes were very minor products of the decomposition (Table 9), but the ratio of the trans- to the cis-isomer offers another possible estimate of the effective temperature at which the decomposition is occurring. An average ratio of 1.20 ± 0.06 was found in the irradiations of ethylene at 3000 Torr and fluence of 0.75 J cm^{-2}. The temperature dependence of the trans-2-C_4H_8/cis-2-C_4H_8 equilibrium ratio given by Meyer and Stroz [134], is

$$\log_{10} K_{t/c} = 0.01947(10^3/T)^2 + 0.08663(10^3/T) \quad 0.006692 \qquad (75)$$

and if it is assumed that the two isomers were formed in the equilibrium ratio in the reaction, then the experimental ratio indicates a temperature of 1200 ± 300 K. This average temperature is comparable to the "effective" temperature of 1310 K obtained from measurement of the cyclobutane constant final value, assuming constant volume, under identical conditions of pressure and fluence. The smaller yields of 2-butene obtained at lower pressures of ethylene, 1000 and 2000 Torr, made measurements of the trans/cis ratio too inaccurate to be useful.

ii. Effect of pressure

The yields of products as a function of ethylene pressure at 250 and 2000 pulses are shown in Figures 33 and 34 and are summarized in Tables 19 and 20. The dependence on pressure is complex, involving concurrent changes in temperature, absorption coefficient and reaction volume. When initiation is second-order and propagation first-order, the over-all rate of the radical chain reaction will be second order in the pressure of ethylene, at a constant temperature, as mentioned in the introduction to this section, and as observed

Figure 33. Yields of products as a function of ethylene pressure at 250 pulses.

10 P(14) line, $\tilde{\nu} = 949.48\ cm^{-1}$,
average incident fluence = $0.67 \pm 0.07\ J\ cm^{-2}$

A. main products

○ : 1,3-butadiene
□ : acetylene
△ : propylene
▽ : 1-butene
◇ : methane

B. minor products

■ : n-butane
● : allene
▲ : trans-2-butene
▼ : cis-2-butene

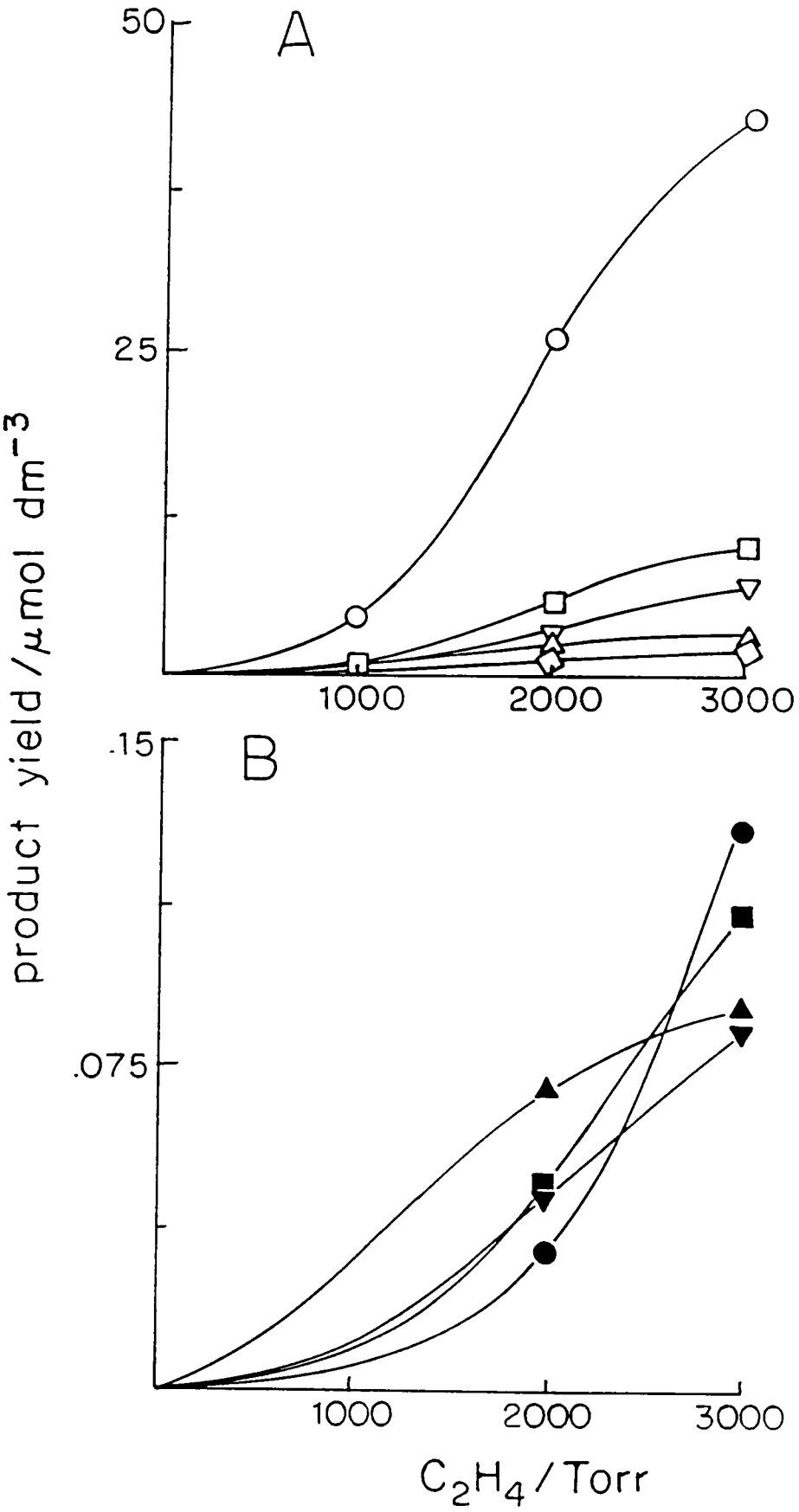
A
B
50
25
.15
.075
1000
2000
3000
product yield / μmol dm⁻³
C₂H₄ / Torr

Table 19. Yields of products as a function of ethylene pressure at 250 pulses.

10 P(14) line, $\tilde{\nu} = 949.48\ cm^{-1}$, $F_0 = 0.67 \pm 0.07\ J\ cm^{-2}$.

	product yield/μmol dm^{-3}								
C_2H_4/Torr	CH_4	C_2H_2	C_3H_4	C_3H_6	1,3-C_4H_6	1-C_4H_8	trans-2-C_4H_8	cis-2-C_4H_8	n-C_4H_{10}
1000	0.17	0.80	—	0.50	4.5	0.62	—	—	—
2000	1.2	5.7	0.32	2.6	26	3.4	0.07	0.04	0.05
3000	2.0	10	0.13	3.0	43	7.0	0.09	0.08	0.11

Figure 34. Yields of products as a function of ethylene pressure at 2000 pulses.

10 P(14) line, $\tilde{\nu} = 949.48\ cm^{-1}$,
average incident fluence = $0.67 \pm 0.07\ J\ cm^{-2}$.

A. main products

○ : 1,3-butadiene
□ : acetylene
△ : propylene
▽ : 1-butene
◇ : methane

B. minor products

■ : n-butane
● : allene
▲ : trans-2-butene
▼ : cis-2-butene

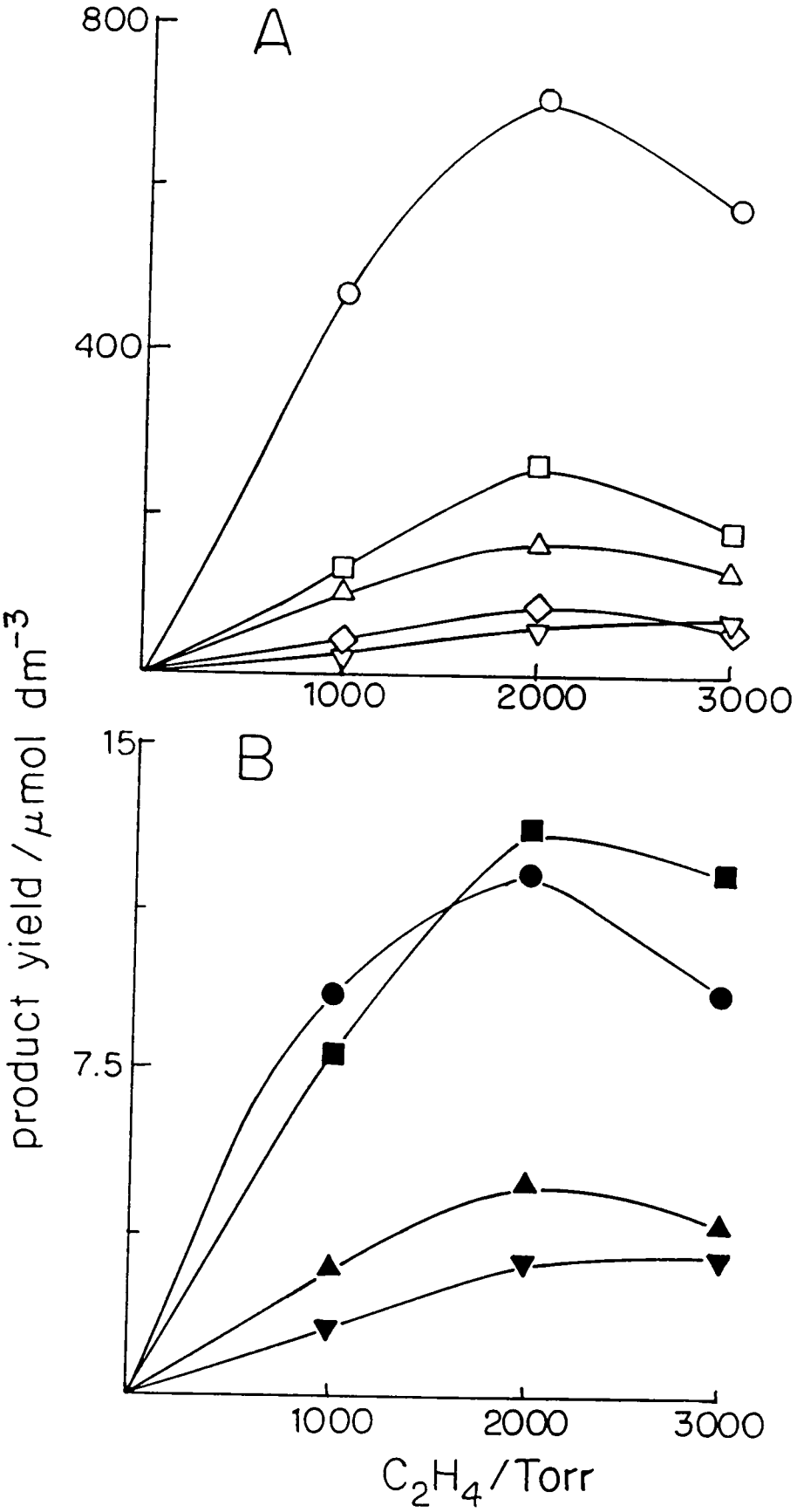
800
400
A
1000
2000
3000
15
7.5
B
1000
2000
3000
product yield / μmol dm⁻³
C2H4 / Torr

Table 20. Yields of products as a function of ethylene pressure at 2000 pulses.

10 P(14) line, $\tilde{\nu} = 949.48\ cm^{-1}$, $F_0 = 0.67 \pm 0.07\ J\ cm^{-2}$

	product yield/μmol dm^{-3}								
C_2H_4/Torr	CH_4	C_2H_2	C_3H_4	C_3H_6	1,3-C_4H_6	1-C_4H_8	trans-2-C_4H_8	cis-2-C_4H_8	n-C_4H_{10}
1000	44	136	9.2	103	466	26	2.9	1.6	7.8
2000	87	258	12	164	709	59	4.9	3.1	13
3000	60	180	9.3	130	576	69	4.0	3.2	12

by Back and coworkers [94,96,98,99]. Counter-balancing this strong dependence on pressure is the effect of pressure on the reaction volume. Since absorption in the irradiation vessel (l = 0.52 cm) is complete in this range of pressure (Figure 29), increasing the pressure has the effect of reducing the reaction volume and hence the total yield. This reduction in volume is even more pronounced because of the increase in absorption coefficient with increasing pressure, which also, however, increases the temperature and thus increases the reaction rate (see Figure 29 and Table 11). An additional possible effect is a faster rate of cooling and hence a shorter reaction time as the reaction volume becomes smaller. A further effect of increasing the pressure might be a change in the product distribution, with more radical addition to ethylene at higher pressures yielding more higher products (which were not measured) and fewer products from radical decomposition. Figures 33 and 34 in fact show a rapid increase in yield at low pressure, then a levelling out, and even indicate a drop in yields of some products at the highest pressure of 3000 Torr. Certainly changes in many factors affecting reaction rate and product yields occur concurrently with changes in pressure in this system, and these can only be assessed in a qualitative manner.

iii. Effect of fluence

The effect of varying the incident fluence (from 0.55 to 0.77 J cm^{-2}) on the various product yields measured in a 500-pulse irradiation of 3000 Torr C_2H_4 with the 10 P(14) line, is shown in Figure 35 and Table 21. All the products except cyclobutane show a very strong dependence, increasing sharply with increasing fluence. The dependence on fluence is similar for 1,3-C_4H_6, C_2H_2 and 1-C_4H_8, while a more pronounced increase is observed for

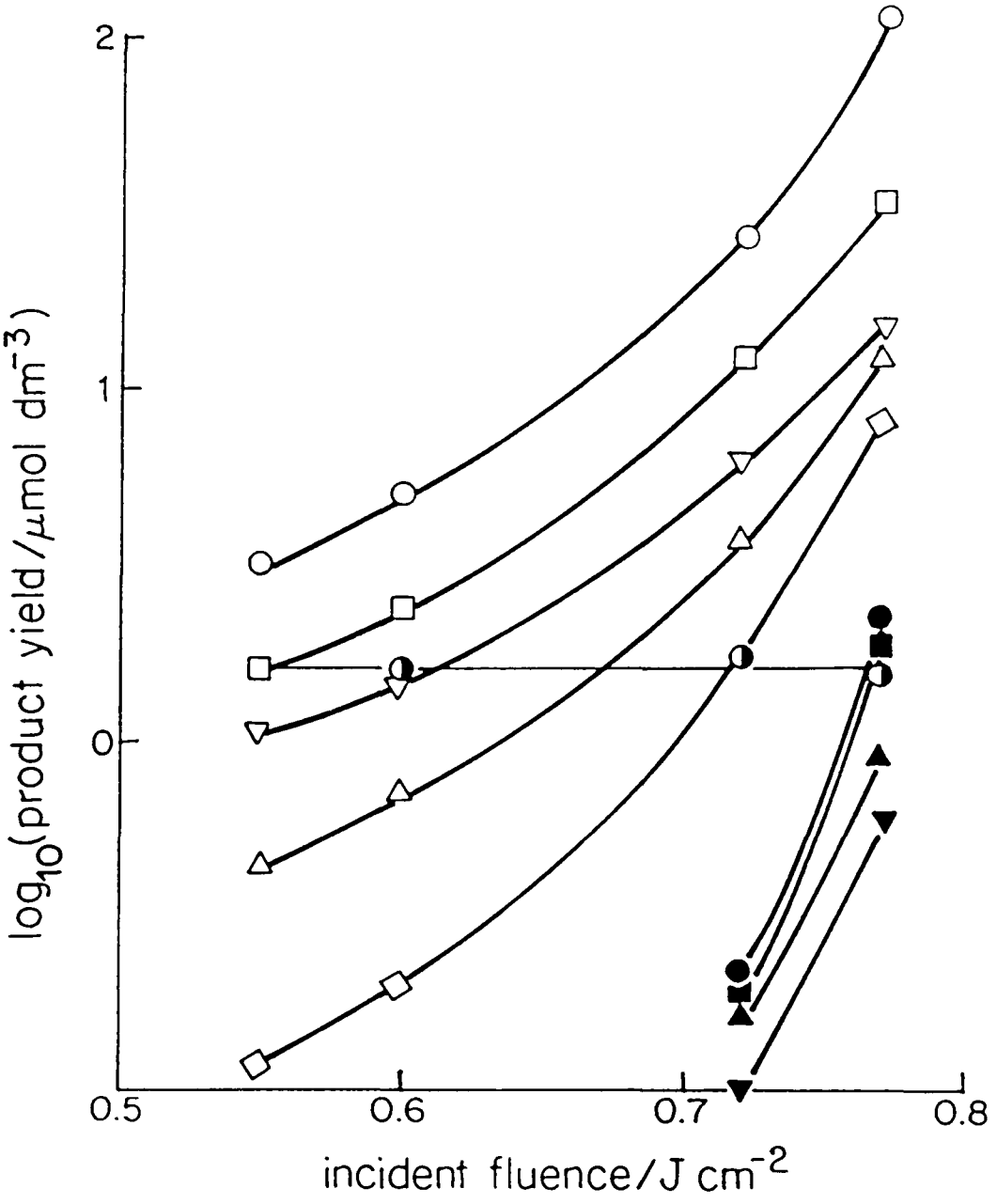

Figure 35. Yields of products as a function of incident fluence.

$P_{C_2H_4}$ = 3000 Torr

t = 500 pulses

10 P(14) line, $\tilde{\nu}$ = 949.48 cm^{-1}.

products

○ : 1,3-butadiene
□ : acetylene
▽ : 1-butene
△ : propylene
◇ : methane
● : allene
■ : n-butane
▲ : trans-2-butene
▼ : cis-2-butene
◑ : cyclobutane

Table 21. Yields of products as a function of incident fluence.

$P_{C_2H_4}$ = 3000 Torr, t = 500 pulses, 10 P(14) line, $\tilde{\nu}$ = 949.48 cm^{-1}.

incident fluence/ J cm^{-2}	product yield/μmol dm^{-3}									
	CH_4	C_2H_2	C_3H_4	C_3H_6	1,3-C_4H_6	1-C_4H_8	trans-2-C_4H_8	cis-2-C_4H_8	n-C_4H_{10}	c-C_4H_8
0.55	0.12	1.6	—	0.44	3.2	1.0	—	—	—	1.6
0.60	0.20	2.3	—	0.71	5.0	1.4	—	—	—	1.6
0.72	1.8	12	0.21	3.6	27	6.0	0.16	0.10	0.18	1.7
0.77	8.1	33	2.2	12	110	15	0.87	0.58	1.8	1.5

CH_4, C_3H_6 as well as for the minor products C_3H_4, n-C_4H_{10} and 2-C_4H_8. The unique behavior of cyclobutane supports the conclusion that it is a molecular product, produced in equilibrium concentrations, while the other products arise from a radical chain mechanism.

PART II

Photolysis of ethylene

in the ultraviolet region

between 193 and 308 nm

with pulsed excimer lasers

INTRODUCTION

Experimental and theoretical research on the electronic absorption spectrum of ethylene and its interpretation has been an ongoing activity since Stark and Lipp [135] first recorded the first far ultraviolet absorption spectrum exactly 75 years ago. The sustained interest shown by molecular spectroscopists [53,127,135-166] and quantum theoreticians [167-183] in this particular molecule stems from the fact that even now there is still no clear understanding or agreement about some features of the electronic excitation in ethylene, particularly the T-N and V-N systems. Difficulties in interpreting the spectrum of the simplest olefin is an embarrassment, since if ethylene, the prototype π system, presents any unsolved problems this casts some doubt on the understanding of π-electron molecules of greater complexity.

In its electronic ground state (^1A_g), called the N (normal) state by Mulliken [168], the ethylene molecule is planar and belongs to the point group D_{2h}. Following the convention recommended by the Joint Commission on Spectroscopy of the International Astronomical Union and IUPAP [184], the x-axis is perpendicular to the plane of the molecule, and the z-axis lies along the C-C axis. This leads to a ground-state electronic configuration:

$$(\sigma 1a_g)^2(\sigma 1b_{1u})^2(\sigma 2a_g)^2(\sigma 2b_{1u})^2(\sigma 1b_{2u})^2(\sigma 3a_g)^2(\sigma 1b_{3g})^2(\pi 1b_{3u})^2$$

Promotion of an electron from the HOMO $1b_{3u}$, a π-bonding orbital, to the LUMO $1b_{2g}$, a π^*-antibonding orbital, results in both a triplet (T) and a singlet (V) state, while excitation of a π-electron into a 3s Rydberg orbital gives a Rydberg (R) state.

Much time and effort has been expended by theoreticians in the prediction of the changes in geometry of ethylene upon its promotion to the

various excited electronic states [167-183]. Such studies have predicted a change from a coplanar to a perpendicular arrangement of the methylene groups when ethylene is excited from its ground state to the first excited electronic (T and V) states.

First observed by Reid [139] in long pathlengths (1.25-2.5 m) of liquid ethylene, the ultraviolet absorption at the longest wavelengths consisted of an extremely weak progression of diffuse bands extending with increasing intensity from 340 to 260 nm. This band system was tentatively assigned to the T ← N electronic transition but the possibility that it could be due to an extension of the V ← N transition or to impurities [142], was not rejected. One decade later, Evans [144] found the same bands in a gas phase mixture of 50 atm. C_2H_4 and 25 atm. O_2 in a 5.2 cm high-pressure cell. The T ← N absorption system in "pure" ethylene is forbidden by the multiplicity rule and would be greatly weakened by unfavorable Franck-Condon factors arising from the expected change in geometry. In the presence of high pressures of oxygen, which because of its triplet ground state is known to induce singlet-triplet transitions, the T ← N absorption is greatly enhanced. A remeasurement of the spectrum of liquid ethylene in the absence and presence of dissolved oxygen led McDiarmid [156] to conclude that the T ← N absorption system found by Reid was detectable only because of an oxygen impurity in the liquid sample.

Several attempts were made to analyze the vibrational structure of the T ← N system in terms of progression(s) in upper-state vibration(s) [144,152]. In a review of the experimental evidence up to 1976, Mulliken [179] argued that a single progression in the C=C stretching frequency ν_2', accounts for the observed bands, an assignment based on the average spacing between bands of

about 990 cm^{-1}, and its small change upon deuteration [152]. Mulliken also noted the lack of any band structure which could be assigned to the torsional frequency ν_4', despite the expectation that vertical excitation from the planar ground state would give a conformation of the T state twisted almost 90° from its potential minimum and maximum Franck-Condon overlap between high levels of ν_4' in the T state and the $\nu''_4 = 0$ level of the ground state. Wilden and Comer have measured a high-resolution (~ 200 cm^{-1} (FWHM) electron energy-loss) spectrum of ethylene [127] and found the vibrational structure of the T ← N transition to consist of very long progressions of the C=C stretching mode ν_2' ($\tilde{\nu}_2' = 1048$ cm^{-1}), and in addition at least three quanta of ν_4', the torsional mode, with both even and odd levels excited at high scattering angles and low impact energies. Comparison of Franck-Condon factors with the observed spectrum led to an estimate of the C-C bond length of 0.154 nm, considerably longer than in the ground state where $r_{C-C} = 0.1339$ nm [185], and lying between calculated values of 0.15 nm [174,178] (for perpendicular geometry) and 0.16 nm [174] (for planar geometry). The energy-loss spectrum of ethylene in the region of the triplet band measured by Wilden and Comer [127] is shown in Figure 36. Values of the vertical energy of the T state at its planar maximum have been quoted in the range 400-450 kJ mol^{-1} [148,157] above the ground state, while an energy of 309 kJ mol^{-1} has been calculated for the T state at its 90° minimum [178,180].

In comparison with the very weak T ← N transition ($\epsilon \sim 10^{-4}$ M^{-1} cm^{-1} [139]), the much stronger V ← N absorption system begins at 206.9 nm [136] consisting of a long series of broad diffuse bands somewhat irregularly spaced about 800 cm^{-1} apart [142,149,152,158] whose intensities were found to

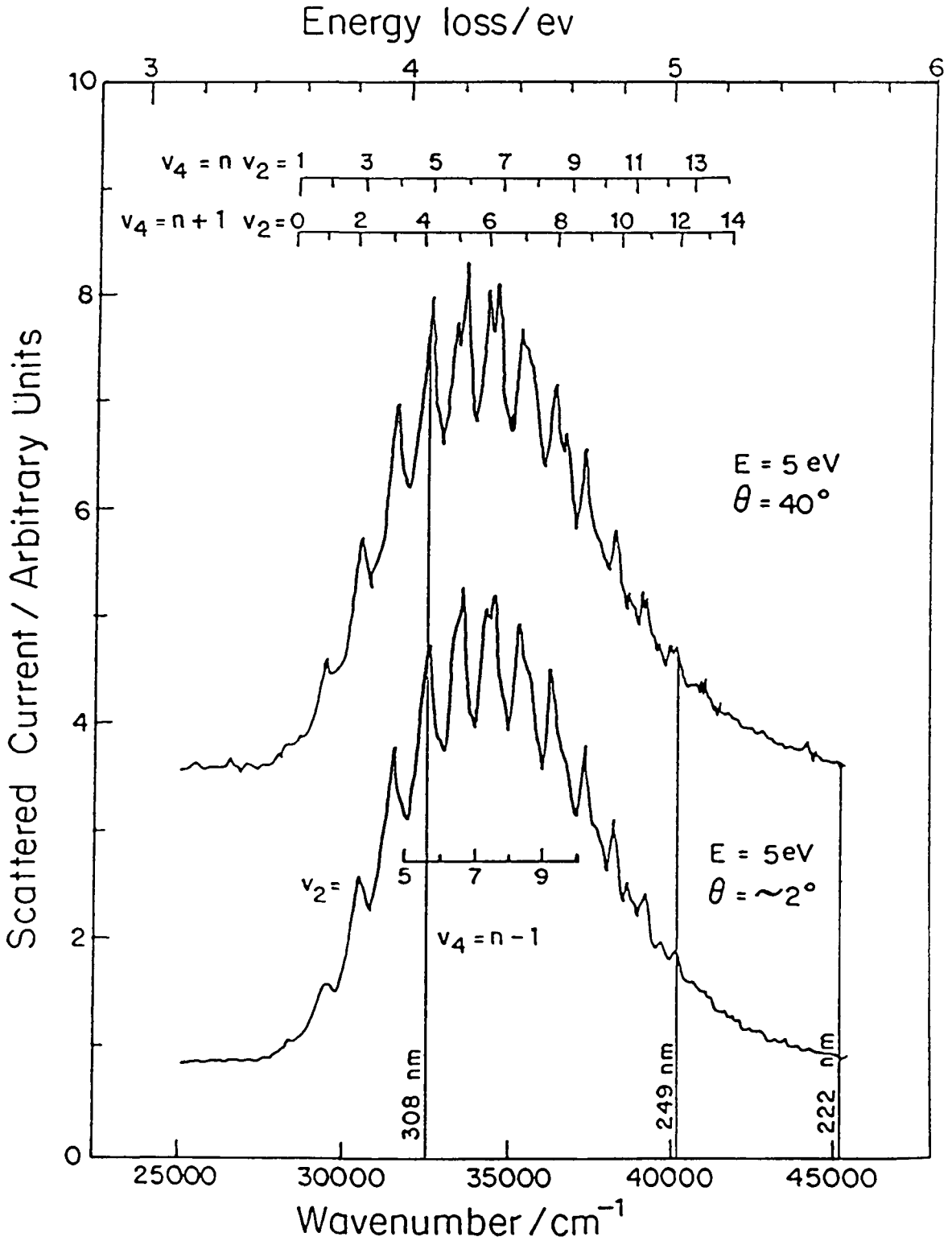

Figure 36. Low-energy electron loss spectra of ethylene in the T ← N region showing the vibrational structure assigned to progressions of ν'_2 (C=C stretch) and ν'_4 ($H_2C{=}CH_2$ torsion); reproduced from [127]. Photolysis wavelengths of 222, 249 and 308 nm are indicated in the spectra.

increase progressively by about a factor of three down to about 175 nm. At this wavelength, the V ← N bands disappear under the stronger and sharper bands of the first Rydberg transition, R(3s) ← N, beginning at 174.4 nm [138], and merge into an apparent continuum which reaches a broad maximum at 162 nm [142], and declines. Several other weak Rydberg systems have been identified at 159 nm ($3p_x \leftarrow \pi$) and 149.5 nm ($3p_y \leftarrow \pi$) in a two-photon absorption study [164]. At even shorter wavelengths, transitions to other Rydberg states have been observed [138,142,146,164,180]. The absorption spectrum of ethylene in the region of the singlet (V) band measured by Wilkinson and Mulliken [142] is shown in Figure 37.

Three major questions still in dispute about the V ← N transition of ethylene are the position of its origin, the assignment of the observed vibrational bands, and the extent of valence/Rydberg mixing in the V ← N system.

Although Merer and Mulliken [152] had tentatively suggested that the (0,0) band of the V ← N system corresponded with the steep rise in the absorption observed by Reid [139] in long paths of liquid ethylene near 265 nm, McDiarmid [156] convincingly showed that this absorption disappeared upon excluding traces of oxygen from the sample. On these grounds, the 265 nm absorption was attributed to the oxygen-enhanced absorption previously seen in the spectrum of gaseous C_2H_4-O_2 mixtures by Evans [144]. While the unequivocal observation at 206.9 nm [136] of the first band of the V ← N system sets a lower limit for the origin, an upper limit at 228.5 nm was predicted by Foo and Innes in a vibrational analysis of the spectra of four deuterated ethylenes in terms of progressions in the torsional mode, ν_4' [158]. In liquid ethylene, although the bands are red shifted from the gas phase

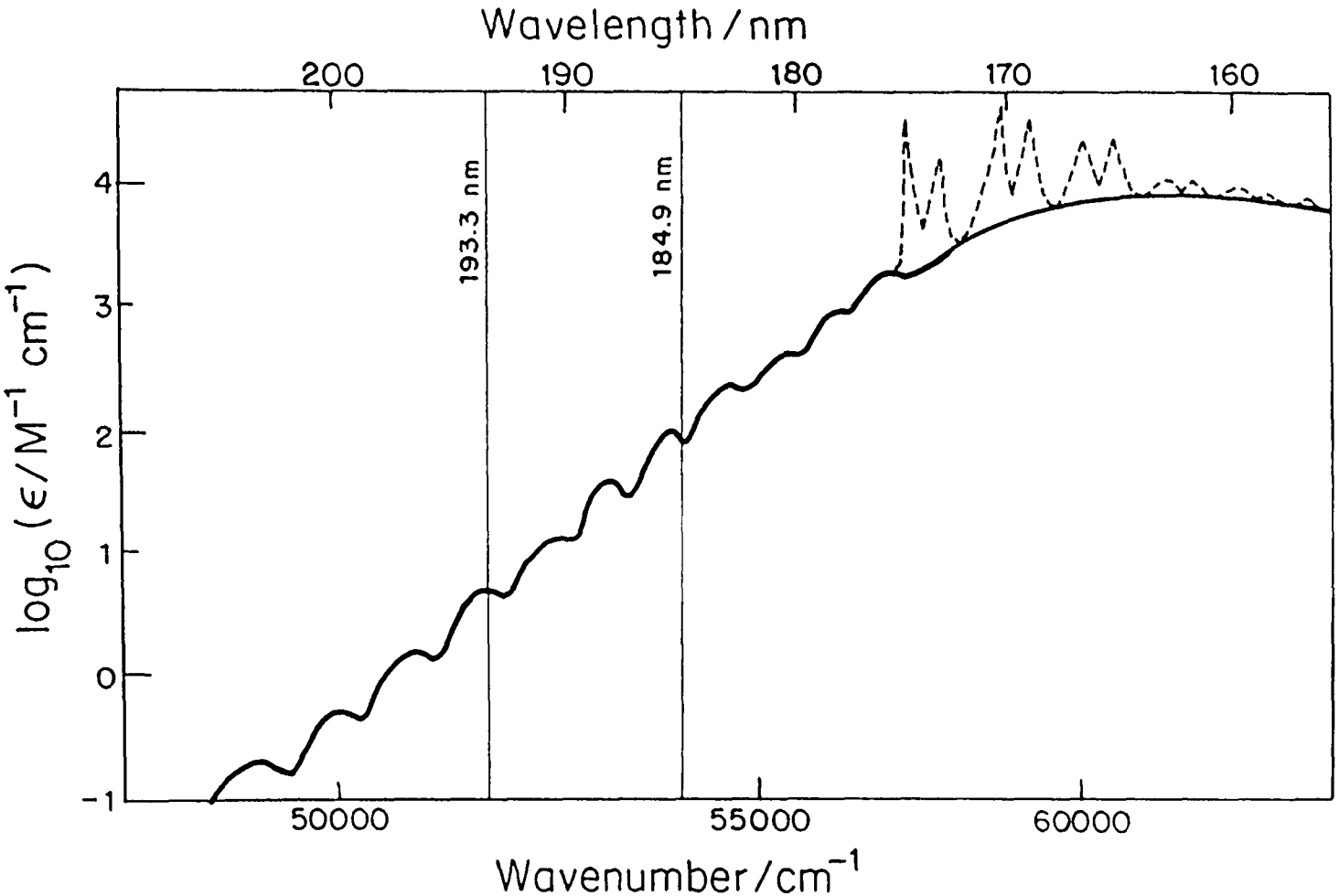

Figure 37. Absorption spectrum of ethylene in the V←N region. The R(3s)←N absorption band is indicated by the dashed line; reproduced from [142]. Photolysis wavelengths of 184.9 and 193.3 nm are indicated in the spectrum.

spectrum by an unknown amount, observation of weak bands ($10^{-2} \geq \epsilon \geq 10^{-3}$) in the range between 208 and 228 nm by McDiarmid [161] led her to conclude that the origin was probably close to the extrapolated value of Foo and Innes. Theoretical calculations of the origin of the V ← N transition of ethylene have given values ranging between 200 nm [178] and 206.7 nm [183].

By analogy with the Schumann-Runge ($\tilde{B}\ ^3\Sigma_u^- \rightarrow \tilde{X}\ ^3\Sigma_g^-$) system of isoelectronic oxygen, Mulliken originally attributed the shape of the V ← N band of ethylene to a long progression in ν_2', the stretching vibration [169]. The bond length of the O_2 molecule increases from 0.121 nm in the N state to 0.160 nm in the V state [186], and by analogy the C-C bond length in ethylene should significantly increase in the V ← N transition. Some experimental support was given to Mulliken's prediction in a vibrational analysis first made by Wilkinson and Mulliken [142] of the spectrum of C_2H_4. However, while they explained the ~ 800 cm^{-1} intervals in the V ← N spectrum in terms of a single, slightly irregular, progression in ν_2', they did not rule out some complications involving ν_4', the torsional vibration. McDiarmid and Charney [149] subsequently interpreted the V ← N vibrational structure in terms of a single progression in ν_4' and in 1969, Merer and Mulliken [172] reproduced many features of the spectrum in a calculation involving a coupling of the twisting and stretching vibrations. Several workers have also suggested the possibility of CH_2 wagging (ν_7' and ν_8') distortions in the 90°-twisted V state [187,188] as well as CH_2 rocking (ν_6' and ν_{10}') vibrations. However, a high-resolution study of the V ← N bands of four deuterioisotopes of C_2H_4 by Foo and Innes [158] indicated that the ν_4' twisting mode was the only one active in the spectrum except in C_2D_4, in which some activity of the ν_2' stretch was also detected. This led them to propose a C-C distance in the

V state of 0.140 nm, only a ~ 5% increase from the ground state, which is consistent with some of the numerous bond length calculations [178]. Ziegler and Hudson [165] have measured a resonance Raman scattering spectrum of ethylene excited by radiation at 212.8 and 193.4 nm, which provides some new information about the vibrational bands involved in the electronic excitation. The appearance of the even ν_4 torsional harmonics i.e. $2\nu''_4$ excited at 212.8 nm, as well as $4\nu''_4$ excited at 193.4 nm, could be explained only if the V state has a twisted, 90° equilibrium configuration in agreement with theoretical calculations and lending support to the involvement of ν'_4 in the absorption spectrum of the isotopic ethylenes [158]. In addition to the strong resonance enhancement observed for the even overtones of the twisting vibration, enhancements of the ν_2 (C=C stretching) and ν_3 (symmetric CH_2 deformation) fundamentals were also found. The lack of resonance scattering activity for the ν_7 or ν_8 wagging modes does not support suggestions by Ogilvie [187] of pyramidal geometry at the carbon atoms in the V state. The absence of the ν_6 and ν_{10} CH_2 rocking modes also rules out Walsh's suggestion that in the V state, each carbon atom may lie out of the plane bisecting the HCH angle of the other CH_2 group [188]. Sension, Mayne and Hudson have very recently extended the technique of UV resonance Raman scattering spectroscopy to a study of the ethylene spectrum with excitation wavelengths as short as 141.2 nm [166]. While the resonance Raman spectra obtained exhibited many highly excited vibrational levels, these were, as in a previous investigation [165], mainly dominated by enhancements of the ν_2, ν_3 and ν_4 modes. The finding of a very long series of even overtones (with up to 14 quanta of excitation) of the torsional mode (ν_4) lent additional support to the importance of ν'_4 in the promotion of ethylene from its ground state to its low lying excited states [53,152,158].

Turning briefly to the extent of Rydberg orbital character in the V state of ethylene, the most recent theoretical studies have agreed that even though there is important mixing of the $^1(nd\pi \leftarrow \pi)$ Rydberg configurations with $^1(\pi^* \leftarrow \pi)$ in the V state, the latter still behaves like a valence state [177,178,182,183]. Further support for the valence-shell nature of the V state is the insensitivity of the position and width of the vibrational features upon either pressurization with nitrogen gas [145,154] or a change to condensed phases [150,155]. Rydberg bands under these conditions typically exhibit marked pressure broadening and shifts to shorter wavelengths.

The vacuum ultraviolet ($\lambda \leq 200$ nm) photolysis of ethylene has been studied extensively by a number of investigators. Most of the work has been carried out between 122 and 185 nm, the shorter wavelengths (≤ 163 nm) corresponding to excitation to various Rydberg states [189-201], while at 185 nm, the V state of ethylene is excited [193-195,197,202-205]. Very few experiments have been conducted at wavelengths longer than 185 nm, with two brief reports of the photolysis at 193 nm [195,206]. At still longer wavelengths, a variety of photosensitized decompositions of ethylene have been studied, using Zn, Cd and Hg atoms: Zn (4^1P_1) at 214 nm [207], Cd (5^1P_1) at 229 nm [208], Hg (6^3P_1) at 254 nm [209-216], Zn (4^3P_1) at 308 nm [207,217] and Cd (5^3P_1) at 326 nm [218-223].

The photolysis of ethylene (with 2% oxygen, added as a radical scavenger) at 121.6 nm [191] using a Lyman-α resonance lamp at an energy only 30 kJ mol^{-1} below the ionization potential [147], yielded acetylene (major), hydrogen, allene, methylcyclopropane (minor) along with small amounts of propylene and 1,3-butadiene. C_5 and C_6 hydrocarbons were only detected at increased pressures or lamp intensities. The pathway suggested for acetylene formation was as follows:

$$C_2H_4 + h\nu(\lambda = 121.6\ nm) \rightarrow C_2H_4^* \quad (76)$$

$$C_2H_4^* \rightarrow C_2H_2 + H_2 \quad (77a)$$

$$\rightarrow C_2H_3\cdot + H\cdot \quad (77b)$$

$$\rightarrow C_2H_2 + 2H\cdot \quad (77c)$$

Reaction (77c) was suggested to account for the excess of acetylene over hydrogen (C_2H_2/H_2 ~ 3). The small amount of methylcyclopropane, ≤ 1% of total product, was thought to come from the direct addition of an excited ethylene molecule to a ground state molecule:

$$C_2H_4^* + C_2H_4 \rightarrow c\text{-}CH_3C_3H_5 \quad (78)$$

The results obtained by the authors of this work [191], however did not permit them to speculate on the structure of $C_2H_4^*$.

The main products of the direct photolysis of CH_2CD_2 (35 Torr) and trans-CHDCHD (15 Torr) at 123.6 nm with a Kr resonance lamp were acetylene, hydrogen, ethane and n-butane [193]. Since the measured acetylene/hydrogen ratio was again greater than one, being 2.8 ± 0.2, a similar mechanism to that reported at 121.6 nm was suggested with some reservations, however, concerning the decomposition route yielding a vinyl radical and a hydrogen atom i.e. reaction (77b). This pathway was tentatively rejected on the basis that no product expected from vinyl, such as 1-butene, was observed. However, as was described by Innel, Siddiqi and Meisels at 121.6 nm [191], Okabe and McNesby [193] also speculated on the fact that if reaction (77b) above occurred, the excited vinyl radical would have a very short lifetime for dissociation into H plus acetylene, process (77c). On the other hand, the ratio of ethane/n-butane of 0.18 ± 0.02 was in reasonable agreement with the well established value of 0.14 for the disproportionation/recombination ratio of ethyl radicals [224].

Two independent photolyses of $C_2H_4 + C_2D_4$ mixtures at 147 nm [192,194] have reported formation of H_2 and D_2 but not HD. Such a finding, which was also verified at 123.6 nm [193], can be accounted for only by the molecular elimination of hydrogen. While the products of the photolysis of ethylene at 147 nm [192,196] are identical to those observed at 123.6 nm, except for the presence of 1-butene at this wavelength, the reported ratios of acetylene/hydrogen (2.0 ± 0.1 [192,193] and 2.3 ± 0.1 [195]), are somewhat smaller.

In an investigation of the flash photolysis of ethylene (1-20 Torr) with a quartz flash lamp emitting light of a broad wavelength distribution from about 155 to 190 nm, Back and Griffiths [199] found mainly such products as acetylene, hydrogen, ethane, propane, n-butane and methane along with minor yields of 1-butene and propylene. The products were accounted for by a hydrogen atom "cracking" mechanism followed by radical combination, which differed from that at low-intensity because of the much greater hydrogen atom concentration produced by the high intensity flash. At an ethylene pressure of 1 Torr, an observed decrease in the acetylene/hydrogen ratio with increasing flash energy was explained by the probable formation of H_2 by atom recombination:

$$H + H + M \rightarrow H_2 + M \qquad (79)$$

The presence of propylene and 1-butene among the products indicated the stabilization of vinyl radicals (reaction (77b)) at the higher pressures and their efficient trapping by methyl and ethyl radicals. It was also suggested that less highly excited vinyl radicals were produced near the absorption threshold of C_2H_4 and were thus more easily stabilized.

In recent vacuum UV flash photolysis studies of ethylene also carried out between 155 nm and the onset of C_2H_4 absorption, Laufer and coworkers [200,201] have observed formation of the triplet vinylidene ($^3B_2$) radical intermediate. Vinylidene radical formation had previously been suggested in the low intensity VUV photolysis of ethylene at 123.6 and 147 nm [193] where it had been demonstrated that the majority of the H_2 was formed from elimination at the same C atom:

$$CH_2CD_2 \rightarrow D_2C{=}C{:} + H_2 \qquad (80)$$

In reference [193], however, since no butadiene or C-4 compounds other than n-butane were observed, the vinylidene formed very rapidly rearranged to acetylene;

$$D_2C{=}C{:} \rightarrow C_2D_2 \qquad (81)$$

The photolysis of ethylene at 163.4 nm has been studied by Potzinger, Glasgow and von Bünau [195] and by Hara and Tanaka [197,198], using a bromine lamp. The measured products in order of decreasing importance were acetylene, hydrogen, n-butane, ethane and 1-butene. An acetylene/hydrogen ratio of 1.6 ± 0.03 was reported in [195].

The majority of studies on the photolysis of ethylene in the vacuum ultraviolet have been conducted at 185 nm with a low-pressure mercury resonance lamp. At this wavelength, the photolysis has been shown to involve the three primary dissociation processes (77a-c) [193-195,197,202-205]. Potzinger and coworkers [195] have suggested that more than one excited state of ethylene plays a role in its decomposition. The major products detected in order of decreasing importance were acetylene, hydrogen, n-butane, ethane and 1-butene. A scheme in which the three primary processes are followed by the rapid addition of hydrogen atoms to ethylene, and by

reactions of ethyl and vinyl radicals, quite successfully accounted for the products. While Potzinger et al. [195] have reported an acetylene/hydrogen ratio of 1.45, ratios of 1.19 and 1.01 were given by Borrell, Cervenka and Turner [202] and Hirokami and Cvetanovic [203] respectively.

At 193 nm, only two brief studies of the photolysis of ethylene have been reported [195,206]. Using a carbon resonance lamp, Potzinger and coworkers [195] made a single photolysis experiment at 193.1 nm, and measured some yields relative to that of H_2. The yield of acetylene was close to that of hydrogen, while relative yields of n-butane, ethane and 1-butene were much lower than at 185 nm, and they suggested that H_2 elimination dominated the photolysis at 193 nm.

Irion, in an unpublished report from the Max Planck Institüt für Quantenoptik [206], gives a brief account of the photolysis of 100 Torr ethylene with an ArF excimer laser at 193.3 nm. Products found in order of decreasing importance were H_2, C_2H_2, n-C_4H_{10}, C_3H_8, C_2H_6, C_4H_2 (diacetylene), CH_4 and i-C_5H_{12}. The C_2H_2/H_2 ratio was 0.54, and the fractional decomposition was very high, ~ 70% and a variety of secondary reactions and photolysis were undoubtedly occurring.

In a rather different study, Jackson, Halpern and Lin claim to have observed a sequential two photon absorption process in ethylene, based on fluorescence from excited states of the CH radical, using the unfocussed beam of an ArF laser at 193 nm [225].

The present investigation consists of a more systematic study of the photolysis of ethylene using an ArF excimer laser at 193 nm, including its dependence on time (10-250 pulses) and pressure (50-3000 Torr). Accurate quantum yields of product formation are also reported.

Somewhat less complete results are also presented from the photolysis of ethylene with excimer laser sources at 222 nm (KrCl), 249 nm (KrF), and 308 nm (XeCl). While absorption at these wavelengths is very weak, the high power available in the excimer lasers makes these experiments feasible, and measurable decomposition was observed at all wavelengths. While absorption at 222 nm, located near the origin of the V $\leftarrow$ N transition at 228.5 nm [158], possibly involves a "hot" band, absorption at 249 and 308 nm probably involves excitation into the triplet state, as indicated by the electron energy loss spectrum of the T $\leftarrow$ N band of ethylene, measured by Wilden and Comer [127], and shown in Figure 36.

EXPERIMENTAL

1. Irradiation system

The ethylene photolysis in the UV region between 193 and 308 nm was done with unfocussed pulsed excimer (exciplex*) lasers (Lumonics TE-860 series) operated at pulse rates from 1 to 100 Hz. Experiments were made at 193 nm (ArF), 222 nm (KrCl), 249 nm (KrF) and 308 nm (XeCl), using the appropriate rare gas halide mixtures.

The rectangular laser beam was stopped down by a circular aperture of 1.04 cm diameter positioned immediately in front of the reaction vessel so that the beam passed cleanly through without striking its walls. The light transmitted through the cell impinged on a Scientech Model 36-0001 disc calorimeter and the signal monitored with a Scientech Model 36-2002 power and energy meter. For both the absorption measurements and irradiation experiments made at 193 nm, the meter was set on the energy mode since the laser was operated at a pulse frequency of 1 Hz. The accumulated energy of a number of pulses was measured and the average energy per pulse calculated. At the longer wavelengths, the meter was set on the power mode because the laser was operated at higher pulse frequencies usually 10 or 100 Hz. When the laser cavity had been properly passivated, pulse energies typically decreased by about 10-25% over the course of a series of irradiations at 193 nm, or during a single long irradiation at 222, 249 or 308 nm. Typical incident pulse energies

---

* This particular class of laser has become known as "excimer" lasers; they are more properly called exciplex lasers since light emission occurs from a bound electronic state of the exciplex RgX*, usually the strongly bound, ionic B $^2\Sigma_{\frac{1}{2}}$ state down to the weakly bound or dissociative ground X $^2\Sigma_{\frac{1}{2}}$ state.

ranged from about 4-10 mJ (KrCl, KrF) up to 25-30 mJ (ArF, XeCl), corresponding to fluences between 5 and 35 mJ cm^{-2}. Pulselengths ranged between 5 and 20 ns.

2. Procedure for the absorption measurements

The value of the molar absorption coefficient for ethylene at 193 nm was determined according to the following procedure. The evacuated photolysis cell was placed in front of the stopped-down laser and the disc calorimeter was placed just behind the cell. With the power meter set on the energy mode and stable at the zero energy reading, a set of 100 laser pulses was accumulated and the corresponding total energy read directly from the meter scale, and the average energy per pulse transmitted by the empty cell, $\bar{E}_{cell}$, was calculated. The cell was then filled with a known pressure of ethylene and again the total energy accumulated from 100 laser pulses was measured providing a value of the average energy per pulse transmitted by the cell in the presence of ethylene, $\bar{E}_{C_2H_4+cell}$. Optical absorbance A is additive, so that $A_{(C_2H_4+cell)} \quad A_{cell} = A_{C_2H_4} = \log_{10} (\bar{E}_{cell}/\bar{E}_{C_2H_4+cell}) = \epsilon cl$ (assuming the Beer-Lambert law). As shown in Figure 38, a plot of $\log_{10} (\bar{E}_{cell}/\bar{E}_{C_2H_4+cell})$ against ethylene concentration yielded a straight line of slope $\epsilon l = 2.93 \pm 0.07\ M^{-1}\ cm^{-1}$ from a least-squares fit of two separate sets of measurements made at different times. From the cell's pathlength of 0.52 cm, a molar absorption coefficient $\epsilon(193\ nm) = 5.63 \pm 0.14\ M^{-1}\ cm^{-1}$ was obtained, which is about 30% greater than the only other accurate measurement reported at 193.1 nm by Potzinger, Glasgow and von Bünau [195] using a carbon resonance lamp. It should be noted that the actual center wavelength of the

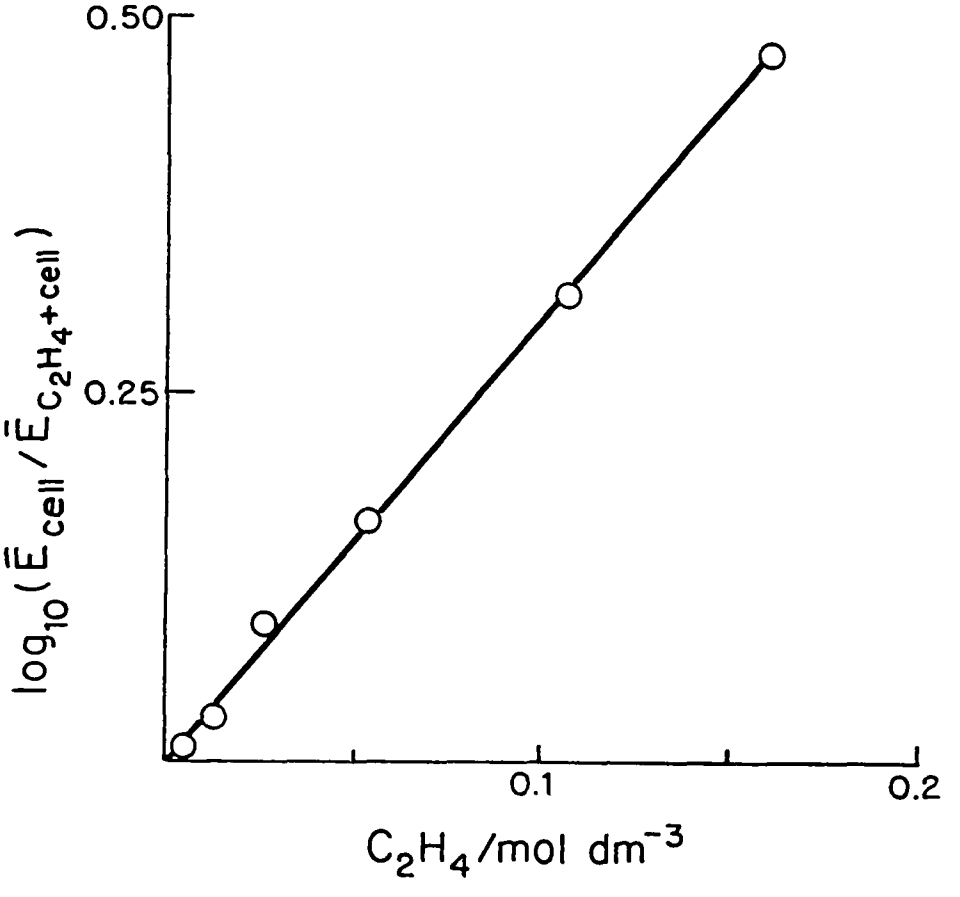

Figure 38. Absorbance of ArF laser radiation as a function of ethylene concentration.

ArF laser is 193.3 nm, with a bandwidth of 0.5 nm (FWHM) [226].

Absorption coefficients for ethylene at 222, 249 and 308 nm are very small and difficult to measure. A preliminary set of absorption measurements carried out in this laboratory [227] at room temperature in a 3 m cell filled with 900 Torr of ethylene, which had been thoroughly degassed and rendered free of traces of water vapor, yielded the following values (average of 5 measurements):

$$\epsilon(222\ \text{nm}) = 1.25 \times 10^{-3}\ M^{-1}\ cm^{-1}$$

$$\epsilon(249\ \text{nm}) = 5.16 \times 10^{-4}\ M^{-1}\ cm^{-1}$$

$$\epsilon(308\ \text{nm}) = 2.27 \times 10^{-4}\ M^{-1}\ cm^{-1}.$$

3. Procedure for irradiation

All irradiations were made in a flat cylindrical vessel, 0.52 cm long, located about 0.5 m from the laser. The laser was not focussed to minimize heating of the front cell window which might induce undesirable thermal reactions. Care was also taken to prevent buildup of solid polymeric material inside the front window which could undergo heating and decomposition and could again yield thermal products. Decrease in window transmission was monitored with the power meter, and when the windows became significantly less transparent to UV radiation, they were removed from the cell and appropriately cleaned. Following irradiation, the entire contents of the vessel were injected into a Hewlett-Packard F&M model 5750 B gas chromatograph equipped with a flame ionization detector for analysis, as in the infrared laser experiments. During each photolysis experiment at 193 nm, the average energy per pulse transmitted by the cell, $\bar{E}_{C_2H_4+cell}$ was measured. Knowing the

value of ϵ(193 nm) and the cell absorbance, A_{cell} measured previously, the average value of the incident energy per pulse, $\bar{E}_0$, was then obtained from the equation:

$$\log_{10} (\bar{E}_0/\bar{E}_{C_2H_4+cell}) = \epsilon cl + A_{cell} \qquad (82)$$

Values of the average energy per pulse absorbed by ethylene in each experiment was then calculated:

$$\bar{E}_{abs(C_2H_4)} = \bar{E}_0(1-10^{-\epsilon cl}) \times T_{window} \times R_f \qquad (83)$$

where T_{window} = transmittance of front window obtained from the relation $\frac{1}{2}A_{cell} = A_{window} = -\log_{10} T_{window}$ and R_f is a factor correcting for light reflected from the windows, and passing back through the cell. Evaluation of R_f is discussed in Appendix E. A simple calculation gave the number of einsteins (moles) of 193 nm light absorbed by C_2H_4:

(i) The energy of one photon of light at 193 nm is:

$h\nu = hc/\lambda = 1.03 \times 10^{-18}$ J

(ii) The energy of one einstein of 193 nm light is:

$E = h\nu \times N_A = 6.20 \times 10^5$ J

where N_A = Avogadro's number

(iii) Einsteins of 193 nm light absorbed in C_2H_4:

$E_{abs(C_2H_4)}$(J)/6.20×10^5 J einstein^{-1}

Product quantum yields, ϕ(product), were then given by

$$\phi(\text{product}) = \frac{\text{yield of product(moles)}}{\text{light absorbed in } C_2H_4 \text{ (Einsteins)}} \qquad (84)$$

Similar methods and procedures were used for calculating quantum yields at 222, 249 and 308 nm, except that values of ϵ were not measured in the photolysis cell.

4. Reaction vessel

The photolysis vessel was identical to that used in the infrared experiments, but with plane fused silica (Suprasil) windows fixed to each side of the brass annulus instead of NaCl, with a space between the windows of 0.52 ± 0.01 cm, giving a volume of 1.63 ± 0.05 cm^3. The vessel in this case was demountable and could be connected to a vacuum line for evacuation or filling, or mounted in front of the laser for irradiation, or attached with Cajon fittings to the gas chromatograph for analysis. The photolysis cell is shown in Figure 39. Prior to each irradiation, the outside surfaces of the Suprasil windows were cleaned with a jet of Freon gas to remove dust which could lead to gradual degradation of the window quality.

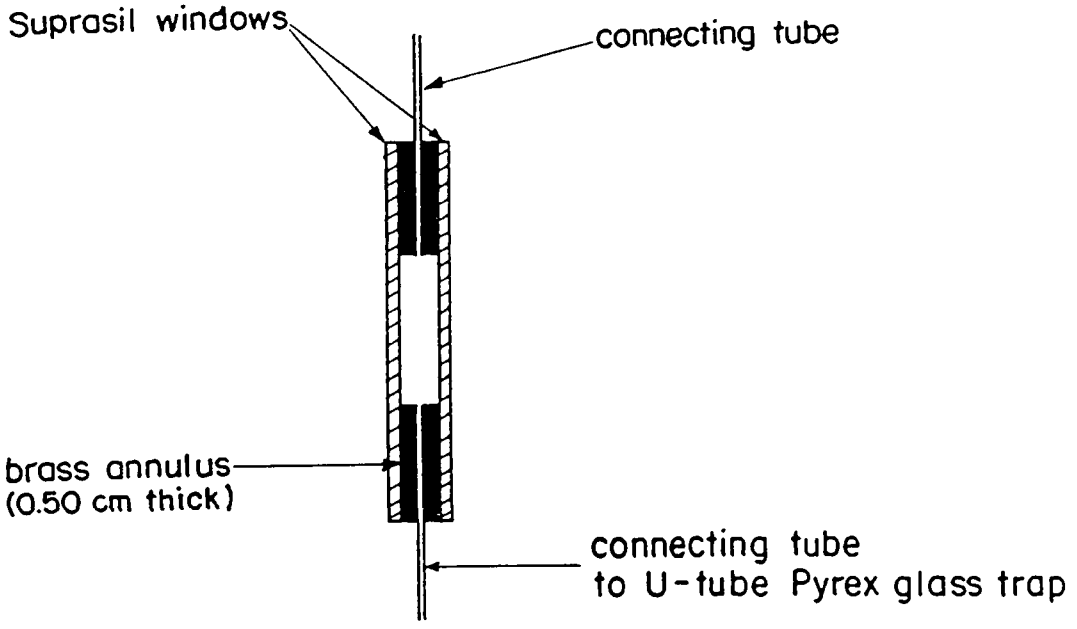

Figure 39. UV photolysis cell.

5. Materials

Ethylene and its preparation was the same as used in the infrared experiments. Except for methylcyclopropane (Columbia Organic Chemicals, Columbia, S.C.) which contained 10% ethane, 2% cyclopropane and 1% of 1-butene and the C_5 and C_6 standard liquid samples (Aldrich, Chemical Company, Inc. Milwaukee, Wis.) which had stated minimum purities of 99%, other standard hydrocarbons were identical to those used in the IR part of this study.

6. Columns used in chromatography

The columns were chiefly those used in the IR experiments described previously, with the following exceptions: A silica gel column (6.2 m x 6 mm o.d. at 373 K) was helpful in yielding somewhat better measurements of methane, ethane and propane compared to those made with the tandem column consisting of sections of VZ-7 and phenylisocyanate on Porasil C. In the 193 nm experiments, a 3.7 m x 6 mm o.d. Porapak Q column operating at 388 K also served to identify some of the minor products formed. The rather few measurements made on C_5 and C_6 hydrocarbons were obtained on a 6.2 m x 6 mm o.d. column of squalane (30%) on Chromosorb P AW-DMCS (80-100 mesh) kept at 345 K. A mass spectrometer (VG ANALYTICAL 7000 E) was also used in identifying some of the heavier products obtained.

7. Calibrations and corrections

The calibrations and corrections in this part were basically identical to those described in the experimental section of the free-radical chain reaction products in the IR part.

PHOTOLYSIS OF ETHYLENE AT 193 nm

1. Results

Under all conditions at this wavelength, the main products observed in approximate order of decreasing importance were acetylene, n-butane, 1-butene, ethane and 1,3-butadiene. The minor products, propane, propylene, methane, allene, 2-butene and methylcyclopropane were measured in most experiments, while other minor products, including C_5 (n-pentane, 1-pentene, 1,4-pentadiene) and C_6 (n-hexane, 1-hexene, 1,5-hexadiene) hydrocarbons, were analyzed only in a few cases. Although yields of hydrogen were not measured it was almost certainly a major product in the present study since it has been found to accompany acetylene in all previous VUV photolysis investigations of ethylene. On the other hand, while efforts were made to detect small yields of cyclobutane, this product was not found.

The product analysis at 193 nm is consistent with the occurrence of the three primary dissociation processes which have previously been observed in the VUV photolysis of ethylene between 121.6 and 193 nm [189-206]:

	ΔH/ kJ mol^{-1}	
$C_2H_4 + h\nu \rightarrow C_2H_2 + H_2$	174	(85)
$\rightarrow C_2H_2 + 2H\cdot$	610	(86)
$\rightarrow C_2H_3\cdot + H\cdot$	431	(87)

The energy of the absorbed quantum (620 kJ einstein^{-1}) exceeds the energy requirements of all three primary reactions. The hydrogen atoms [192-194] produced in (86) and (87), are expected to add rapidly to ethylene, yielding the ethyl radical: $H\cdot + C_2H_4 \rightarrow C_2H_5\cdot$ (88)

At room temperature the radicals formed have been shown to undergo mainly recombination and disproportionation reactions [224], while radical addition to ethylene, which requires appreciable activation energies, occurs to a much lesser degree. The following reaction scheme, which appears to account for the majority of products observed in this work, was in part suggested by Back and Griffiths [199] in the flash photolysis of ethylene in the range of 155-190 nm, and by Borrell, Cervenka and Turner [202] in an investigation of the photolysis of ethylene at 185 nm:

$$2C_2H_5^{\cdot} \rightarrow n\text{-}C_4H_{10} \quad (89)$$

$$\rightarrow C_2H_6 + C_2H_4 \quad (90)$$

$$C_2H_5^{\cdot} + C_2H_3^{\cdot} \rightarrow 1\text{-}C_4H_8 \quad (91)$$

$$\rightarrow C_2H_6 + C_2H_2 \quad (92)$$

$$\rightarrow 2C_2H_4 \quad (93)$$

$$2C_2H_3^{\cdot} \rightarrow 1,3\text{-}C_4H_6 \quad (94)$$

$$\rightarrow C_2H_2 + C_2H_4 \quad (95)$$

$$H^{\cdot} + C_2H_5^{\cdot} \rightarrow [C_2H_6^{*}] \quad (96)$$

$$[C_2H_6^{*}] \xrightarrow{(+M)} C_2H_6 + M \quad (97)$$

$$\rightarrow 2CH_3^{\cdot} \quad (98)$$

$$2CH_3^{\cdot} \rightarrow C_2H_6 \quad (99)$$

$$CH_3^{\cdot} + C_2H_5^{\cdot} \rightarrow C_3H_8 \quad (100)$$

$$\rightarrow CH_4 + C_2H_4 \quad (101)$$

$$CH_3\cdot + C_2H_3\cdot \rightarrow C_3H_6 \quad (102)$$

$$\rightarrow CH_4 + C_2H_2 \quad (103)$$

$$H\cdot + CH_3\cdot \xrightarrow{(+M)} CH_4 + M \quad (104)$$

A count of the products derived from ethyl and vinyl radicals in reactions (89)-(95) gives approximate values for $\phi(85)^*$, $\phi(86)$ and $\phi(87)$. In this treatment, reactions (96)-(99), which are possible sources of ethane and reactions (100)-(104), which may yield small amounts of methane and C_3 hydrocarbons, were neglected.

$$\phi(85) = \phi(C_2H_2) \quad \phi(86) \quad (A)$$

$$\phi(86) = \tfrac{1}{2}[2\phi(n\text{-}C_4H_{10})(1+k_{90}/k_{89}) + \phi(1\text{-}C_4H_8)(1+(k_{92}+k_{93})/k_{91}) \quad \phi(87)] \quad (B)$$

$$\phi(87) = 2\phi(1,3\text{-}C_4H_6)(1+k_{95}/k_{94}) + \phi(1\text{-}C_4H_8)(1+(k_{92}+k_{93})/k_{91}) \quad (C)$$

The values of rate constant ratios used in the expressions above are given in the following table.

Table 22. Rate constant ratios used for obtaining primary quantum yield values in the 193 nm photolysis of ethylene.

ratio	value	T/K	reference
k_{90}/k_{89}	0.14	298	[224]
k_{92}/k_{91}	0.12	434-448	[228]
k_{93}/k_{91}	0.03	434-448	[228]
k_{95}/k_{94}	0.02	323	[229]

* This primary quantum yield is based exclusively on hydrocarbon analysis; i.e. on the measurement of acetylene, as given by expression (A).

A. Time-dependent series (10-250 pulses) at 760 Torr

Product quantum yields from the photolysis at a pressure of 760 Torr of ethylene are plotted in Figure 40 as a function of number of pulses; the same data are shown in Table 23, together with extrapolated initial values from Figure 40. In this series, the average incident pulse energy was 20.4 ± 1.2 mJ, corresponding to an average incident light intensity of $2.4 \pm 0.2 \times 10^{16}$ photons cm^{-2} $pulse^{-1}$. The average pulse energy absorbed was 4.9 ± 0.3 mJ which corresponded to an average light intensity absorbed of $5.7 \pm 0.4 \times 10^{15}$ photons cm^{-2} $pulse^{-1}$. While the quantum yield for disappearance of ethylene based on product formation remained constant at $\phi(-C_2H_4) = 0.82 \pm 0.01$, the percentage of ethylene in the reaction vessel converted to products ranged from 0.10 up to 2.1%.

The acetylene quantum yield remained constant at $\phi(C_2H_2) = 0.42 \pm 0.01$. Quantum yields of ethane and n-butane increased with increasing number of pulses, while those of 1-butene and 1,3-butadiene decreased. The quantum yields of all the minor products measured, which include methane, propane, propylene, allene and methylcyclopropane increased with number of pulses; extrapolated initial yields are close to zero, and all these products appear to be largely of secondary origin.

Since depletion of ethylene is negligible in these experiments, the observed changes with number of pulses must be caused by loss of products through secondary reactions or photolysis. The decreasing trends in the 1,3-butadiene and 1-butene quantum yields is almost certainly caused by their secondary photolyses, since both have appreciable molar absorption coefficients at 193 nm, $\epsilon(1,3\text{-}C_4H_6) \sim 10^4$ M^{-1} cm^{-1} and $\epsilon(1\text{-}C_4H_8) \sim 5 \times 10^2$ M^{-1} cm^{-1}

Figure 40. Product quantum yields from the 193 nm photolysis of ethylene at a pressure of 760 Torr as a function of number of pulses.

A. main products

□ : acetylene
▼ : 1-butene
▲ : n-butane
▽ : ethane

B. minor products

■ : 1,3-butadiene
○ : propylene
● : propane
△ : methane
◪ : allene

Error bars (± 5%), which are estimates based on measurements, are only shown in cases where the uncertainties are greater than the dimension of the individual symbols.

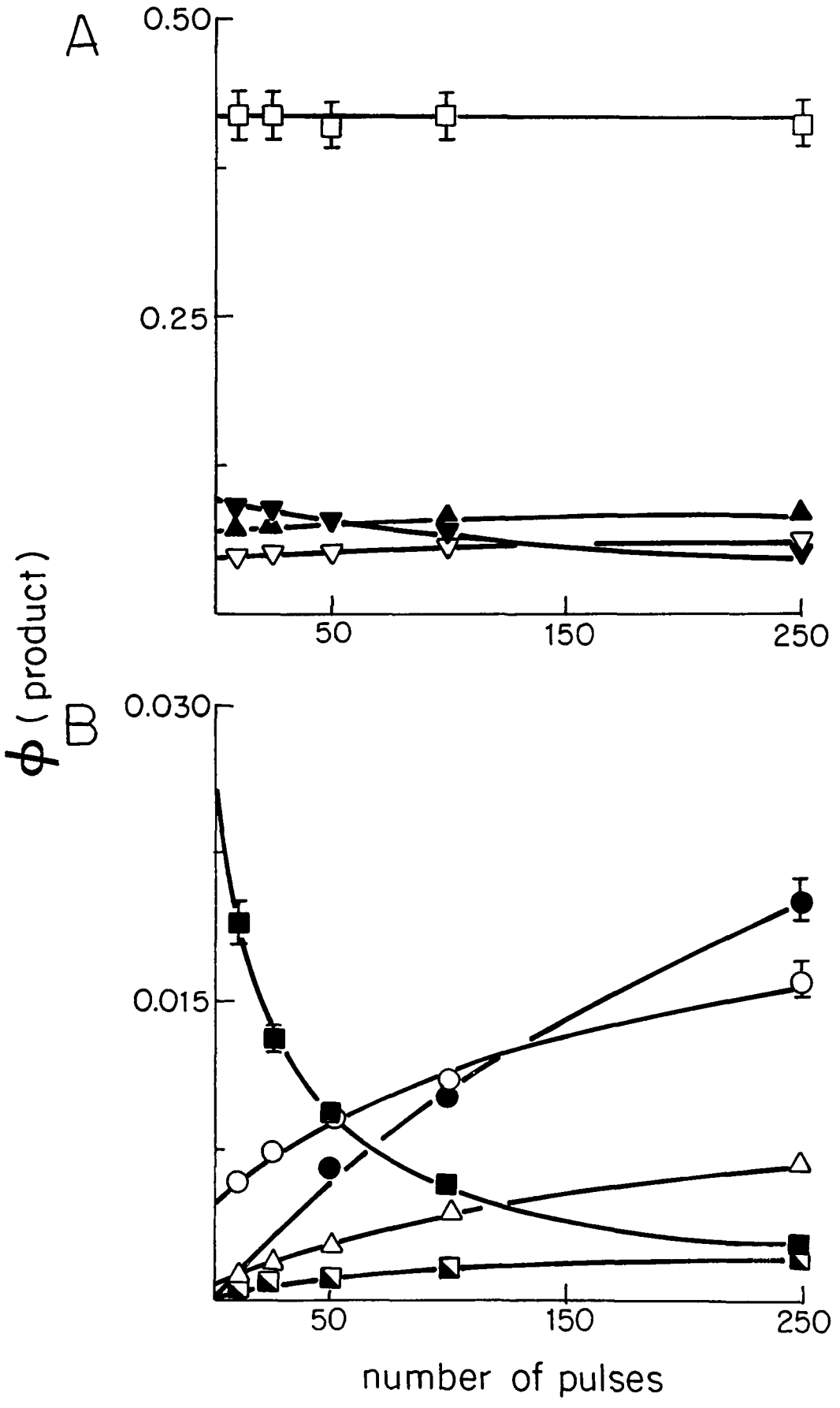
A
0.50
0.25
50
150
250
B
0.030
0.015
50
150
250
ϕ (product)
number of pulses

Table 23. Product quantum yields from the 193 nm photolysis of ethylene at a pressure of 760 Torr as a function of number of pulses.

product	initial extrapolated value	number of pulses 10	25	50	100	250
CH_4	$0.7 \pm 0.04 \times 10^{-3}$	1.2×10^{-3}	1.9×10^{-3}	2.7×10^{-3}	4.4×10^{-3}	6.9×10^{-3}
C_2H_6	$4.7 \pm 0.2 \times 10^{-2}$	4.8×10^{-2}	5.1×10^{-2}	5.2×10^{-2}	5.5×10^{-2}	6.1×10^{-2}
C_2H_2	$4.2 \pm 0.2 \times 10^{-1}$	4.2×10^{-1}	4.2×10^{-1}	4.1×10^{-1}	4.2×10^{-1}	4.1×10^{-1}
C_3H_8	0	———	———	6.5×10^{-3}	1.0×10^{-2}	2.0×10^{-2}
C_3H_6	$5.0 \pm 0.2 \times 10^{-3}$	5.9×10^{-3}	8.9×10^{-3}	9.0×10^{-3}	1.1×10^{-2}	1.6×10^{-2}
C_3H_4	0	3.7×10^{-4}	7.9×10^{-4}	1.1×10^{-3}	1.6×10^{-3}	2.1×10^{-3}
$n\text{-}C_4H_{10}$	$6.9 \pm 0.4 \times 10^{-2}$	7.1×10^{-2}	7.5×10^{-2}	7.6×10^{-2}	8.1×10^{-2}	8.4×10^{-2}
$c\text{-}CH_3C_3H_5$	0	———	———	———	5.5×10^{-5}	1.2×10^{-4}
$1\text{-}C_4H_8$	$9.6 \pm 0.5 \times 10^{-2}$	8.9×10^{-2}	8.8×10^{-2}	7.8×10^{-2}	6.9×10^{-2}	4.9×10^{-2}
$1,3\text{-}C_4H_6$	$2.5 \pm 0.1 \times 10^{-2}$	1.9×10^{-2}	1.3×10^{-2}	9.2×10^{-3}	5.7×10^{-3}	2.8×10^{-3}

[141]. The minor secondary products are very probably formed, directly or indirectly, by the same photolyses. The shape of the curve for propylene (Figure 40), itself a secondary product, suggests that it is also subject to secondary photolysis. Yields of the very minor product methylcyclopropane are too small to say with certainty if it is primary or secondary in origin. It is of interest because it may arise from reaction of an ethylidene radical with ethylene,

$$CH_3\ddot{C}H + C_2H_4 \rightarrow c\text{-}CH_3C_3H_5 \qquad (105)$$

since ethylidene has been postulated before as an intermediate in the photochemistry of ethylene [189-191,203,213,215,216]. Whether because it is not formed in the present system in substantial yields, or because it is formed but does not react efficiently, reaction (105) is of little importance, as the yield of methylcyclopropane is very low. It appears unlikely that this product would arise from the secondary photolysis of 1-butene on the basis of an investigation made by Harumiya, Shida and Arai [230] of the direct photolysis of this alkene at 185 nm in which they did not find methylcyclopropane. On the other hand, in a study of the Hg-photosensitized reaction of 1-butene, Cvetanovic and Doyle [231] measured methylcyclopropane and suggested that it was formed by a molecular rearrangement involving an internal 1,2- or a 1,4-migration of an H atom in the excited 1-butene.

Table 24 shows some significant product ratios. If ethane were formed only by the disproportionation reactions (90) and (92), then the ratio ethane/(n-butane + 1-butene) should have been ~ 0.13 (Table 22). From Table 24, the initial extrapolated value is about 0.28, suggesting that there is another source of ethane in the system, although it is just possible that the combined uncertainties in the initial extrapolation and in the

Table 24. Product ratios and secondary quantum yields from the 193 nm photolysis of ethylene at a pressure of 760 Torr as a function of number of pulses.

	number of pulses					
	initial extrapolated value	10	25	50	100	250
$C_2H_6/(n\text{-}C_4H_{10} + 1\text{-}C_4H_8)$	2.8×10^{-1}	3.0×10^{-1}	3.1×10^{-1}	3.4×10^{-1}	3.7×10^{-1}	4.6×10^{-1}
$(1\text{-}C_4H_8)^2/(n\text{-}C_4H_{10})(1,3\text{-}C_4H_6)$	5.3	5.9	7.9	8.7	1.03×10^{1}	1.02×10^{1}
C_2H_6 (secondary)	0	1.0×10^{-3}	4.0×10^{-3}	5.0×10^{-3}	8.0×10^{-3}	1.4×10^{-2}
$n\text{-}C_4H_{10}$ (secondary)	0	2.0×10^{-3}	6.0×10^{-3}	7.0×10^{-3}	1.2×10^{-2}	1.5×10^{-2}
C_2H_6 (secondary, corrected)	0	9.0×10^{-4}	3.4×10^{-3}	4.3×10^{-3}	6.9×10^{-3}	1.2×10^{-2}
$(C_3H_8)^2/4(n\text{-}C_4H_{10})$	0	———	———	1.4×10^{-4}	3.1×10^{-4}	1.2×10^{-3}

disproportionation/combination ratios could explain the difference. It is interesting that values of 0.25 and 0.21 for the same product ratio can be obtained from the data reported in two previous studies of the photolysis of ethylene at 185 nm [197,204]. It will be seen later that the most probable cause of the high ratio in the present work is the formation of ethane by the combination of H· with C_2H_5·, reactions (96) and (97). The increase in the ratio ethane/(n-butane + 1-butene) with increasing number of pulses reflects the changes in these three products evident in Table 23.

The second ratio of interest included in Table 24 is $(1\text{-butene})^2/(\text{n-butane})(1,3\text{-butadiene})$, which should have a value of about 4 if these three products were formed by random combination of ethyl and vinyl radicals, reactions (89), (91) and (94). The initial extrapolated value of this ratio is 5.3, and it rises to a value of 10.2 with increasing conversion. This rise is due to the sharp fall in 1,3-butadiene, partly compensated by the decrease in 1-butene and the increase in n-butane (Figure 40). Given the uncertainties in the initial extrapolations, particularly for 1,3-butadiene, the initial extrapolated value of 5.3 is close enough to the expected value of 4 to support the conclusion that n-butane, 1-butene and 1,3-butadiene were formed by radical combination.

As noted earlier, methyl radicals are probably involved in the secondary formation of propane and perhaps ethane via reactions (100) and (99). For random combination of ethyl and methyl radicals, the ratio $\phi(C_3H_8)^2/\phi(\text{n-}C_4H_{10})\phi(C_2H_6)_{(99)}$ should equal about 4 and $\phi(C_2H_6)_{(99)}$, the expected yield of ethane from reaction (99), should be given by $\phi(C_3H_8)^2/4\phi(\text{n-}C_4H_{10})$. These values may then be compared with the secondary yield of ethane corrected for that formed by reaction (90) accompanying the

secondary production of n-butane. This is given by:

$$\phi(C_2H_6)_{sec.cor.} = \phi(C_2H_6)_{tot.} - \phi(C_2H_6)_{init.} - 0.14[\phi(n\text{-}C_4H_{10})_{tot.} - \phi(n\text{-}C_4H_{10})_{init.}] \quad (106)$$

The relevant data are shown in Table 24, and it is clear that combination of methyl radicals made little contribution to the observed secondary formation of ethane. Again it seems probable that the source was instead reactions (96) and (97), and possibly the secondary reaction of ethyl radicals with 1-butene, which is very reactive towards abstraction:

$$C_2H_5^{\cdot} + 1\text{-}C_4H_8 \rightarrow C_2H_6 + H_2C{=}CH\text{-}\dot{C}H\text{-}CH_3 \quad (107)$$

Table 25 shows primary quantum yields, $\phi(85)$, $\phi(86)$ and $\phi(87)$ obtained from expressions (A)-(C), using initial extrapolated yields from Table 23. If, however, the additional initial ethane (in excess of that expected from disproportionation reactions (90) and (92) accompanying respectively the formation of n-butane and 1-butene) comes from $H^{\cdot} + C_2H_5^{\cdot}$, this amount should be added to $\phi(86)$, which in turn leads to a decrease in $\phi(85)$; $\phi(87)$ is unchanged. The corrected primary quantum yields are also included in Table 25.

Table 25. Primary quantum yields from the 193 nm photolysis of ethylene at a pressure of 760 Torr based on extrapolated initial values and corrected for the additional initial ethane coming from $H^{\cdot} + C_2H_5^{\cdot}$.

$\phi(85)$	0.37
$\phi(85)_{corrected}$	0.34
$\phi(86)$	0.05
$\phi(86)_{corrected}$	0.08
$\phi(87)$	0.16
ϕ(total)	0.58

B. Pressure-dependent series (50-3000 Torr) at 10 pulses

Product quantum yields in the 10 pulse photolysis series in which the average incident pulse energy was 29.2 ± 2.3 mJ, corresponding to an average incident light intensity of 3.3 ± 0.3 x 10^{16} photons cm^{-2} $pulse^{-1}$, are plotted in Figure 41 as a function of ethylene pressure (50-3000 Torr); the same data are shown in Table 26. Between the lowest and highest ethylene pressures, the average pulse energy absorbed ranged from 0.5 to 18.4 mJ, corresponding to a range of light intensity absorbed between 0.05 and 2 x 10^{16} photons cm^{-2} $pulse^{-1}$. In this pressure-dependent series, the percentage ethylene conversion to products decreased from 0.16% at 50 Torr down to 0.08% at 3000 Torr, reflecting the non-linear increase in percentage absorption with pressure.

The acetylene quantum yield decreased from a value of 0.47 at 50 Torr to 0.37 at 3000 Torr. The quantum yield of 1-butene remained constant at 0.086 ± 0.02, that of n-butane decreased from 0.082 to 0.067, while that of ethane increased from 0.037 to 0.059. The quantum yield of 1,3-butadiene increased, while that of propylene decreased. The other secondary products were not measured, as their yields were small.

Table 27 shows values of $\phi(85)$, $\phi(86)$ and $\phi(87)$ obtained from expressions (A)-(C) as a function of ethylene pressure. Also included are the corrected primary quantum yield values for the additional ethane formed by the combination of $H^{\cdot}$ and $C_2H_5^{\cdot}$; reactions (96) and (97). Shown in Figure 42A are values of $\phi(85)$, $\phi(86)$, $\phi(87)$, $\phi(86+87)$ and $\phi(total)$ as a function of ethylene pressure in the range between 50 and 3000 Torr. Reaction (85), the molecular elimination of hydrogen, is the main process at all pressures although its quantum yield declines slowly (~ 20-25%) between 50 and 3000 Torr.

Figure 41. Product quantum yields from the 193 nm photolysis of ethylene at 10 pulses as a function of ethylene pressure.

A. main products

□ : acetylene
▼ : 1-butene
▲ : n-butane
△ : ethane

B. minor products

■ : 1,3-butadiene
○ : propylene

Error bars (± 5%), which are estimates based on measurements, are only shown in cases where the uncertainties are greater than the dimension of the individual symbols.

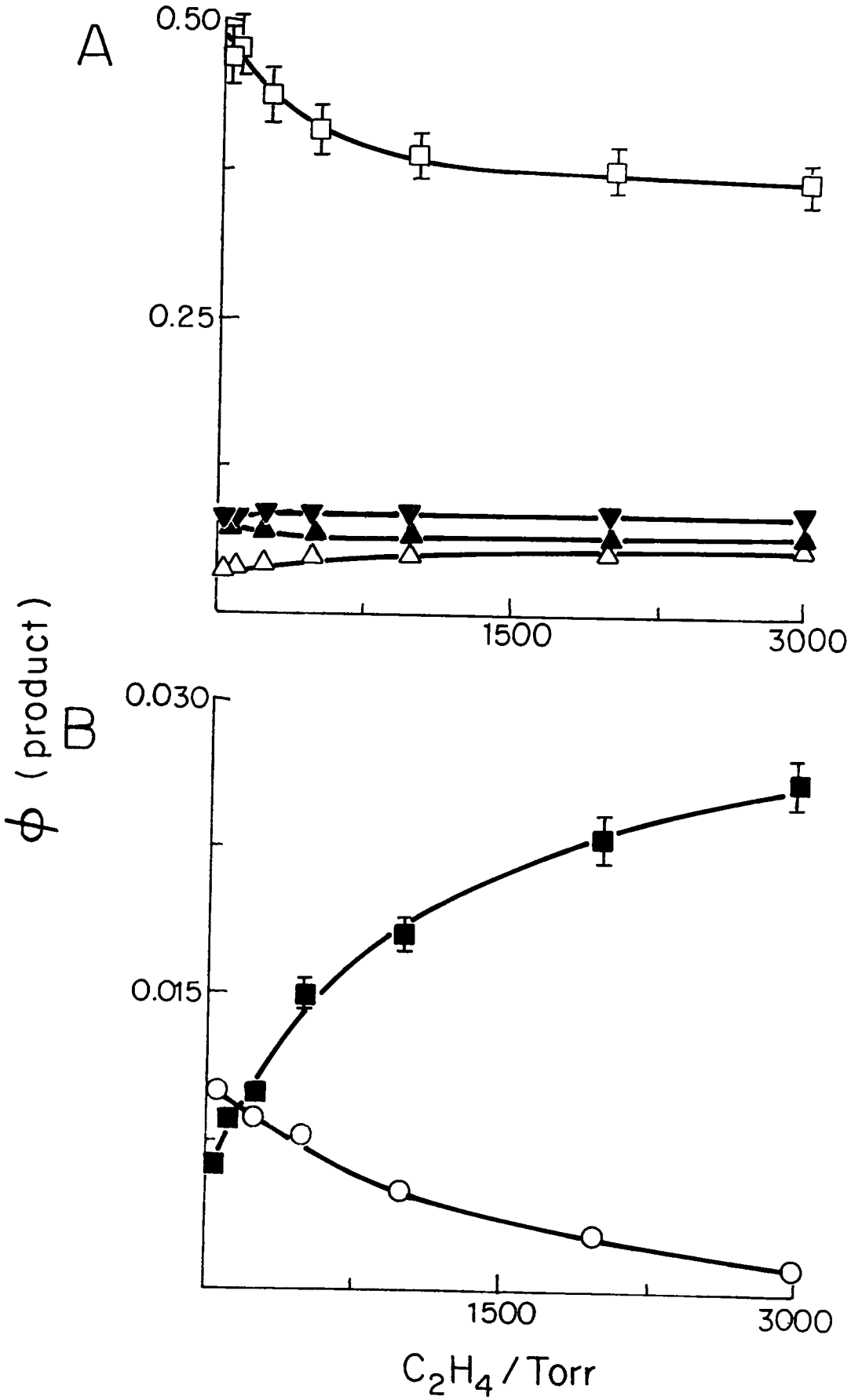
A
0.50
0.25
1500
3000
B
0.030
0.015
1500
3000
ϕ (product)
C2H4 / Torr

Table 26. Product quantum yields from the 193 nm photolysis of ethylene at 10 pulses as a function of ethylene pressure.

	C_2H_4/Torr						
product	50	100	250	500	1000	2000	3000
C_2H_6	3.7×10^{-2}	3.8×10^{-2}	4.2×10^{-2}	4.7×10^{-2}	5.2×10^{-2}	5.4×10^{-2}	5.9×10^{-2}
C_2H_2	4.7×10^{-1}	4.8×10^{-1}	4.4×10^{-1}	4.1×10^{-1}	3.9×10^{-1}	3.8×10^{-1}	3.7×10^{-1}
C_3H_6	9.9×10^{-3}	8.6×10^{-3}	8.5×10^{-3}	7.8×10^{-3}	5.0×10^{-3}	2.9×10^{-3}	1.4×10^{-3}
n-C_4H_{10}	8.2×10^{-2}	7.3×10^{-2}	7.1×10^{-2}	6.8×10^{-2}	6.8×10^{-2}	6.6×10^{-2}	6.7×10^{-2}
1-C_4H_8	8.2×10^{-2}	8.3×10^{-2}	8.7×10^{-2}	8.6×10^{-2}	8.8×10^{-2}	8.6×10^{-2}	8.8×10^{-2}
1,3-C_4H_6	6.3×10^{-3}	8.6×10^{-3}	9.9×10^{-3}	1.5×10^{-2}	1.8×10^{-2}	2.3×10^{-2}	2.6×10^{-2}

Table 27. Uncorrected and corrected primary quantum yields for the additional ethane coming from $H^{\cdot} + C_2H_5^{\cdot}$ from the 193 nm photolysis of ethylene at 10 pulses as a function of ethylene pressure.

	C_2H_4/Torr						
	50	100	250	500	1000	2000	3000
$\phi(85)$	0.38	0.40	0.37	0.35	0.33	0.33	0.32
$\phi(85)_{corrected}$	0.36	0.38	0.35	0.32	0.30	0.30	0.28
$\phi(86)$	0.09	0.08	0.07	0.06	0.06	0.05	0.05
$\phi(86)_{corrected}$	0.11	0.10	0.09	0.09	0.09	0.08	0.09
$\phi(87)$	0.11	0.11	0.12	0.13	0.14	0.15	0.15
ϕ(total)	0.58	0.59	0.56	0.54	0.53	0.53	0.52

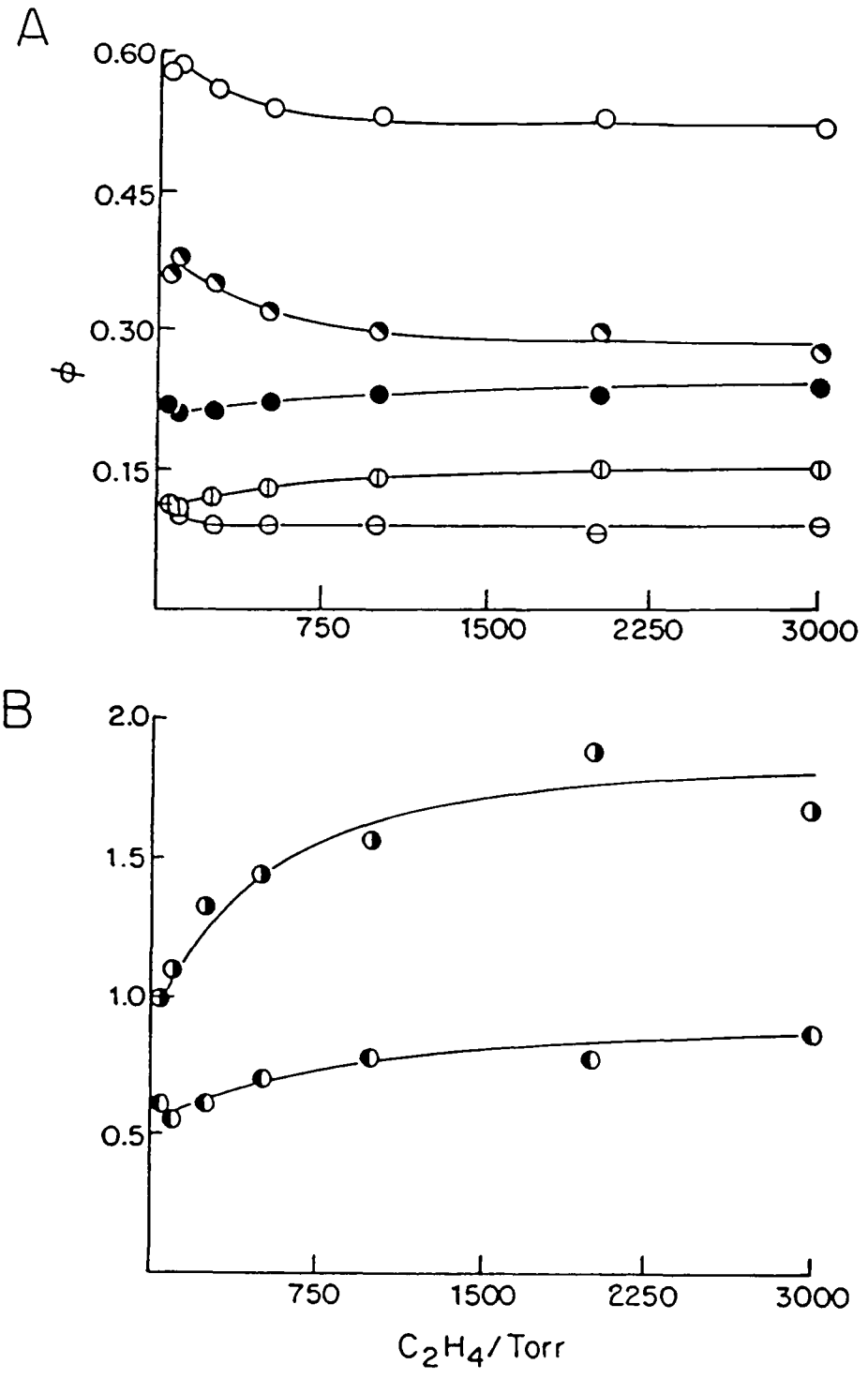

Figure 42. Primary quantum yield data from the 193 nm photolysis of ethylene at 10 pulses as a function of ethylene pressure.

A. ◔ : φ(85), ⊖ : φ(86), ◐ : φ(87),
● : φ(86+87), ○ : φ(total)

B. ◑ : φ(87)/φ(86), ◐ : φ(86+87)/φ(85)

Reaction (87) increases while reaction (86) decreases in the same pressure range. The observed decrease in the total quantum yield from a value of 0.58 at 50 Torr to 0.52 at 3000 Torr is almost entirely accounted for by the decrease in $\phi(85)$, since the changes in $\phi(86)$ and $\phi(87)$ approximately compensate one another. The observed decrease in $\phi(C_2H_2)$ with pressure is thus attributable to the decreasing importance of both primary processes (85) and (86). The decrease in process (86) and the compensating increase in (87) point to collisional stabilization of the vinyl radical as suggested previously [198,199] or possibly to vibrational de-excitation of a precursor. In the photolysis of ethylene at 185 nm, both Potzinger and coworkers [195] and Borrell et al. [202] also observed a decrease in the acetylene quantum yield, and proposed collisional quenching of several different excited states of ethylene. A constant quantum yield of 1-butene was also reported by Potzinger et al. [195] at 185 nm between ethylene pressures of 0.1-100 Torr; they also found a decrease in $\phi(n\text{-}C_4H_{10})$ from 0.24 to 0.18. The decrease in n-butane in the present work, and probably in the earlier studies, can be attributed to the decrease in process (86) and thence in H-atoms and C_2H_5 radicals. The increase in $\phi(C_2H_6)$ is probably best explained by the enhancement of reactions (96) and (97) due to the higher concentrations of $H\cdot$ and $C_2H_5\cdot$ at higher pressures, and by increased stabilization of the $C_2H_6^*$ produced. The increasing trend in $\phi(1,3\text{-}C_4H_6)$ can be attributed to the increase in $\phi(87)$ with increasing pressure.

Table 28 shows the ratios $C_2H_6/(n\text{-}C_4H_{10} + 1\text{-}C_4H_8)$ and $(1\text{-}C_4H_8)^2/(n\text{-}C_4H_{10})(1,3\text{-}C_4H_6)$, both as a function of pressure. As before, the first ratio exceeds 0.13, the value expected if ethane were all formed by disproportionation, and increases with increasing pressure, probably due to an

Table 28. Product ratios from the 193 nm photolysis of ethylene at 10 pulses as a function of ethylene pressure.

	C_2H_4/Torr						
ratio	50	100	250	500	1000	2000	3000
$C_2H_6/(n\text{-}C_4H_{10} + 1\text{-}C_4H_8)$	2.3×10^{-1}	2.4×10^{-1}	2.7×10^{-1}	3.1×10^{-1}	3.3×10^{-1}	3.6×10^{-1}	3.8×10^{-1}
$(1\text{-}C_4H_8)^2/(n\text{-}C_4H_{10})(1,3\text{-}C_4H_6)$	1.30×10^{1}	1.10×10^{1}	1.08×10^{1}	7.2	6.3	4.9	4.4

increase in reactions (96) and (97). The second ratio again should be equal to about 4 for a random combination of ethyl and vinyl radicals. The decrease in this ratio with pressure suggests a decrease in secondary photolysis of 1,3-butadiene with increasing pressure, probably due to collisional stabilization of the photoexcited 1,3-C_4H_6 molecules [232].

2. Discussion

Because the wavelengths of 185 and 193 nm are rather close to one another, corresponding to an energy difference of only ~ 27 kJ mol^{-1}, it is useful to compare the primary quantum yields obtained by Potzinger and coworkers at 185 nm [195] at pressures from 0.12 to 100 Torr with those obtained in the present investigation at 193 nm at higher pressures (50-3000 Torr).

Figure 43 is a semilogarithmic plot of $\phi(85)$, $\phi(86+87)$ and ϕ(total) as a function of ethylene pressure, and includes both the data of Potzinger et al. and those of the present study, all based on hydrocarbon analysis. It is interesting to note that within the scatter of the experimental measurements, both sets of data can be reasonably well combined in single smooth curves. In the work of Potzinger et al., $\phi(85)$ remained constant at about 0.45 between 0.12 and 0.63 Torr and then declined to a value of 0.37 at 100 Torr, while in the present work, $\phi(85)$ is subject to a relatively smooth decrease from 0.36 at 50 Torr to 0.28 at 3000 Torr. The trend in the quantum yield of the radical processes, $\phi(86+87)$, found by Potzinger and coworkers is similar to that for $\phi(85)$, a constant value of ~ 0.35 at $P \leq 0.63$ Torr, followed by a decrease to 0.25 at 100 Torr. The present data on the other hand exhibit a slight increase

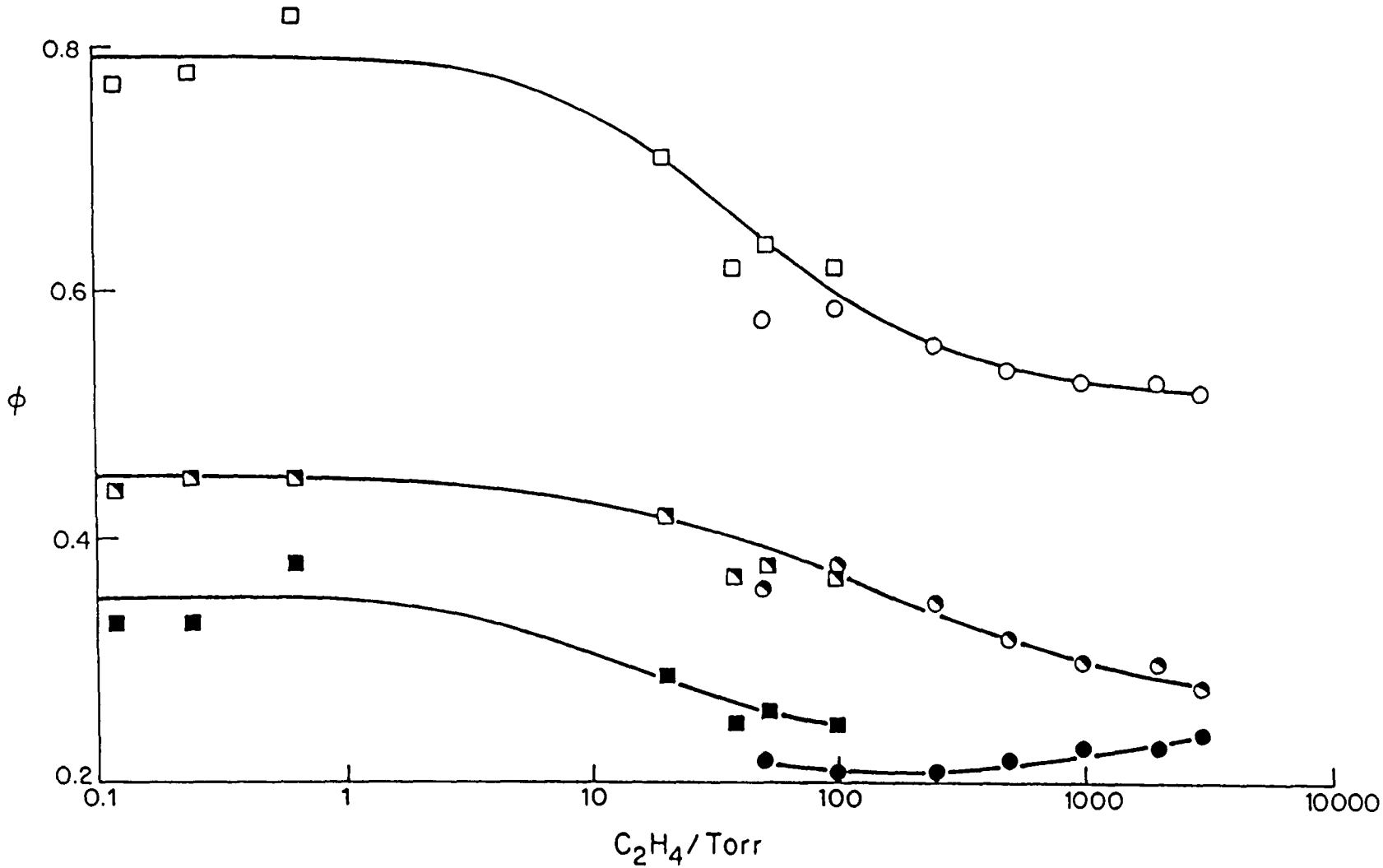

Figure 43. Primary quantum yield data from the 184.9 nm [195] and 193 nm photolysis of ethylene at 10 pulses as a function of ethylene pressure.

184.9 nm: ◪ : ϕ(85), ■ : ϕ(86+87), □ : ϕ(total)

193 nm : ◔ : ϕ(85), ● : ϕ(86+87), ○ : ϕ(total)

in $\phi(86+87)$ with increasing pressure. For ϕ(total), Potzinger et al. reported a constant value of 0.79 at $P \leq 0.63$ Torr, and then a smooth decrease to 0.62 at 100 Torr. The present data which slightly overlaps the pressures of the previous work, shows a continuing decrease in ϕ(total) from 0.58 at 50 Torr down to 0.52 at 3000 Torr.

The major difference between the data at 185 and 193 nm appears in the ratio $\phi(87)/\phi(86)$ (Figure 42B). While this ratio is observed to increase with increasing pressure at both wavelengths, it is much smaller, by a factor of ~ 5 at 50 and 100 Torr, at 185 nm. It will be seen that the increase of this ratio with increasing pressure can almost certainly be attributed to the collisional stabilization of vinyl radicals which otherwise would decompose further to acetylene and a hydrogen atom. The smaller value of $\phi(87)/\phi(86)$ at 185 nm must reflect a higher level of vibrational excitation of the vinyl radicals produced at this wavelength, and a consequent shorter lifetime for decomposition.

Also included in Figure 42B is the ratio of $\phi(86+87)/\phi(85)$ as a function of ethylene pressure at 193 nm. The increase in this ratio, which represents the proportion of radical to molecular processes, is due in part to the slight increase in $\phi(86+87)$ with pressure but mainly to the greater decrease in $\phi(85)$. At the lower pressures of the earlier work at 185 nm [195], this ratio decreased slightly with increasing pressure.

It seems reasonable to continue the comparison of the present data at 193 nm with the earlier work at lower pressures at 185 nm by discussing the combined results in terms of the scheme proposed by Potzinger and coworkers for the photolysis of ethylene between 147 and 193 nm [195]. This scheme suggested that participation of at least three different states of ethylene had to be invoked to explain the results of a kinetic analysis of the system:

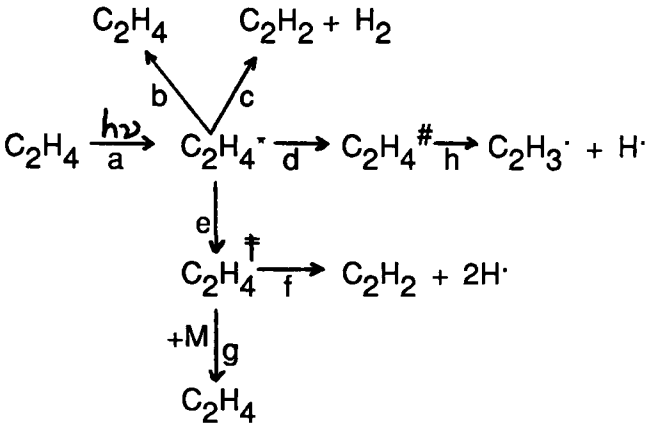

The three states of ethylene in this scheme, $C_2H_4^*$, $C_2H_4^{\#}$ and $C_2H_4^{\ddagger}$, were not all clearly specified, and it is useful at this point to examine closely the electronic states of ethylene most likely to be involved in its photochemistry at $\lambda \geq 185$ nm.

Schematic potential energy diagrams of these states are shown as a function of torsional angle in Figure 44. Absorption of a photon at 193 nm excites ethylene from its planar electronic ground state, $N(^1A_g)$, (point group D_{2h}), into its first excited electronic singlet state, $V(^1B_2)$, in which in the equilibrium configuration one CH_2 group has been twisted by 90° relative to the other (point group D_{2d}). The origin of the $V \leftarrow N$ ($\pi^* \leftarrow \pi$) band at 228.5 nm (523.7 kJ mol^{-1}) shown in this figure as well as the vibrational energy levels of the V state were obtained from the work of Foo and Innes [158]. The value of the vertical excitation energy (at 0°) of the V state of 733 kJ mol^{-1} was taken from Robin [53]. The curve for the spectroscopically unseen $Z(^1A_g)$ state, which possesses an ion-pair or zwitterionic structure and results from the excitation of two electrons from the π orbital to the π^* orbital is shown as a dotted line, and is only a rough estimate. When the ethylene molecule is twisted to 90° geometry the π and π^* orbitals become

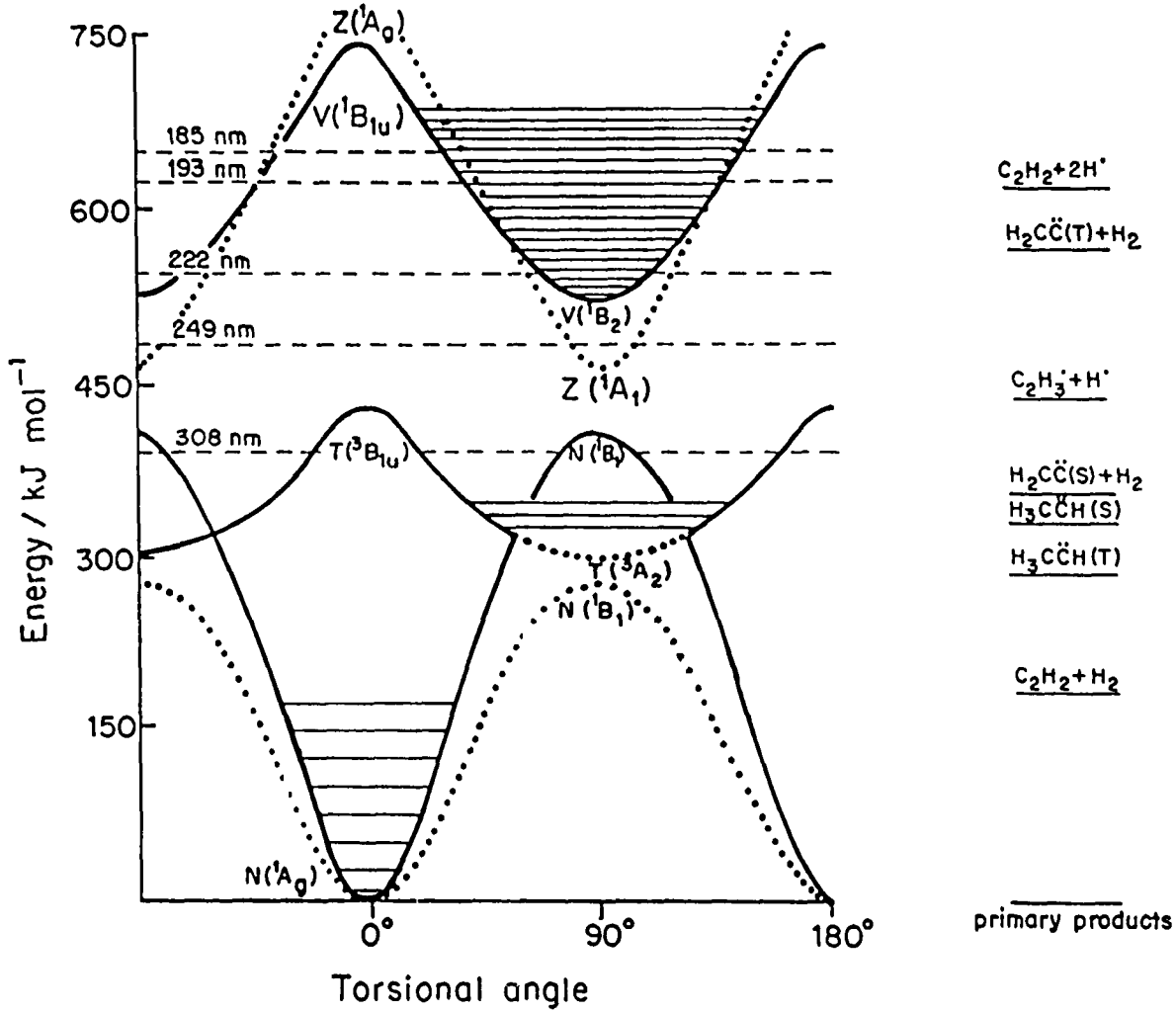

Figure 44. Schematic potential energy diagrams of the N, T, V and Z electronic states of ethylene as a function of torsional angle.
Heats of formation from ethylene for the three primary dissociation processes ((85)-(87) in the text) are taken from standard sources [79,99] while those involving the intermediates ethylidene and vinylidene are taken from the work of Luke, Pople and coworkers [233].

degenerate, and the N- and Z- state configurations interact to generate, through an avoided crossing, the maximum in the N state and the minimum in the Z state, which in this geometry are the ($^1B_1$) and ($^1A_1$) states respectively. The Z-state minimum has been drawn to be somewhat below that of the V state as has been suggested, although its position is by no means certain [178,183,234]. On the other hand, the vertical energy (at 0°) of the planar doubly excited Z state must lie far above that of the V state.

Besides the V state and the Z state, the electronic ground state, N(^1A_g), and the first excited triplet state, T($^3A_2$), may also be important intermediates in the photolysis of ethylene.

Figure 44 shows two potential energy curves for the ground state having different barriers to internal rotation. The one drawn as a dotted line has a barrier of 272 kJ mol^{-1} which is the activation energy for the thermal cis-trans isomerization of dideuteroethylene obtained by Douglas, Rabinovitch and Looney [235]. This value is usually taken as the minimum barrier to internal rotation. The full line shows the pure torsional barrier of ~ 400 kJ mol^{-1} obtained by Sension, Mayne and Hudson [166] who fitted a long progression of even overtones of the torsional mode, ν''_4, observed in a far UV resonance Raman study, to a potential function of standard form. The even vibrational levels in the ground state shown in the figure are taken from this work.

Because the origin of the T ← N band in ethylene is not well established, the potential minimum of this state is shown as a dashed line at an energy of 290 kJ mol^{-1}. The three adjacent ν_4 vibrational levels of the T state shown in Figure 44 were taken from the low-energy electron loss spectrum of the T ← N band in ethylene measured at high scattering angles by Wilden and

Comer [127] (Figure 36). The vertical excitation energy of the planar T state of 421 kJ mol^{-1} was taken from a threshold electron-impact spectrum of ethylene obtained by van Veen [160].

Also included in Figure 44 are the photon energies for the several wavelengths between 185 and 308 nm used in the photolysis and heats of formation from ethylene of the possible primary products.

In the scheme put forward by Potzinger et al. [195], four processes b, c, d and e were postulated for the originally formed $C_2H_4^*$, which at 185 and 193 nm is undoubtedly the V state. Since none of these processes are apparently affected by collisions, they must be occurring very rapidly, hence implying a short-lived V state. An estimate of the lifetime at 760 Torr based on a collisional deactivation rate of 82 ns Torr in ethylene [236], yields a value ≤ 0.11 ns.

Process b was postulated to account for the loss without product formation of about 20% of the V state originally excited, even at a pressure as low as 0.12 Torr, and thus a maximum ϕ(total) of ~ 0.8 at 185 nm. Potzinger and coworkers do not specify how this loss occurs, but it appears that it must involve formation of a long-lived intermediate, B, that can be completely deactivated by collisions even at 0.12 Torr and eventually reverts to ground state ethylene with insufficient energy to decompose or react:

$$V \xrightarrow[(0.21)]{\text{fast}} B^{\ddagger} \xrightarrow{+M} B \longrightarrow C_2H_4$$

There is no obvious candidate for B. The known behavior of the triplet state and the vibrationally excited ground state in the mercury photosensitized decomposition rule these out [211,213,216]. Ethylidene is an interesting possibility because of its low energy (see Figure 44); if it were totally relaxed vibrationally by collisions before reverting to C_2H_4, the resulting molecule

would be below the energy threshold for decomposition to $C_2H_2 + H_2$, which is probably ~ 350 kJ mol^{-1} [105]. A problem with ethylidene is whether it would be sufficiently unreactive towards C_2H_4; one might expect sizeable yields of methylcyclopropane at high pressure from such a reaction. The very small yields of methylcyclopropane obtained in the present study (193 nm) suggest that ethylidene, if it is formed, is indeed unreactive towards C_2H_4. Furthermore, in recent vacuum UV flash photolysis studies of ethylene (λ > 155 nm), Laufer and coworkers [200,201] reported a very long-lived vinylidene triplet ($^3B_2$), which perhaps suggests that the ethylidene triplet ($^3A''$) might also be unreactive.

Process c giving $C_2H_2 + H_2$ is equivalent to our reaction (85); its pressure dependence is complex. Measurements of $\phi(H_2)$ by Potzinger and coworkers show it to be unaffected by pressure up to a pressure of 100 Torr, but found $\phi(85)$, based on hydrocarbon analysis (C_2H_2), to decline from about 0.45 to 0.37 between 0.12 and 100 Torr. It would be interesting to know whether this difference in $\phi(H_2)$ and $\phi(85)$ continued at higher pressure and at 193 nm, but the present experiments were not designed to measure H_2 and this question must therefore await future measurements. A difference in $\phi(H_2)$ and $\phi(85)$ could arise from reactions removing vinylidene radicals before they can rearrange to C_2H_2, since Laufer's work appears to show that H_2CC: is an intermediate in the formation of C_2H_2, and is relatively long-lived [200,201]. There is no evidence for such reactions in the products observed, but yields would be small and may not have been detected by the analysis employed.

The decline in $\phi(85)$ with increasing pressure continues in our experiments, falling from about 0.37 at 50 Torr to 0.28 at our highest pressure (Figures 42A and 43). Stern-Volmer plots of Potzinger's data and the present

results (Figure 45) indicate two quenching processes consisting of an efficient one at low pressure (0.12-50 Torr) and a less efficient one between 50 and 1000 Torr. From the combined data at 185 and 193 nm, the molecular C_2H_2 yield can be divided in 3 parts:

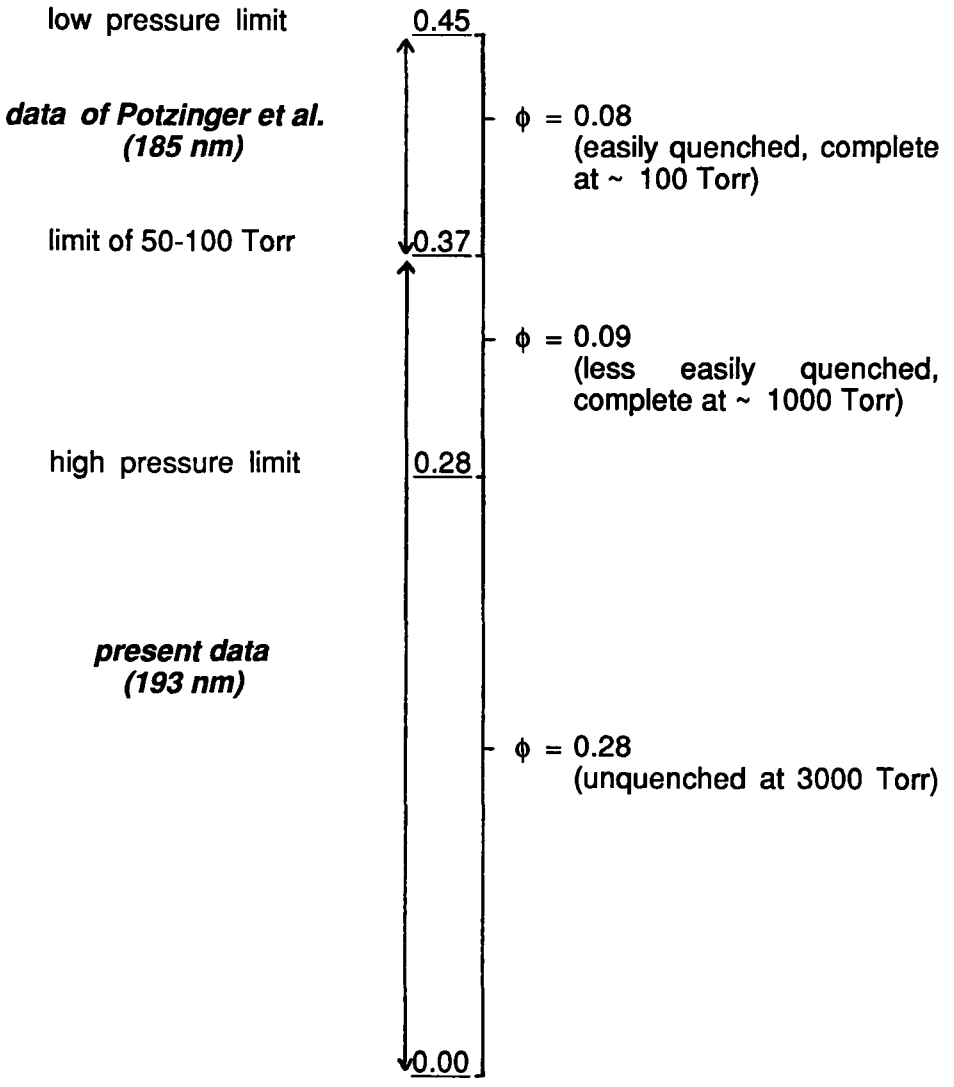

The easily quenched yield of 0.08 might correspond to loss of H_2CC: radicals, as discussed. The less easily quenched yield of 0.09 suggests decomposition via an unspecified intermediate C. The yield of 0.28 unquenched at 3000 Torr

Figure 45

A. Stern-Volmer plot for the portion of reaction (85) quenchable below 50 Torr.

An intermediate having a lifetime of ~ 25 μs was estimated from the slope assuming a quenching rate constant of k_q (dm^3 mol^{-1} s^{-1}) = 10^9.

B. Stern-Volmer plot for the portion of reaction (85) quenchable between 50 and 1000 Torr.

An intermediate having a lifetime of ~ 0.7 μs was estimated from the slope assuming a quenching rate constant of k_q (dm^3 mol^{-1} s^{-1}) = 10^9.

◪ : 184.9 nm ◔ : 193 nm

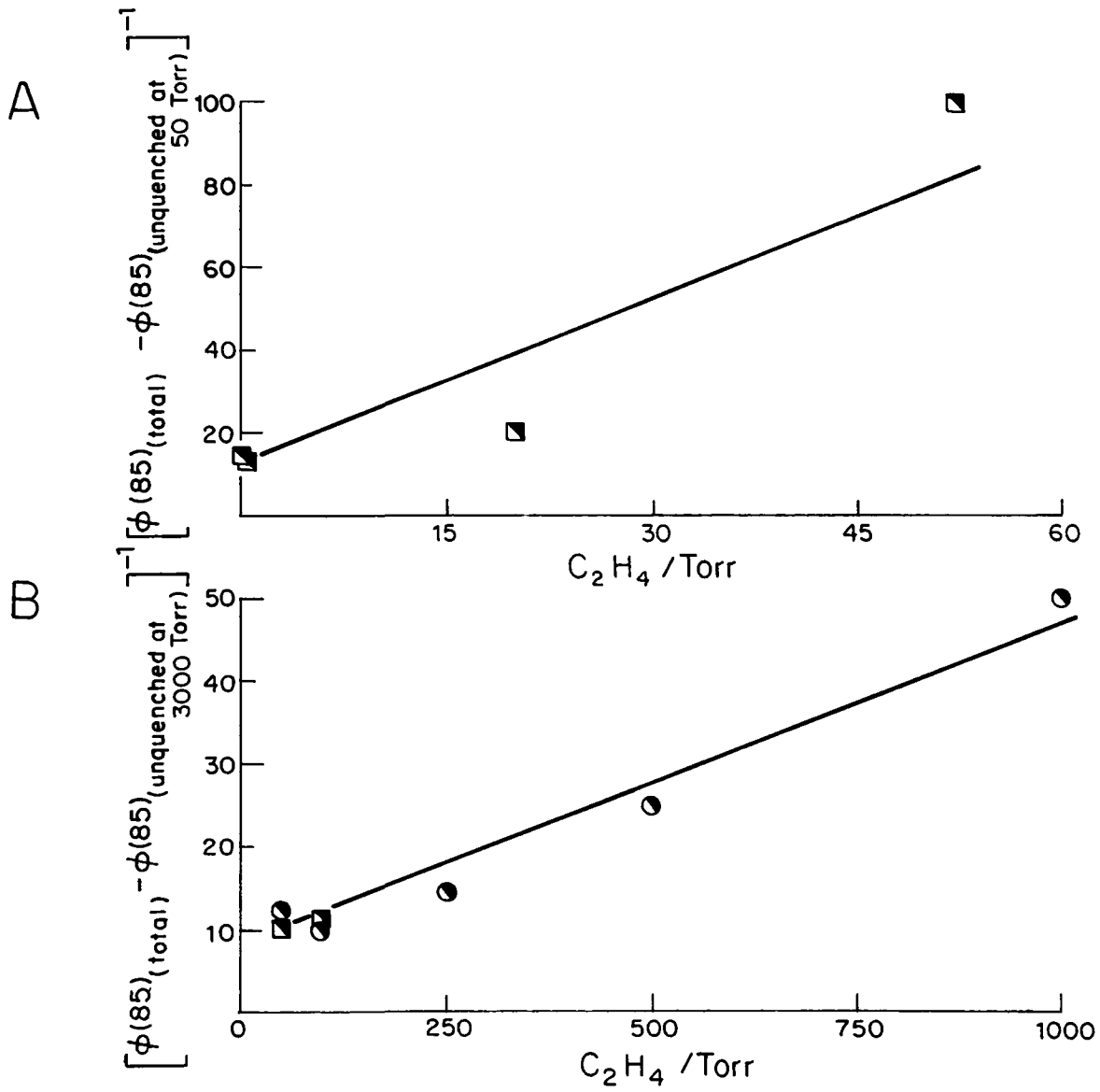
A
$[\phi(85)_{(total)} - \phi(85)_{(unquenched\ at\ 50\ Torr)}]^{-1}$
100
80
60
40
20
15
30
45
60
C_2H_4 / Torr
B
$[\phi(85)_{(total)} - \phi(85)_{(unquenched\ at\ 3000\ Torr)}]^{-1}$
50
40
30
20
10
0
250
500
750
1000
C_2H_4 /Torr

most probably corresponds to direct dissociation of the V state. The above three yields are included between parentheses in the following modification to process c in the scheme:

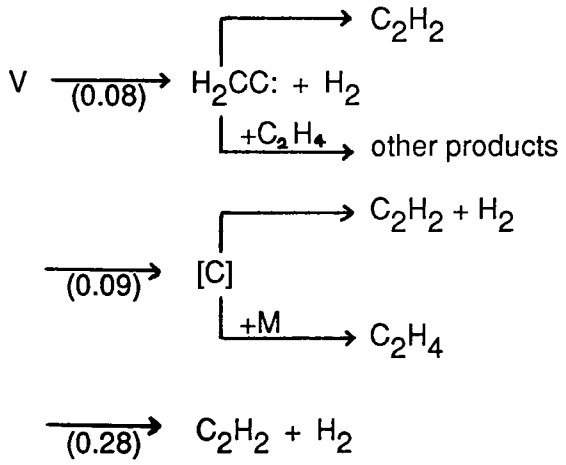

Process d was suggested by Potzinger and coworkers to account for vinyl radical production and for $C_2H_2 + 2H^{\cdot}$, which contributes to the yield of acetylene along with process c up to their highest pressure of 100 Torr. The present results suggest a modification, the formation of vibrationally hot vinyl radicals which decompose at low pressure but can be stabilized by collision, also suggested in an earlier flash photolysis study [199] and in a 163.4 nm photolysis of ethylene [198]. The data at 193 nm indicate complete stabilization of $C_2H_3^{\cdot}$ by about 2000 Torr, evident in the plot of $\phi(87)$ in Figure 42A. Process k then yields directly $C_2H_2 + 2H^{\cdot}$ while process h gives $C_2H_3^{\cdot\ddagger} + H^{\cdot}$. There seems no need for an intermediate ($C_2H_4^{\#}$), since h and k could occur directly from the V state; if there is an intermediate it is unaffected by pressure at 3000 Torr, i.e. very short-lived. Process d in Potzinger's scheme would be omitted, and replaced by h and k, along with the yields of these processes shown between parentheses:

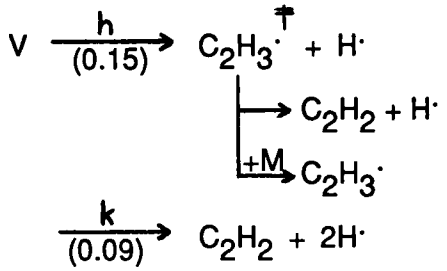

Process e was suggested by Potzinger et al. to explain the decrease in ϕ(86+87) from ~ 0.35 at low pressure to ~ 0.25 at 100 Torr; the decrease in fact occurred only in ϕ(86) and not in ϕ(87) which remained constant at ~ 0.044. Values of ϕ(86+87) in the present study lie slightly lower at about 0.21 at pressures from 50 to 250 Torr. This most probably is because yields of 1-butene and 1,3-butadiene in the 10-pulse pressure dependent series are not initial values extrapolated to zero time, and thus are slightly lower than the initial extrapolated values of Potzinger and coworkers. The slight rise in ϕ(86+87) between 250 and 3000 Torr (Figures 42A and 43) supports this explanation, since loss of products by secondary photolysis would decrease at higher pressure as discussed earlier and also observed by Srinivasan [232]. Process e thus requires the formation of an intermediate E with a quantum yield of about 0.10 which is fully quenched at ~ 100 Torr, and which decomposes to C_2H_2 + 2H· at low pressure. A lifetime of ~ 16 μs can be estimated for E from a Stern-Volmer plot of Potzinger's data (Figure 46), assuming a quenching rate constant of $k_q(dm^3\ mol^{-1}\ s^{-1}) = 10^9$.

Firm identification of the intermediate E is difficult, but the T state or the Z state, especially if the latter lies below the V state, are the most probable candidates. The vibrationally excited ground state is less likely, as some molecular dissociation to C_2H_2 + H_2 might be expected.

Figure 46. Stern-Volmer plot for the quenchable portion of reactions (86+87).

From the slope, a lifetime of ~ 16 μs was estimated for intermediate ^1E assuming a quenching rate constant of k_q ($dm^3\ mol^{-1}\ s^{-1}$) = 10^9.

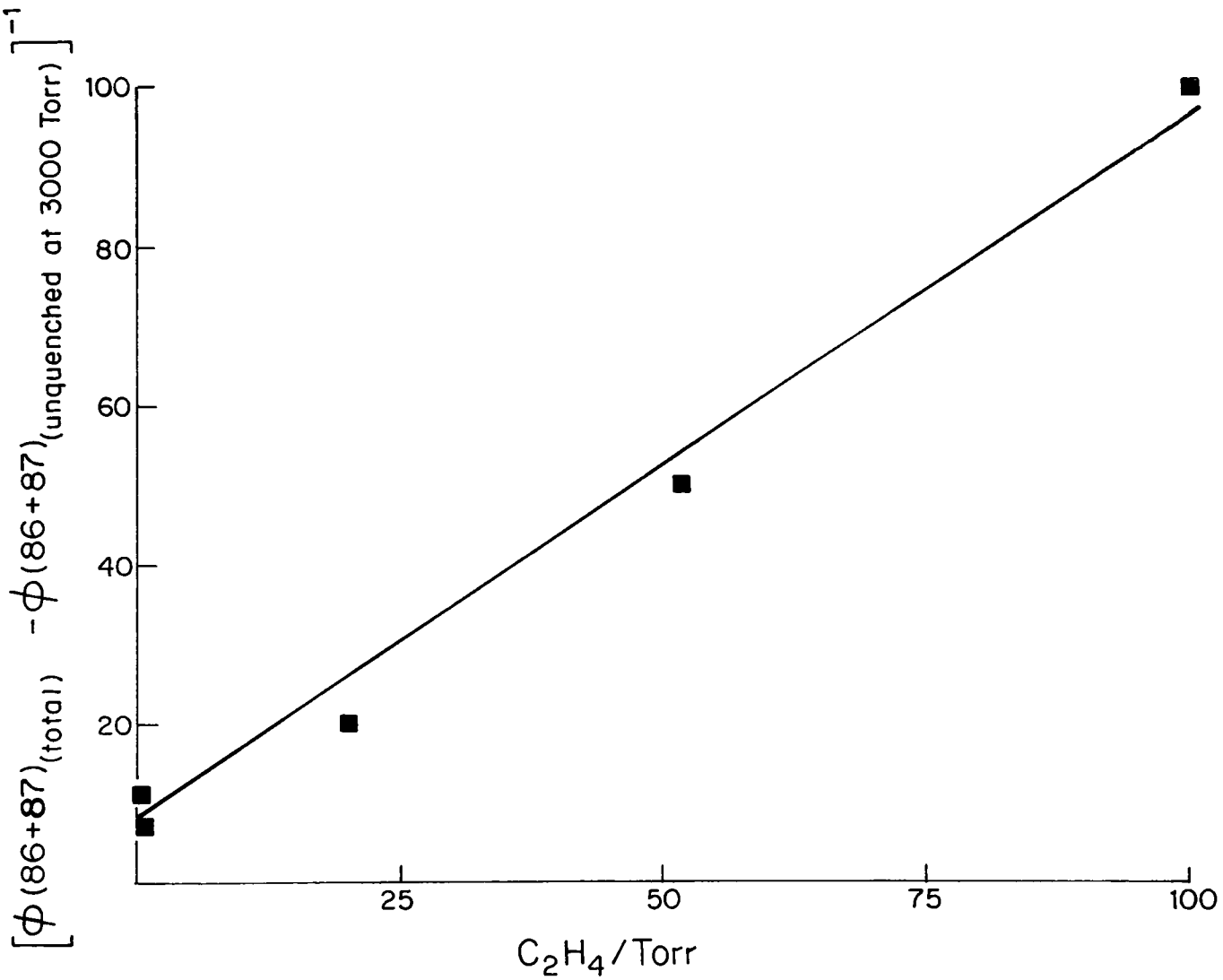
$\left[\phi_{(86+87)_{(total)}} - \phi_{(86+87)_{(unquenched\ at\ 3000\ Torr)}}\right]^{-1}$
100
80
60
40
20
25
50
75
100
C_2H_4 / Torr

The complete modified mechanism for the combined results from 185 and 193 nm can now be summarized by the following scheme in which numbers included between parentheses refer to the quantum yields of the individual processes discussed above:

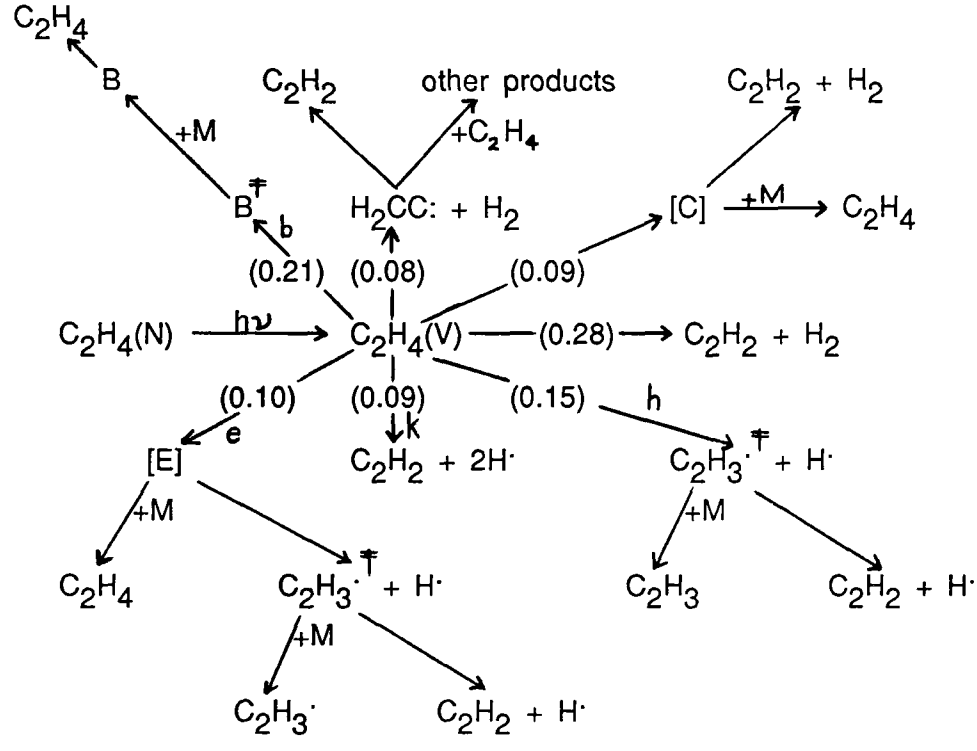

The photodissociation of C_2H_4 following excitation of the V state is surprisingly complex for such a simple molecule. Some details of the mechanism remain uncertain, especially the precise roles played by the several electronic states that may be involved. Both Evleth and Sevin in a theoretical study of the proposed primary photoprocesses in ethylene [237] and Collin in a recent review on the present status of the UV photochemistry of this molecule [54], have suggested that many reaction paths involving a variety of excited states are possible and that ethylidene and vinylidene intermediates may also play some part.

In order to further clarify the mechanism for the UV photodecomposition of ethylene at 193 nm, the following experiments need to be done: (1) A careful measurement of the quantum yields of products at ethylene pressures below 0.12 Torr, the lowest pressure in Potzinger's investigation, to study the behavior of ϕ(total) to find out if it increases towards a value of 1.0 as the pressure approaches zero, where deactivating collisions become negligible. (2) A measurement of the quantum yield of hydrogen, $\phi(H_2)$, at pressures above 100 Torr, to determine whether it remains constant at ~ 0.43, as found by Potzinger and coworkers at $P \leq 100$ Torr, or whether it decreases as ϕ(85) is observed to do. These experiments should be done at low conversion, and yields extrapolated to initial values at zero time to avoid loss of products by secondary photolysis.

PHOTOLYSIS OF ETHYLENE BETWEEN 222 AND 308 nm

1. Results and Discussion

The much weaker absorption by ethylene at these longer wavelengths required much longer irradiation time (1 h) at a higher pulse repetition rate (100 Hz) in order to observe photolysis. The main products measured at 222, 249 and 308 nm in approximate order of decreasing importance were acetylene, ethane, n-butane, propylene, methane and 1-butene. Minor products included n-pentane, 1,3-butadiene, allene, 2-butene, methylcyclopropane and i-pentane. Propane was probably also formed but the small amounts were obscured by the tail of the large ethylene peak on the chromatogram. As at 193 nm, hydrogen was very probably also a product but its yields were not measured. No formation of cyclobutane was detected at these wavelengths.

To obtain quantum yields, energy absorbed in the reaction cell was calculated from measurements of incident power and absorption coefficients taken from absorption measurements made in this laboratory [227] in a 3 m cell at 900 Torr, as noted earlier.

Table 29 shows quantum yields of products at 222, 249 and 308 nm with initial extrapolated values at 193 nm and 760 Torr for comparison. Several features of these data may be noted:

(1) The quantum yield of acetylene, $\phi(C_2H_2)$, falls sharply from 0.42 at 193 nm to much lower values at the longer wavelengths, continuing the trend seen by Potzinger et al. [195] and other workers [192,193,196-198,202,203] at shorter wavelengths. It appears to reach a minimum of 0.063 at 249 nm and rises again slightly up to 0.096 at 308 nm, although these variations are probably

within the errors of measurement. At 222, 249 and 308 nm, the quantum energy is insufficient to give C_2H_2 + 2H· (reaction (86)) so that acetylene may probably be taken as a measure of reaction (85), the molecular dissociation to C_2H_2 + H_2.

(2) There are more free radical products, relative to acetylene, at the longer wavelengths than at 193 nm. If these arose only from reaction (87) followed by reactions (88) to (104), one would expect the yields of n-butane and 1,3-butadiene to be about equal. There is in fact a large excess of n-butane suggesting loss of 1,3-butadiene and/or some additional source of H atoms leading to ethyl radicals.

(3) Ethane becomes a major product at these longer wavelengths and methane yields are also significantly larger, both products again probably coming from radical reactions.

Table 29. Product quantum yields from the photolysis of ethylene between 193 and 308 nm at a pressure of 760 Torr.

	λ/nm			
product	193*	222	249	308
CH_4	0.00070	0.0027	0.017	0.0039
C_2H_6	0.047	0.035	0.048	0.024
C_2H_2	0.42	0.072	0.063	0.096
C_3H_6	0.0050	0.0072	0.012	0.0060
n-C_4H_{10}	0.069	0.010	0.012	0.018
1-C_4H_8	0.096	0.0066	0.0097	0.0053
1,3-C_4H_6	0.025	0.00016	0.0017	0.00074

* Initial extrapolated value

Secondary photolysis of products such as 1,3-butadiene and 1-butene probably account for some of these observations, especially at 222 nm and perhaps at 249 nm; absorption coefficients are not accurately known at these wavelengths. Sensitized decomposition by energy transfer from relatively long lived excited ethylene molecules might also play a role, and a variety of other secondary reactions may be important. In the absence of measurements over a range of reaction times and pressures, further speculation about the detailed mechanism of product formation is unwarranted.

Finally, the excited states of ethylene that may be involved at the longer wavelengths require some comment.

From the vibrational analysis of Foo and Innes [158] and their proposed band origin at 228.5 nm, a 222 nm photon can excite ethylene to the first vibrational level (4_o^1) of the V state (Figure 44). Absorption measurements at 195 K [227] suggest that "hot bands" may make some contribution to the absorption at 222 nm, thereby exciting some molecules to the $v'_4 = 2$, and perhaps $v'_4 = 3$ levels. There seems little doubt that at 222 nm, the V state is the one initially excited, the same state as that involved at 193 and 185 nm. The lower quantum yield of C_2H_2 presumably reflects the lower energy content at the longer wavelength.

As indicated by the electron energy loss spectrum measured by Wilden and Comer [127] (Figure 36) and by the schematic potential energy diagrams of the different electronic states of ethylene (Figure 44), excitation at both 249 and 308 nm falls within the triplet absorption band of ethylene. Simple Boltzmann calculations show that hot band excitation of the V $\leftarrow$ N transition is completely negligible at these wavelengths. In fact, the absorption showed a considerable enhancement on cooling to 195 K, and a pressure dependence,

which together suggest that weakly bound ethylene dimers might be involved [227]. The absorption at 249 and 308 nm, while very weak, is stronger than might be expected for the forbidden T $\leftarrow$ N transition.

A quantum yield of H_2 of ~ 8 x 10^{-3} can be estimated for the $Hg(^3P_1)$ sensitized decomposition of C_2H_4 [213] which almost certainly excites the triplet state. The present measurements of $\phi(C_2H_2)$ at 249 and 308 nm are about 8-12 times larger than this value. A very tentative explanation of this difference, suggested by the possibility that ethylene dimers might be involved in the absorption, is a molecular disproportionation occurring in the dimer after excitation,

$$(C_2H_4)_2 + h\nu \rightarrow C_2H_4 \cdot C_2H_4\ (T)$$

$$\downarrow$$

$$C_2H_6 + C_2H_2$$

which would also account for the large yields of ethane observed. Further speculation is unwarranted until a better understanding of the optical absorption spectrum at these wavelengths is obtained. Further studies of the photolysis of ethylene at these longer wavelengths is also obviously desirable, but the combination of weak absorption and low quantum yields make these very difficult.

CONTRIBUTIONS TO ORIGINAL RESEARCH

1. In the thermal decomposition of ethylene induced with a pulsed CO_2 laser the reversible reaction

$$2C_2H_4 \rightleftarrows c\text{-}C_4H_8$$

was explored as a potential monitor of the average temperature of the reaction.

2. Measurements of the absorption of the 10 P(12) and 10 P(14) emission lines of the CO_2 laser by ethylene showed that the effective absorbance was a complex function of both the pressure and temperature. The variation in ϵ_{eff} with pressure was shown to be caused largely by pressure-broadening of the sharp absorption lines while its dependence on temperature was explained in terms of the depopulation of the absorbing (ground state) level in ethylene.

3. Measurement of the energy absorbed permitted the calculation of the temperature profile along the reaction vessel and led to an estimate of the effective reaction zone immediately following the laser pulse.

4. Computer modelling of the rate of approach to equilibrium of the reversible reaction over a range of conditions of pressure, maximum temperature and cooling and heating rates showed that the constant final value of cyclobutane indicated an effective reaction temperature somewhat lower than the maximum temperature achieved during the pulse.

5. The experimental measurement of a constant final value of the product cyclobutane allowed an estimate of an effective reaction temperature in the system under various reaction conditions.

6. A comparison between the temperatures estimated from the product cyclobutane and from the energy absorbed suggested that little expansion occurred during heating of the gas by the laser pulse. Thus the present system was probably closer to the limiting assumption of constant volume during the pulse rather than constant pressure.

7. The distribution of products of the reaction (other than cyclobutane) was shown to be consistent with the occurrence of a radical chain reaction with characteristics intermediate between those at about 750 K (static studies) and 1500 K (shock-tube investigations).

8. In a study of the UV photolysis of ethylene using a pulsed ArF excimer laser at 193 nm, measurement of the absorption coefficient $\epsilon = 5.6\ M^{-1}\ cm^{-1}$ provided accurate product quantum yields as a function of both time (10-250 pulses) and pressure (50-3000 Torr).

9. A count of the products derived from ethyl and vinyl radicals provided approximate values of the primary quantum yields $\phi(1)$, $\phi(2)$, $\phi(3)$ of the following three dissociation reactions:

$$C_2H_4 + h\nu(\lambda = 193\ nm) \rightarrow C_2H_2 + H_2 \quad (1)$$

$$\rightarrow C_2H_2 + 2H\cdot \quad (2)$$

$$\rightarrow C_2H_3\cdot + H\cdot \quad (3)$$

10. The quantum yields of 1-butene and 1,3-butadiene were found to decrease with increasing number of pulses. The minor products measured were suggested to arise from the secondary photolysis of these two main products which have appreciably greater absorption coefficients than ethylene at 193 nm.

11. In the pressure-dependent series while the quantum yield of primary process (1), $\phi(1)$, decreased from 0.36 to 0.28, $\phi(2)$ decreased from 0.11 to 0.09 and $\phi(3)$ increased from 0.11 to 0.15 between the lowest (50 Torr) and highest (3000 Torr) pressures.

12. The total primary quantum yield varied between 0.5 and 0.6 decreasing with increasing pressure. A mechanism was proposed to account for the pressure dependence of the quantum yields of the three primary processes both in the present work and that of Potzinger and coworkers at 185 nm. This mechanism is similar to that suggested by the latter, but with significant modifications, and involves a very short-lived V state which disappears by a number of competing channels. In one of the channels, vibrationally excited vinyl radicals are formed which can decompose to $C_2H_2 + H^{\cdot}$ or can be stabilized by collision, accounting for the pressure dependence of primary processes (2) and (3).

13. A preliminary investigation of the photolysis of ethylene at wavelengths between 222, 249 and 308 nm with excimer lasers yielded measurable decomposition products despite the very weak absorption of ethylene at these longer wavelengths where $\epsilon \sim 10^{-3}$-10^{-4} M^{-1} cm^{-1} At the two

longer wavelengths, the triplet state is probably excited, and possible mechanisms of product formation are discussed.

REFERENCES

[1] T.H. Maiman, Nature 187, 493 (1960).

[2] N.R. Isenor and M.C. Richardson, Appl. Phys. Lett. 18, 224 (1971).

[3] N.R. Isenor, V. Merchant, R.S. Hallsworth and M.C. Richardson, Can. J. Phys. 51, 1281 (1973).

[4] V.S. Letokhov, E.A. Ryabov and O.A. Tumanov, Sov. Phys. JETP 36, 1069 (1973).

[5] R.V. Ambartzumian, V.S. Letokhov, E.A. Ryabov, and N.V. Chekalin, JETP Lett. 20, 273 (1974).

[6] R.J. Jensen, J.G. Marinuzzi, C.P. Robinson and S.D. Rockwood, Laser Focus 12, 51 (1976).

[7] I.P. Herman and J.B. Marling, Chem. Phys. Lett. 64, 75 (1979).

[8] J.L. Lyman and S.D. Rockwood, J. Appl. Phys. 47, 595 (1976).

[9] J.G. Black, E. Yablonovitch, N. Bloembergen and S. Mukamel, Phys. Rev. Lett. 38, 1131 (1977).

[10] C.D. Cantrell and H.W. Galbraith, Opt. Commun. 18, 513 (1976).

[11] R.V. Ambartzumian, Yu.A. Gorokhov, V.S. Letokhov, G.N. Makarov and A.A. Puretzkii, JETP Lett. 22, 177 (1975).

[12] R.S. McDowell, H.W. Galbraith, B.J. Krohn, C.D. Cantrell and E.D. Hinkley, Opt. Commun. 1, 178 (1976).

[13] N. Bloembergen, Opt. Commun. 15, 416 (1975).

[14] R.V. Ambartzumian, Yu.A. Gorokhov, V.S. Letokhov and G.N. Makarov, Sov. Phys. JETP 42, 993 (1975).

[15] P.A. Schulz, Aa.S. Subdo, D.J. Krajnovich, H.S. Kwok, Y.R. Shen and Y.T. Lee, Ann. Rev. Phys. Chem. 30, 379 (1979).

[16] R. Naaman and R.N. Zare, Faraday Discuss. Chem. Soc. 67, 242 (1979).

[17] J.L. Lyman, G.P Quigley and O.P. Judd, in "Multiple Photon Excitation and Dissociation of Polyatomic Molecules", (C. Cantrell, ed.), Top. Curr. Phys., Springer-Verlag, New York, 1986, Vol. 35, pp. 9-94.

[18] W.C. Danen and J.C. Jang, in "Laser Induced Chemical Processes", (J.I. Steinfeld, ed.), Plenum Press, New York, 1981, pp. 45-164.

[19] W.C. Danen, V.C. Rio and D.W. Setser, J. Am. Chem Soc. 104, 5431 (1982).

[20] D.W. Setser, H.H. Nguyen and W.C. Danen, J. Phys. Chem. 87, 408 (1983).

[21] J.C. Jang-Wren, D.W. Setser and J.C. Ferrero, J. Phys. Chem. 89, 414 (1985).

[22] D.W. Setser, T.S. Lee and W.C. Danen, J. Phys. Chem. 89, 5799 (1985).

[23] J.G. Black, P. Kolodner, M.J. Shultz, E. Yablonovitch and N. Bloembergen, Phys. Rev. A 19, 704 (1979).

[24] P.A. Hackett, V. Malatesta, W.S. Nip, C. Willis and P.B. Corkum, J. Phys. Chem. 85, 1152 (1981).

[25] A. Pasternak, D.J. James, J.A. Nilson, D.K. Evans, R.D. McAlpine, H.M. Adams and E.B. Selkirk, Appl. Opt. 20, 3849 (1981).

[26] D.K. Evans, R.D. McAlpine and H.M. Adams, J. Chem. Phys. 77, 3551 (1982).

[27] D.K. Evans, R.D. McAlpine, H.M. Adams and A.L. Creagh, Chem. Phys. 80, 379 (1983).

[28] D.K. Evans, R.D. McAlpine and H.M. Adams, Isr. J. Chem. 24, 187 (1984).

[29] M.N.R. Ashfold, C.G. Atkins, G. Hancock and A.J. MacRobert, Isr. J. Chem. 24, 197 (1984).

[30] R.A. Back, D.K. Evans and H.M. Adams, Can. J. Chem. 62, 1525 (1984).

[31] N. Bloembergen, I. Burak, E. Mazur and T.B. Simpson, Isr. J. Chem. 24, 179 (1984).

[32] T.B. Simpson, J.G. Black, I. Burak, E. Yablonovitch and N. Bloembergen, J. Chem. Phys. 83, 628 (1985).

[33] M.J. Coggiola, P.A. Schulz, Y.T. Lee and Y.R. Shen, Phys. Rev. Lett. 38, 17 (1977).

[34] W.M. Shaub and S.H. Bauer, Int. J. Chem. Kinet. 7, 509 (1975).

[35] E. Grunwald, D.F Dever and P.M. Keehn, "Megawatt Infrared Laser Chemistry", Wiley, New York, 1978.

[36] C. Steel, V. Starov, R. Leo, P. John and R.G. Harrison, Chem. Phys. Lett. 62, 121 (1979).

[37] N. Selamoglu and C. Steel, J. Phys. Chem. 87, 1133 (1983).

[38] N. Selamoglu, Ph.D. Thesis, Brandeis University, Massachusetts (1983).

[39] W.C. Danen, W.D. Munslow and D.W. Setser, J. Am. Chem. Soc. 99, 6961 (1977).

[40] A.T. Blades, Can. J. Chem. 47, 615 (1969).

[41] M.H. Back and R.A. Back, Can. J. Chem. 57, 1511 (1979).

[42] R.G. Harrison, H.L. Hawkins, R.M. Leo and P. John, Chem. Phys. Lett. 70, 555 (1980).

[43] V. Starov, N. Selamoglu and C. Steel, J. Phys. Chem. 85, 320 (1981).

[44] R.A. Back, Can. J. Chem. 60, 2542 (1982).

[45] P. John, M.R. Humphries, R.G. Harrison and P.G. Harper, J. Chem. Phys. 79, 1353 (1983).

[46] M.-K. Au, P.A. Hackett, M. Humphries and P. John, Laser Chem. 4, 275 (1984).

[47] R.N. Rosenfeld, J.I. Brauman, J.R. Barker and D.M. Golden, J. Am. Chem. Soc. 99, 8063 (1977).

[48] J.M. Preses, R.E. Weston, Jr. and G.W. Flynn, Chem. Phys. Lett. 46, 69 (1977).

[49] L.M. Quick, D.A. Knecht and M.H. Back, Int. J. Chem. Kinet. 4, 61 (1972).

[50] L. Giroux, M.H. Back and R.A. Back, "Thermal reactions of ethylene induced by pulsed infrared laser radiation", Laser Applications in Chemistry, (D.K. Evans, ed.), Proc. SPIE 669, 72 (1986).

[51] K. Hohla, H. Pummer and C.K. Rhodes, in "Excimer Lasers", (C.K. Rhodes, ed.) Top. Appl. Phys., Springer-Verlag, New York, 1984, Vol. 30, pp. 229-257.

[52] C.A. Brau, in "Excimer Lasers", (C.K. Rhodes, ed.), Top. Appl. Phys., Springer-Verlag, New York, 1984, Vol. 30, pp. 87-137.

[53] M.B. Robin, "Higher Excited States of Polyatomic Molecules", Academic Press, New York, 1975, Vol. 2, pp. 2-22, 1985, Vol. 3, pp. 213-227.

[54] G.J. Collin, in "Advances in Photochemistry", (D.H. Volman, G.S. Hammond and K. Gollnick, eds.), Wiley, New York, 1988, Vol. 14, pp. 136-140.

[55] H.H. Li, J. Phys. Chem. Ref. Data 5, 329 (1976).

[56] N.P. Barnes and M.S. Piltch, J. Opt. Soc. Am. 69, 178 (1979).

[57] D.F. Dever and E. Grunwald, J. Am. Chem Soc. 98, 5055 (1976).

[58] K.J. Olszyna, E. Grunwald, P.M. Keehn and S.P. Anderson, Tetrahedron Lett. 19, 1609 (1977).

[59] F.M. Lussier, J.I. Steinfeld and T.F. Deutsch, Chem. Phys. Lett. 58, 277 (1977).

[60] B.G. Gowenlock, P. John, R. Leo, R.G. Harrison, S. Butcher and C. Steel, J. Photochem. 9, 200 (1978).

[61] V. Starov, C. Steel and R.G. Harrison, J. Chem. Phys. 71, 3304 (1979).

[62] V. Starov, N. Selamoglu and C. Steel, J. Am. Chem. Soc. 103, 7276 (1981).

[63] R.A. Gorber, R.E. McNair, S.F. Fulghum, M.S. Feld and B.J. Feldman, J. Chem. Phys. 72, 4693 (1980).

[64] D.S. King, in "Dynamics of the Excited State", (K.P Lawley, ed.), Adv. Chem. Phys., Wiley, New York, 1982, Vol. 50, pp. 105-189.

[65] V.N. Bagratashvili, V.S. Letokhov, A.A. Makarov and E.A. Ryabov, "Multiple Photon Infrared Laser Photophysics and Photochemistry", Harwood, New York, 1985.

[66] J. Blazejowski and F.W. Lampe, J. Photochem. 29, 285 (1985).

[67] J. Blazejowski and F.W. Lampe, Spectrochimica Acta 43A, 265 (1987).

[68] S.K. Sarkar, V. Parthasarathy, K.V.S. Rama Rao and J.P. Mittal, J. Photochem. 35, 13 (1986).

[69] E.M. Alonso, A.L. Peuriot and V.B. Slezak, Appl. Phys. B 40, 39 (1986).

[70] J.L. Lyman, J.M. Telle and R.C. Eckhart, Spectrochimica Acta 43A, 141 (1987).

[71] G.D.T. Tejwani and E.S. Yeung, J. Quant. Spectrosc. Radiat. Transfer 20, 499 (1978).

[72] F. Herlemont, M. Lyszyk, J. Lemaire, CH. Lambeau and A. Fayt, J. Mol. Spectrosc. 74, 400 (1979).

[73] CH. Lambeau, A. Fayt, J.L. Duncan and T. Nakagawa, J. Mol. Spectrosc. 81, 227 (1980).

[74] F. Herlemont, M. Lyszyk, J. Lemaire, CH. Lambeau, M. De Vleeshouwer and A. Fayt, J. Mol. Spectrosc. 94, 309 (1982).

[75] R.B. Woodward and R. Hoffmann, "The Conservation of Orbital Symmetry", Academic Press, New York, 1970.

[76] S.W. Benson and P.S. Nangia, J. Chem. Phys. 38, 18 (1963).

[77] R. Huisgen, Acc. Chem. Res. 10, 117 (1977).

[78] R.W. Carr, Jr. and W.D. Walters, J. Phys. Chem. 67, 1370 (1963).

[79] S.W. Benson, "Thermochemical Kinetics", 2nd ed., Wiley, New York, 1976.

[80] G.P. Smith and R.M. Laine, J. Phys. Chem. 85, 1620 (1981).

[81] D.F. McMillen, K.E. Lewis, G.P. Smith and D.M. Golden, J. Phys. Chem. 86, 709 (1982).

[82] H.-L. Dai, E. Specht, M.R. Berman and C.B. Moore, J. Chem. Phys. 77, 4494 (1982).

[83] P.W. Fairchild, G.P. Smith and D.R. Crosley, in "Nineteenth Symposium (International) on Combustion", The Combustion Institute, Pittsburgh, 1982, pp. 107-115.

[84] M.D. Scheer, J.R. McNesby and W. Braun, J. Phys. Chem. 88, 1850 (1984).

[85] M.J. Shultz, E.J. Rock, R.E. Tricca and L.M. Yam, J. Phys. Chem. 88, 5157 (1984).

[86] J.R. Guckert and R.W. Carr, J. Phys. Chem. 90, 4286 (1986).

[87] C. Steel, R. Schatzberger and S. Kimel, Spectrochimica Acta 43A, 149 (1987).

[88] S.W. Benson, "The Foundations of Chemical Kinetics", McGraw-Hill, New York, 1960, p. 476.

[89] C.R. Moylan and J.I. Brauman, Int. J. Chem. Kinet. 18, 379 (1986).

[90] J.N. Butler, J. Am. Chem. Soc. 84, 1393 (1962).

[91] R.F. Marchand, J. prakt. Chem. 26, 478 (1842).

[92] G. Dahlgren, Jr. and J.E. Douglas, J. Am. Chem. Soc. 80, 5108 (1958).

[93] M.P. Halstead and C.P. Quinn, Trans. Far. Soc. 64, 103 (1968).

[94] M.L. Boyd, T.M. Wu and M.H. Back, Can. J. Chem. 46, 2415 (1968).

[95] M. Simon and M.H. Back, Can. J. Chem. 47, 251 (1969).

[96] M.H. Back and R. Martin, Int. J. Chem. Kinet. 11, 757 (1979).

[97] D. Delliste, C. Richard and R. Martin, J. chim. phys. 78, 655 (1981).

[98] G. Ayranci and M.H. Back, Int. J. Chem. Kinet. 13, 897 (1981).

[99] G. Ayranci and M.H. Back, Int. J. Chem. Kinet. 15, 83 (1983).

[100] H. Mellottée, J. Tardieu de Maleissye and R. Delbourgo, Bull. Soc. chim. 448 (1969).

[101] J. Tardieu de Maleissye, H. Mellottée and R. Delbourgo, Bull. Soc. chim. 2268 (1965).

[102] G.B. Skinner and E.M. Sokoloski, J. Phys. Chem. 64, 1028 (1960).

[103] I.D. Gay, R.D. Kern, G.B. Kistiakowsky and H. Niki, J. Chem. Phys. 45, 2371 (1966).

[104] J.B. Homer and G.B. Kistiakowsky, J. Chem. Phys. 47, 5290 (1967).

[105] S.W. Benson and G.R. Haugen, J. Phys. Chem. 71, 1735 (1971).

[106] T. Just, P. Roth and R. Damm, in "Sixteenth Symposium (International) on Combustion", The Combustion Institute, Pittsburgh, 1976, pp. 961-969.

[107] T. Tanzawa and W.C. Gardiner, Jr., Combust. Flame 39, 241 (1980).

[108] C. Bordé, A. Henry and L. Henry, C.R. Acad. Sc. Paris 263B, 619 (1966).

[109] C. Cohen, C. Bordé and L. Henry, C.R. Acad. Sc. Paris 265B, 267 (1967).

[110] E. Quel and X. de Hemptinne, Ann. Soc. Sc. Brux. 83, II, 262 (1969).

[111] J.P. Bell, R.V. Edwards, B.R. Nott and J.C. Angus, Ind. Educ. Chem. Fund. 13, 89 (1974).

[112] J.W. Robinson, P.J. Moses and P.M. Boyd, Spectrosc. Lett. 7, 395 (1974).

[113] J. Tardieu de Maleissye, F. Lempereur and C. Marsal, Chem. Phys. Lett. 42, 472 (1976).

[114] X. de Hemptinne and D. De Keuster, J. Chem. Phys. 73, 3170 (1980).

[115] J. Bastiaens, D. De Keuster and X. de Hemptinne, Bull. Soc. Chim. Belg. 85, 833 (1976).

[116] R.V. Ambartzumian, N.V. Chekalin, V.S. Letokhov and E.A. Ryabov, Chem. Phys. Lett. 36, 301 (1975).

[117] N.V. Chekalin, V.S. Dolzhikov, V.S. Letokhov, V.N. Lokhman and A.N. Shibanov, Appl. Phys. 12, 191 (1977).

[118] N.V. Chekalin, V.S. Letokhov, V.N. Lokhman and A.N. Shibanov, Chem. Phys. 36, 415 (1979).

[119] J.H. Hall, Jr., M.L. Lesiecki and W.A. Guillory, J. Chem. Phys. 68, 2247 (1978).

[120] S.V. Filseth, J. Danon, D. Feldmann, J.D. Campbell and K.H. Welge, Chem. Phys. Lett. 66, 329 (1979).

[121] O.N. Avatkhov, V.N. Bagratashvili, I.N. Knyazev, Yu.R. Kolomiiskii, V.S. Letokhov, V.V. Lobko and E.A. Ryabov, Sov. J. Quantum Electron. 7, 412 (1977).

[122] N.C. Peterson, R.G. Manning and W. Braun, J. Res. Natl. Bur. Stand. 83a, 117 (1978).

[123] K. Nagai and M. Katayama, Bull. Chem. Soc. Jap. 51, 1269 (1978).

[124] H. Albrecht, H. Hohmann and R. Grunwald, in "Laser Processing and Diagnostics", (D. Bäuerle, ed.), Springer Ser. Chem. Phys., Springer-Verlag, New York, 1984, Vol. 39, pp. 536-541.

[125] W. Radloff, H. Hohmann, H. Albrecht and T. Freudenberg, Spectrochimica Acta 43A, 225 (1987).

[126] L. Nemes and T. Székely, Spectrochimica Acta 43A, 243 (1987).

[127] D.G. Wilden and J. Comer, J. Phys. B: Atom. Molec. Phys. 12, L371 (1979).

[128] D.F. McMillen and D.M. Golden, Ann. Rev. Phys. Chem. 33, 493 (1982).

[129] D.R. Powers and W.H. Corcoran, in "Industrial and Laboratory Pyrolyses", ACS Symposium Series, 32, 117 (1976).

[130] R.J. Cvetanovic and R.S. Irwin, J. Chem. Phys. 46, 1694 (1967).

[131] D. Rowley and H. Steiner, Disc. Faraday Soc. 10, 198 (1951).

[132] T. Sakai, K. Soma, Y. Sasaki, H. Tominaga and T. Kanugi, in "Refining Petroleum for Chemicals", Adv. Chem. series 97, 68 (1970).

[133] J.H. Kiefer, H.C. Wei, R.D. Kern and C.H. Wu, Int. J. Chem. Kinet. 17, 225 (1985).

[134] E.F. Meyer and D.G. Stroz, J. Am. Chem. Soc. 94, 6344 (1972).

[135] J. Stark and P. Lipp, Z. physik. Chem. 86, 36 (1913).

[136] C.P. Snow and C.B. Allsopp, Trans. Faraday Soc. 30, 93 (1934).

[137] G. Scheibe and H. Grieneisen, Z. physik. Chem. 25B, 52 (1934).

[138] W.C. Price and W.T. Tutte, Proc. Roy. Soc. (London) A174, 207 (1940).

[139] C. Reid, J. Chem. Phys. 18, 1299 (1950).

[140] M. Zelikoff and K. Watanabe, J. Opt. Soc. Am. 43, 756 (1953).

[141] L.C. Jones and L.W. Taylor, Anal. Chem. 27, 228 (1955).

[142] P.G. Wilkinson and R.S. Mulliken, J. Chem. Phys. 23, 1895 (1955).

[143] P.G. Wilkinson, Can. J. Phys. 34, 643 (1956).

[144] D.F. Evans, J. Chem. Soc. 1735 (1960).

[145] D.F. Evans, Proc. Chem. Soc. (London), 378 (1963).

[146] A. Kuppermann and L.M. Raff, Discuss. Faraday Soc. 35, 30 (1963).

[147] G. Herzberg "Electronic Spectra of Polyatomic Molecules", Van Nostrand, Princeton, 1966, Vol. 3.

[148] J.P. Doering, J. Chem. Phys. 46, 1194 (1967).

[149] R. McDiarmid and E. Charney, J. Chem. Phys. 47, 1517 (1967).

[150] B. Katz and J. Jortner, Chem. Phys. Lett. 2, 437 (1968).

[151] R. McDiarmid, J. Chem. Phys. 50, 1794 (1969).

[152] A.J. Merer and R.S. Mulliken, Chem. Rev. 69, 639 (1969).

[153] S. Trajmar, K. Rice and A. Kuppermann, Adv. Chem. Phys. 18, 15 (1970).

[154] M.B. Robin and N.A. Kuebler, J. Mol. Spectrosc. 33, 274 (1970).

[155] E. Miron, B. Raz and J. Jortner, Chem. Phys. Lett. 6, 563 (1970).

[156] R. McDiarmid, J. Chem. Phys. 55, 4669 (1971).

[157] D.F. Dance and I.C. Walker, Proc. Roy. Soc. (London) A334, 259 (1973).

[158] P.D. Foo and K.K. Innes, J. Chem. Phys. 60, 4582 (1974).

[159] W.M. Flicker, O.A. Mosher and A. Kuppermann, Chem. Phys. Lett. 36, 56 (1975).

[160] E.H. van Veen, Chem. Phys. Let. 41, 540 (1976).

[161] R. McDiarmid, J. Chem. Phys. 67, 3835 (1977).

[162] K.E. Johnson, D.B. Johnston and S. Lipsky, J. Chem. Phys. 70, 3844 (1979).

[163] R. McDiarmid, J. Phys. Chem. 84, 64 (1980).

[164] A. Gedanken, N.A. Kuebler and M.B. Robin, J. Chem. Phys. 76, 46 (1982).

[165] L.D. Ziegler and B.S. Hudson, J. Chem. Phys. 79, 1197 (1983).

[166] R.J. Sension, L. Mayne and B. Hudson, J. Am. Chem. Soc. 109, 5036 (1987).

[167] R.S. Mulliken, Phys. Rev. 41, 751 (1932).

[168] R.S. Mulliken, Phys. Rev. 43, 297 (1933).

[169] R.S. Mulliken, Rev. Mod. Phys. 14, 265 (1942).

[170] R.S. Mulliken and C.C.J. Roothaan, Chem. Rev. 41, 219 (1947).

[171] U. Kaldor and I. Shavitt, J. Chem. Phys. 48, 191 (1968).

[172] A.J. Merer and R.S. Mulliken, J. Chem. Phys. 50, 1026 (1969).

[173] G.H. Kirby and K. Miller, Chem. Phys. Lett. 3, 643 (1969).

[174] H. Basch and V. McKoy, J. Chem. Phys. 53, 1628 (1970).

[175] R.J. Buenker, S.D. Peyerimhoff and H.L. Hsu, Chem. Phys. Lett. 11, 65 (1971).

[176] A. Warshel and M. Karplus, Chem. Phys. Lett. 17, 7 (1972).

[177] R.J. Buenker and S.D. Peyerimhoff, Chem. Phys. Lett. 36, 415 (1975).

[178] R.J. Buenker and S.D. Peyerimhoff, Chem. Phys. Lett. 9, 75 (1975).

[179] R.S. Mulliken, J. Chem. Phys. 66, 2448 (1977).

[180] L.E. McMurchie and E.R. Davidson, J. Chem. Phys. 67, 5613 (1977).

[181] R.S. Mulliken, J. Chem. Phys. 71, 556 (1979).

[182] R.J. Buenker, S.D. Peyerimhoff and S.K. Shih, Chem. Phys. Lett. 69, 7 (1980).

[183] C. Petrongolo, R.J. Buenker and S.D. Peyerimhoff, J. Chem. Phys. 76, 3655 (1982).

[184] R.S. Mulliken, J. Chem. Phys. 23, 1997 (1955).

[185] G. Herzberg, "Infrared and Raman Spectra of Polyatomic Molecules", Van Nostrand, Princeton, 1945, Vol. 1.

[186] G. Herzberg, "Spectra of Diatomic Molecules", Van Nostrand, Princeton, 1950, Vol. 2.

[187] J.F. Ogilvie, J. Chem. Phys. 49, 474 (1968).

[188] A.D. Walsh, J. Chem. Soc. 2325 (1953).

[189] E. Tschuikow-Roux, J.R. McNesby, W.M. Jackson and J.L. Faris, J. Phys. Chem. 71, 1531 (1967).

[190] R. Gorden, Jr. and P. Ausloos, J. Res. Natl. Bur. Stand. 75a, 141 (1971).

[191] Y. Inel, A. Siddiqi and G.G. Meisels, J. Phys. Chem. 75, 1317 (1971).

[192] H. Okabe and J.R. McNesby, J. Chem. Phys. 36, 601 (1962).

[193] J.R. McNesby and H. Okabe, in "Advances in Photochemistry", (W.A. Noyes, Jr., G.S. Hammond and J.N. Pitts, Jr., eds.), Wiley, New York, 1964, Vol. 3, pp. 228-231.

[194] M.C. Sauer and L.M. Dorfman, J. Chem. Phys. 35, 497 (1961).

[195] P. Potzinger, L.C. Glasgow and G. von Bünau, Z. Naturforsch. 27a, 628 (1972).

[196] H. Hara, K. Kodama and I. Tanaka, Bull. Chem. Soc. Jap. 48, 711 (1975).

[197] H. Hara and I. Tanaka, Bull. Chem. Soc. Jap. 46, 3012 (1973).

[198] H. Hara and I. Tanaka, Bull. Chem. Soc. Jap. 47, 1543 (1974).

[199] R.A. Back and D.W.L. Griffiths, J. Chem. Phys. 46, 4839 (1967).

[200] A.H. Laufer, J. Photochem. 27, 267 (1984).

[201] A. Fahr and A.H. Laufer, J. Photochem. 34, 261 (1986).

[202] P Borrell, A. Cervenka and J.W. Turner, J. Chem. Soc. B 2293 (1971).

[203] S. Hirokami and R.J. Cvetanovic, J. Phys. Chem. 78, 1254 (1974).

[204] D.G. Hooper, M. Simon and M.H. Back, Can. J. Chem. 53, 1237 (1975).

[205] M. Simon and M.H. Back, Can. J. Chem. 53, 1245 (1975).

[206] M.P. Irion, "Beiträge zur Anwendung des ArF-Exciplex Lasers in der Photochemie", Max-Planck-Institut für Quantenoptik, 1981.

[207] H. Habeeb, D.J. Le Roy and E.W.R. Steacie, J. Chem. Phys. 10, 261 (1942).

[208] E.W.R. Steacie and D.J. Le Roy, J. Chem. Phys. 10, 22 (1942).

[209] J.R. Bates and H.S. Taylor, J. Am. Chem. Soc. 49, 2438 (1927).

[210] D.J. Le Roy and E.W.R. Steacie, J. Chem. Phys. 9, 829 (1941).

[211] B. de B. Darwent, J. Chem. Phys. 20, 1673 (1952).

[212] R.J. Cvetanovic and A.B. Callear, J. Chem. Phys. 23, 1182 (1955).

[213] A.B. Callear and R.J. Cvetanovic, J. Chem. Phys. 24, 873 (1956).

[214] J.R. Majer, B. Mile and J.C. Robb, Trans. Faraday Soc. 57, 1342 (1961).

[215] D.W. Setser, B.S. Rabinovitch and D.W. Placzek, J. Am. Chem. Soc. 85, 862 (1963).

[216] R.J. Cvetanovic, Prog. Rxn. Kinet. 2, 39 (1964).

[217] S. Hirokami and S. Sato, Bull. Chem. Soc. Jap. 41, 2226 (1968).

[218] E.W.R. Steacie and R. Potvin, Can. J. Research B18, 47 (1940).

[219] D.J. Le Roy and E.W.R. Steacie, J. Chem. Phys. 10, 683 (1942).

[220] S. Tsunashima, S. Hirokami and S. Sato, Can. J. Chem. 46, 995 (1968).

[221] S. Sato, Pure Appl. Chem. 16, 87 (1968).

[222] H. Hunziker, J. Chem. Phys. 50, 1288 (1969).

[223] S. Tsunashima and S. Sato, Rev. Chem. Intermed. 2, 201 (1979).

[224] Handbook of Bimolecular and Termolecular Gas Reactions, (J.A. Kerr and S.J. Moss, eds.), CRC Press, Boca Raton, 1981, Vol. 2, Table 205.

[225] W.M. Jackson, J.B. Halpern and C.S. Lin, Chem. Phys. Lett. 55, 254 (1978).

[226] R. Burnham and N. Djeu, Appl. Phys. Lett. 29, 707 (1976).

[227] R.A. Back, to be published.

[228] D.G.L. James and G.E. Troughton, Trans. Faraday Soc. 62, 145 (1966).

[229] A.G. Sherwood and H.E. Gunning, J. Phys. Chem. 69, 2323 (1965).

[230] N. Harumiya, S. Shida and S. Arai, Bull. Chem. Soc. Jap. 38, 142 (1965).

[231] R.J. Cvetanovic and L.C. Doyle, J. Chem. Phys. 37, 543 (1962).

[232] R. Srinivasan, J. Am. Chem. Soc. 82, 5063 (1960).

[233] B.T. Luke, J.A. Pople, M-B. Krogh-Jespersen, Y. Apeloig, M. Karni, J. Chandrasekhar and P.v.R. Schleyer, J. Am. Chem. Soc. 108, 270 (1986).

[234] Y-P. Lee and G.C. Pimentel, J. Chem. Phys. 75, 4241 (1981).

[235] J.E. Douglas, B.S. Rabinovitch and F.S. Looney, J. Chem. Phys. 23, 315 (1955).

[236] R.C.L. Yuan, J.M. Preses, G.W. Flynn and A.M. Ronn, J. Chem. Phys. 59, 6128 (1973).

[237] E.M. Evleth and S. Sevin, J. Am. Chem. Soc. 103, 7414 (1981).

APPENDIX A: Tables of data accompanying Figures 8-15 of the absorption measurements in PART I.

Table A-1. Absorbance of CO_2 laser radiation as a function of ethylene concentration in cell A, l = 0.52 cm.

A. 10 P(12) line

	Incident fluence / J cm^{-2}		
	0.18	0.30	0.65
$C_2H_4/10^{-2}$ mol dm^{-3}	Absorbance / $\log_{10}(E_0/E_T)$		
0.134	0.012	0.0098	0.0063
0.269	0.030	0.024	0.017
0.538	0.070	0.062	0.054
0.807	0.12	0.11	0.10
1.08	0.19	0.17	0.16
1.34	0.25	0.24	0.22
1.61	0.34	0.32	0.30
2.15	0.54	0.50	0.48
2.69	0.73	0.69	0.66

B. 10 P(14) line

	Incident fluence/J cm^{-2}		
	0.10	0.36	0.69
$C_2H_4/10^{-2}$ mol dm^{-3}	Absorbance/$\log_{10}(E_0/E_T)$		
0.134	0.025	0.021	0.018
0.269	0.059	0.049	0.042
0.404	0.10	—	—
0.538	0.15	0.12	0.11
0.847	0.26	0.21	0.19
1.08	0.40	0.33	0.29
1.34	0.55	0.46	0.40
1.48	—	0.53	0.46
1.88	0.91	0.75	0.65

Table A-2. Absorbance of CO_2 laser radiation as a function of ethylene concentration in cell B, l = 0.051 cm.

A. 10 P(12) line

	Incident fluence/J cm^{-2}			
	0.20	0.29	0.37	0.52
$C_2H_4/10^{-2}$ mol dm^{-3}	Absorbance/$\log_{10}$ (E_0/E_T)			
1.34	0.024	0.022	0.017	0.015
2.69	0.066	0.062	0.055	0.049
4.04	0.11	0.099	0.090	0.075
5.38	0.15	0.14	0.13	0.11
8.07	0.25	0.24	0.22	0.20
10.76	0.36	0.34	0.32	0.29
13.45	0.48	0.46	0.43	0.38
16.14	0.60	0.57	0.54	0.48

B. 10 P(14) line

	Incident fluence/J cm^{-2}			
	0.18	0.25	0.38	0.53
$C_2H_4/10^{-2}$ mol dm^{-3}	Absorbance/$\log_{10}$ (E_0/E_T)			
1.34	0.044	0.038	0.029	0.027
2.69	0.10	0.089	0.070	0.063
4.04	0.17	0.15	0.12	0.10
5.38	0.24	0.22	0.18	0.15
8.07	0.41	0.37	0.30	0.25
10.76	0.62	0.56	0.45	0.36
13.45	0.89	0.76	0.61	0.48
16.14	1.17	0.95	0.75	0.60

Table A-3. Effective molar absorption coefficient as a function of ethylene pressure in cell A, l = 0.52 cm.

A. 10 P(12) line

	Incident fluence/J cm^{-2}		
	0.18	0.30	0.65
C_2H_4/Torr	$\epsilon_{effective}$/dm^3 mol^{-1} cm^{-1}		
25	17	14	9
50	21	17	12
100	25	22	19
150	29	27	24
200	34	31	28
250	38	35	32
300	41	38	36
400	48	45	43
500	52	49	47

B. 10 P(14) line

	Incident fluence/J cm^{-2}		
	0.10	0.36	0.69
C_2H_4/Torr	$\epsilon_{effective}$/dm^3 mol^{-1} cm^{-1}		
25	36	30	26
50	42	35	30
75	48	—	—
100	54	43	38
150	62	50	45
200	71	59	52
250	79	66	58
275	—	69	60
350	93	77	67

Table A-4. Effective molar absorption coefficient as a function of ethylene pressure in cell B, l = 0.051 cm.

A. 10 P(12) line

	Incident fluence/J cm^{-2}			
	0.20	0.29	0.37	0.52
C_2H_4/Torr	$\epsilon_{effective}$/dm^3 mol^{-1} cm^{-1}			
250	35	32	24	22
500	48	45	40	36
750	52	48	44	39
1000	55	52	47	42
1500	61	58	53	48
2000	66	62	58	53
2500	69	67	63	56
3000	72	70	66	58

B. 10 P(14) line

	Incident fluence/J cm^{-2}			
	0.18	0.25	0.38	0.53
C_2H_4/Torr	$\epsilon_{effective}$/dm^3 mol^{-1} cm^{-1}			
250	65	56	43	39
500	72	65	51	46
750	79	72	58	51
1000	86	79	66	54
1500	100	91	73	60
2000	113	102	82	66
2500	129	111	89	70
3000	142	116	91	74

Table A-5. Absorbance of CO_2 laser radiation as a function of ethylene concentration in ethylene-ethane mixtures in cell A, l = 0.52 cm.

A. 10 P(12) line, $F_0 = 0.65$ J cm^{-2}

	C_2H_6/C_2H_4 ratio		
	5.2	10.3	20.8
$C_2H_4/10^{-2}$ mol dm^{-3}	Absorbance/$\log_{10}$ (E_0/E_T)		
0.134	0.020	0.027	0.037
0.269	0.056	0.066	0.089
0.404	—	—	0.15
0.538	0.14	0.16	0.22
0.646	—	—	0.27
0.753	—	—	0.32
0.807	0.24	0.28	—
1.08	0.37	0.41	—
1.34	—	0.54	—
1.47	—	0.62	—
1.61	0.61	—	—
2.15	0.87	—	—
2.69	1.12	—	—

B. 10 P(14) line, $F_0 = 0.69$ J cm^{-2}

	C_2H_6/C_2H_4 ratio		
	5.2	10.3	20.8
$C_2H_4/10^{-2}$ mol dm^{-3}	Absorbance/$\log_{10}$ (E_0/E_T)		
0.134	0.045	0.092	0.12
0.269	0.15	0.22	0.29
0.404	—	—	0.46
0.538	0.40	0.54	0.64
0.646	—	—	0.77
0.673	0.55	—	—
0.753	—	—	0.90
0.807	0.73	0.88	—
1.08	1.06	1.21	—
1.34	1.38	1.56	—
1.47	—	1.72	—
1.61	1.68	—	—

Table A-6. Effective molar absorption coefficient as a function of ethylene pressure in ethylene-ethane mixtures in cell A, l = 0.52 cm.

A. 10 P(12) line, $F_0 = 0.65$ J cm^{-2}

	C_2H_6/C_2H_4 ratio		
	5.2	10.3	20.8
C_2H_4/Torr	$\epsilon_{effective}$/dm^3 mol^{-1} cm^{-1}		
25	29	39	53
50	40	47	64
75	—	—	71
100	50	57	79
120	—	—	80
140	—	—	82
150	57	67	—
200	66	73	—
250	—	77	—
275	—	81	—
300	73	—	—
400	78	—	—
500	80	—	—

B. 10 P(14) line, $F_0 = 0.69$ J cm^{-2}

	C_2H_6/C_2H_4 ratio		
	5.2	10.3	20.8
C_2H_4/Torr	$\epsilon_{effective}$/dm^3 mol^{-1} cm^{-1}		
25	64	132	172
50	107	157	207
75	—	—	219
100	143	193	227
120	—	—	229
125	157	—	—
140	—	—	230
150	174	210	—
200	189	215	—
250	198	224	—
275	—	225	—
300	201	—	—

Table A-7. Effective molar absorption coefficient as a function of total pressure of ethylene and ethane in cell A, l = 0.52 cm.

A. 10 P(12) line, F_0 = 0.65 J cm^{-2}

C_2H_6/C_2H_4 = 5.2		C_2H_6/C_2H_4 = 10.3		C_2H_6/C_2H_4 = 20.8	
$C_2H_4+C_2H_6$/Torr	ϵ_{eff}/dm^3 mol^{-1} cm^{-1}	$C_2H_4+C_2H_6$/Torr	ϵ_{eff}/dm^3 mol^{-1} cm^{-1}	$C_2H_4+C_2H_6$/Torr	ϵ_{eff}/dm^3 mol^{-1} cm^{-1}
155	29	282	39	545	53
310	40	565	47	1090	64
465	—	848	—	1635	71
620	50	1130	57	2180	79
744	—	1356	—	2616	80
868	—	1582	—	3052	82
930	57	1695	67		
1240	66	2260	73		
1550	—	2825	77		
1705	—	3108	81		
1860	73				
2480	78				
3100	80				

B. 10 P(14) line, F_0 = 0.69 J cm^{-2}

C_2H_6/C_2H_4 = 5.2		C_2H_6/C_2H_4 = 10.3		C_2H_6/C_2H_4 = 20.8	
$C_2H_4+C_2H_6$/Torr	ϵ_{eff}/dm^3 mol^{-1} cm^{-1}	$C_2H_4+C_2H_6$/Torr	ϵ_{eff}/dm^3 mol^{-1} cm^{-1}	$C_2H_4+C_2H_6$/Torr	ϵ_{eff}/dm^3 mol^{-1} cm^{-1}
155	64	282	132	545	172
310	107	565	157	1090	207
465	—	848	—	1635	219
620	143	1130	193	2180	227
744	—	1356	—	2616	229
775	157	1412	—	2725	—
868	—	1582	—	3052	230
930	174	1695	210		
1240	189	2260	215		
1550	198	2825	224		
1705	—	3108	225		
1860	201				

Table A-8. Effective molar absorption coefficient as a function of total pressure of ethylene and ethane in cell A, l = 0.52 cm.

A. 10 P(12) line, $F_0 = 0.65$ J cm^{-2}

	$C_2H_6/C_2H_4 = 5.2$		$C_2H_6/C_2H_4 = 10.3$		$C_2H_6/C_2H_4 = 20.8$	
C_2H_4/Torr	$C_2H_4+C_2H_6$/Torr	ϵ_{eff}/dm^3 mol^{-1} cm^{-1}	$C_2H_4+C_2H_6$/Torr	ϵ_{eff}/dm^3 mol^{-1} cm^{-1}	$C_2H_4+C_2H_6$/Torr	ϵ_{eff}/dm^3 mol^{-1} cm^{-1}
25	155	29	282	39	545	53
50	310	40	565	47	1090	64
75	465	—	848	—	1635	71
100	620	50	1130	57	2180	79
120	744	—	1356	—	2616	80
140	868	—	1582	—	3052	82
150	930	57	1695	67		
200	1240	66	2260	73		
250	1550	—	2825	77		
275	1705	—	3108	81		
300	1860	73				
400	2480	78				
500	3100	80				

B. 10 P(14) line, $F_0 = 0.69$ J cm^{-2}

	$C_2H_6/C_2H_4 = 5.2$		$C_2H_6/C_2H_4 = 10.3$		$C_2H_6/C_2H_4 = 20.8$	
C_2H_4/Torr	$C_2H_4+C_2H_6$/Torr	ϵ_{eff}/dm^3 mol^{-1} cm^{-1}	$C_2H_4+C_2H_6$/Torr	ϵ_{eff}/dm^3 mol^{-1} cm^{-1}	$C_2H_4+C_2H_6$/Torr	ϵ_{eff}/dm^3 mol^{-1} cm^{-1}
25	155	64	282	132	545	172
50	310	107	565	157	1090	207
75	465	—	848	—	1635	219
100	620	143	1130	193	2180	227
120	744	—	1356	—	2616	229
125	775	157	1412	—	2725	—
140	868	—	1582	—	3052	230
150	930	174	1695	210		
200	1240	189	2260	215		
250	1550	198	2825	224		
275	1705	—	3108	225		
300	1860	201				

APPENDIX B: Temperature and fluence profile calculation as a function of distance at an incident fluence of 0.3 J cm^{-2}

The calculations were made as follows:

(1) Each cell was subdivided into cylinders of equal length. Thus the short cell was divided into 5 cylinders and the long cell into 50 cylinders.

(2) The absorption coefficient will be the same for both cells just inside the front window and to a first approximation the value for ϵ_{eff} measured in the short cell, where the temperature gradient is small, will be used. In addition, this value will be assumed constant over the length of each vessel, although this will over-estimate the temperature gradient in the long vessel. The energy absorbed per mole of ethylene in each cylinder was obtained from the following equation:

$$E_{abs} = [F_0 \times S \times (1-10^{-\Delta A})]/n \qquad \text{(B-1)}$$

where $\Delta A = \epsilon c \Delta l$, Δl is the length of the cylinder and c is the concentration of ethylene in the cylinder. F_0 is the fluence incident on the front of each cylinder, S is the cross-sectional area of the beam and n is the number of moles of ethylene in the cylinder. For example, with an incident fluence of 0.3 J cm^{-2}, and cross-sectional area of the beam, 0.75 cm^2, pressure of ethylene 1000 Torr, $\Delta l = l/50 = 0.0104$ cm, and $\Delta A = 1.43/50 = 0.0286$, the energy absorbed in the first cylinder is

$$E_{abs} = \frac{0.3 \text{ J cm}^{-2} \times 0.75 \text{ cm}^2 \times (1 \quad 10^{-0.0286})}{4.2 \times 10^{-7} \text{ mol}}$$

$$= 3.41 \times 10^4 \text{ J mol}^{-1}$$

(3) The temperature in each cylinder was calculated assuming a constant volume process as follows:

$$E_{abs} = \int_{298}^{T} C_V dT \qquad \text{(B-2)}$$

where C_V is the heat capacity of ethylene at constant volume [B-1], and E_{abs} is the energy absorbed per mole of ethylene in the cylinder. These calculations assumed complete thermalization of the absorbed energy and no energy losses during the pulse. Values are summarized in Table B-1.

(4) The assumption of complete thermalization of absorbed energy requires some comment. While rotational and translational energy will equilibrate rapidly in the present system, laser schlieren measurements of the vibrational relaxation of ethylene behind shock waves [B-2] indicate a relaxation time given by $p\tau$ = 0.08 atm μs at 1000 K. Thus vibrational-translational equilibration at 500 Torr and 1000 K would occur in a time comparable to the duration of the laser pulse. The result would be that the true T_{max} for a given energy input would be somewhat higher than calculated, (because translational components of specific heat would not be fully active) and this would be a rotational-vibrational temperature with translational temperatures appreciably lower. A further effect would be to delay somewhat the adiabatic expansion of the hot gas, since this requires translational heating. These effects would largely disappear at higher pressures, and none of the conclusions reached in this thesis would be substantially altered.

Table B-1. Temperature and fluence profile calculation as a function of distance at an incident fluence of 0.3 J cm^{-2}.

A. 10 P(12) line

T/K*	F_0/J cm^{-2} **	l/cm
895	0.300	0.0
870	0.281	0.0102
845	0.264	0.0204
820	0.247	0.0306
795	0.232	0.0408
770	0.217	0.051
665	0.155	0.104
510	0.080	0.208
415	0.042	0.312
355	0.022	0.416
325	0.011	0.52

* $\bar{T}_{cell\ A}$ = 511 K, $\bar{T}_{cell\ B}$ = 832 K

** $\bar{F}_{cell\ A}$ = 0.091 J cm^{-2}, $\bar{F}_{cell\ B}$ = 0.256 J cm^{-2}

B. 10 P(14) line

T/K*	F_0/J cm^{-2} **	l/cm
1040	0.300	0.0
1010	0.275	0.0102
975	0.251	0.0204
930	0.230	0.0306
890	0.211	0.0408
850	0.193	0.051
685	0.122	0.104
480	0.049	0.208
375	0.020	0.312
330	0.008	0.416
305	0.003	0.52

* $\bar{T}_{cell\ A}$ = 508 K, $\bar{T}_{cell\ B}$ = 950 K

** $\bar{F}_{cell\ A}$ = 0.069 J cm^{-2}, $\bar{F}_{cell\ B}$ = 0.243 J cm^{-2}

REFERENCES

[B-1] JANAF Thermochemical Tables, 3rd ed; J. Phys. Chem. Data 14, Suppl. 1 (1985), p.661.

[B-2] H. Teitlebaum, in "Proceedings of the 13th International Symposium on Shock Tubes and Waves", (C.E. Treanor and J.G. Hall, eds.), State University of New York Press, Albany, New York, 1981, pp. 560-569.

APPENDIX C: Thermodynamic data for the ethylene-cyclobutane system

Table C-1 Thermodynamic data for ethylene and cyclobutane

Species	ΔH°_{f300}/ kJ mol^{-1}	S°_{300}/ J mol^{-1} K^{-1}	C_p°/J mol^{-1} K^{-1}				
			300 K	500 K	800 K	1000 K	1500 K
C_2H_4	52.3	219.2	43.1	62.3	83.7	93.7	110.0
c-C_4H_8	26.4	265.3	72.4	124.9	177.5	200.7	235.7

Standard state: P = 1 atm, T = 300 K

Relationship between thermodynamic properties for standard state of 1 atmosphere (pressure) and 1 mol dm^{-3} (concentration)

$$\Delta H_p^\circ = \Delta H_c^\circ + \Delta nRT \qquad \text{(C-1)}$$

$$\Delta S_p^\circ = \Delta S_c^\circ + R\,\Delta n + \Delta nR\ln(R'T) \qquad \text{(C-2)}$$

$$K_p = K_c(RT)^{\Delta n} \qquad \text{(C-3)}$$

$$\log_{10} K_c = (\Delta S_c^\circ/2.3R)\quad(\Delta H_c^\circ/2.3RT) \qquad \text{(C-4)}$$

For the reversible reaction, $2C_2H_4 \rightleftarrows$ c-C_4H_8, $\Delta n = -1$. In the logarithmic term in (C-2), $R' = 0.08206$ dm^3 atm mol^{-1} K^{-1}.

Table C-2 Thermodynamic data for the reaction, $2C_2H_4 \rightleftarrows$ c-C_4H_8

T/K	ΔH_c°/kJ mol^{-1}	ΔS_c°/J mol^{-1}K^{-1}	K_c/dm^3 mol^{-1}
300	-75.7	-138.2	9.30×10^{5}
500	-75.4	-137.3	5.08
800	-71.3	-130.9	6.54×10^{-3}
1000	-67.4	-126.3	8.31×10^{-4}
1500	-55.9	-117.1	6.68×10^{-5}

Standard state: c = 1 mol dm^{-3}, T = 300 K

Values for k_f over the temperature range were obtained using values of k_r extrapolated from the measurements of Carr and Walters [C-1] and combined with the values of K_c in Table C-2 through the equation $K_c = k_f/k_r$. Some uncertainty is introduced by this use of k_r outside the range (692-733 K) over which it was measured. In other words, we assume that E_r is constant over the whole range of temperature and all the change in ΔH_c° becomes included in E_f. An estimate of the error in E_f introduced in this way is therefore approximately the change in ΔH_c° from 800 K to 1500 K, or 15.4 kJ mol^{-1}. Thus k_f used in the calculations may be written as

$$\log_{10} k_f \, (dm^3 \, mol^{-1} \, s^{-1}) = (9.2 \pm 0.8) - (196000 \pm 15000)/2.3 \, RT$$

The error in E_f is thus approximately 8%, with a corresponding error in $\log_{10} A_f$.

Although some uncertainty is associated with k_f and k_r, outside the temperature range of measurement, these errors will affect only the rate of approach to the constant final value, if the values of K_c listed in Table C-2 are maintained.

The errors in both ΔH_c° and ΔS_c° in Table C-2 should now be examined. The largest errors are associated with the ΔH_f° and S° for cyclobutane, and only these need be considered. The error in ΔH_f° was estimated as $\pm$ 0.7 kJ mol^{-1} [C-2]. O'Neal and Benson [C-3] suggested an uncertainty in the entropy of cyclobutane of $\pm$ 4.2 J mol^{-1} K^{-1} These errors may be combined to estimate a maximum range for the values of K_c at 1000 K using equation (C-4). This procedure gives $\log_{10} K_c(dm^3 \, mol^{-1}) = -3.10 \pm 0.25$. Thus from a measurement of the equilibrium concentration of cyclobutane, the value of the temperature in the reaction zone in the region of 1000 K would have an uncertainty of approximately $\pm$ 70 K.

REFERENCES

[C-1] R.W. Carr, Jr. and W.D. Walters, J. Phys. Chem. 67, 1370 (1963).

[C-2] S. Kaarsemaker and J. Coops, Rec. Trav. Chim. 71, 261 (1952).

[C-3] H.E. O'Neal and S.W. Benson, J. Phys. Chem. 72, 1866 (1968).

APPENDIX D: Description of the computer program used to calculate cyclobutane production during a laser pulse

The calculation consists of the numerical integration of the differential equation for the rate of formation of cyclobutane, (equation (16)). Appropriate time increments were chosen, small enough to be accurate and to prevent artificial oscillations in the calculated cyclobutane concentration, yet large enough to obtain results in a reasonable time of computation. The program consisted of two parts:

(1) Heating period

The temperature increased linearly with time from 300 K up to the maximum temperature, T_{max}, in a time of 110 ns.

(2) Cooling period

The temperature decreased linearly with time at a rate equal to or slower than the heating rate, from T_{max} down to 300 K. In some cases, the cooling period was divided into an adiabatic expansion part and a constant pressure part, with different cooling rates.

For every time interval in the calculation (Δ t), corresponding to a known temperature interval (Δ T), the following variables were calculated both at the middle and at the end of the interval:

1. The forward and reverse rate constants:

$$k_f \ (dm^3\ mol^{-1}\ s^{-1}) = 10^{(9.2 \pm 0.8 \quad (196000 \pm 15000)/2.3RT)} \qquad \text{(D-1)}$$

$$k_r \ (s^{-1}) = 10^{(15.62 \pm 0.01 \quad (262000 \pm 1700)/2.3RT)} \qquad \text{(D-2)}$$

2. The equilibrium constant:

$$K = k_f/k_r \qquad \text{(D-3)}$$

3. Ethylene concentration and pressure:

Case I - Under conditions of constant volume, the ethylene concentration remains at its original value,

$$[C_2H_4]_{(To)} = P_{C_2H_4(To)}/RT_0 \quad \text{(D-4)}$$

where $R = 62.36$ Torr M^{-1} K^{-1} and $T_0 = 300$ K

The pressure of ethylene increases with increasing temperature:

$$P_{C_2H_4(T)} = [C_2H_4]_{(To)}RT \quad \text{(D-5)}$$

Case II Under conditions of constant pressure, the concentration of ethylene varies inversely with temperature because of the thermal expansion of the gas:

$$[C_2H_4]_{(T)} = [C_2H_4]_{(To)}(T_0/T) \quad \text{(D-6)}$$

The pressure of ethylene, of course, remains constant:

$$P_{C_2H_4(T)} = P_{C_2H_4(To)} \quad \text{(D-7)}$$

Case III- Finally, for adiabatic cooling of the gas from T_{max}, the ethylene pressure at a temperature T is given by:

$$P_{C_2H_4(T)} = P_{C_2H_4(Tmax)}(T_{max}/T)^{\gamma/(1-\gamma)} \quad \text{(D-8)}$$

where $\gamma = C_p/C_V$, the heat capacity ratio for ethylene [B-1] for which an average value was taken for temperatures between T_{max} and the temperature at the end of the adiabatic expansion. The pressure and temperature decrease during the expansion and the ethylene concentration is given as follows:

$$[C_2H_4]_{(T)} = [C_2H_4]_{(To)}(P_{C_2H_4(T)}/P_{C_2H_4(To)})(T_0/T) \quad \text{(D-9)}$$

4. Equilibrium cyclobutane concentrations:

$$[c\text{-}C_4H_8]_{equil(T)} = K_{(T)}[C_2H_4]^2_{(T)} \quad \text{(D-10)}$$

5. For the three different cases considered dealing with the thermal expansion of the gas during a heating-cooling cycle, the following "approximate" treatment provided the concentrations of cyclobutane in the respective time intervals (Δt). Considering 5 times t_1,...t_5, corresponding to 5 temperatures T_1,...T_5 during the calculation:

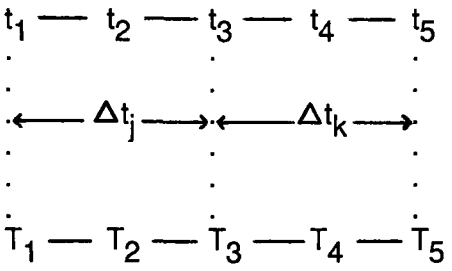

where t_2 and t_4 respectively are mid-points of the t_1-t_3 and t_3-t_5 time intervals. The cyclobutane concentration at time t_2, $[c\text{-}C_4H_8]_{t_2}$, is estimated by extrapolation based on the increment in cyclobutane concentration in the preceding time interval (Δt_i). The increment in concentration of cyclobutane formed during the time interval Δt_j, was then calculated at the average temperature T_2:

$$\Delta [c\text{-}C_4H_8]_{\Delta t_j} = (k_f[C_2H_4]^2 \quad k_r[c\text{-}C_4H_8])\, \Delta t \qquad \text{(D-11)}$$

where k_f, k_r, $[C_2H_4]$, and $[c\text{-}C_4H_8]$ are the values at T_2 (average between T_1 and T_3). The cyclobutane concentration at the end of the time interval Δt_j, at t_3, was given by:

$$[c\text{-}C_4H_8]_{t_3} = [c\text{-}C_4H_8]_{t_1} + \Delta [c\text{-}C_4H_8]_{\Delta t_j} \qquad \text{(D-12)}$$

In all the calculations each of the concentrations in equation (D-12) was normalized to the original volume before performing the addition. When no change in volume occurred no corrections were required but when a change in volume took place, during either a heating or a cooling period, normalization was made by appropriate corrections involving the pressure and the temperature. Also, in all the figures the concentration refers to the value in the original volume.

The computer program in question used in the calculation of the constant final value of cyclobutane in the case of heating the gas under constant volume (from T_0 to T_{max}), followed by cooling first by adiabatic expansion (from T_{max} to $T_{adiab.exp.}$), and then under constant pressure (from $T_{adiab.exp.}$ to T_0), i.e. Case III, is included in the following pages.

FILE: CASE3 FORTRAN * UNIV D'/OF OTTAWA CMS

```
C*************************************************************************
C*************************************************************************
C   THIS PROGRAM IS CONCERNED WITH THE TIME AND TEMPERATURE DEPENDENCE
C   OF THE PRODUCT CYCLOBUTANE FORMED IN THE REVERSIBLE REACTION,
C   2C2H4⇌c-C4H8, OVER THE COURSE OF A SINGLE PULSE CALCULATION
C   (WHICH INCLUDES A HEATING AS WELL AS A COOLING PERIOD).
C   IN A CALCULATION AIMED AT ESTIMATING THE CYCLOBUTANE CONSTANT FINAL
C   CONCENTRATION, THE INITIAL CYCLOBUTANE CONCENTRATION AT 300K (IN THE
C   HEATING PERIOD) IS GIVEN A NONZERO VALUE, AND FOR THAT MATTER IT IS
C   GIVEN A NUMERICAL VALUE IN THE NEIGHBORHOOD OF THE CALCULATED
C   EQULIBRIUM CYCLOBUTANE CONCENTRATION AT THE CHOSEN MAXIMUM
C   TEMPERATURE (TMAX).
C   THIS PARTICULAR CALCULATION, INVOLVES THE SUMMATION OF THE
C   CYCLOBUTANE CONCENTRATION FORMED FROM ITS INITIAL VALUE AT 300K IN
C   THE HEATING PERIOD ALL THE WAY TO ITS FINAL VALUE AT 300K IN THE
C   COOLING PERIOD.
C   FOR CASE 3 OR THE COMBINED CASE, (WHERE A LINEAR HEATING RATE WAS
C   ASSUMED FROM 300 K TO TMAX, REACHED AFTER 110 NANOSECOND, AS
C   ESTABLISHED FROM MEASUREMENT OF THE CO2 LASER PROFILE AT HALF THE
C   MAXIMUM INTENSITY), THE FOLLOWING ASSUMPTIONS WERE MADE:
C   (1) IN THE HEATING PERIOD (PART 1), NO EXPANSION OF THE GASEOUS
C   SYSTEM OCCURED (CONSTANT VOLUME); (2) IN THE COOLING PERIOD
C   (PART 2),TWO DIFFERENT COOLING MECHANISMS WERE ASSUMED (A) THE GAS
C   WAS INITIALLY COOLED BY AN ADIABATIC EXPANSION (OCCURING AT A RATE
C   (DELTA TEMPERATURE / DELTA TIME) 10 TIMES SLOWER THAN THE
C   RATE OF HEATING), TAKING PLACE FROM THE MAXIMUM TEMPERATURE DOWN TO
C   A LOWER TEMPERATURE T, AT WHICH THE ETHYLENE PRESSURE IN THE
C   ORIGINAL VOLUME (V0) HAS BEEN REESTABLISHED FOLLOWED BY (B) FURTHER
C   COOLING UNDER THE ASSUMPTION THAT THE GAS REMAINED AT A CONSTANT
C   PRESSURE (EQUAL TO THAT AT THE END OF THE ADIABATIC EXPANSION) BACK
C   DOWN TO 300K AT A COOLING RATE ASSUMED TO BE 100 TIMES SLOWER
C   THAN THE HEATING RATE.
C*************************************************************************
C*************************************************************************
C   INITIALIZATION OF A SERIES OF CONSTANTS AND VARIABLES USED IN THE
C   CALCULATION
C*************************************************************************
C   R=62.3656 DM3 TORR PER DEGREE KELVIN PER MOLE
C   RA=8.314 JOULE PER DEGREE KELVIN PER MOLE
C   GAMMA=HEAT CAPACITY RATIO (CP/CV) FOR ETHYLENE; ASSUMED CONSTANT
C   OVER A LIMITED TEMPERATURE RANGE; (FROM THE MAXIMUM TEMPERATURE TMAX
C   DOWN TO A LOWER TEMPERATURE T AT THE END OF THE ADIABATIC COOLING
C   PERIOD)
C   TIME=TIME IN THE CALCULATION / S
C   DTIME=TIME INCREMENT IN PART 1; (HEATING PART) / S
C   DTIME1=FIRST TIME INCREMENT IN PART 2; (COOLING BY ADIABATIC
C   EXPANSION) / S
C   DTIME2=SECOND TIME INCREMENT IN PART 2; (COOLING UNDER CONSTANT
C   PRESSURE) / S
C   T0= INITIAL TEMPERATURE OF THE GASEOUS SYSTEM; 300K
C   TMID=MID TEMPERATURE IN DTIME / K
C   TEND=FINAL TEMPERATURE IN DTIME / K
C   DTEMP=TEMPERATURE INCREMENT IN PART 1; (HEATING PART) / K
C   DTEMP1=FIRST TEMPERATURE INCREMENT IN PART 2; (COOLING PART) / K
C   DTEMP2=SECOND TEMPERATURE INCREMENT IN PART 2; (COOLING PART) / K
```

```
FILE: CASE3     FORTRAN  *    UNIV D'/OF OTTAWA CMS

C    TMAX=MAXIMUM TEMPERATURE REACHED AT A TIME OF 110 NANOSECOND / K
C    MKF=FORWARD RATE CONSTANT AT TMID IN DTIME / DM3 PER MOLE PER SECOND
C    FKF=FORWARD RATE CONSTANT AT TEND IN DTIME / DM3 PER MOLE PER SECOND
C    MKR=REVERSE RATE CONSTANT AT TMID IN DTIME / DM3 PER MOLE PER SECOND
C    FKR=REVERSE RATE CONSTANT AT TEND IN DTIME / DM3 PER MOLE PER SECOND
C    MKEQU=EQUILIBRIUM CONSTANT AT TMID IN DTIME / DM3 PER MOLE
C    FKEQU=EQUILIBRIUM CONSTANT AT TEND IN DTIME / DM3 PER MOLE
C    PC2H4M=PRESSURE OF ETHYLENE AT TMID / (TORR)
C    PC2H4F=PRESSURE OF ETHYLENE AT TEND / (TORR)
C    PC2H4MAX=PRESSURE OF ETHYLENE AT TMAX / (TORR)
C    C2H40=INITIAL CONCENTRATION OF ETHYLENE AT T0 / (MOLE/DM3)
C    C2H4M=CONCENTRATION OF ETHYLENE AT TMID / (MOLE/DM3)
C    C2H4F=CONCENTRATION OF ETHYLENE AT TEND / (MOLE/DM3)
C    PC4H8M=PRESSURE OF CYCLOBUTANE AT TMID / (TORR)
C    PC4H8F=PRESSURE OF CYCLOBUTANE AT TEND / (TORR)
C    PC4H8MAX=PRESSURE OF CYCLOBUTANE AT TMAX / (TORR)
C    C4H8M=ESTIMATED CYCLOBUTANE CONCENTRATION AT TMID / (MOLE/DM3)
C    C4H8MC=CORRECTED MID-CYCLOBUTANE CONCENTRATION TO V0 / (MOLE/DM3)
C    C4H8F=FINAL CYCLOBUTANE CONCENTRATION AT TEND / (MOLE/DM3)
C    C4H8FC=CORRECTED FINAL CYCLOBUTANE CONCENTRATION TO V0 / (MOLE/DM3)
C    DC4H8=NET CYCLOBUTANE CONCENTRATION FORMED IN DTIME / (MOLE/DM3)
C    CDC4H8=CORRECTED DC4H8 TO V0 / (MOLE/DM3)
C    SC4H8=CONCENTRATION OF CYCLOBUTANE FORMED DURING A PULSE i.e. FROM
C    ITS INITIAL CONCENTRATION AT 300 K (IN PART 1) TO ITS FINAL
C    CONCENTRATION AT 300 K (IN PART 2) / (MOLE/DM3)
C    C4H8EM=EQUILIBRIUM CYCLOBUTANE CONCENTRATION AT TMID CORRECTED TO
C    V0 / (MOLE/DM3)
C    C4H8EF=EQUILIBRIUM CYCLOBUTANE CONCENTRATION AT TEND CORRECTED TO
C    V0 / (MOLE/DM3)
C*************************************************************************
C    SPECIFICATION OF VARIABLE TYPE USED IN THE PROGRAM PRIOR TO THE
C    START OF THE CALCULATION.
C*************************************************************************
      DIMENSION PC2H4M(1000),PC2H4F(1000),C2H4M(1000),C2H4F(1000),
     +PC4H8M(1000),PC4H8F(1000),C4H8M(1000),C4H8MC(1000),C4H8EM(1000),
     +C4H8F(1000),C4H8FC(1000),C4H8EF(1000),DC4H8(1000),CDC4H8(1000),
     +SC4H8(1000),TMID(1000),TEND(1000),TIME(1000),MKF(1000),FKF(1000),
     +MKR(1000),FKR(1000),MKEQU(1000),FKEQU(1000)
      INTEGER J,K,L,M,N,O
      REAL*8 PC2H4M,PC2H4F,PC2H4MAX,C2H4M,C2H4F,PC4H8M,PC4H8F,PC4H8MAX,
     +C4H8M,C4H8MC,C4H8EM,C4H8F,C4H8FC,C4H8EF,DC4H8,CDC4H8,SC4H8,T0,TMAX
     +,TMID,TEND,TIME,DTIME,DTIME1,DTIME2,DTEMP,DTEMP1,DTEMP2,MKF,MKR,
     +FKF,FKR,MKEQU,FKEQU
C*************************************************************************
      R=62.3656
      RA=8.314
      GAMMA=1.08368
      TIME(1)=0
      DTIME=1.10D-09
      DTIME1=1.6069D-09
      DTIME2=9.39309D-10
      T0=300
      TMAX=1500
      DTEMP=12.0
      DTEMP1=1.75299
```

FILE: CASE3 FORTRAN * UNIV D'/OF OTTAWA CMS

```
      DTEMP2=0.1024701
      TMID(1)=T0-DTEMP/2
      TEND(1)=T0
      MKF(1)=10**(9.17-196000/(2.3*RA*TMID(1)))
      MKR(1)=10**(15.62-262000/(2.3*RA*TMID(1)))
      MKEQU(1)=MKF(1)/MKR(1)
      FKF(1)=10**(9.17-196000/(2.3*RA*TEND(1)))
      FKR(1)=10**(15.62-262000/(2.3*RA*TEND(1)))
      FKEQU(1)=FKF(1)/FKR(1)
      PC2H40=1000
      PC2H4MAX=PC2H40*(TMAX/T0)
      C2H40=PC2H40/(R*T0)
      C2H4M(1)=C2H40
      C4H8EM(1)=MKEQU(1)*(C2H4M(1)**2)
      C2H4F(1)=C2H40
      C4H8EF(1)=FKEQU(1)*(C2H4F(1)**2)
      PC2H4M(1)=C2H4M(1)*R*TMID(1)
      C4H8M(1)=0
      C4H8MC(1)=C4H8M(1)
      DC4H8(1)=0
      CDC4H8(1)=DC4H8(1)
      SC4H8(1)=0
      C4H8F(1)=6.4D-08
      C4H8FC(1)=C4H8F(1)
      PC4H8M(1)=0
      PC4H8F(1)=C4H8F(1)*R*TEND(1)
C*************************************************************************
C              PART 1 - HEATING PERIOD FROM 300 K TO TMAX
C*************************************************************************
      WRITE(6,10)
10    FORMAT( '      PC2H4F       DC4H8                    SC4H8        C4H8
     +F                    C4H8EF        TIME         TMID         TEND ' )
C   WRITE RESULTS LINED UP WITH HEADER
      WRITE(6,20)PC2H40,DC4H8(1),SC4H8(1),C4H8F(1),C4H8EF(1),TIME(1),
     +TMID(1),TEND(1)
20    FORMAT(1X,2(D11.4,1X),12X,2(D11.4,1X),14X,4(D11.4,1X))
         DO 30 J=2,102
         TIME(J)=TIME(J-1)+DTIME
         TMID(J)=TMID(J-1)+DTEMP
         TEND(J)=TEND(J-1)+DTEMP
         MKF(J)=10**(9.17-196000/(2.3*RA*TMID(J)))
         MKR(J)=10**(15.62-262000/(2.3*RA*TMID(J)))
         MKEQU(J)=MKF(J)/MKR(J)
         C2H4M(J)=C2H40
         C4H8EM(J)=MKEQU(J)*(C2H4M(J)**2)
         PC2H4M(J)=C2H4M(J)*R*TMID(J)
         FKF(J)=10**(9.17-196000/(2.3*RA*TEND(J)))
         FKR(J)=10**(15.62-262000/(2.3*RA*TEND(J)))
         FKEQU(J)=FKF(J)/FKR(J)
         C2H4F(J)=C2H40
         PC2H4F(J)=C2H4F(J)*R*TEND(J)
         C4H8EF(J)=FKEQU(J)*(C2H4F(J)**2)
         C4H8M(J)=C4H8F(J-1)+DC4H8(J-1)/2
         PC4H8M(J)=C4H8M(J)*R*TMID(J)
         DC4H8(J)=(MKF(J)*C2H4M(J)**2-MKR(J)*C4H8M(J))*DTIME
```

```
FILE: CASE3    FORTRAN  *   UNIV D'/OF OTTAWA CMS


          SC4H8(J)=DC4H8(J)+SC4H8(J-1)
          C4H8F(J)=C4H8F(J-1)+DC4H8(J)
          PC4H8F(J)=C4H8F(J)*R*TEND(J)
30        CONTINUE
       DO 50 K=2,101
       WRITE(6,40)PC2H4F(K),DC4H8(K),SC4H8(K),C4H8F(K),C4H8EF(K),TIME(K),
      +TMID(K),TEND(K)
40     FORMAT(1X,2(D11.4,1X),12X,2(D11.4,1X),14X,4(D11.4,1X))
50     CONTINUE
       WRITE(6,60)
60     FORMAT('  ')
C*************************************************************************
C        PART 2 - COOLING PERIOD FROM TMAX TO 300 K
C*************************************************************************
       WRITE(6,70)
70     FORMAT( '      ' )
       WRITE(6,80)
80     FORMAT( '      PC2H4F       DC4H8       CDCC4H8       SC4H8        C4H8
      +F       C4H8FC         C4H8EF        TIME         TMID         TEND ' )
C   SINCE THE COOLING RATE OF THE GAS IS DIFFERENT FROM ITS HEATING RATE
C   SOME CORRECTIONS WILL BE REQUIRED TO (A) THE TEMPERATURE AT THE
C   MIDDLE OF THE NEW TEMPERATURE INTERVAL, TO (B) THE PRESSURES OF
C   ETHYLENE AND OF CYCLOBUTANE ESTIMATED AT THE NEW TMID AT THE
C   BEGINNING OF PART 2 AS WELL AS TO (C) THE CONCENTRATIONS OF ETHYLENE
C   AND OF CYCLOBUTANE AT THE NEW TMID AND TO (D) THE CORRECTED FINAL
C   CONCENTRATION OF CYCLOBUTANE FORMED AT TMAX AND TO (E) THE NET
C   CONCENTRATION OF CYCLOBUTANE FORMED IN THE NEW TEMPERATURE INTERVAL.
       TMID(101)=TMID(101)+5.123505
       MKF(101)=10**(9.17-196000/(2.3*RA*TMID(101)))
       MKR(101)=10**(15.62-262000/(2.3*RA*TMID(101)))
       MKEQU(101)=MKF(101)/MKR(101)
       PC2H4M(101)=PC2H4MAX*((TMAX/TMID(101))**(GAMMA/(1-GAMMA)))
       PC4H8MAX=PC4H8F(101)
       PC4H8M(101)=PC4H8MAX*((TMAX/TMID(101))**(GAMMA/(1-GAMMA)))
       C2H4M(101)=C2H40*(PC2H4M(101)/PC2H40)*(T0/TMID(101))
       C4H8M(101)=(C4H8F(101)*(PC4H8M(101)/PC4H8F(101))*(TEND(101)/
      +TMID(101)))+((DC4H8(100)/2*(TMID(101)+DTEMP1)/TMID(101)))
       C4H8MC(101)=C4H8M(101)*(PC2H40/PC2H4M(101))*(TMID(101)/T0)
       C4H8EM(101)=MKEQU(101)*(C2H4M(101)**2)*(PC2H40/PC2H4M(101))*
      +(TMID(101)/T0)
       C4H8FC(101)=C4H8F(101)*(PC2H40/PC2H4F(101))*(TEND(101)/T0)
       DC4H8(101)=(MKF(101)*C2H4M(101)**2-MKR(101)*C4H8M(101))*DTIME1
       CDC4H8(101)=DC4H8(101)*(PC2H40/PC2H4M(101))*(TMID(101)/T0)
C   WRITE RESULTS LINED UP WITH HEADER
       WRITE(6,90)PC2H4F(101),DC4H8(101),CDC4H8(101),SC4H8(101),
      +C4H8F(101),C4H8FC(101),C4H8EF(101),TIME(101),TMID(101),TEND(101)
90     FORMAT(1X,6(D11.4,1X),2X,D11.4,3(1X,D11.4))
C   IN THIS PART, THE FINAL PRESSURES OF ETHYLENE AND OF CYCLOBUTANE
C   ARE CALCULATED FIRST AND ARE SUBSEQUENTLY USED TO CALCULATE THE
C   FINAL CONCENTRATIONS OF ETHYLENE AND OF CYCLOBUTANE. IN THIS PART,
C   THE FINAL PRESSURES AND CONCENTRATIONS ARE CALCULATED BEFORE THE
C   MIDDLE PRESSURES AND CONCENTRATIONS.
          DO 100 L=102,202
          TIME(L)=TIME(L-1)+DTIME1
          TEND(L)=TEND(L-1)-DTEMP1
```

FILE: CASE3 FORTRAN * UNIV D'/OF OTTAWA CMS

```
          TMID(L)=TMID(L-1)-DTEMP1
          FKF(L)=10**(9.17-196000/(2.3*RA*TEND(L)))
          FKR(L)=10**(15.62-262000/(2.3*RA*TEND(L)))
          FKEQU(L)=FKF(L)/FKR(L)
          PC2H4F(L)=PC2H4MAX*((TMAX/TEND(L))**(GAMMA/(1-GAMMA)))
          C2H4F(L)=C2H40*(PC2H4F(L)/PC2H40)*(T0/TEND(L))
          C4H8EF(L)=FKEQU(L)*(C2H4F(L)**2)*(PC2H40/PC2H4F(L))*
     +    (TEND(L)/T0)
          MKF(L)=10**(9.17-196000/(2.3*RA*TMID(L)))
          MKR(L)=10**(15.62-262000/(2.3*RA*TMID(L)))
          MKEQU(L)=MKF(L)/MKR(L)
          PC2H4M(L)=PC2H4MAX*((TMAX/TMID(L))**(GAMMA/(1-GAMMA)))
          C2H4M(L)=C2H40*(PC2H4M(L)/PC2H40)*(T0/TMID(L))
          C4H8EM(L)=MKEQU(L)*(C2H4M(L)**2)*(PC2H40/PC2H4M(L))*
     +    (TMID(L)/T0)
          PC4H8F(L)=PC4H8MAX*((TMAX/TEND(L))**(GAMMA/(1-GAMMA)))
          C4H8F(L)=(C4H8F(L-1)*((TEND(L)+DTEMP1)/TEND(L))*(PC4H8F(L)/
     +    PC4H8F(L-1)))+(DC4H8(L-1)*((TMID(L)+DTEMP1)/TEND(L))*
     +    (PC4H8F(L)/PC4H8M(L-1)))
          C4H8FC(L)=C4H8F(L)*(PC2H40/PC2H4F(L))*(TEND(L)/T0)
          PC4H8M(L)=PC4H8MAX*((TMAX/TMID(L))**(GAMMA/(1-GAMMA)))
          C4H8M(L)=(C4H8F(L)*(TEND(L)/TMID(L))*(PC4H8M(L)/PC4H8F(L)))+
     +    (DC4H8(L-1)/2*((TMID(L)+DTEMP1)/TMID(L))*(PC4H8M(L)/PC4H8M(L-1)
     +    ))
          C4H8MC(L)=C4H8M(L)*(PC2H40/PC2H4M(L))*(TMID(L)/T0)
          SC4H8(L)=CDC4H8(L-1)+SC4H8(L-1)
          DC4H8(L)=(MKF(L)*C2H4M(L)**2-MKR(L)*C4H8M(L))*DTIME1
          CDC4H8(L)=DC4H8(L)*(PC2H40/PC2H4M(L))*(TMID(L)/T0)
100       CONTINUE
       DO 120 M=102,201
       WRITE(6,110)PC2H4F(M),DC4H8(M),CDC4H8(M),SC4H8(M),C4H8F(M),
      +C4H8FC(M),C4H8EF(M),TIME(M),TMID(M),TEND(M)
110    FORMAT(1X,6(D11.4,1X),2X,D11.4,3(1X,D11.4))
120    CONTINUE
       WRITE(6,130)
130    FORMAT(' ')
C    AT THIS POINT IN THE CALCULATION,THE COOLING OF THE GAS BY ADIABATIC
C    EXPANSION HAS CEASED AND FURTHER COOLING OCCURS UNDER CONSTANT
C    PRESSURE AT A RATE WHICH IS ASSUMED TO BE 100 TIMES SLOWER THAN THE
C    HEATING RATE AND 10 TIMES SLOWER THAN THE COOLING RATE BY ADIABATIC
C    EXPANSION. THEREFORE BEFORE CONTINUING THE CALCULATION,CORRECTIONS
C    TO SUCH VARIABLES AS (A) THE MIDDLE TEMPERATURE AT THE BEGINNING
C    OF THE NEW TEMPERATURE INTERVAL AS WELL AS TO (B) THE PRESSURES OF
C    ETHYLENE AND OF CYCLOBUTANE AND TO (C) THE CONCENTRATIONS OF
C    ETHYLENE AND OF CYCLOBUTANE AS WELL AS TO (D) THE NET CONCENTRATION
C    OF CYCLOBUTANE ARE REQUIRED.
       TMID(201)=TMID(201)+0.82526
       MKF(201)=10**(9.17-196000/(2.3*RA*TMID(201)))
       MKR(201)=10**(15.62-262000/(2.3*RA*TMID(201)))
       MKEQU(201)=MKF(201)/MKR(201)
       C2H4M(201)=C2H40*(T0/TMID(201))
       C4H8EM(201)=MKEQU(201)*(C2H4M(201)**2)*(TMID(201)/T0)
       C4H8M(201)=(C4H8F(201)*(TEND(201)/TMID(201)))+(DC4H8(200)/2*
      +(TMID(201)+DTEMP2)/TMID(201))
       C4H8MC(201)=C4H8M(201)*(TMID(201)/T0)
```

FILE: CASE3 FORTRAN * UNIV D'/OF OTTAWA CMS

```
      C4H8FC(201)=C4H8F(201)*(TEND(201)/T0)
      DC4H8(201)=(MKF(201)*C2H4M(201)**2-MKR(201)*C4H8M(201))*DTIME2
      CDC4H8(201)=DC4H8(201)*(TMID(201)+DTEMP2)/TEND(201)*(TEND(201)/T0)
      PC2H4M(201)=PC2H40*(C2H4M(201)/C2H40)*(TMID(201)/T0)
      PC4H8M(201)=PC4H8F(201)*(C4H8M(201)/C4H8F(201))*(TMID(201)/
     +TEND(201))
      WRITE(6,140)PC2H4F(201),DC4H8(201),CDC4H8(201),SC4H8(201),
     +C4H8F(201),C4H8FC(201),C4H8EF(201),TIME(201),TMID(201),TEND(201)
140   FORMAT(1X,6(D11.4,1X),2X,D11.4,3(1X,D11.4))
      DO 170 N=1,100
         DO 150 O=202,302
         TIME(O)=TIME(O-1)+DTIME2
         TEND(O)=TEND(O-1)-DTEMP2
         TMID(O)=TMID(O-1)-DTEMP2
         FKF(O)=10**(9.17-196000/(2.3*RA*TEND(O)))
         FKR(O)=10**(15.62-262000/(2.3*RA*TEND(O)))
         FKEQU(O)=FKF(O)/FKR(O)
         C2H4F(O)=C2H40*(T0/TEND(O))
         PC2H4F(O)=PC2H40*(C2H4F(O)/C2H40)*(TEND(O)/T0)
         MKF(O)=10**(9.17-196000/(2.3*RA*TMID(O)))
         MKR(O)=10**(15.62-262000/(2.3*RA*TMID(O)))
         MKEQU(O)=MKF(O)/MKR(O)
         C2H4M(O)=C2H40*(T0/TMID(O))
         PC2H4M(O)=PC2H40*(C2H4M(O)/C2H40)*(TMID(O)/T0)
         C4H8F(O)=(C4H8F(O-1)*(TEND(O)+DTEMP2)/TEND(O))+(DC4H8(O-1)*
     +   (TMID(O)+DTEMP2)/TEND(O))
         C4H8FC(O)=C4H8F(O)*(TEND(O)/T0)
         C4H8EF(O)=FKEQU(O)*(C2H4F(O)**2)*(TEND(O)/T0)
         PC4H8F(O)=PC4H8F(O-1)*(C4H8F(O)/C4H8F(O-1))*(TEND(O)/(TEND(O)+
     +   DTEMP2))
         C4H8M(O)=(C4H8F(O)*(TEND(O)/TMID(O)))+(DC4H8(O-1)/2*(TMID(O)+
     +   DTEMP2)/TMID(O))
         C4H8MC(O)=C4H8M(O)*(TMID(O)/T0)
         C4H8EM(O)=MKEQU(O)*(C2H4M(O)**2)*(TMID(O)/T0)
         PC4H8M(O)=PC4H8F(O)*(C4H8M(O)/C4H8F(O))*(TMID(O)/TEND(O))
         SC4H8(O)=CDC4H8(O-1)+SC4H8(O-1)
         DC4H8(O)=(MKF(O)*C2H4M(O)**2-MKR(O)*C4H8M(O))*DTIME2
         CDC4H8(O)=DC4H8(O)*(TMID(O)+DTEMP2)/TEND(O)*(TEND(O)/T0)
150      CONTINUE
      WRITE(6,160)PC2H4F(301),DC4H8(301),CDC4H8(301),SC4H8(301),
     +C4H8F(301),C4H8FC(301),C4H8EF(301),TIME(301),TMID(301),TEND(301)
160   FORMAT(1X,6(D11.4,1X),2X,D11.4,3(1X,D11.4))
      TIME(201)=TIME(301)
      TMID(201)=TMID(301)
      TEND(201)=TEND(301)
      MKF(201)=MKF(301)
      MKR(201)=MKR(301)
      FKF(201)=FKF(301)
      FKR(201)=FKR(301)
      MKEQU(201)=MKEQU(301)
      FKEQU(201)=FKEQU(301)
      C2H4M(201)=C2H4M(301)
      PC2H4M(201)=PC2H4M(301)
      C2H4F(201)=C2H4F(301)
      PC2H4F(201)=PC2H4F(301)
```

FILE: CASE3 FORTRAN * UNIV D'/OF OTTAWA CMS

```
      C4H8EM(201)=C4H8EM(301)
      C4H8EF(201)=C4H8EF(301)
      C4H8M(201)=C4H8M(301)
      C4H8MC(201)=C4H8MC(301)
      PC4H8M(201)=PC4H8M(301)
      C4H8F(201)=C4H8F(301)
      C4H8FC(201)=C4H8FC(301)
      PC4H8F(201)=PC4H8F(301)
      SC4H8(201)=SC4H8(301)
      DC4H8(201)=DC4H8(301)
      CDC4H8(201)=CDC4H8(301)
170   CONTINUE
      WRITE(6,180)SC4H8(201)
180   FORMAT(T38,D11.4)
      WRITE(6,190)
190   FORMAT( '      ' )
      WRITE(6,200)
200   FORMAT( ' END OF PROGRAM -- ETHYLENE-CYCLOBUTANE SYSTEM ' )
      STOP
      END
```

APPENDIX E: Calculation of R_f, the reflectance factor correcting for light reflected from the cell windows and absorbed by ethylene

Since reflectance from a quartz window is substantial in the UV region, approaching 10% at 193 nm, a correction must be made from light reflected back through the cell which can be absorbed by ethylene. Table E-1 shows the normal reflectance at a fused silica gas interface at the excimer laser wavelengths derived from Fresnel's equation $\rho = (n - 1)^2/(n + 1)^2$ using published values of n, the index of refraction of fused silica [E-1,E-2].

Table E-1. Normal reflectance as a function of $\lambda_{excimer\ laser}$

λ/nm	ρ	2ρ
193	0.0481	0.0962
222	0.0434	0.0868
249	0.0410	0.0820
308	0.0385	0.0770

We shall assume that the two surfaces of each window contribute equally to the total reflectance of the window, which will then be 2ρ. (This assumption neglects losses to the second surface reflection due to absorption within the window material and the two reflections at the first surface. When corrected for these reflective losses, total second surface reflection is given by $\rho(1-\rho)^2$ instead of ρ, which for ρ = 0.0481 has a value of 0.0436, neglecting absorption in the window. The effect of these approximations on calculation of the total energy absorbed in ethylene is less than 1%).

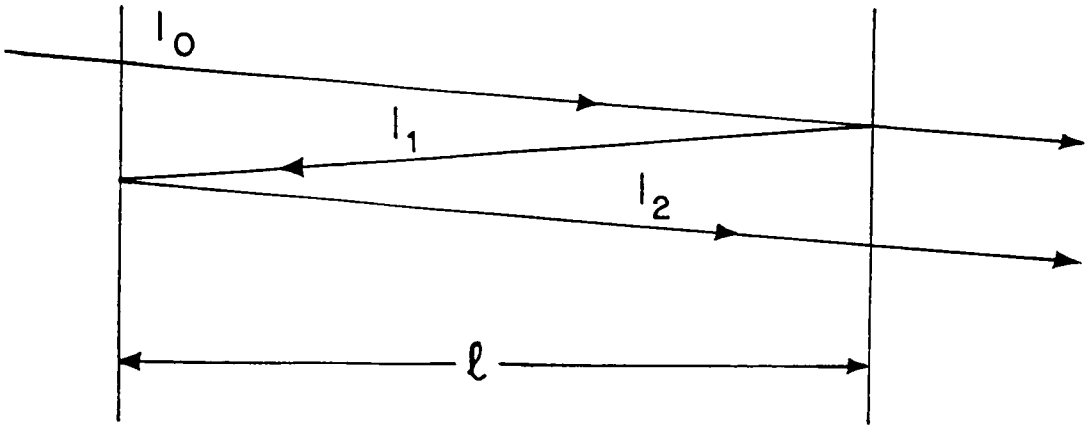

The diagram shows two reflections between the cell windows, where I_0 is the light intensity transmitted by the front window, and I_1 and I_2 are intensities of the two reflected beams. For clarity, beams are shown at an angle to the normal; in the experiments, light beams were normal to the windows. Because each reflected beam traverses the same path length in ethylene as the primary beam, the effect of the reflected light on the photolysis can be treated as an increase in the intensity of light incident on the gas, and the correction factor will be given by $R_f = (I_0 + I_1 + I_2)/I_0$. At low ethylene pressure, when attenuation of the light beams in the cell is negligible, for $\rho = 0.0481$,

$$R_f = [I_0(1 + 2\rho + 4\rho^2)]/I_0 = 1 + 0.0962 + 0.0092 = 1.1054$$

from which it is clear that further reflections can be neglected. At higher ethylene pressures, attenuation in the gas must be taken into account, and $R_f = (1 + 2\rho T + 4\rho^2 T^2)$ where T is the transmittance of the gas. Table E-2 shows calculated values of R_f for various pressures of ethylene from 50 to 3000 Torr at 193 nm, together with the corresponding percent absorption by ethylene in the cell, taking $\epsilon(193\ nm) = 5.63\ M^{-1}\ cm^{-1}$. These data are shown in Figure E-1.

Table E-2. Values of R_f and the corresponding percent absorption for various pressures of ethylene in the cell at 193 nm.

C_2H_4/Torr	R_f	percent absorption
0	1.105	0
50	1.103	1.8
100	1.101	3.6
250	1.096	8.7
500	1.087	16.6
760	1.078	24.1
1000	1.071	30.4
2000	1.049	51.6
3000	1.033	66.3

At wavelengths of 222, 249 and 308 nm, the photolysis of ethylene was investigated only at a single pressure of 760 Torr. Table E-3 gives calculated values of R_f. The correction for attenuation at these wavelengths is negligible.

Table E-3. Values of R_f and the corresponding percent absorption at 760 Torr ethylene in the cell at λ = 222, 249 and 308 nm.

λ/nm	R_f	percent absorption
222	1.094	0.0044
249	1.089	0.12
308	1.083	0.40

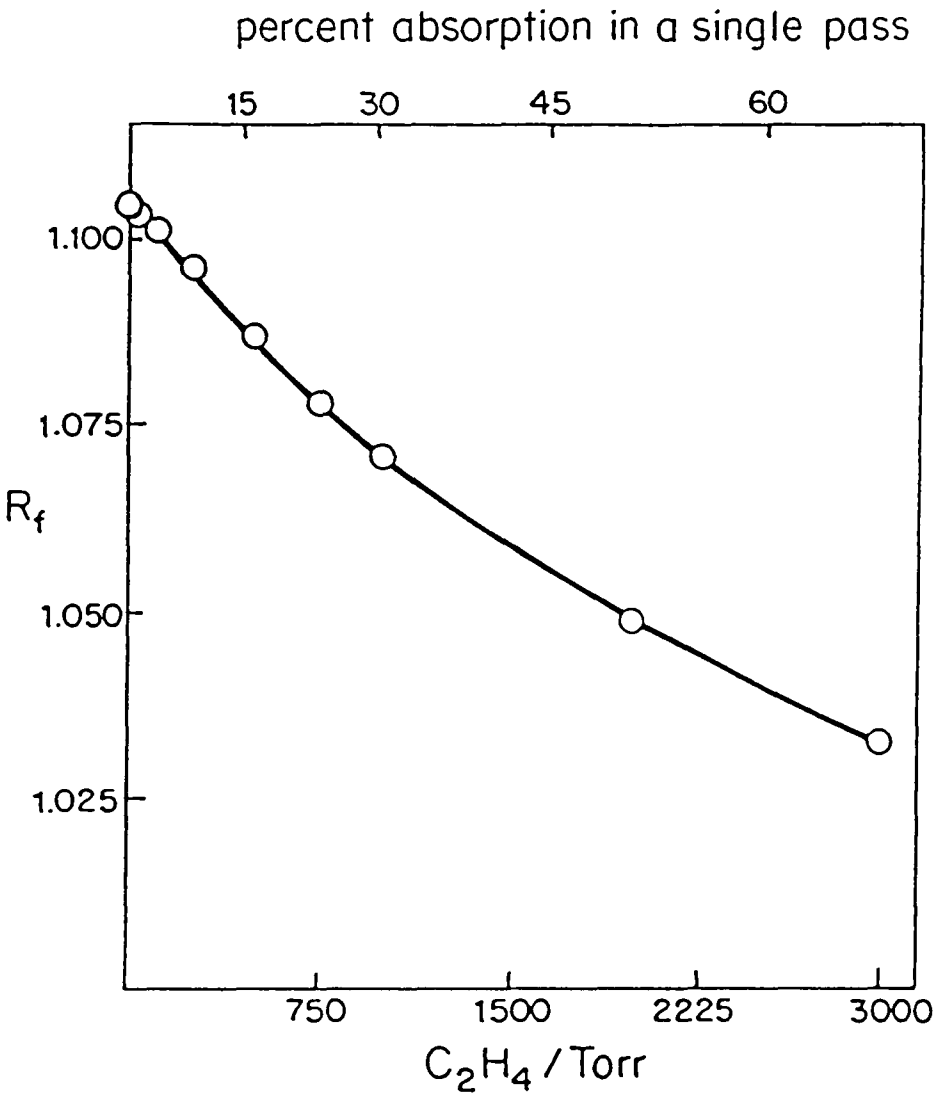

Figure E-1. Reflectance factor as a function of ethylene pressure and the corresponding percent absorption of 193 nm radiation by ethylene.

REFERENCES

[E-1] H.R. Philipp, J. Phys. Chem. Solids 32, 1935 (1971).

[E-2] B. Brixner, J. Opt. Soc. Am. 57, 674 (1967).